Electromagnetic Interference Shielding and Microwave Absorption Performance of Hybrid Nanoparticles Filled Epoxy Composites

Thesis

submitted in partial fulfillment
of the requirements to

Birla Institute of Technology & Science, Pilani (BITS Pilani)
For the award of the degree

of

Doctor of Philosophy

by

Bheema Rajesh Kumar

Under the guidance of

Dr. Krishna C. Etika

DEPARTMENT OF CHEMICAL ENGINEERING
BIRLA INSTITUTE OF TECHNOLOGY & SCIENCE, PILANI,
PILANI CAMPUS-333031 (RAJASTHAN) INDIA
July, 2023

BIRLA INSTITUTE OF TECHNOLOGY & SCIENCE, PILANI

<u>CERTIFICATE</u>

This is to certify that the thesis entitled **"*Electromagnetic Interference Shielding and Microwave Absorption Performance of Hybrid Nanoparticles Filled Epoxy Composites*"** submitted by **Mr. *Bheema Rajesh Kumar*** ID No**. *2018PHXF0005P*** for the award of Ph.D. of the institute embodies original work done by him under my supervision.

Signature of the Supervisor:

Name in capital letters: **Dr. KRISHNA C. ETIKA**

Designation: Assistant Professor,

                                              Department of Chemical Engineering,

                                              Birla Institute of Technology & Science, Pilani

                                              Pilani Campus, Rajasthan.

Date: 04/07/2023

DEDICATION

This thesis is dedicated to both my parents and my wife, whose continuous love and support helped me achieve my Doctoral degree goal. It is also dedicated to my supervisor, who assisted me in achieving a dream that I had never imagined possible, and I completed my work because of his ongoing competent support academically, professionally, and personally.

ACKNOWLEDGMENTS

This thesis is the cumulation of four and half years of work (2018-2023) at the Birla Institute of Technology & Science (BITS), Pilani. There are many people I would like to thank for their constant encouragement and assistance in completing my Ph.D. work. First, I would like to express my deepest and most sincere gratitude to my supervisor Dr. Krishna C. Etika, for the continuous guidance, motivation, encouragement, and affection throughout the research period at BITS, Pilani. He is a teacher that strives to bring out the best in each of his students. "The best teachers are those who show you where to look but don't tell you what to see." He always followed this standard approach, and it allowed me to expand my horizons beyond the confines of my regular lab work and explore new things. I believe this approach will be useful in the future. In addition to research, he taught us the importance of punctuality, planning, ethics, and modesty. He believed in logical thinking, extensive planning, and strategy necessary to execute any work. In addition, he was always available for assistance and advice on personal or professional matters. The amount of effort, thinking, and time given by him to this thesis work is appreciable, due to which this thesis work has some substance and does better reading.

I express my sincere thanks to Prof. Banasri Roy and Prof. A.V. Praveen Kumar, the members of the Doctoral Advisory Committee (DAC), for their valuable suggestions and remarks at every point of this thesis work. I would like to thank the Head of the Department (HOD) of Chemical Engineering, Prof. Pratik N Sheth, and former HOD, Prof. Banasri Roy and Prof. Hare Krishna Mohantta, for their valuable suggestions and for providing the required facilities in the Department of Chemical Engineering. Also, I would like to thank Prof. V Ramgopal Rao (Vice-Chancellor), Prof. S. K. Barai (Director), and Prof. Sanjay Kumar Verma (Dean of administration) for providing the required facilities. I wish to extend special thanks to Col Soumyabrata Chakraborty (Registrar) and Prof. Shamik Chakraborty (Associate Dean of Academic Graduate Studies and Research Division) for their administrative support.

I would also like to extend my sincere gratitude to the faculty members Prof. Arvind K Sharma, Prof. Bhanu Vardhan Reddy Kuncharam, Prof. Srinivas Appari, Prof. Somak Chatterjee, Prof. Priya C Sande, Prof. Amit Jain, Prof. Ajaya Kumar Pani, Prof. Smita Raghuvanshi, Prof. Pradipta Chattopadhyay, Prof. Suresh Gupta who have supported me during my research and teaching practice. I wish to thank all non-teaching staff, Mr. Suresh Kumar Sharma, Mr. Kuldeep Kumar,

Table of Contents

Electromagnetic Interference (EMI) refers to the electromagnetic radiation emitted by electronic devices, which can interfere with other nearby devices and cause performance issues. EMI shielding is the process of enclosing an electronic device or component in a material that blocks electromagnetic radiation from escaping or entering. EMI shielding is crucial for protecting electronic devices, complying with regulations, improving performance, ensuring safety, and saving costs. The choice of an EMI shielding material depends on several factors, including the frequency of the electromagnetic radiation, the size and shape of the electronic device, and the required level of shielding effectiveness. Traditionally, metals were used for EMI shielding due to their excellent shielding effectiveness and durability. However, metals are prone to corrosion, are bulky, and can only reflect the electromagnetic energy, which at best partially mitigates the EMI issue. Polymer composites, on the other hand, offer a range of advantages for EMI shielding, including their light weight, flexibility, customizability, and cost-effectiveness. In this work, the EMI shielding and microwave absorption performance of epoxy composites containing hybrid nanoparticles in the X-band frequency range, i.e., 8-12.4 GHz, is investigated. The X-Band frequency range plays an important role in various industries and applications that require high-speed data transfer, high-resolution imaging, and reliable communication over long distances.

Copper nanowires (CuNW) are being increasingly used as a filler material in polymer composites for EMI shielding applications. This is because copper has high electrical conductivity and is an effective EMI shielding material. CuNW, with its high aspect ratio, offers several advantages over other copper filler materials. Driven by this aspect, the EMI shielding performance of CuNW-filled epoxy composites was evaluated over the X-band frequency range and the results are discussed in detail in Chapter 3 of this thesis. Briefly, the CuNWs used in this study were produced

using a facile one-pot hydrothermal synthesis method. A series of CuNW-epoxy nanocomposites containing various filler contents were fabricated and compared for their electrical conductivity and EMI shielding effectiveness. The obtained results indicated that 12 wt% CuNW sample demonstrated the highest total shielding effectiveness, i.e., SE_T value of 6.5 dB, which corresponds to 77.1 % attenuation of incident EM wave. Although encouraging, the realized SE_T performance was inferior when compared to values reported for carbon-filled polymer systems.

It has been demonstrated by several researchers that the addition of magnetic and/or dielectric particles can enhance the EMI shielding effectiveness in conducting polymer composites. Driven by the motivation to increase the SE_T values of the CuNW-epoxy system, the influence of Fe_3O_4 nanoparticles on the EMI shielding and microwave absorption performance in these composites was subsequently investigated. The chapter 4 of this thesis summarizes the detailed results from this effort. A series of composites containing 12 wt% CuNW and varying weight percentages of Fe_3O_4 were prepared and tested. The composite sample containing 12 wt% CuNW and 8 wt% Fe_3O_4 demonstrated the highest SE_T value of 14.6 dB in the X-band frequency range among all the composites tested. Furthermore, the SE_T value for a composite containing both particles was found to be significantly more than the composites containing equivalent loading of only either of these particles, which suggested a synergistic effect between these particles. To explore further on the observed synergy between conductive and magnetic nanoparticles, an epoxy composite containing an altogether different filler system, i.e., graphene nanoplatelets (GNP) and Barium hexaferrite (BaM), was also studied. A set of epoxy composites were made using varying weight ratios of GNP:BaM and tested for their EMI shielding performance. The results obtained were similar to that of CuNW/Fe_3O_4 epoxy composites, wherein the composite containing both magnetic and conductive filler particles exhibited larger SE_T values when compared to those

composites that had equivalent loading of only one type of filler. A one-millimeter-thick composite sample containing 8 wt% BaM and 10 wt% GNP exhibited a SE_T value of 17.2 dB in the X-band frequency range, which equates to attenuation of 98.17% of incident wave power.

It was noted from the literature review that the direct incorporation of conductive nanoparticles along with magnetic nanoparticles in the polymer matrix can lead to phase segregation, which can deteriorate the shielding performance. Driven by this observation, an attempt was made to test the EMI shielding performance of epoxy composites containing hybrid particles, i.e., Fe_3O_4@CuNW. It was envisioned that these hybrid filler particles would reduce phase separation and can further enhance the EMI shielding performance. Accordingly, the Fe_3O_4@CuNW hybrid particles were synthesized using the hydrothermal method and were characterized for their microstructure using XRD, SEM, and XPS. The composites containing varying content of these hybrid particles were made and tested for their EMI shielding performance. A one-millimeter thick 12:8 (wt%/wt%) CuNW: Fe_3O_4 hybrid epoxy composite exhibited a SE_T value of 19.3 dB in the X-band, which translates to attenuation of 98.8% of the microwave power. Furthermore, 60% of the microwave power was found to be attenuated by the absorption mechanism in these composites. These results indicate that magnetic and conductive particles, when used together, have the potential to significantly augment the shielding performance in polymer composites.

As mentioned earlier, the addition of dielectric particles to conducting polymer composites has also resulted in good improvement in their SE_T values. To understand the influence of dielectric fillers on the SE_T values, epoxy composite filled with CuNW and/or barium strontium titanate (BST) and their hybrid, i.e., BST@CuNW, were prepared and tested. The chapter 5 of this thesis comprises of the results from the above effort. The BST@CuNW hybrid composite exhibited superior EMI shielding performance when compared to samples containing equivalent loading of

only CuNW and/or BST. The 1-mm thick composite sample containing 10:15 (wt%/wt%) CuNW: BST hybrid attenuated 99.2 % of incident wave power and exhibited a SE_T value of 21.2 dB in the X-band. As a continuation to the above work, microwave absorbing characteristics of epoxy composites containing both BST and Fe_3O_4 nanoparticles deposited on copper nanowires (i.e., $Fe_3O_4@BST@ CuNW$ hybrids), CuNW, BST, and Fe_3O_4 over the X-band frequency range of 8–12.4 GHz was also investigated and the results are presented in chapter 6 of this thesis. The SE_T values obtained on epoxy composites containing $Fe_3O_4@BST@CuNW$ hybrid were significantly more than those containing equivalent loading of CuNW, BST, or Fe_3O_4. A one-millimeter thick sample containing 4:8:10 (wt%:wt%:wt%) Fe_3O_4: BST: CuNW hybrid composite attenuated 99.91 % of incident power with absorption power of 80.2% in the X-band frequency range of 8–12.4 GHz. Overall, the results suggest that EMI shielding of CuNw-epoxy composites can be significantly improved with the addition of CuNW-based hybrid nanostructures and an absorption-dominated attenuation mechanism exists in these composites.

Keywords: Copper nanowires, Hybrid structures, Microwave absorbing materials, Epoxy composites, EMI shielding materials, Ferrites, Fe_3O_4, Dielectrics, Barium strontium titanate, Polymer nanocomposites, X-band frequency range.

List of the Figures

List of Tables

List of Abbreviations

ABS: Acrylonitrile-butadiene-styrene

AEM: Ethylene acrylic elastomers

AIBN: Azoisobutyronitrile

Ag: Silver nanoparticles

Ag@HGM: Silver nanoparticles on the surface of hollow glass microspheres

APS: Aminopropyltrimethoxysilane

BaM: M-type barium hexaferrites nanoparticles

BC: Bacterial cellulose

BITS: Birla Institute of Technology and Science

BN: Boron nitride

BNSF: $BaNd_{0.2}Sm_{0.2}Fe_{11.6}O_{19}$

BRF: Polypyrrole matrix encapsulated with BST, RGO and Fe_3O_4

BST: Barium strontium titanate

CB: Carbon black

CCTO: $CaCu_3Ti_4O_{12}$

CDCA: Cellulose-derived carbon aerogels

CEERI: Central Electronics Engineering Research Institute

CF: Carbon fibre

CIP: Carbonyl iron powder

CLF: Carbonized loofah fiber

CNF: Cellulose nanofiber

CNT: Carbon nanotubes

CPC: conductive polymer composites

CPEGDA: Crosslinked poly (ethylene glycol) diacrylate

CSA: Camphor sulfonic acid

CTAB: Cetyl trimethyl ammonium bromide

CuNW: Copper nanowires

DAC: Doctoral Advisory Committee

EDA: ethylenediamine

EDS: energy dispersive spectroscopy

EM: Electro-magnetic

EMA: Ethylene-co-methyl acrylate

EMI: Electro-magnetic Interference

EMI SE: Electro-magnetic Interference shielding effectiveness.

EOC: Ethylene octene copolymer

FAC: Fly ash cenosphere

FNP: Fe_3O_4 nanoparticles

f-MWCNT: Functionalized Multiwalled Carbon Nanotubes

GFBT: Graphene nanoplate/ Fe_3O_4@$BaTiO_3$ hybrid

GN: Graphene nanosheets

GN-CN: graphene nanoplates-carbon nanotubes

GNP: Graphene nanoplatelets

GO: graphene oxide

HDA: hexadecyl amine

HDPE: High density polyethylene

HGM: Hollow glass microspheres

HOD: Head of the Department

HS-CB: High-structure carbon black

IL-MWCNT: Ionic Liquid- Multiwalled Carbon Nanotubes

IoT: Internet of things

LC: Lignin-derived carbon

M: Multiple internal reflection

MA: Maleic anhydride

MAM: Microwave absorbing materials

MNP: Metal nanoparticles

MPU: Mill able polyurethane

MWNT or MWCNT: Multi-walled carbon nanotubes

NCF: Nickel doped cobalt ferrites

NE: Neat epoxy

NF: Nonwoven fabric

Ni: Nickel

Ni@CNT: Carbon nanotubes encapsulated nickel nanowires

NR: Natural Rubber

NRW: Nicholson–Ross–Weir

NWF: Non-woven fabrics

OA: Oleic acid

ODA: octadecylamine

ODE: 1-octadecene

OM: Oleyl amine

PAM: Polyazomethine

PANI: Polyaniline

PBAT: Poly (butylene adipate-co-terephthalate)

PBO: Poly(p- phenylenebenzobisoxazole)

PC: Polycarbonate

PCL: Polycaprolactone

PDMS: Polydimethylsiloxane

PEDOT: Poly(3,4-ethylene dioxythiophene)

PEEK: Polyether ether ketone

PEG: polyethylene glycol

PET: Polyethylene terephthalate

PET Oxide: Poly (ethylene oxide)

PHDDT: Phosphorus-containing liquid crystalline co-polyester

PI: Power density of incident electromagnetic waves

PLA: Poly (lactic acid)

PLLA: Poly(l-lactide)

PMMA: Poly (methyl methacrylate)

PNC: Polymer nanocomposites

POE: Poly(ethylene-co-1-octene)

PP: Polypropylene

PPy: Polypyrrole

PPEK: Poly (phthalazinone etherketone)

PPS: Poly (phenylene sulphide)

PR: Power density of reflected electromagnetic waves

PS: Polystyrene

PSS: Polystyrene sulfonate

PT: Power density of transmitted electromagnetic waves

p-TSA: para-Toluene Sulphonic Acid

PVA: Polyvinyl Alcohol

PVB: Poly (vinyl butyral)

PVP: polyvinylpyrrolidone

PVDF: Polyvinylidene fluoride

PU: Polyurethane

PyC: Pyrolytic carbon

RG-CN: Chemically reduced graphene oxide-carbon nanotubes

rGH: Honeycomb structural RGO

rGMH: Honeycomb structural RGO-MXene

RGO: Reduced graphene oxide

SBR: Styrene-butadiene rubber

SCF: Short carbon fiber

SDBS: Sodium dodecyl benzenesulfonate

SDS: sodium dodecyl sulfate

SE$_A$: EMI shielding effectiveness due to absorption loss

SE$_R$: EMI shielding effectiveness due to reflection loss

SEM: Scanning electron microscopy

SE$_T$: Total EMI shielding effectiveness

SGM: Solid glass microspheres

SLS: sodium lauryl sulfate

SSE: Specific shielding effectiveness

SSF: Stainless steel fibre

Sub-SF: Substituted strontium ferrite

SWNT: Single-walled carbon nanotube

TAGA: Thermally annealed graphene aerogel

TDA: tetradecylamine

TGO: Thermally reduced graphene oxide

TGO-CN: Thermally reduced graphene oxide-carbon nanotubes

TPU: Thermoplastic polyurethane

TOA: tri-n-octylamine

UHMWPE: Ultrahigh-molecular-weight polyethylene

VNA: vector network analyzer

WPU: Waterborne polyurethane

WTP: Wastepaper

XRD: X-ray powder diffraction

List of Symbols

A: Absorption

t: Conductivity exponent

f_r: Cut-off frequency

D: Dimensional

σ: Electrical conductivity

Φ: Filler content

E: Electric field strength

ε'': Imaginary permittivity or dielectric loss

μ'': Imaginary permeability

Z_o: Impedance

Z_w: Impedance of the material

H: Magnetic field strength

M_s : Magnetic saturation

μ: Magnetic permeability

M: Multiple internal reflections

Φ_c: Percolation threshold

ε': Real part of permittivity

μ': Real permeability

μ_r: Relative permeability

R: Reflection

Γ: Reflection coefficient

δ: Skin depth

d: Thickness

T: Transmission coefficient

1 Introduction

1.1 Electromagnetic interference

The rapid growth of instrumentation and electronics in various sectors, such as information technology, military, defense safety systems, healthcare, business electronics, commercial appliances, *etc.*, have led to electromagnetic interference (EMI) as an undesirable by-product [1,2]. Furthermore, concepts such as the internet of things (IoT) and smart villages are rapidly gaining momentum, wherein the products involve some wireless data transfer that can potentially further enhance the already widespread problem of signal interference [3]. The EMI in electronic devices and industrial instruments can cause a deterioration in normal functioning or a total malfunction of the instrument. If these problems are unattended, they can cause major harm to electrical and communication systems as well as the safe operation of numerous electronic products. Consequently, EMI can be regarded as a new type of pollution that can be mitigated using EMI shielding materials [4]. This EMI not only attempts to disrupt the regular operation of electronic equipment but can also have a negative impact on human health, such as nervousness, insomnia, languidness, and headache, as reported in the recent literature [5,6]. To prevent this issue, the signal interferences generated from electrical instruments and communication gadgets must be suppressed or bypassed [7], which necessitates the invention of EMI shielding materials.

1.2 Importance of EMI shielding

EMI shielding is described as the reflection and/or absorption of electromagnetic (EM) waves by a specific material that serves as a barrier against interfering EM waves [8]. Hence, the shielding materials prevent the interference of EM waves with the operation and longevity of electrical instruments. Each year, the need for EMI shielding materials in industries such as aircraft, electrical and communication, and the military has increased [9]. EMI shielding materials have been practically employed as anti-radiation devices and stealth surface coatings on airplanes,

battleships, and automobiles, to safeguard electronic devices and human health from EMI [10]. Signal interference can be observed not only in industrial equipment or electronic communication systems but also in our everyday life. A few examples of EMI that hinder everyday life could be cited as visual flickering or distortion of noise in television sets, jamming and distortions of signals in mobile phones, and signal interference among wireless microphones with mobile or electronic gadgets signals in the vicinity [11]. Such signal interferences can be reduced or mitigated by employing suitable EMI shielding material.

Modern electrical gadgets make use of several frequency bands for various applications. The S-band (2–4 GHz) is widely employed for a variety of uses, including wireless networking, radio, and television. Next, the C-band (4 –8.2 GHz) is often used for long-distance radio, telecommunications, and wifi devices. Further, the X-band (8.2 –12.4 GHz) is used for applications such as air traffic control, weather monitoring, satellite communication, defense tracking, vehicle speed detection for law enforcement, radar, and wireless computer networks. The large utilization of the X-band frequency can be developed signal interference between electronic gadgets. As a result, it is crucial to create EMI shielding materials operating in the X-band frequency region, where most signal interference occurs.

1.3 EMI Shielding Effectiveness

EMI shielding effectiveness (SE_T) is a standard metric to measure the performance of any shielding materials [12]. It may be defined as

$$SE_T = 20\log_{10} \frac{H_I}{H_T} = 20\log_{10} \frac{E_I}{E_T} = 10\log_{10} \frac{P_I}{P_T} \ldots\ldots (1.1)$$

Where H_I and H_T are magnetic fields, E_I and E_T are electric fields, and P_I and P_T are the power of the incident and transmitted EM waves. Based on electromagnetic theory, EMI shielding results from absorption, reflection, and multiple internal reflection losses. According to EMI shielding

principles, the SE_T of shielding material is the sum of the shielding effectiveness by reflection (SE_R), multiple reflections (SE_M), and absorption (SE_A) of EM waves. It can be defined as

$$SE_T \text{ (dB)} = SE_R + SE_M + SE_A \qquad \ldots\ldots\ldots (1.2)$$

The SE_M value may be zero, negative, or positive, which is negligible when $SE_A \geq 10$dB [12].

1.4 Mechanism of EMI shielding

The EMI shielding was realized by three mechanisms, i.e., reflection (R), absorption (A), and multiple internal reflections (M) of the EM waves [8]. When an EM wave impinges on the shielding material, the EM wave energy is attenuated by reflection and absorption. The remaining EM wave energy travels across the material through multiple internal reflections (M) and is transmitted out of the EMI shielding material, as shown in Figure 1.1 [13–17].
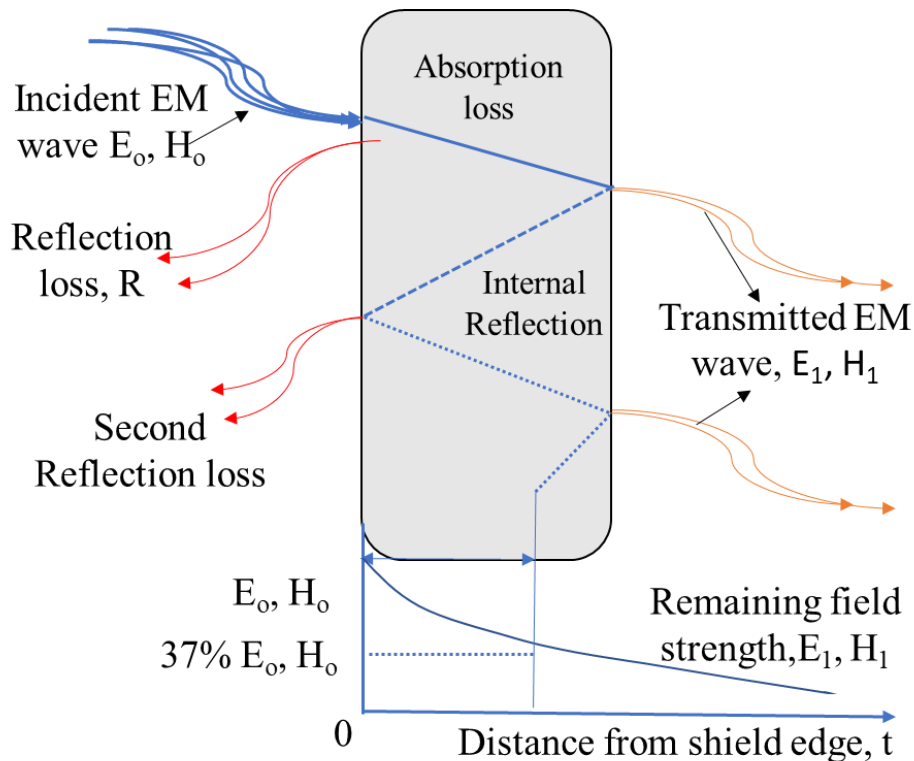
Fig.1.1. Interaction of electromagnetic waves with shield material [12]

1.4.1 Absorption loss

The EM wave absorption and/or reflection capability influences the overall performance of an EMI shielding material. The absorption of EM waves in a material mainly depends on the material's ability to cause dielectric, magnetic, or conductive losses when the wave traverses through them. [18–23]. The dielectric losses arose due to the polarization effects, where the periodic rotation of dipoles inside the material cannot keep up with the frequency of the EM field [5,24–27]. On the other hand, the conduction losses arose in materials that contain a large number of free electronic carriers that could induce a conduction current in the presence of an EM wave to attenuate the EM energy and generate heat [12,28]. In contrast to electrical losses (i.e., conductive and dielectric losses), the magnetic loss mechanism was observed in magnetic materials due to the occurrence of various phenomena that include hysteresis loss, eddy current, domain-wall resonance, natural resonance, etc. [29].

The absorption loss is defined as the amplitude of EM waves exponentially decaying as the EM waves pass through the material. The field intensity entering the shielding material is $E(H)_i$, and the field intensity of the EM wave after it travels a distance d is $E(H)_t$

$$E(H)_i = E(H)_t\, e^{\frac{-d}{\delta}} \qquad \ldots\ldots\ldots\ldots\ldots\ldots\ldots\ldots (1.3)$$

The absorption loss is given as follows:

$$A = 20\log\left(\frac{E(H)_i}{E(H)_t}\right) = 20\log e^{\frac{-d}{\delta}} \qquad \ldots\ldots\ldots\ldots\ldots\ldots\ldots\ldots\ldots(1.4)$$

$$A = 8.69\left(\frac{d}{\delta}\right)\, dB \qquad \ldots\ldots\ldots\ldots\ldots\ldots\ldots\ldots (1.5)$$

Skin depth (δ) is defined as the distance taken by the field of the amplitude of EM waves to be attenuated to 37% of its initial value and given as:

$$\delta = \sqrt{\frac{2}{\sigma \mu_r \omega}} \qquad \ldots\ldots\ldots\ldots\ldots\ldots\ldots\ldots\ldots (1.6)$$

On substituting the skin depth values in the above equation (5) reduces to

$$A=3.34d\sqrt{f\mu_r\sigma} \text{ dB} \quad \ldots\ldots\ldots\ldots\ldots\ldots\ldots\ldots (1.7)$$

where d is the thickness of the shielding material, σ is the conductivity, and μ_r is the relative permeability with respect to the copper.

1.4.2 Reflection loss

In addition to the absorption loss, the reflection and multiple internal reflection losses are also responsible for the performance of EMI shielding material. The reflection losses occur because of the impedance mismatch between the surface of the shielding material and free space [3]. This mismatch of impedance causes the wave to get deflected from the material's surface rather than entering its bulk. The impedance (Z_o) is described as the ratio of the electric field strength (E) to the magnetic field strength (H) and given as:

$$Z_o=\frac{E}{H} \quad \ldots\ldots\ldots\ldots\ldots\ldots\ldots (1.8)$$

Whereas the impedance of the material (Z_w) is defined as:

$$Z_w=\sqrt{\frac{j\omega\mu}{\sigma+j\omega\varepsilon}} \quad \ldots\ldots\ldots\ldots\ldots\ldots\ldots\ldots (1.9)$$

In case of insulating materials, the electrical conductivity (σ) $\ll$ j$\varepsilon\omega$ and above equation converts to:

$$Z_w=\sqrt{\frac{\mu}{\epsilon}} \quad \ldots\ldots\ldots\ldots\ldots\ldots\ldots\ldots (1.10)$$

In the case of conducting materials, $\sigma \gg$ j$\varepsilon\omega$ the equation (9) is reducing to:

$$Zm=\sqrt{\frac{j\omega\mu}{\sigma}}=\sqrt{\frac{j\omega\mu}{2\sigma}}(1+j)$$

$$|Z_m|=\left|\sqrt{\frac{j\omega\mu}{2\sigma}}\right| \quad \ldots\ldots\ldots\ldots\ldots\ldots\ldots (1.11)$$

The impedance of conducting material (Z_m) is given as:

$$|Z_m|=3.368\times10^{-7}\sqrt{\frac{f\mu_r}{\sigma}} \quad\quad\quad \dots\dots\dots\dots\dots\dots\dots\dots\dots (1.12)$$

where σ is the conductivity, and μ_r is the relative permeability with respect to the copper.

The reflection coefficient (Γ) given as:

$$\Gamma=\frac{Z_m-Z_o}{Z_m+Z_o} \quad\quad\quad\quad \dots\dots\dots\dots\dots\dots\dots\dots (1.13)$$

The transmission coefficient (T) is given as follows:

$$T =1-\Gamma = 1-\frac{Z_m-Z_o}{Z_m+Z_o} = \frac{2Z_o}{Z_m+Z_o} \quad\quad \dots\dots\dots\dots\dots\dots\dots\dots (1.14)$$

The EM wave is incident with the electric field intensity of E_i on the EMI shielding material, as shown in Fig.1.1. The EM waves get reflected with the electric field intensity of E_r. The rest of the EM wave energy is passed through the EMI shielding material with an electric field intensity of E_t.

Then, E_t in the free space is given as:

$$E_t= TE_i=\frac{2Z_o}{Z_m+Z_o}E_i \quad\quad\quad \dots\dots\dots\dots\dots\dots\dots\dots (1.15)$$

The transmission coefficient (T_m) in the shielding material is given as follows:

$$T_m=\frac{2Z_m}{Z_m+Z_o} \quad\quad\quad\quad \dots\dots\dots\dots\dots\dots\dots\dots (1.16)$$

The electrical field intensity in the shielding material (E_m) is given as follows:

$$E_m= TE_i=\frac{2Z_o}{Z_m+Z_o}E_i \quad\quad\quad\quad \dots\dots\dots\dots\dots\dots\dots\dots (1.17)$$

The transmitted electric field intensity (E_t) from the shielding material is given as follows:

$$E_t= T_mE_s=\frac{2Z_m}{Z_m+Z_o}E_s$$

$$E_t=\frac{2Z_m}{Z_m+Z_o}\frac{2Z_o}{Z_m+Z_o}E_i$$

$$E_t=\frac{4Z_oZ_m}{(Z_m+Z_o)^2} E_i \quad\quad\quad\quad \dots\dots\dots\dots\dots\dots\dots\dots (1.18)$$

For a plane wave, the impedance of air is Z_o=377 Ω. In conductive materials, the impedance of material $(Z_m) \ll (Z_o)$, therefore:

$$E_t = \frac{4Z_m}{Z_o} E_i \qquad \text{……………………} (1.19)$$

Thus, the reflection (R) is defined as:

$$R = 20 \log_{10}\left(\frac{E_i}{E_t}\right) = 20\log_{10}\left(\frac{377}{4Z_m}\right) \qquad \text{…………………} (1.20)$$

After substituting the Z_m value in the above equation, the equation is reduced to

$$R = 168 + \log_{10}\left(\frac{\sigma}{\mu_r f}\right) \quad dB \qquad \text{……………………} (1.21)$$

1.4.3 Multiple internal reflection loss

The contribution of multiple reflection losses to overall shielding efficiency was dominant at the kHz frequency range and only significant if the shielding material was thin. The SE_M is negligible at higher frequencies for thick conductive shielding materials (skin depth $< t_n$) [12].

In the case of highly conductive materials such as metals, the EM waves get reflected from the surface of EMI shielding materials. Therefore, multiple reflections can be neglected. For other materials, the multiple internal reflection losses are given as

$$M = 20\log_{10}\left(1 - e^{\frac{-2t}{\delta}}\right) dB \qquad \text{…………………} (1.22)$$

1.5 Factors influencing the performance of EMI shielding material

Based on the above EMI shielding principles, it is reasonable to deduce that the performance of EMI shielding materials depends on several material properties, such as permittivity, permeability, electrical conductivity, thickness, size, distribution, and morphology of filler.

1.5.1 Permittivity

Permittivity is a material property that considers a critical factor for developing EMI shielding performance. When the EM waves incident on the material, the electric dipoles present in the

materials were polarized and aligned with an applied electric field. The degree of electric polarization of the material is expressed in terms of dielectric permittivity. The permittivity is in a complex form and has a real part and an imaginary part. It can be written as the following equation:

$$\varepsilon = \varepsilon' - i\varepsilon'' \qquad\qquad \ldots\ldots\ldots\ldots\ldots\ldots\ldots\ldots\ldots (1.23)$$

The real part of permittivity (ε') is called the dielectric constant, which corresponds to the ability of the material to store charge. Imaginary permittivity (ε''), referred to as dielectric loss, corresponds to energy dissipation in the material. The dielectric polarization mechanism in the materials mainly relies on the frequency, size, and shape of the material [30]. In the materials, the contribution of dielectric permittivity was majorly dependent on interfacial, electronic, dipolar, and atomic polarization mechanisms. It should be noted here that ionic and electronic polarization mechanisms only act at extremely higher frequencies (over 10^3 GHz). Therefore, these effects may be ignored in the X-band. Furthermore, dipole polarization occurred owing to the existence of imperfections and residual groups present in the material, and this mostly depends on the production procedures, materials used, the sintering process, and so on [31,32]. The interfacial polarization and other relaxations occur in the composite due to entrapped space charges at the interface.

The dielectric losses of material corresponding to the dissipation of energy in the material while an electric field is applied. The dielectric losses were a combination of conduction loss and polarization loss [33–35]. The conduction losses arose as a result of the conduction mechanism in the material, as the EM waves were dissipated by the mobility of charge carriers in the material. In addition to this loss, the energy of the EM wave also dissipated while nomadic charges interacted with other particles present in the material. It is reasonable to mention that all polarization mechanisms could contribute to dielectric loss at a lower frequency (i.e., MHz

frequency range), while only a few polarization mechanisms could contribute to dielectric loss at higher frequencies (i.e., GHz frequency range), so there is a decrease in the dielectric loss at higher frequencies.

The dielectric permittivity of insulating polymers is very low compared to ferroelectric ceramic materials. Ceramic materials with a high dielectric constant were generally added to the polymeric materials to increase their dielectric constant. Polymer composites containing ferroelectric ceramic materials could increase not only the dielectric constant of pure polymers but also improve dielectric losses, which are essential for the absorption of propagating EM waves in the material. Yousefi et al. studied dielectric properties and EMI shielding performance of epoxy composite containing reduced graphene oxide (RGO). They reported that the epoxy composite containing 3 wt% of RGO had demonstrated a very high dielectric constant of 14000 at 1 kHz. The same composite also presented a superior SE_T value of 38 dB in the 0.54-4 GHz frequency range [36]. Chiang et al. studied the addition of ferroelectric materials to polymers could improve the dielectric constant of the composite. Cherqaoui et al. reported the dielectric properties of polyvinylidene fluoride (PVDF) polymer matrix with the addition of ferroelectric material. They reported that PVDF has a dielectric constant of 12 at 1kHZ frequency at room temperature. The dielectric constant of the polymer can be increased to 82 with the addition of high loadings of $BaTiO_3$ [37].

1.5.2 Permeability

Permeability is considered to be an important property in the development of an effective EMI shielding material. The magnetic permeability of the material is in a complex form and has a real part and an imaginary part. It can be written as the following equation:

$$\mu = \mu' - i\,\mu'' \qquad \ldots\ldots\ldots\ldots\ldots\ldots\ldots\ldots\ldots (1.24)$$

The real permeability (μ') of the materials relates to the storage of magnetic energy, and the imaginary permeability (μ'') of the materials relates to magnetic loss. In the EMI shielding materials, magnetic permeability can be induced with the addition of magnetic materials. Some magnetic materials such as Fe, FeNi, and FeCo exhibit good magnetic saturation (M_s) values and good permeability at the MHz frequency range [38,39]. However, bulk ferrites possess significantly lower M_s values, so cut-off frequency (fr) occurs at the GHz frequency range [40]. These circumstances limited the maximum use of bulk magnetic materials at higher GHz frequency bands. This phenomenon was explained by Snoek's limit. According to Snoek's limit, the magnetic permeability (μ) of magnetic materials is drastically decreased at the f_r, which is expressed by the equation:

$$f_r(\mu-1)\alpha M_s \qquad \ldots\ldots\ldots\ldots\ldots\ldots (1.25)$$

In other words, higher M_s in magnetic materials exhibit a smaller anisotropy field that improves the absorption bandwidth [40]. To address the aforementioned issue, researchers have concentrated on nanosized or micro-sized materials since their anisotropic morphology reduces eddy current loss [41].

Polymers are generally non-magnetic in nature. The addition of magnetic materials to the polymer composites, such as ferrites and hexaferrite, has increased their magnetic properties. The magnetic filler in the polymer composites can create magnetic dipoles in the materials that can absorb the energy of EM waves. So, once again, increasing the magnetic loss in the material can improve the absorption of EM waves. Furthermore, the magnetic loss is generated in magnetic materials due to domain-wall resonance, eddy current, natural resonance, hysteresis loss, etc. The conservation of magnetic loss must be required to produce efficient microwave absorbers and EMI shielding materials.

1.5.3 Electrical conductivity

According to EM theory, the impedance match between both the shielding surface and the incident EM wave is necessary to reduce reflection losses [42]. To facilitate maximum interaction of EM waves, the shield material would possess satisfactory electrical conductivity. Therefore, the electrical conductivity of EMI shielding materials is considered one of the important factors in the preparation of EMI shielding materials. The metals are good electrical conductors. Due to their large conductivity, metal-based EMI shielding materials can increase the reflections of EM waves. However, the strong secondary reflections in the metal-based EMI shielding materials also enhance the reflection power in the materials.

On the other hand, polymers are insulative in nature. The incorporation of conductive particles such as carbon-based and metal-based nanofillers can enhance the electrical conductivity of composites. These nanofillers can create mobile charge carriers in the polymer composite, which facilitates the attenuation of EM waves. As the filler loading increases in the composite, the amount of motion of charge carriers increases, resulting increase in the electrical conductivity. This enhancement may improve the reflection-dominated shielding mechanism in the materials.

Based on the EMI shielding mechanism, as discussed in section 1.4, the electrical conductivity (σ) influences both dielectric loss (ε'') as well as reflections of EM waves. It is challenging to build EMI shielding materials by simply increasing electrical conductivity. It is hard to obtain the balance between ε'' and reflection. Therefore, a reasonable electrical conductivity facilitates the impedance match, thereby, the balance between ε'' and reflections of EM waves.

1.5.4 Size, distribution, and morphology

The nanoparticle's properties play a key factor in the preparation of EMI shielding materials and influence the performance of shielding materials. The addition of nano or micro fillers in the

polymer composites improves their electrical, thermal, and mechanical properties. It is reasonable to mention that nanosized fillers possess a larger surface area and better intrinsic properties when compared to micro and macro fillers. For example, two dimensional (D) nanofillers such as graphene, graphene oxide, and graphene nanoplatelet, two dimensions are greater than 100nm, and the other dimension is less than 100 nm. 1D nanofillers, such as nanotubes, nanofibers, nanowires, nanorods, and 0D nanofiller, such as nanoparticles. First, the 1D and 2D anisotropic conductive nanofillers provide suitable electrical conductivity at lower filler loadings in the polymer composites. The polymer composites containing fillers with large aspect ratios and the surface area form multiple interfaces in the polymer composite resulting in the accumulation of bound charges at the interface, causing interfacial polarization. As a result, multi-interfaces in polymer composites may be inferred to be significantly favorable for the attenuation of EM waves due to electric loss. In the porous composites, the porosity created in the polymer composites improves the multiple reflections of EM waves, thereby increasing EMI shielding performance. This suggested that the morphology of nanoparticles has a good impact on the microwave absorption and shielding performance of EMI shielding materials. Apart from morphology, other parameters, such as the filler's dispersion and particle size, will affect the EMI shielding material's properties. Furthermore, Koops et al. studied that the filler's particle size influenced the shielding performance of a polymer composite and noticed that the shielding properties increased as the filler size decreased [43]. On the other hand, there is a strong influence on magnetic permeability with the dimensions of magnetic particles. The researchers discovered that when the particle size falls under a critical size, eddy current losses in magnetic particles begin to reduce as a reduction in generated eddy voltage.

1.5.5 Thickness of the material

The thickness is also an important design parameter for preparing EMI shielding materials. The EMI shielding performance increases as the thickness of the shielding material increases. Chen et al. reported the influence of the thickness on the EMI characteristics of polydimethylsiloxane (PDMS) composite. The single-layer PDMS composite containing graphene exhibited a SE_T value of 24 dB, whereas the three-layer composite demonstrated a SE_T value of 33 dB [44]. In another study, the polyurethane (PU) composite containing carbon nanotube (CNT) exhibited a SE_T value from 12 dB to 35 dB with a varying thickness from 0.91 mm to 2 mm [45]. In addition to usual nanocomposites, special stack structures were also explored. For example, Pande et al. developed a stack of 7 layered structures of MWNT- polymethylmethacrylate (PMMA) with 0.3mm thick and a two-layered structure with 1.1mm thick and evaluated that a stack of 7 layered exhibited a SE_T value of 40 dB whereas two-layered stack exhibited a SE_T value of 30 dB [46]. It is reasonable to deduce that increasing the thickness of the material has improved the EMI shielding performance.

1.6 Materials for EMI shielding

1.6.1 Metals

To reduce signal interference, the EMI shielding material must possess good electrical conductivity, magnetic loss, and dielectric loss. Metals such as aluminum, copper, and steel have been extensively applied as EMI Shielding applications for more than a decade due to their superior electrical properties and mechanical strength. The excellent electrical conductivity in metals results in the reflection of EM waves [47]. This suggested that the metals exhibited a reflection-dominated shielding mechanism, which may not always be a preferable choice. Furthermore, certain properties of metals, including relatively large densities, complex molding

process, expensive material cost, inadequate physical flexibility, high cost of fabrication, and prone to oxidation, limit their widespread use in EMI shielding applications [48].

1.6.2 Polymer composites

Polymer nanocomposites (PNC) represent a class of materials that possess a unique combination of electrical, thermal, dielectric, magnetic and/or mechanical properties. Compositionally, PNC comprises a continuous polymer matrix in which a nanosized filler is dispersed. Depending on the type of polymer and filler used, the properties of PNC can be tailored for the suppression of EM waves. Owing to such attractive qualities, PNC has been proposed as an attractive substitute for metals as EMI shielding materials.

The polymer composites should possess certain advantages, including ease of manufacturing, flexibility, lightweight, and non-corrosive as well as this is effective in providing the EMI shielding performance [49]. Polymer composites may be developed depending on the requirements by selecting the shape, size, amount of fillers, and type incorporated in various polymer matrices. Hence, the polymer composites are prepared with either ferromagnetic materials, dielectric materials, conductive materials, or a combination of these materials for EMI shielding application.

1.6.2.1 Ferrite-based polymer composites

The EMI shielding materials often contain magnetic materials that have good permeability, such as metal oxide and magnetic alloys that exhibit magnetic loss-dominated shielding mechanisms [50–53]. Several researchers studied the EMI shielding characteristics of magnetic materials for EMI shielding and microwave absorption application. Iqbal et al. reported the EMI shielding characteristics of barium ferrites pellets sintered at two different temperatures of 700 $^{\circ}$C and 850 $^{\circ}$C. The barium ferrites sintered at 700 $^{\circ}$C exhibited a SE_T value of 11 dB, and sintered at 850 $^{\circ}$C demonstrated a SE_T value of 7 dB in the X-band [50]. Madhuri et al. reported the EMI shielding

characteristics of NiMg ferrites. The $Ni_{0.4}Mg_{0.6}Fe_2O_4$ pellets have demonstrated a SE_T value of 17

dB in the X-band [54]. Several researchers utilized ferrite-based composites in preparing the EMI

shielding materials. Guo et al. reported EMI shielding properties of the paraffin wax containing

$Ba_3Co_2Fe_{24}O_{41}$ hexaferrite composites. These composites demonstrated a reflection loss of 30 dB

at 9.7 GHz frequency [55]. Gordani et al. reported the epoxy composite containing

$SrZn_{1.6}Co_{0.2}Ni_{0.2}Fe_{16}O_{27}$ ferrites demonstrated a reflection loss of 29.1 dB at 14.57 GHz [56]. Chen

et al. studied the polystyrene composite containing Fe_3O_4 composite and demonstrated a SE_T value

of 2.5 dB in the X-band [57]. Krithika et al. reported the epoxy composite containing Fe_3O_4

exhibited a SE_T value of 2 dB in the X-band frequency range [3].

1.6.2.2 Conductive polymer composites

Over the last decade, conductive polymers and intrinsically conductive composites have been

widely employed in the application of EMI shielding. Several researchers prepared EMI shielding

materials utilizing different materials, including metal-based and carbon-based particles. The

conductive fillers such as multi-walled carbon nanotube (MWNT), carbon fibers (CF), single-

walled carbon nanotube (SWNT), graphite flakes, carbon black, graphene, and Cu, Ni, and Al in

the form of nanoparticles, nanocubes, nanorods, and nanowires are extensively utilized as fillers

in the polymer matrix to prepare the EMI shielding material [58–64]. Kim et al. explained that the

EMI shielding effectiveness of nylon-6 composite containing poly(pyrrole) depends on properties

such as the aspect ratio of filler, dielectric constant, and electrical conductivity [65]. Mishra et al.

reported the influence of filler size and shape on the EMI shielding performance of PNC [66]. The

15 wt% CF or 30 wt% CB particles filled composite exhibited inferior shielding performance than

the composite containing the 10 wt% CNT. The EMI shielding performance in polymer

composites containing SWNT was explained by Li et al. The composites filled with SWNT were

lightweight and had a SE_T value 20 dB in an X-band [67]. These composites exhibited a SE_T value of 49 dB at 10 MHz and 15-20 dB at the 1.5 GHz range. Huang et al. fabricated epoxy composites with 0.01–15 wt% SWNT loadings and evaluated the EMI shielding effectiveness in the X-band [68]. The researcher reported that the SE_T value of PNC is affected by SWNT structure and aspect ratio. The SWNT-filled epoxy composites exhibited a percolation threshold limit of 0.062 vol% and SE_T value of 20-30 dB in the X-band. Liang et al. developed a lightweight epoxy polymer composite with functionalized graphene [69]. These composites exhibited a percolation threshold limit of 0.52 vol% and a SE_T value of 21 dB in an X-band. Al-Saleh et al. prepared an acrylonitrile-butadiene-styrene (ABS) polymer composite with MWNT, high-structure carbon black (HS-CB), and carbon nanofibers (CNF) [70]. ABS polymer composite containing 10 wt% filler loading of CNF, HS-CB, and MWNT exhibited the SE_T value of 15.3 dB, 26.1 dB, and 40.7 dB, respectively. Ameli et al. reported that 10 vol.% CF-filled solid polypropylene composite exhibited a SE_T value of 24.9 dB [71]. Liu et al. developed lightweight SWNT-filled polyurethane composites, which exhibited a SE_T value of 14 dB in the X-band [72]. Joseph et al. prepared polyvinylidene fluoride (PVDF) /carbonyl iron powder (CIP) composite [57]. The SE_T value was 20 dB at 50 vol% of CIP in PVDF in the 8-12.4 GHz. This research on conductive polymer composites is helpful in understanding the influence of electrical conductivity on EMI shielding effectiveness. However, developing a high electrical conductivity or permittivity will result on the contrary because the large difference in electrical conductivity among shielding materials and free space contributes to an impedance mismatch which will induce the majority of the EM waves can be reflected prior to actually impinging into the shielding materials. As a consequence, the researchers have focused on developing hybrid shielding materials to achieve high absorption capacity, wide absorbing bandwidth, and lightweight requirements.

1.6.2.3   Hybrid polymer composites containing ferrites

According to recent research, hybrid polymer composites comprising magnetic particles as well as conductive particles can be used for the application of EMI shielding materials. The improvement of shielding performance with the incorporation of magnetic particles was studied by Saini et al. [73]. The Fe_3O_4-coated polyaniline (PANI) composite was prepared and exhibited a SE_T value of 19 dB. Subsequently, Che et al. demonstrated that CNT/Fe hybrid epoxy composite exhibits good EMI shielding performance at low filler loading, and a better SE_T value of 25 dB were ascribed to a large aspect ratio of the CNT filler used [74]. This suggests that EMI shielding effectiveness will be improved by adding magnetic filler (i.e., Fe) and conductive filler (i.e., CNT) in an epoxy matrix. In another study, Chen et al. demonstrated that polystyrene (PS) composites filled with thermally exfoliated reduced graphene oxide (TGO) and Fe_3O_4 exhibited better EMI shielding performance than PS composites containing reduced graphene oxide (RGO) and Fe_3O_4 in X-band range [75]. The SE_T value of PS filled with Fe_3O_4 @TGO was 25 dB at 2.27 vol% graphene content. Subsequently, Wu et al. fabricated RGO-carbon fiber / Fe_3O_4 deposited rGO nanohybrids/epoxy composites, and a SE_T value of 30 dB was exhibited [76]. Additionally, Liu et al. added graphene to chitosan and iron pentacarbonyl porous films and improved the SE_T value to 38 dB in the 8.2-59.6 GHz frequency range [77]. It is reasonable to deduce that conductive fillers in association with magnetic fillers yield better EMI shielding effectiveness.

1.6.2.4   Hybrid structured polymer composites containing dielectrics

Similar to magnetic materials, the dielectric materials, including $BaTiO_3$, ZnO, MnO_2, TiO_2, SiC, and SiO_2, demonstrated a dielectric-loss-dominated shielding mechanism in the EMI shielding materials [78–81]. The presence of a dielectric loss in EMI shielding materials improves the performance of EMI shielding and microwave absorption properties. Cao et al. reported the

microwave absorption and EMI shielding properties of short carbon fiber (CF) and silica composites. These composites demonstrated a SE_T value of 11.7 dB with microwave absorption of 35% of incident EM power [82]. Hao et al. reported the dielectric, microwave absorption, and EMI Shielding properties of the phenolic composite containing silicon nitride (Si_3N_4), nickel (Ni), and pyrolytic carbon (PyC). These composites containing 4.1 vol% of PyC and 5 wt% of Si_3N_4, and 1 wt% Ni exhibited 15.1 dB in the X-band [83]. Jia et al. studied the EMI shielding and microwave absorption properties of aminopropyltrimethoxysilane (APS) composite containing carbonyl iron, TiO_2, and SiO_2. The composite containing TiO_2 exhibited the SE_T value of 34 dB with 36% of absorption of incident EM power. Furthermore, the composite containing SiO_2 exhibited the SE_T value of 29 dB with 43.3% of absorption of incident EM power [84]. All these studies postulated that the addition of dielectric material along with conductive material could improve the dielectric loss of composite; thereby, the performance of EMI shielding and microwave absorption can be increased.

1.6.2.5 Hybrid structured polymer composites

Over the last two decades, continued attempts have been made to minimize EMI utilizing a variety of methods and materials, including metals, magnetic materials, conducting polymers, carbon-based materials, and dielectric materials, as mentioned above. One of the strategies is to develop hybrid nanostructures with a combination of dielectric and/or magnetic materials. These nanostructures achieve outstanding absorbing characteristics of EM waves that surpass the same synthetic nanomaterials. The EMI shielding materials containing these special nanostructures can reduce the reflection of the radar cross-section and develop the impedance match, thereby reducing the reflection of EM waves [10]. Moreover, the hybrid nanostructures developed with conductive and magnetic/dielectric particles are primarily attributed to their unique synthetic structures. These

structural systems exhibit good electric and magnetic characteristics (i.e., good permittivity and permeability) [3]. The successive structure aids in obtaining outstanding absorbing characteristics of the EM waves that are significantly superior to what the substances can attain. In fact, hybrid structures can exhibit good microwave absorption properties. Currently, the hybrid structures can be reduced the EM waves reflection by reducing the impedance mismatch, thereby improving the shielding performance by magnetic and electric losses in the hybrid structures [85–90]. Especially, the studies on hybrid structures applied in EMI shielding materials have gained extensive interest. The recent studies performed on the microwave absorption characteristics of hybrid polymer composites containing various nanomaterial systems were listed in the literature review.

1.7 Gaps Identified Based on Literature Review

Based on the literature review, It can be observed that the metals such as Cu, Al, stainless steel, etc., have been employed as EMI shielding materials over the decade. These bulk metal applications as EMI shielding materials are limited due to material properties such as large densities, prone to oxidation, and exhibiting reflection-dominated shielding mechanism [47]. Addressing these issues, polymer composites have been used as an alternative to metals. Furthermore, polymer composites comprising carbon-based materials such as graphene, GNP, RGO, CB, and CNT have been widely employed as EMI shielding materials. However, large-scale production, high cost, and easy aggregation of carbon fillers limited their applications as an EMI shielding material [91]. On the other hand, copper nanowires (CuNW) are one-dimensional nanomaterials that are low in cost compared to carbon-based materials, have a large aspect ratio, and have better electrical and thermal conductivities. Owing to such attractive properties, the preparation of CuNW-filled nanocomposites has been proposed as a promising method for producing EMI shielding materials. In spite of this merit, there has been very limited research reported on the preparation of EMI shielding materials using CuNW [92–94]. Moreover, these

studies mostly employ thermoplastic polymers as a matrix to produce EMI shields. In comparison to thermoplastic polymers, thermosets are more rigid, have greater working temperatures, and can be manufactured at a lower cost [95]. Employing a thermosetting polymer as a matrix for EMI shielding material could significantly enhance their usage in applications that require high strength and temperature. Epoxy resin is a versatile commercial thermosetting polymer that has been used in several industries due to its exceptional properties, such as insulating behavior, lightweight, corrosion resistance, low cost, and flexibility, and it is also compatible with an extensive range of nanofillers. However, the literature on the EMI shielding performance of CuNW dispersed in thermosetting polymers does not exist.

One of the drawbacks associated with the use of conductive polymer composites for EMI shielding is that high filler loadings are often required to achieve significant improvement in the shielding effectiveness. Such high filler content increases the EM wave reflectivity of the shielding material due to the impedance mismatch [3]. Although the EMI shielding effectiveness values of such shields are good, a large portion of wave energy is deflected into the surroundings, which can create interference issues elsewhere. To counteract the reflection issue, conducting polymer composites are often filled with additional magnetic and/or dielectric fillers that could enhance the absorption of the EM wave. For example, it has already been demonstrated that the addition of magnetic fillers, along with conductive fillers in polymer composites-based EMI shielding materials increases the absorption of the EM waves [3,90,96,97]. However, the effects of magnetic nanoparticles on microwave absorption in CuNW-based composites are not explored, given the limited availability of literature on copper nanowires.

It can further be observed from past studies that not only conduction and magnetic losses but dielectric losses also play a vital role in enhancing the EMI shielding and microwave absorption

characteristics in polymer composites. However, compared to magnetic fillers, relatively fewer efforts have been made to understand the influence of dielectric fillers on the EMI shielding characteristics of conducting polymer composites (CPC). Although limited, the studies clearly suggested that a mixture of conductive and dielectric nanoparticle-filled polymer composites exhibited superior EMI shielding and microwave absorption performance [98,99]. This aspect remains unexplored for the CuNW-filled conductive polymer composites, and efforts in this direction were needed to further enhance the fundamental understanding of microwave absorption in polymer composites.

The direct incorporation of conductive particles along with magnetic particles in the polymer matrix could lead to phase segregation, which could deteriorate the microwave absorption in shielding materials [100]. Therefore, the use of hybrid nanostructures (i.e., mangetic@conductive, dielectric @conductive, or dielectric@magnetic@conductive) has been proposed to achieve superior dispersion and microwave absorption in polymer composites. It is believed that such hybrid nanoparticles impart larger interfacial polarization by limiting the phase segregation of the fillers. Accordingly, few studies have investigated the microwave absorption properties of hybrid magnetic@conductive and dielectric@conductive nanoparticles [3],[97–109]. Furthermore, the majority of efforts put towards the development of hybrid structures employ mostly carbon-based conductive materials or conducting polymers as the conductive particles over which different types of magnetic and/or dielectric particles are anchored [3,90,99,114–116]. However, such attempts to study the influence of hybrid nanostructures with CuNW as conductive particles have not been reported. To summarize, a thorough investigation of microwave absorption and EMI shielding behavior of thermoset composites containing either the pristine CuNW or their hybrids have not been explored in the past. This work precisely focused on the above-mentioned gaps in the existing

literature and aimed to further the understanding of EMI shielding characteristics of polymer nanocomposites.

1.8 Motivation

The metals have been traditionally utilized as EMI shielding materials over the decade. However, metals have a high cost, large weight, and anomalous reflections of EM waves, limiting their application [117]. Therefore, to resolve this problem, PNC was developed as a replacement for traditional metals because of their lightweight, low-cost processing, corrosion resistance, and good mechanical properties [14]. Furthermore, PNC offered a decrease in surface reflections as compared to metals, which is desirable in military and stealth technology applications. In the PNC, the conductive fillers, including conductive polymers, carbon materials, metallic powders, and their hybrids, were incorporated into the insulating polymers to create the conductive network. Carbon fillers, such as CNT, GNP, CF, graphene, and others, have become popular due to their low density and strong conductivity [118] and could also be utilized as a filler in the preparation of EMI shielding materials. However, practical applicability is still limited because of expensive costs, high agglomeration, and instability [119]. On the other hand, metal-based nanofillers such as Ni, Cu, Ag, MXene, and others might endow good conductivity in polymer composites with effective EMI shielding materials. It is mainly believed that low concentrations of metallic nanofillers in the form of nanorods, nanotubes, or nanowires in an insulator matrix can yield reasonably excellent electrical conductivity. Furthermore, the low filler loading in the polymer has no significant impact on the density, hence the advantage of polymeric materials' low density is maintained.

Moreover, copper nanoparticles are low-cost, excellent electrical and thermal conductors that may be produced in a variety of structures, such as spherical particles, nanocubes, nanorods, and nanowires [120]. In these particles, copper nanowires (CuNW) were particularly intriguing

because of their special structure with high aspect ratio, low cost, optical, and good electrical conductivity characteristics. Furthermore, CuNW's electrical conductivity was equivalent to that of silver. These attractive properties of CuNW made them suitable fillers in the preparation of EMI shielding material. As aforementioned, an effective EMI shielding material should have satisfactory electrical conductivity to penetrate microwaves through the material. Thus, the preparation of CuNW-based nanocomposites has been mentioned as a potential method for producing EMI shielding materials. Furthermore, no research including CuNW in a regularly used commercial thermosetting polymer, such as an epoxy resin, has been published, which was the motivation for the current work. Despite such merits of CuNW, relatively few studies were conducted to investigate the EMI shielding properties of CuNW-filled polymer composites in the X-band. It might be due to the poor performance of polymer composites containing CuNW when compared to carbon-based composites. As a result of this, there is a need to boost the EMI shielding performance of CuNW-based polymer composites in order to guarantee their widespread use, which is what drives the motivation for current work.

The present state of the art is to employ polymer-based composites that provide a tailorable combination of dielectric and magnetic properties. In order to prepare such hybrid polymer composites, the dielectric or magnetic particles were incorporated along with conductive particles (i.e., CuNW) in the polymer composite. This strategy helps to enhance their microwave absorption capability due to the addition of magnetic loss or dielectric loss along with conduction loss in these hybrid composites. For example, the addition of conductive fillers such as nickel, graphene, and graphene oxide, along with dielectric or magnetic fillers in the polymer matrix, demonstrated an increase in the microwave absorption capability in the composites [74,79,80,111–122]. However, it is important to note that no research on the preparation of EMI shielding materials with magnetic

materials (i.e., Fe_3O_4) or dielectric materials (i.e., BST) along with CuNW has been reported. Driven by this motivation, epoxy composites containing magnetic materials (i.e., Fe_3O_4) along with CuNW were prepared for EMI shielding applications. To validate these results, a hybrid system of GNP-BaM was developed, and similar studies were performed. These hybrid systems also exhibited an increase in EMI shielding effectiveness when GNP was added in combination with BaM magnetic filler. This is clearly evident that a universal improvement was observed in hybrid systems containing conductive fillers modified with magnetic fillers.

It is important to mention that the majority of the research that has been done in the literature demonstrates that it is feasible to achieve excellent EMI shielding performance by combining magnetic filler with conducting filler [3,125–137]. It has been hypothesized that the EMI shielding characteristics are significantly impacted not only by conduction and magnetic loss but also by dielectric loss in polymer composites [3,133]. Despite this potential, very little amount of study has been published on the microwave absorption and EMI shielding characteristics of BST [98,134,135]. Additionally, the EMI shielding performance of polymer composites comprising BST and conductive nanoparticles has not been investigated at large [98,99]. Interestingly, no published study has reported microwave absorption and EMI shielding properties of an epoxy composite incorporating CuNW and BST particles over the X-band frequency range, which drives the motivation for current work. However, the direct incorporation of conductive particles along with dielectric or magnetic particles in the polymer matrix could lead to phase separation, which could deteriorate the microwave absorption capability of shielding materials [100]. This limited the wide-band utilization of hybrid composites as EMI shielding materials.

One such strategy to reduce the phase separation of nanoparticles is to employ a hybrid nanostructure comprising magnetic and/or dielectric nanoparticles deposited to an electrically

conductive nanoparticle (i.e., magnetic@conductive, dielectric@conductive, magnetic@dielectric@conductive). The hybrid nanostructure is one of the structural systems that display favorable dielectric and magnetic characteristics, primarily attributed to their unique synthetic structures. The successive formation of these structures facilitates attractive microwave absorbing capabilities that are significantly superior to what the substances can attain; in fact, certain lossless substances can exhibit large absorption of microwaves. The increase in absorption capability in composites containing hybrid nanostructures may be attributed to the combined effects of multiple interfacial polarization along with the magnetic, dielectric, and conduction losses [3],[136]. A few studies on polymer composites comprising hybrid nanostructures in the preparation of EMI shielding materials have been published [3,101,102,133,136]. However, it is important to note that no research on the preparation of hybrid structures of the magnetic materials (i.e., Fe_3O_4) or dielectric materials (i.e., BST) deposited on the CuNW (i.e., Fe_3O_4@CuNW or BST@CuNW) particulate system has been reported. This drives the motivation for developing hybrid particles and their epoxy composites for EMI shielding applications. Consequently, very few researchers have studied the EMI shielding characteristics of composites that incorporate a combination of dielectric and magnetic materials along with conductive materials [98,99]. It is still essential to do exhaustive research on the impact of microwave absorption of CuNW-epoxy composites when dielectric and magnetic components are present. It is worth mentioning that none of them reported microwave-absorbing characteristics of epoxy-containing Fe_3O_4@BST@CuNW. The outcome of this research was to contribute to a better understanding of the EMI shielding mechanism. The research could be valuable for applications such as radar absorption materials and stealth technologies.

1.9. Research Objectives

The main focus of this research is to study the influence of different nano-sized fillers on the EMI shielding properties of epoxy nanocomposites. The following objectives outline the emphasis of the proposed study.

1. To determine the effect of copper nanowires (CuNW) on the EMI shielding effectiveness of epoxy nanocomposite.

2. To understand the influence of the addition of magnetic Fe_3O_4 nanoparticles to CuNW-filled epoxy nanocomposites on EMI shielding and microwave absorption characteristics.

3. To probe the effect of dielectric barium strontium titanate nanoparticles on the EMI shielding and microwave absorption characteristics of CuNW-filled epoxy nanocomposites.

The outcome of this study could help in gaining a further understanding of the aspects of the EMI shielding mechanism in polymer nanocomposites.

2 Literature Review

2.1 Hybrid polymer composites for EMI shielding application

Over the years, hybrid polymer composites have been employed as EMI shielding materials. It is postulated in some studies that the combination of two or more fillers addition in the polymer composite can result in a synergistic effect between them and improve the performance of hybrid composites [133]. Additionally, combining magnetic and/or dielectric and conductive fillers facilitates good magnetic and dielectric losses in hybrid composites [3]. The significant rise of these losses in the hybrid composites can increase the performance of EMI shielding materials [85,137,138]. Moreover, the concepts like the structural refinement and hybrid structures of nanofillers, such as magnetic@conductive, dielectric@conductive, conductive@magnetic, conductive@dielectric, magnetic@dielectric@conductive demonstrated better properties than synthetic nanomaterials [3,86,96,131,139,140]. Thus, introducing this additional benefit for preparing EMI shielding material helps achieve better microwave absorption capability and EMI shielding performance [3,133,141]. Previously, several researchers published numerous studies on structure-based strategies for the fabrication of EMI shielding materials, as seen in Table 2.1. The increased EMI shielding effectiveness in composites containing structure-based nanoparticles can be attributed to the combined effects of dielectric losses coupled with the magnetic losses arising due to the presence of structure-based nanoparticles [85,137,138].

2.1.1 Conductive hybrid polymer composites for EMI shielding application

The first approach was to create a hierarchical structure containing materials with similar or distinct impedance properties that can attenuate incident EM waves. These structures include combinations of two or more conductive materials in the polymer composite. These hybrid structures were synthesized by physical mixing, synthesis of one filler in the presence of another, or co-synthesis of two or more fillers, which leads to the growth of a decorated structure of one or

more fillers on the surface [34,142]. The increased EMI shielding in composites containing structure-based nanoparticles can be attributed to the effects of dielectric losses arising due to the presence of structure-based nanoparticles. Previously, several researchers published numerous studies on hybrid structures and used them to fabricate the EMI shielding materials, as seen in Table 2.1.

Table 2.1. EMI shielding values of conductive hybrid structures composites

Materials	Filler content	Conductivity (s/m)	SE_T (dB)	Frequency (GHz)	Ref
rGO-CF	0.75 wt%	7.13	37.8	8.2 -12.4	[142]
GNP-MWNT	10 wt%	9.5	47	20-40	[143]
CNT/CF	0.35 wt%	0.8×10^{-3}	42	8.2 -12.4	[34]
MNP@MWNT	4 wt%	1070	30-60	0.5-12.0	[144]
SSF-CNT	3.5vol%	100	47.5	8.2 -12.4	[145]
Polyamide-6/CNT	0.3 wt%	100	25	8.2 -12.4	[146]
PANI/CNT	25 wt%	1907	27.5-39.2	12.4-18	[147]
PCL-MWNCT	0.25vol%	4.8	60-80	0.04- 40	[148]
CuNW-TAGA/epoxy	7.2 wt%	120.8	47	8.2-12.4	[149]
PDMS/rGO/AgNW	0.43, 0.33 wt%,	1210	34.1	8.2-12.4	[150]

2.1.2 Magnetic and conductive materials hybrid structures

The second approach is to employ a hybrid structure with a combination of magnetic material and a conductive filler in the polymer composite for the enhancement of EMI shielding effectiveness. Subsequently, the addition of conductive material along with magnetic materials generates the dual benefit of magnetic loss and dielectric loss and produces additional effects such as high multiple-interface polarization, all of which are useful in increasing shielding effectiveness. These losses help to enhance the microwave absorption capability in the shielding materials. Generally, these losses are generated in the material due to dipole polarization, electronic polarization, natural resonance, magnetic dipoles, magnetic losses, eddy, and hysteresis losses [3,133]. Therefore, many researchers have focused specifically on the complex hybrid structure of nanofillers to fabricate an efficient EMI shielding material, which is listed in Table 2.2.

Table 2.2. EMI shielding values of conductive and magnetic hybrid structures composites

Materials	Synthesis Method	Thick (mm)	Polymer matrix	SE_T (dB)	Freq. (GHz)	Ref
PANI/15 wt% $BaFe_{12}O_{19}$ (BF)	Co-precipitation	2	PANI	19.7	2-18	[151]
PANI/28 wt% $Mn_{0.5}Zn_{0.5}Fe_2O_4$		2	PANI	6-20	0.03-1	[152]
3% Graphene decorated with Nickel NPs	Co-precipitation	1	Polybenzoxazine	>20	8.2 -12.4	[153]
10 wt% CNT/12 wt% Ni@CNT	Magnetic field-supported solvothermal	0.5	PVDF	51.4	12.4-18	[154]

Material	Method		Matrix			Ref
rGO-FeCo- diamine monomer 4,4′-diamino diphenyl methane, MWCNT	*Insitu* reduction using a solvothermal		PVDF	41	12.4-18	[155]
10 wt% Fe$_3$C-carbon	Carbonization of melamine and iron salt		PVDF	35	14-18	[156]
90:10 ratio of Fe$_3$O$_4$ and carbon black (CB)			Natural rubber	14.7 - 23.1	1-12	[157]
0.25vol% of Fe$_3$O$_4$-MWCNT		5	PC/PVDF	38	18	[158]
0.25vol% of Fe$_3$O$_4$-MWCNT		5	PC/PVDF	30-36	8-18	[159]
0.15 vol% NiFe$_2$O$_4$-MWCNT		5	PC/PVDF	19.7	2-18	[159]
0.28 vol% CoFe$_2$O$_4$-MWCNT		5	PC/PVDF	6-20	0.03-1	[159]
Modified Gr nanoplatelets and MWCNT-Fe$_3$O$_4$			PU	27.5	8 -12.4	[88]
Fe$_3$O$_4$-CNT		1.1	PVDF	32.7	18-26	[160]
Fe$_3$O$_4$-GNP		1.1	PVDF	35.6	18-26	[160]
rGO@Fe$_3$O$_4$- MWCNT		5	PC/PS	> 30	8-18	[161]
0.5 wt% rGO deposited with		7	Epoxy	> 30	8.2-26.5	[76]

Material	Thickness	Matrix	SE	Frequency	Ref.
carbon fiber-Fe_3O_4 -9 wt% modified rGO					
rGO-Fe_3O_4		PC	28	8-18	[162]
rGO-Fe_3O_4		PC	33	8-18	[162]
4 wt% CNT-5 wt% rGO-Fe_3O_4		PC	43.5	8 -12.4	[22]
45 wt% $NiFe_2O_4$-5 wt% rGO	2	PP	28.5	5.8-8.2	[163]
$NiCoFe_2O_4$ (NCF)- CB	1.5	PVA	27	8-18	[164]

2.1.3 Magnetic-Dielectric-Conductive hybrid structures

The third approach is to create a hybrid structure in the polymer composite containing a combination of magnetic and dielectric materials along with a conductive filler. In these hybrid structures, decorating magnetic nanoparticles on dielectric materials or vice versa facilitated a protective encapsulation of decorated nanoparticles on the surface of other nanoparticles to prevent agglomeration of the nanoparticles [165–169].

Recent studies have investigated that dielectric materials, including, SnO_2, TiO_2, ZrO_2, ZnO, Al_2O_3, carbon materials, and polymers, are used as a dielectric source to impart dielectric losses and are used alone or in combination with magnetic and conductive materials [170]. For example, S. Biswas et al. synthesized graphene oxide sheets decorated with $BaTiO_3$ and Fe_3O_4 nanoparticles. These nanoparticles are combined with modified MWNT and embedded in the PC/PVDF matrix. The nanocomposite reported SE_T values of 32.5-35 dB over the frequency range of 12-18 GHz. It can be observed that the composites demonstrated an increase in SE_T values due to the synergistic effect of hybrid lossy materials and selective localization of GO in PC and MWNT in PVDF, which retains the electrical conductivity of composites [170]. The authors also fabricated

composites through multilayer assembly, in which outer layers with modified $BaTiO_3$ /Fe_3O_4 co-doped GO/modified MWCNT/PC/PVDF composite and inner layers with modified MWCNT/PVDF in the composite [170]. The authors also reported that the SE_T values of composites fabricated through multilayer assembly further increased to 46 dB over the frequency range of 12-18 GHz.

L. Jin et al. synthesized a hybrid structure made of graphene along with Fe_3O_4 decorated on $BaTiO_3$ (GFBT) in two steps hydrothermal process. The $BaTiO_3$ particles of 20 nm are primarily coated on the Fe_3O_4 nanospheres forming the hybrid structure of Fe_3O_4 and $BaTiO_3$. The hybrid structure contained $BaTiO_3$/Fe_3O_4 nanoparticles of about 200 nm diameter anchored on the surface of graphene and was used along with MWNT in methyl vinyl silicone rubber. The composite containing 16 wt% with the ratio of 1:5 of MWNT: GFBT filler loading exhibited SE_T values of 26.7 dB in the frequency range of 1-20 GHz for a sample thickness of 2.6 mm [171]. P.Sambyal et al. reported an encapsulated polypyrrole composite with the combination of rGO, Fe_3O_4, and barium strontium titanate (BST) nanoparticles. The BST/rGO/Fe_3O_4 (BRF) hybrid was synthesized by co-precipitation. In this process, the precursors rGO and BST nanoparticles were added to the precursor solution of Fe_3O_4, thus forming the hybrid structure of nanoparticles. The hybrid composite showed an EMI SE of around 48 dB for a thickness of 2.5 mm in the X-Band frequency range [99].

2.2 Synthesis of Copper nanowires

Copper nanowires (CuNW) are a unique class of materials in the copper family with high electrical and thermal conductivities. Since their cost advantage over other conductive fillers, their use as a filler improves the properties of the composite. In the literature, several studies reported various processing methods to synthesize the CuNW. For example, a novel method was developed by Li et al. for synthesizing CuNW with cupric chloride dihydrate ($CuCl_2 \cdot 2H_2O$), glucose, oleyl amine

(OM), oleic acid (OA), and ethanol to prepare CuNW in an electric pressure cooker [172]. 2.1 g of CuNW was prepared in a batch with a cost of INR 298/g. Chang et al. developed a process for high-quality ultra-long CuNW with an aspect ratio >350-450 using $Cu(NO_3)_2$, NaOH, ethylenediamine (EDA), and hydrazine, as shown in reaction (1) [173].

$$2Cu^{+2} + N_2H_4 + 4OH^- \longrightarrow 2Cu + N_2 + 4H_2O \quad \dots\dots\dots\dots (1)$$
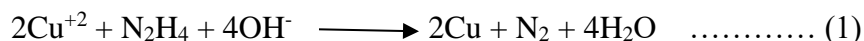
Subsequently, Rathmell et al. scaled up Chang's method from 0.006 to 1.2 g of CuNW by heating reagents for 1 hour at 80 °C [174]. Additionally, Mohl et al. synthesized ultralong CuNW using hexadecyl amine (HDA) instead of ethylenediamine and hydrazine [175]. Subsequently, Ye et al. developed another seed method to synthesize the CuNW. In this method, $Cu(SO_4)_2$ solution was treated with N_2H_4 in the presence of NaOH and EDA [176]. The formed final product was washed and stored under hexane. The CuNW synthesized using a hydrothermal process was studied by Kumar et al. using $CuCl_2.2H_2O$ and glucose [177]. This method produced CuNW with a large aspect ratio when the solution was processed in an autoclave for elevated temperatures and pressure. Yet another work, Liu et al. formed the CuNW by the reduction of a Cu(II)-glycerol complex with NaOH, glycerol aqueous solution [178]. Sodium dodecyl benzenesulfonate (SDBS) was used as a surfactant in this process. The final product contained 85 nm CuNW. Shi et al. formed the CuNWs of 48 nm diameter using copper chloride ($CuCl_2$) and octadecyl amine (ODA) in an aqueous solution maintained at 120-180 °C for 48 h [179]. CuNW formed with 48nm diameter. Mohl et al. used HDA or tetradecyl amine (TDA) instead of ODA and demonstrated that the reaction time could be reduced to 10 h for synthesizing CuNW of diameter 40-60 nm [180]. In the synthesis of CuNW, the role of alkyl amines was studied by Kumar et al. [181]. The studies suggested that the CuNW cannot be synthesized with stabilized penta twinned seeds like cetyl trimethyl ammonium bromide (CTAB) and polyvinylpyrrolidone (PVP). However, alkylamines

like EDA and OM make perfect CuNW by forming a metal-amine complex for seed generation. The reduction of this complex generates twinned seeds, which will grow into CuNW.

2.3 Synthesis of magnetite nanoparticles

Magnetite nanoparticles can be synthesized in a variety of ways that include: co-precipitation, hydrothermal, and sol-gel methods, etc. synthesis of Fe_3O_4 nanoparticles (FNP) by the co-precipitation method was demonstrated by Park et al. using ferrous (II) chloride tetrahydrate and ferric (III) chloride hexahydrate in the presence of ammonia solution [182]. The reagents were stirred for two hours, resulting in a black precipitate of Fe_3O_4. Size-controlled synthesis of magnetite nanoparticles was demonstrated by Sun et al. using ferrous (III) acetyl acetate as a precursor to yield as low as 4 nm Fe_3O_4 particles [183]. A mixture of OA and OM was employed by them. Furthermore, Xu et al. presented a method where size-controlled Fe_3O_4 particles could be synthesized using oleyl amine as a reducing agent and stabilizer [184]. Subsequently, Ge et al. synthesized Fe_3O_4 nanoparticles with an average diameter value of 15-31nm by using a one-step hydrothermal synthesis [185]. In this method, $FeCl_2.4H_2O$ and NH_4OH solution was autoclaved for three hours at 134 °C and produced black color magnetite. Subsequently, Lu et al. synthesized Fe_3O_4 nanoparticles using the sol-gel technique, which had a size ranging from 5-15 nm [186]. EMG 340- Ferrofluid, 2-propanol, and NH_4OH were used as reagents. Additionally, Wu et al. studied the effect of surfactants to stabilize the magnetic nanoparticles by forming a strong bond between the amorphous iron oxide and the carboxylic group of OA [187]. The use of surfactant reduced the formation of agglomerates and yielded 10 nm diameter Fe_3O_4 nanoparticles. Mahdavi et al. explained the effect of pH, temperature, and stirring rate on the particle size of Fe_3O_4 nanoparticles [188]. Jain et al. synthesized Fe_3O_4 nanoparticles of size 14-50 nm using the conventional co-precipitation method with OM and benzyl ether as a stabilizer [189].

Zhou et al. prepared Fe_3O_4 nanoparticles using iron oleate, 1-octadecene (ODE) or tri-n-octylamine (TOA), oleic acid, and sodium oleate [190]. Fe_3O_4 shape and size were controlled with different molar ratios of sodium oleate from 0.1 mmol to 0.6 mmol, respectively. However, Singh et al. synthesized Fe_3O_4 nanoparticles using piperidine and $FeCl_2$ [191]. Additionally, Shen et al. synthesized shape-controlled Fe_3O_4 nanoparticles by co-precipitation method using ferrous sulfate ($FeSO_4.7H_2O$) and ferric sulfate ($Fe_2(SO_4)_3$) in the presence of sodium dodecyl sulfate (SDS) [192]. Subsequently, He et al. synthesized Fe_3O_4 nanoparticles by a hydrothermal approach using $FeSO_4 \cdot 7H_2O$ and sodium thiosulfate ($Na_2S_2O_3 \cdot 5H_2O$) in the presence of an aqueous solution of polyethylene glycol (PEG), and NaOH in an autoclave maintained at 150 °C for 24 h [193]. Additionally, Sun et al. synthesized 63 to 140 nm magnetite particles through a solvothermal route using iron pentacarbonyl ($Fe(CO)_5$), OA, and HDA in the presence of oleic acid and n-octanol in an autoclave maintained at 200 °C for 6 h [194].

2.4 Synthesis of BST Nanoparticles

The BST nanoparticles were formed using various techniques, including Co-precipitation, hydrothermal, molten-salt, and sol-gel methods. The BST nanoparticles synthesized by Simoes et al. using the precipitation method by reducing barium acetate ($Ba(CH_3COO)_2$), strontium chloride ($SrCl_2 \cdot 6H_2O$) with an aqueous solution of tetrachloride titanate($TiCl_4$) in the presence of NaOH [195]. Subsequently, Pazik et al. hydrothermally synthesized BST Nanoparticles using Barium acetate ($Ba(CH_3COO)_2$, titanium butoxide ($Ti(OC_4H_9)_4$, and strontium nitrate ($Sr(NO_3)_2$) in the presence of NaOH [196]. Although $Ba_{1-x}Sr_xTiO_3$ powders (at x= 0, 0.3, 0.5, 0.8, and 1) prepared with two different salts were demonstrated by Fuentes et al. using sol-gel followed by the hydrothermal process with an aqueous solution of strontium salts ($SrCl_2$ or $Sr(OH)_2$) and barium salts ($BaCl_2$ or $Ba(OH)_2$) in the presence of $TiCl_4$ and HCl [197]. Furthermore, a cube shape BST nanoparticles were prepared by Liu et al. using the molten salt method [198]. To form cube shape

BST particles, strontium hydroxide (Sr(OH)$_2$) and barium hydroxide (Ba(OH)$_2$) were treated with titanium dioxide (TiO$_2$) in the presence of NaOH and KOH.

2.5 The preparation methods for polymer nanocomposite

Traditional polymer composites can be prepared using a variety of processes that can be broadly classified into four primary routes: exfoliation adsorption, melt intercalation, in situ polymerization intercalation, and template synthesis [199–202].

2.5.1 Melt intercalation

Melt intercalation technique is the most common method for the preparation of nanocomposites with a thermoplastic. The process requires higher melting temperatures, then adding the suitable filler and kneading the nanocomposite to obtain a homogeneous dispersion. It offers the benefit of being environmentally friendly and solvent free. Furthermore, this process is an industrial-friendly process, such as extrusion and injection molding, which makes this process more convenient and economical. However, the high-temperature processing conditions may damage the filler's surface modification. Abedi et al. reported that modified organoclay decomposes at a higher temperature of 140 ℃. However, the melt intercalation process temperature range is maintained at 190-220 ℃ [203]. This suggested that optimization of processing conditions is very important to achieve good distribution of fillers in the polymer. Mittal et al. reported that thermally stable surface-modified nanofillers or lower processing temperatures help to reduce surface degradation [204]. Because of the weaker electrostatic interactions between the fillers and their compatibility, the polymer can tunnel into the interlayers, thereby producing exfoliated or intercalated composites [205].

2.5.2 Exfoliation adsorption

Exfoliation adsorption is the process used for the development of polymer nanocomposite. In this technique, the prepolymer or polymer is dispersed in the solvent. For example, the silicate layers dispersed in the solvent before being in the polymer solution. The polymeric chains subsequently

intercalate and remove the solvent from the silicate layers, causing the silicate layers to reassemble and entrap in the polymeric chains, resulting in the development of a multilayer nanocomposite structure [201,202,206]. This technique is mainly suitable for water-soluble polymers with low polarities, such as PVA, PEO, and PVP, to produce a nanocomposite [201,205]. In contrast, to melt intercalation, this approach is not eco-friendly due to the large volumes of solvents used.

2.5.3 Emulsion polymerization

Emulsion polymerization is another technique used in the production of polymer nanocomposites. In this method, an emulsifier was added along with polymer and nanofillers. For example, an emulsifier used to distribute the methyl methacrylate and styrene is in water and added silicates to the polymer matrix [202]. The monomers are crosslinked with a portion of silicates contained within the polymer matrix and another portion adsorbed on the particle surface, resulting in the formation of a nanocomposite. In the preparation of polystyrene containing CB through emulsion polymerization, a surfactant and Azobisisobutyronitrile (AIBN) initiator were added to form emulsified monomer [207]. Hu et al. and Hassan et al. studied the preparation of graphene-filled polystyrene nanocomposite using sodium lauryl sulfate (SLS) as a surfactant [208,209]. This process facilitates good dispersion and exfoliation of nanofillers in the polymer composite.

2.5.4 In situ polymerization

In situ polymerization is another important method used for the preparation of polymer composites. In this process, the monomer with low molecular weight seeps into the internal layers, causing swelling of the filler. This technique uses either initiator diffusion, radiation, or heat to start cross-linkage, developing the growth of exfoliated or intercalated nanocomposites. The benefit of this process is that it achieves well intercalated than all other techniques, including melt intercalated, emulsion polymerization, and exfoliation adsorption methods. Ray et al. reported the

preparation of nylon-6 composite containing clay through in situ polymerization. The studies reported that the clay is well distributed in the monomer and forms a nanocomposite [200].

2.5.5 Template synthesis

Template-based polymerization process technique is one of the important methods for the preparation of polymer nanocomposites. This technique is different than all other previous techniques. In this technique, the nanofillers are prepared in the form of a gel or an aqueous solution comprising the polymeric and the nanofillers as the building components [201,205]. Thus, a polymer used in the technique act as a nucleating agent, which facilitates the growth of the nanoparticles. Subsequently, the nanofillers are distributed in the polymer to form the nanocomposite. This technique is limited because high processing temperatures during the preparation of polymer nanocomposites can result in the agglomeration of nanofillers. It is primarily employed in the fabrication of a double-layer hydroxide-based composite [201,205].

2.6 Research methodology

2.6.1 Literature review

The literature review helped to get a deeper understanding of the current research scenario and the limitations of the research. The methodology for carrying out this research is illustrated in Fig.2.1
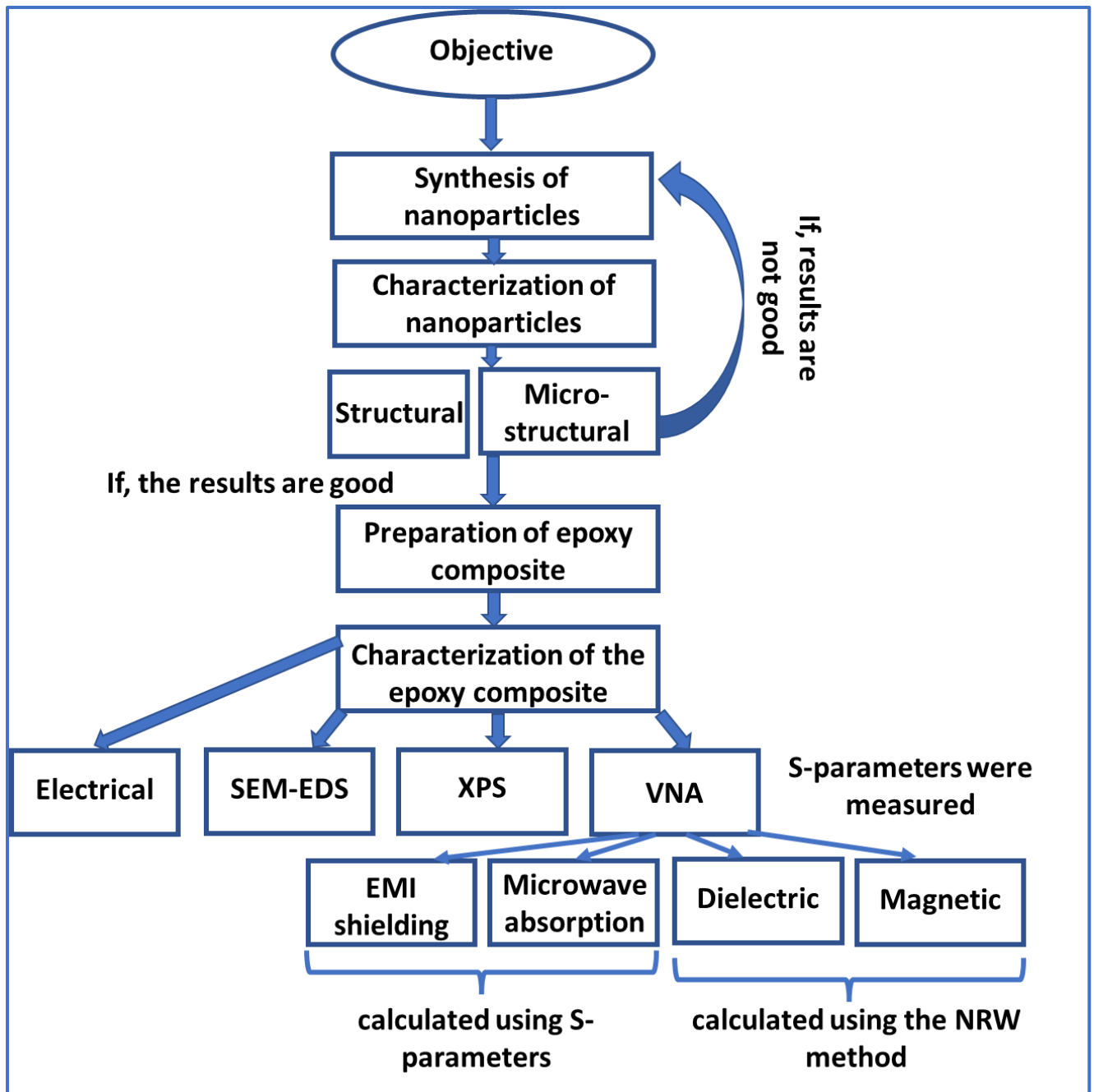
Fig.2. 1. Schematic depicting the methodology to be adopted in the proposed research.

As part of the research studies, the conductive nanoparticles, i.e., CuNW, will be synthesized using

the hydrothermal method. This CuNW preparation method is a modified protocol developed by Li

et al. [172]. The detailed description of this one-pot hydrothermal synthesis method was discussed

in Chapter-3, Thesis. The synthesized CuNW were characterized using X-ray powder diffraction

(XRD) and scanning electron microscopy (SEM) and subsequently used for making nanocomposite. The epoxy composites were prepared through the resin blending technique. Then, the epoxy composites containing CuNW were characterized for electrical, morphological, and EMI shielding properties.

As a continuation of this work, the magnetic particles, i.e., Fe_3O_4 and BaM, were synthesized through the co-precipitation method. These particles were using XRD and SEM. Subsequently, these particles were added along with conductive particles, i.e., CuNW or GNP, in the epoxy matrix through the resin blending technique. The GNP- epoxy composites containing BaM particles were tested for electrical, morphological, dielectric, magnetic, and EMI shielding properties. Similarly, CuNW-based epoxy composites containing Fe_3O_4 particles (non-hybrid) were prepared through a resin blending technique. In addition to this, the hybrid nanostructures (i.e., Fe_3O_4@CuNW and Fe_3O_4@GNP) will be synthesized through a water-based coprecipitation method. The preparation of hybrid particles was clearly described in Chapter 4 of the thesis. The prepared hybrid particles were subsequently used in the preparation of an epoxy composite (hybrid composite). Both the composites are specially tested for microwave absorption properties along with other properties such as electrical, morphological, dielectric, magnetic, and EMI shielding properties, and results are compared.

In contrast to the above studies, the influence of dielectric nanoparticles on the EMI shielding and microwave absorption characteristics were studied. As a part of these studies, the dielectric particles, i.e., barium strontium titanate (BST) particles, were prepared through the co-precipitation technique. The BST particles are added along with CuNW in the epoxy matrix (non-hybrid composite) through the resin blending technique. In addition to this, the hybrid nanostructures, i.e., BST@CuNW through the co-precipitation technique, and used in the

preparation of the composites (hybrid composite). These composites were tested for electrical, EMI shielding, dielectric, and microwave absorption properties. Furthermore, to study the influence of both magnetic and dielectric particles, the hybrid nanostructures, i.e., $Fe_3O_4@BST@CuNW$ were synthesized through the co-precipitation technique. The epoxy composites containing different weight ratios of $Fe_3O_4@BST@CuNW$ particles were prepared through the resin blending technique. These composites were tested for electrical, dielectric, EMI shielding, and microwave absorption properties.

2.6.2 Preparation of epoxy nanocomposites

The nanocomposites were produced by mixing the required quantity of fillers, comprising nanofillers, in the epoxy resin for 12 minutes with an ARE-250 Mixer (Thinky, USA). Subsequently, the epoxy mixture was processed in an ultrasonic processor (Sonics, USA) operated at 500 W for 5 minutes in order to facilitate uniform dispersion of the fillers in the epoxy matrix. Afterward, the requisite quantity of curing agent was added, and the epoxy mixture was even further mixed in the ARE-250 Mixer for 3 minutes to ensure proper mixing of the curing agent. The epoxy mixture was then degassed in the degassing chamber before being cast in a glass mold and cured at room temperature for 12 hours. The thickness of the nanocomposite was measured to be 1 mm and was also set by the mold's dimensions. **Tables 3.1, 4.1, and 5.1** shows the composition of the composites used in this study. The fabricated composites will be characterized for micro-structural, electrical, EMI shielding, microwave absorption, dielectric, and magnetic properties.

2.6.3 Characterization

The X-ray diffractometer (Miniflex, Rigaku, Japan) using the Cu-Kα source with wavelength (λ) = 1.54 Å was used to collect XRD patterns of nanoparticles. The patterns were obtained at a scan

rate of 2 °/min across the 2θ angle range of 20° to 90°. The scanning electron microscope (FEI-APREO, Thermo Fisher, USA) was used to observe the microstructure of nanoparticles and the epoxy composite's freeze-fractured cross-section images. The XPS data were recorded by K-Alpha X-ray photoelectron spectrometer system (Thermo Fisher Scientific, India) using Al Kα (hν = 1486.3 eV) X-ray source with a step size of 0.05 eV at an average of ten scans. It was observed that the analyzer chamber had a residual pressure of 1.3×10^{-8} Pa. A nonlinear curve- fitting method was used so that the core level changes and relative intensities of these components could be determined.

The impedance analyzer (E4990A, Keysight Technologies, India) was used to determine electrical conductivity in a 25 Hz to 25 MHz frequency range using test specimens of dimensions 1 cm×1 cm×1 mm. The microwave absorption in the epoxy composite was determined using scattering parameters (S_{11}, S_{21}, S_{12}, and S_{22}) data across the X-band on a sample of dimensions 22.86 mm×10.16 mm×1 mm from a 2-port MS2038C vector network analyzer (Anritsu, India). First, full 2-port calibration was performed before the measurement in the vector network analyzer. Then the S-parameters were recorded. After that, the sample was loaded in the setup, and S_{11}, S_{21}, S_{12}, and S_{22} were recorded. A total of 3 samples were tested for each composite composition.
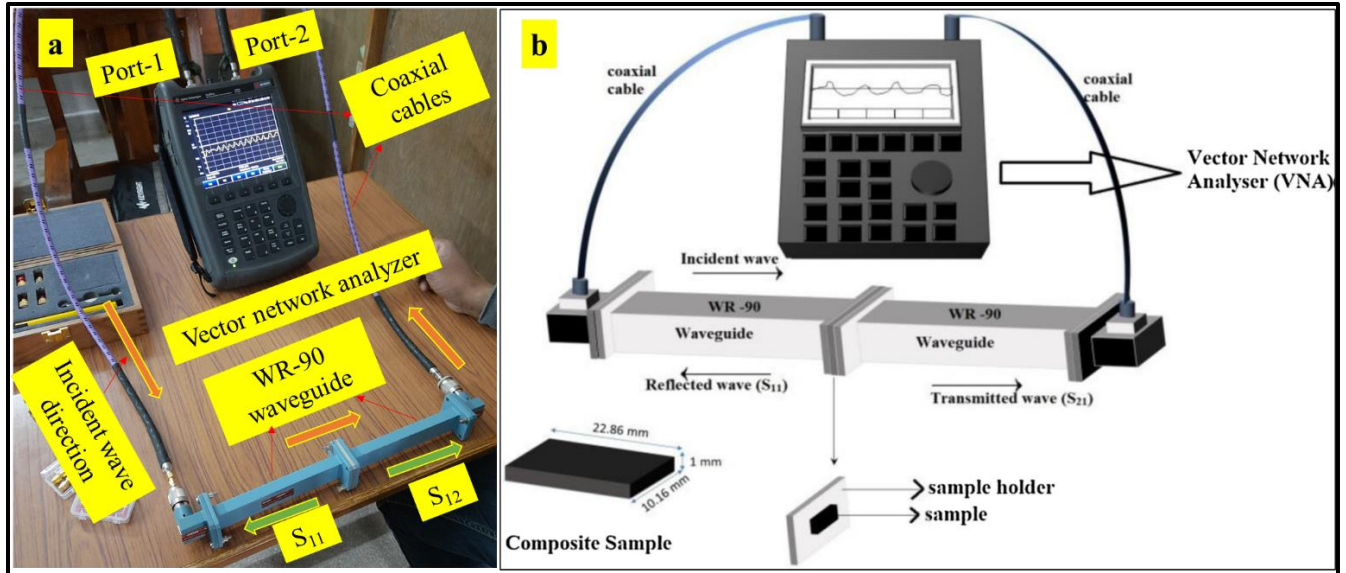
Fig.2.2. Schematic illustrating the vector network analyzer setup.

The power coefficients, absorption coefficient (A), reflection coefficient (R), and transmission coefficient (T) were calculated by the equations,

$$R=|S_{11}|^2 \tag{2.1}$$

$$T=|S_{21}|^2 \tag{2.2}$$

$$A=1\text{-}R\text{-}T \tag{2.3}$$

The S-parameters were used to determine the EMI shielding effectiveness of the composite.

$$SE_T=SE_R+SE_A+SE_M=10\log_{10}\left(\frac{1}{S_{21}^2}\right) \tag{2.4}$$

$$SE_R=10\log_{10}\left(\frac{1}{1-S_{11}^2}\right) \tag{2.5}$$

$$SE_A=10\log_{10}\left(\frac{1-S_{11}^2}{S_{21}^2}\right) \tag{2.6}$$

2.6.4 Nicholson–Ross–Weir (NRW) method:

The complex permeability ($\mu^* = \mu' - i\mu''$) and complex permittivity ($\varepsilon^* = \varepsilon' - i\varepsilon''$) were calculated from S-parameters by using the standard Nicholson–Ross–Weir (NRW) method [70,317–319], as shown Fig.2.2.
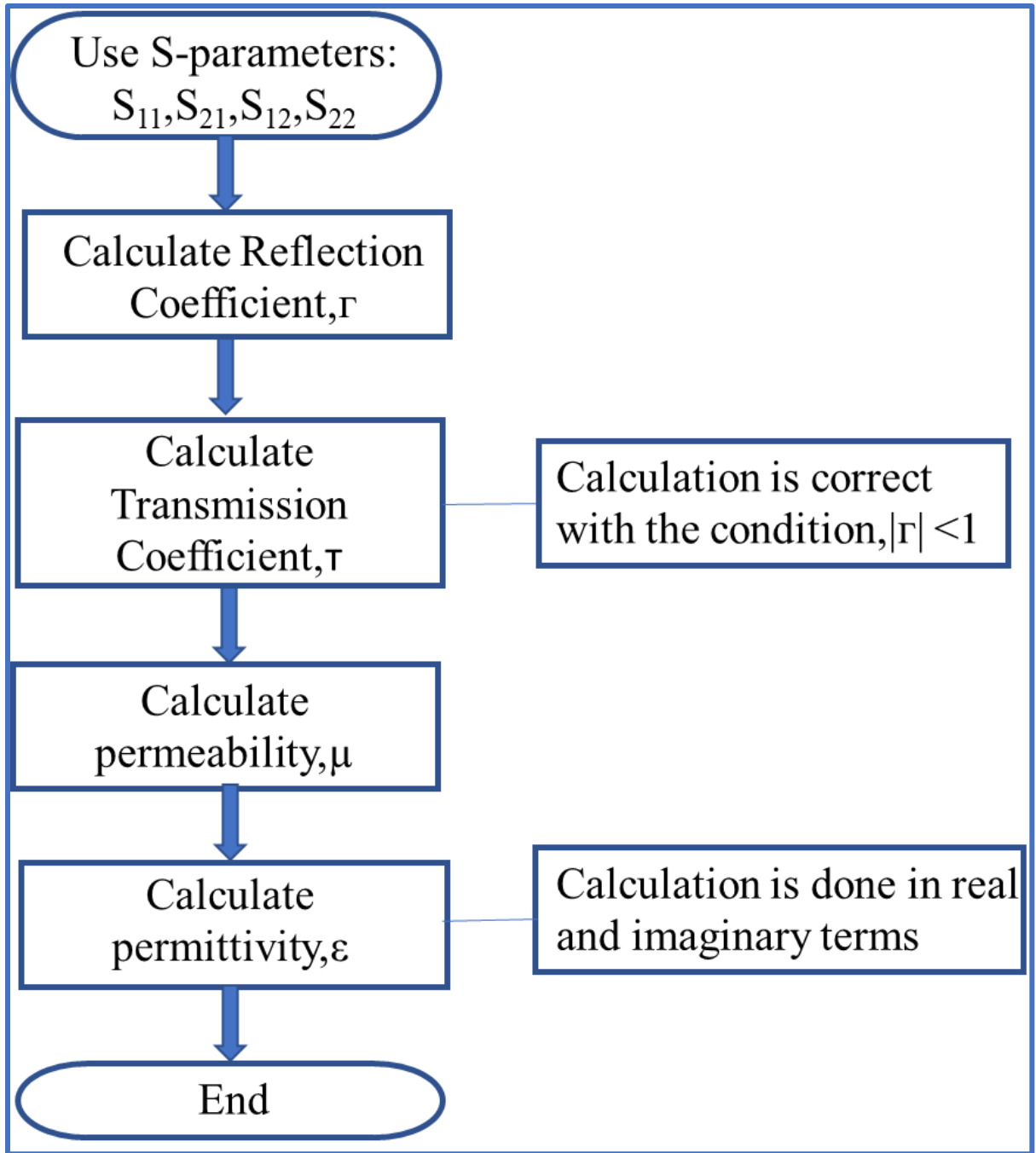
Fig.2.3. The process for the NRW method

The S-parameters: S_{11}, S_{12}, S_{21}, and S_{22} are directly obtained from the vector network analyzer.

The procedure proposed by the NRW method is deduced from the following equations.

The reflection coefficient can be deduced as follows:

$$\Gamma = X \pm \sqrt{X^2 - 1} \qquad \dots\dots\dots\dots\dots\dots\dots(2.7)$$

where $|\Gamma| < 1$ is required to finding

$$\text{Where } X = \frac{S_{11}^2 - S_{21}^2 + 1}{2S_{11}} \quad\quad \dots\dots\dots\dots\dots\dots\text{(2.8)}$$

The transmission coefficient can be written as:

$$T = \frac{S_{11} + S_{21} - \Gamma}{1 - (S_{11} + S_{21})\Gamma} \quad\quad \dots\dots\dots\dots\dots\dots\text{(2.9)}$$

The permeability is given as follows:

$$\mu = \frac{1 + \Gamma}{\Lambda(1 - \Gamma)\sqrt{\frac{1}{\lambda_0^2} - \frac{1}{\lambda_c^2}}} \quad\quad \dots\dots\dots\dots\dots\dots\text{(2.10)}$$

Where λ_0 is the free space wavelength, λ_c is the cut-off wavelength and

$$\frac{1}{\Lambda}^2 = \frac{\varepsilon_{r*}\mu_r}{\lambda_0^2} - \frac{1}{\lambda_c^2} = -\{\frac{1}{2\pi L}\ln\left(\frac{1}{T}\right)\}^2 \quad\quad \dots\dots\dots\dots\dots\dots\text{(2.11)}$$

The permittivity can be defined as:

$$\varepsilon = \frac{\lambda_0^2}{\mu}\{\frac{1}{\lambda_c^2} - \frac{1}{\Lambda}^2\} \quad\quad \dots\dots\dots\dots\dots\dots\text{(2.12)}$$

2.6.5 Analysis of Results

All the experimental results will be well documented and studied. The outcomes of the experiments are compared with the results presented in the existing literature.

3 Influence of CuNW on the EMI shielding effectiveness of epoxy nanocomposite

3.1 Introduction

The rapid growth of instrumentation and electronics in various sectors, such as information technology, military, defense safety systems, healthcare, business electronics, commercial appliances, etc., have led to EMI as an undesirable by-product [1,2]. Furthermore, concepts such as the IoT and smart villages are rapidly gaining momentum, wherein the products involve some wireless data transfer and can potentially further enhance the already widespread problem of signal interference [3]. The EMI in electronic devices and industrial instruments can cause a decrease in normal functioning or a total malfunction of the instrument. EMI can be regarded as a new type of pollution that can be mitigated using EMI shielding materials [4].

As a result, continued efforts have been made over the past two decades to reduce EMI by using several strategies and a variety of materials that include metals, carbon-based materials, dielectric/magnetic materials, and conducting polymers [3,8,49]. Metals are excellent conductors of electricity and can absorb, reflect and transmit electromagnetic waves [12]. Owing to this, metals have been widely employed for EMI Shielding applications. However, the shielding mechanism in metals is dominated by the reflection of the incident electromagnetic wave, which is not always a desirable option. In addition to this, a relatively large density and high cost of fabrication limit its widespread use in EMI shielding applications [210],[211].

Polymer nanocomposites represent a class of materials that possess a unique combination of electrical, thermal, dielectric, magnetic and/or mechanical properties [40,212–215]. Compositionally, nanocomposite comprises a continuous polymer matrix in which a nanofiller is dispersed. Depending on the type of polymer and filler used, the properties of nanocomposite can be tailored for the suppression of EM waves. Owing to such potential, a lot of interest is shown in

employing conductive polymers or conductive polymer composites (CPC) for EMI shielding applications [4,9,12,216].

Several polymers have been used to fabricate nanocomposites, such as poly(styrene), poly(imide), poly(methyl methacrylate), phenolic resin, etc. Among these polymers, epoxy resin is the most widely available thermoset polymer with good chemical, mechanical and thermal properties. In addition to this, it is also a lightweight, corrosion-resistant, flexible, low-cost thermoset polymer, thus used in various applications such as aerospace, die-attach, printed circuit boards, light-emitting devices, etc. [217]. Furthermore, epoxy resin is also an excellent compatible material for a wide range of substrates and additives (nanofillers). Although it exhibits very low electrical and thermal conductivity, limiting its potential applications in instrumentation and electronics. However, these limitations can be overcome by the addition of various reinforced carbon nanofillers such as carbon black, graphene, reduced graphene oxide, carbon nanotubes, and metallic nanoparticles such as gold, silver, copper, etc., [3,8,49],[115,129,212,216,218–221].

It is well known that high aspect ratio conductive nanofillers in the form of nanotubes, nanowires, or nanorods have the advantage of achieving reasonably high electrical conductivity at extremely low filler concentrations in an insulator matrix. This is attributed to the ability of high aspect ratio nanofillers to achieve electrical percolation at extremely low filler loadings [222–225]. Moreover, from a polymer composites' point of view, the low filler loading in the polymer does not influence their density significantly, thereby retaining the low-density advantage of polymeric material [226].

Copper nanoparticles are a good conductor of electricity and can be synthesized in a variety of shapes that include spherical particles, nanorods, nanocubes, and nanowires [177,227,228]. Among these, CuNW are interesting due to their unique structure, high aspect ratio, low cost,

excellent electrical and thermal conductivity, and optical properties. It is worth mentioning here that CuNW exhibits electrical conductivity comparable to that of silver [172]. Such unique properties of CuNW have attracted attention from industrial as well as scientific societies [229–233],[177]. It should be noted here that a good EMI shielding material should possess reasonable electrical conductivity to mitigate EM wave propagation through the material. Thus, the development of nanocomposites with CuNW has been offered as a promising approach to making EMI shielding materials. However, relatively few studies have been reported on utilizing CuNW for producing EMI shielding materials [23]–[25]. Furthermore, to the best of the author's knowledge, no studies are reported wherein CuNW in a widely used engineering thermosetting polymer such as epoxy drives the motivation for the current work.

In this work, the performance of epoxy nanocomposites containing CuNW as an EMI shielding material is presented. The CuNW were produced using a facile one-pot hydrothermal synthesis method, and the EMI shielding effectiveness of the composites in the X-band frequency range (i.e., 8-12.4 GHz) is investigated. The crystallographic and morphological characteristics of the as-synthesized CuNW determined using XRD and SEM, respectively, are presented. Furthermore, microstructure, electrical conductivity, and EMI shielding effectiveness epoxy composites containing varying amounts of CuNW fabricated using solvent-free melt blending method are also included.

3.2 Experimental work

3.2.1 Materials

Copper chloride di hydrated (AR), dextrose extra pure (AR), oleic acid (AR), and oleyl amine (AR) were purchased from Merck (Mumbai, Maharashtra). Liquid epoxy resin araldite® CY230 and hardener aradur® HY-951 were purchased from Huntsman (Mumbai, Maharashtra).

3.2.2 One-pot synthesis of Copper Nanowires

A hydrothermal synthesis method for CuNW was prepared by modifying the protocol developed by Li et al.[172]. First, 40 mmol of copper precursor aqueous solution was prepared by dissolving a stoichiometric amount of copper chloride dihydrate in the double-distilled water and stored in a conical flask. The capping agent solution contained oleyl amine (20 mL), oleic acid (0.2 mL) in ethanol (35 mL) was added to the copper salt solution and mixed thoroughly using a magnetic stirrer for 15 minutes. Additionally, 40 mmol of dextrose solution was prepared, which was used as a reducing agent for the synthesis of CuNW. Subsequently, the dextrose solution was added drop by drop at specific flow rates of 1mL/ min into a copper salt solution under vigorous stirring to form a uniform viscous solution. Then the solution was diluted by adding millipore water and continuously stirred for 12 hours at a temperature of 60°C. At this point, the color of the solution changed from dark blue to caesious. Subsequently, the solution was kept in an autoclave and processed at 120°C for 7 hours, after which the color of the solution turned reddish-brown, indicating the formation of copper nanowires. [172] After the autoclave was cooled down to room temperature, the supernatant was decanted. Subsequently, the final product was washed several times with hexane and was subjected to ultrasonication for 5 minutes at 250 watts and 20 kHz using a tip sonicator (Johnson Plastosonic, India). The CuNW suspended in the solution was separated using a centrifuge (CPR 24, REMI Compufuge, India) operated at 10000 RPM for 15 minutes. The sediment of CuNW was stored in hexane prior to using it for composite preparation.

3.2.3 Preparation of CuNW- epoxy nanocomposites

The CuNW-epoxy composites were made by dispersing the required quantity of CuNW powder in the epoxy resin using a planetary resin mixer (ARE-250, Thinky Corporation, Japan) for 10 minutes. Afterward, the resin mixture was subjected to ultra-sonication in an ultrasonic liquid processor (Johnson Plastosonic, Pune) operated at 20 kHz and 250 W for 10 minutes to facilitate good dispersion of the CuNW in the epoxy matrix. Subsequently, the required quantity of hardener was added, and the mixture was further mixed in a planetary resin mixer (ARE-250, Thinky Corporation, Japan)) for 10 minutes to enable good mixing of the hardener. The resin mixture was then degassed and subsequently cast in a glass mold and cured at room temperature for 24 h. The thickness of the composites was measured to be 1 mm and was controlled by the mold dimensions. Table 1 shows the composition of the composites used in this study.

Table 3. 1: The composition of CuNW/epoxy nanocomposite was used in this study.

S No.	CuNW (wt%)	Epoxy (wt%)
1	0	100
2	2	98
3	4	96
4	6	94
5	8	92
6	10	90
7	12	88
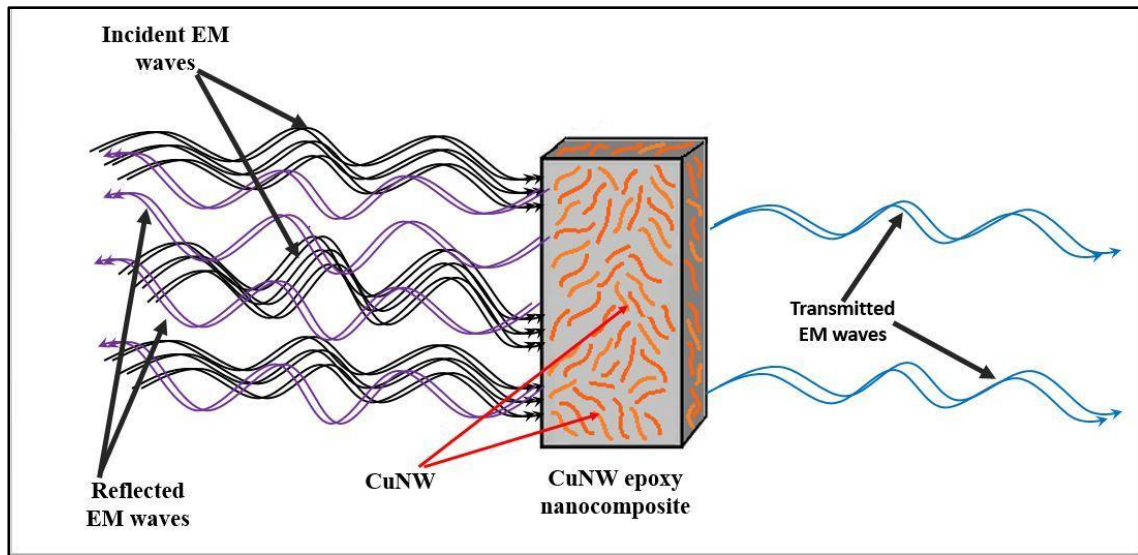
Fig.3. 1. Schematic illustrating the microwave absorptive nature of CuNW epoxy

nanocomposites.

3.2.4 Characterization

The XRD diffractograms of CuNW were obtained using a Miniflex X-ray diffractometer (Rigaku, Japan). The data was collected using the Cu- Kα radiation source of wavelength (λ) = 1.5406 Å over 2θ range from 20 ^{o} to 100 ^{o} at a scan rate of 2 °/min. The microstructure of CuNW and the freeze-fractured cross-section of CuNW-epoxy nanocomposite were recorded using a scanning electron microscope FEI-APREO (Thermo Fisher, USA). All the samples were sputtered with gold prior to recording their SEM images. The electrical conductivity of the composites was measured using the E4990A impedance analyzer (Keysight Technologies, India) over the frequency range of 25 Hz to 25 MHz. The conductivity was calculated from the obtained resistance value. The samples of dimensions 1 cm x 1 cm x 1 mm were used for the measurement. The EMI shielding effectiveness of the composites was determined using a 2-port N5230A PNA-L vector network analyzer (Keysight Technologies, India). The measurement setup comprises a coaxial waveguide adapter attached to an X-band waveguide (WR-90). The nanocomposites of rectangular sections of dimensions 22.86 mm×10.16 mm fit in a cavity of the sample holder. Then the sample holder

was then sandwiched between X-band waveguides, and the scattering parameters (S_{11} and S_{12}) was recorded over an X-band frequency of 8–12.4 GHz. A total of 5 samples were tested for each composite composition, and a full 2-port calibration was performed before the measurement. The obtained s parameters from the VNA were used to calculate the total EMI shielding effectiveness (SE_T), shielding effectiveness due to reflection (SE_R), and shielding effectiveness due to absorption (SE_A) using equations (3.1)-(3.3).

$$SE_T = SE_R + SE_A = 10\log_{10}\left(\frac{1}{S_{21}^2}\right) \tag{3.1}$$

$$SE_R = 10\log_{10}\left(\frac{1}{1-S_{11}^2}\right) \tag{3.2}$$

$$SE_A = 10\log_{10}\left(\frac{1-S_{11}^2}{S_{21}^2}\right) \tag{3.3}$$

3.3 Results and discussion

3.3.1 CuNW Characterization

In an effort to confirm the presence of CuNW in the synthesized product, XRD and SEM were performed, and the results are shown in Fig.3.2 and 3.3, respectively. It can be seen from Fig.3.2 that the sample exhibited XRD peaks at 2θ values of 43.59º, 50.81º,74.43º, 91º, and 95º, which corresponds well with the characteristic peaks of copper as per JCPDS #040836. These results confirm the presence of copper in the synthesized product. It should also be noted here that the synthesized product contained pure copper without any impurities, as no additional peaks in the XRD spectra were recorded. Moreover, it can also be noticed from Fig.3.2 that the XRD peaks of the CuNW sample were relatively broad, which can be attributed to the nano-sized morphology. It can be seen that the most prominent peak was observed at 2θ of 43.6 º, which indicates that the preferred growth direction of nanowires was along the (111) plane. Similar XRD results were obtained for CuNW by other researchers as well [234,235].
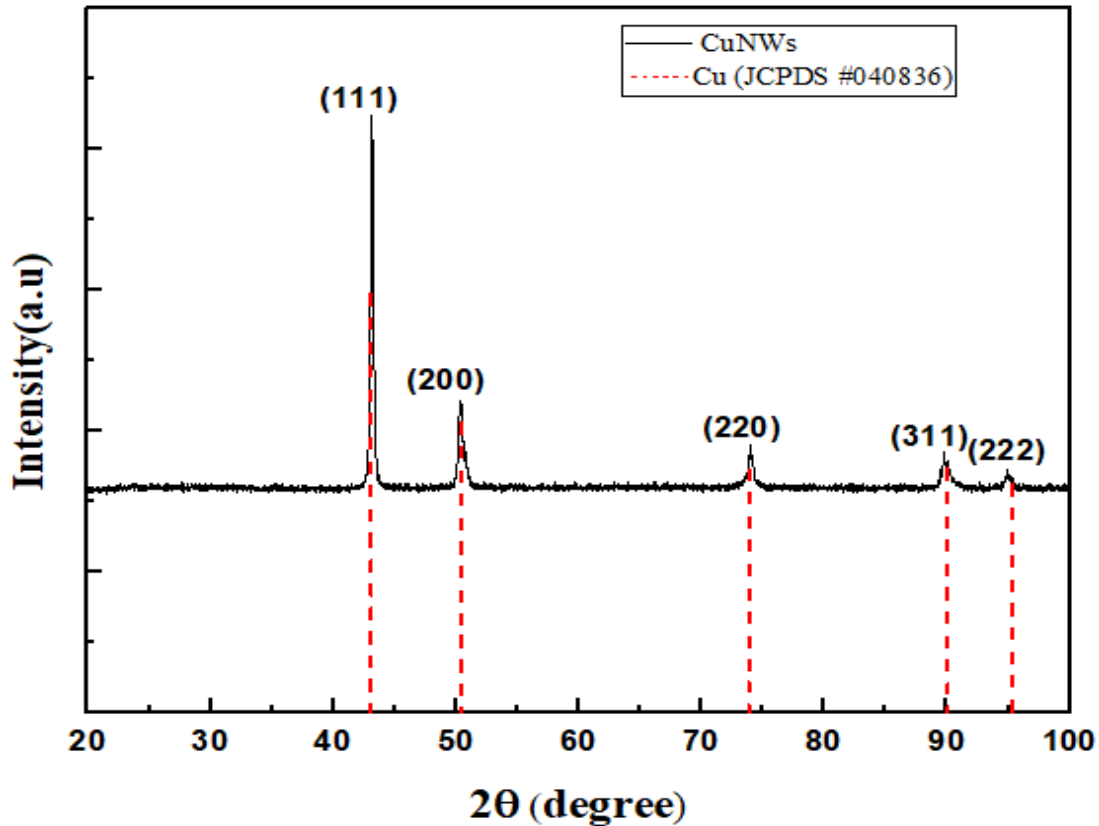
Fig.3. 2. XRD spectra of CuNW along with corresponding JCPDS of copper

The SEM images obtained on the synthesized product are shown in Fig.3.3. It can be observed from the image that the sample contains wire-like particles, which again confirms the successful formation of CuNW. Furthermore, it can be observed that the wires formed are straight without any bends, which distinguishes them from typical SEM observed for other 1-D nanoparticles, such as carbon nanotubes [175,228,236]. The length and diameter of CuNW were determined using Image-J software for 100 different CuNW in the SEM image, and the results are shown in Fig.3.3 ((b) and (c)). The average length and average diameter of CuNW were determined to be 44.9 μm, and 24.3 nm, respectively. The average aspect ratio of CuNW was determined to be 1848, which again suggests that formed particles are nanowires rather than nanorods [120,175,231,237,238].

Based on the results obtained from XRD and SEM, it is reasonable to suggest that CuNW was successfully formed.
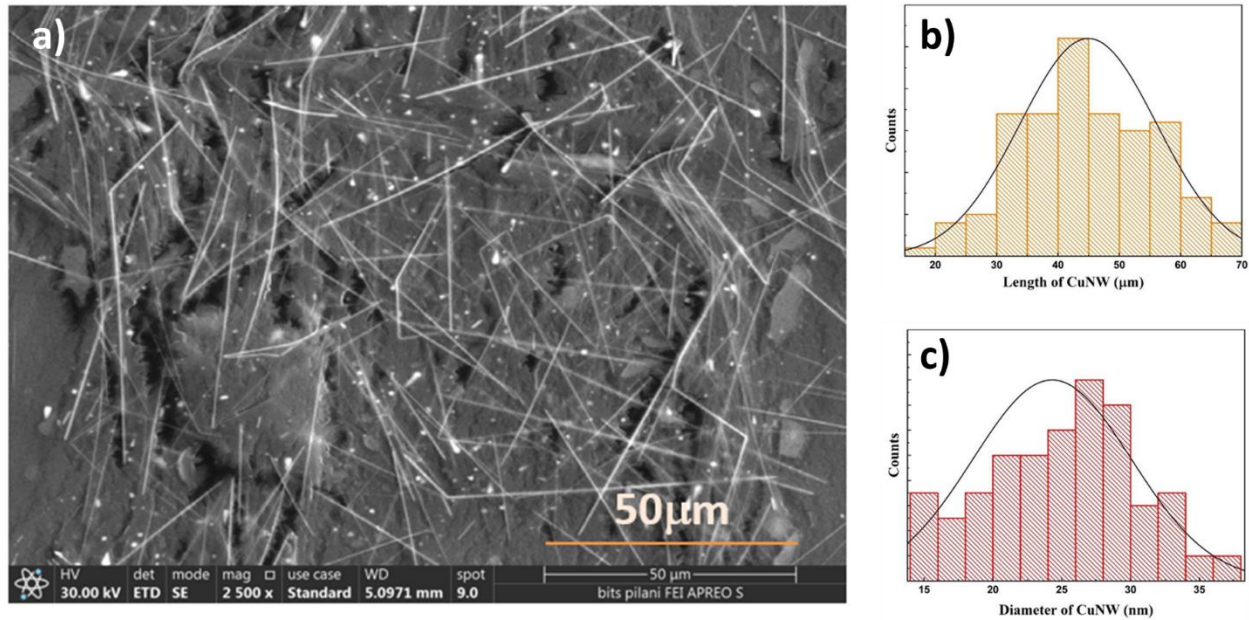
Fig.3.3. SEM images of CuNW sample at a magnification of 2500x (a), length (b), and diameter (c) of the sample obtained using Image J software.

3.3.2 SEM of CuNW-Epoxy Nanocomposite

To investigate the microstructure and dispersion of CuNW in epoxy composites, SEM was performed on the freeze-fractured cross-section of epoxy nanocomposite containing 12 wt% CuNW. The SEM image suggests that CuNW is well dispersed in the epoxy matrix, as is evident by the absence of large agglomerates, as shown in Fig. 3.4(a). This suggests that the composite preparation protocol successfully disentangles and disperses the nanowires in the epoxy matrix. To further characterize the chemical composition of the composite, energy dispersive spectroscopy (EDS) was performed, and the results are shown in Fig. 3.4(b). The presence of copper in the composites was confirmed as an EDS peak corresponding to copper was obtained. This further suggests the presence of CuNW in the composite.
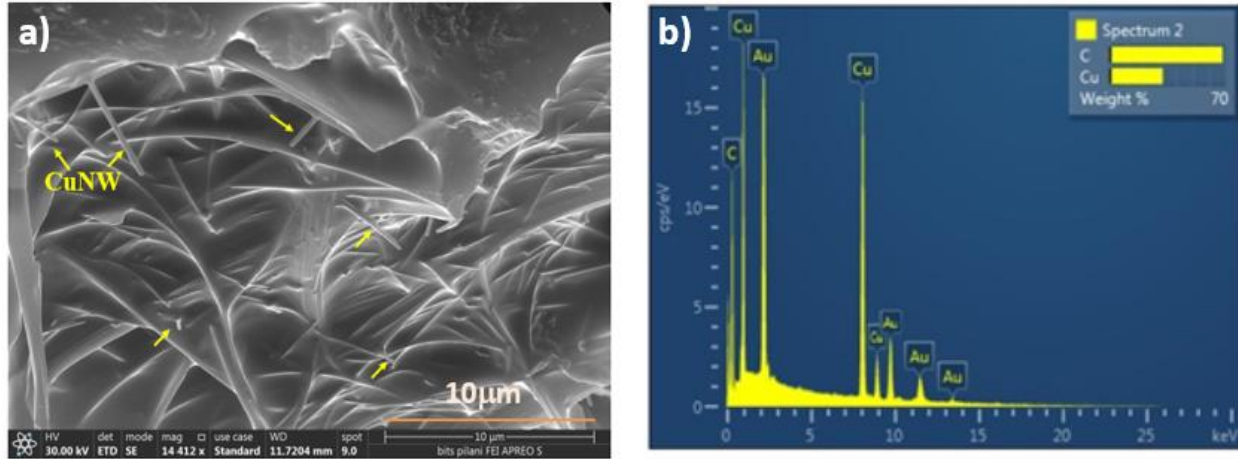
Fig.3.4. SEM images of freeze fractured cross-section of the epoxy composite containing 12 wt% CuNW (a) and the energy-dispersive spectra obtained from the sample (b).

3.3.3 Electrical Conductivity of CuNW-epoxy nanocomposite

The electrical conductivity of a shielding material ultimately influences its EMI shielding effectiveness [3]. Therefore, it is interesting to characterize the composite's electrical properties. With this motivation, the electrical properties of the composites were measured, and the results are shown in Fig.3.5. It can be seen from Fig.3.5(a) that all composites containing CuNW content less than or equal to 10 wt% exhibited frequency-dependent electrical conductivities in the 25 Hz -300 MHz frequency range suggesting a dielectric nature of the samples. However, the sample containing 12 wt.% CuNW showed frequency-independent electrical conductivity in the 25-200 Hz region. Such frequency-independent electrical conductivity is demonstrated by percolated composites wherein a 3-dimensional conductive network is established [3],[239]. Based on these results, it is reasonable to deduce that the 12 wt.% CuNW-containing composites had a percolated network of CuNW. Furthermore, Fig.3.5(b) shows the electrical conductivity at 25 Hz frequency as a function of CuNW content in the composites. The sample containing 12 wt.% CuNW demonstrated the highest conductivity of 1.76×10^{-6} s/m at 25 Hz, which is about three orders of magnitude higher than that of neat epoxy.

In an effort to determine the percolation threshold (ϕ_c) for CuNW-epoxy composites, the conductivity was fitted to the percolation law shown in equation (3.4). The results of the fitting are shown in Fig.3.5(c)

$$\sigma = \sigma_0(\phi - \phi_c)^t \qquad\qquad (3.4)$$

Where ϕ is the filler content, ϕ_c is the percolation threshold, t is the conductivity exponent, and σ is the conductivity of the composite [239]. The following describes the fitting procedure. The electrical conductivity of nanocomposites was plotted as a function of ($\phi - \phi_c$), and a linear fitting was performed by assuming the ϕ_c value, which would yield the highest R^2 value. The ϕ_c value of 10.8 wt.% gave an R^2 and t values of 0.998 and 1.47, respectively. These results suggest that the CuNW-epoxy composites exhibit a percolation threshold of 10.8 wt.%. However, few studies with other polymeric systems have reported a lower percolation threshold for CuNW [92,93,240]. This may be attributed to increased oxidation of CuNW in the epoxy matrix, which results in degradation in their conductivity. Similar observations were made in other studies as well [241].
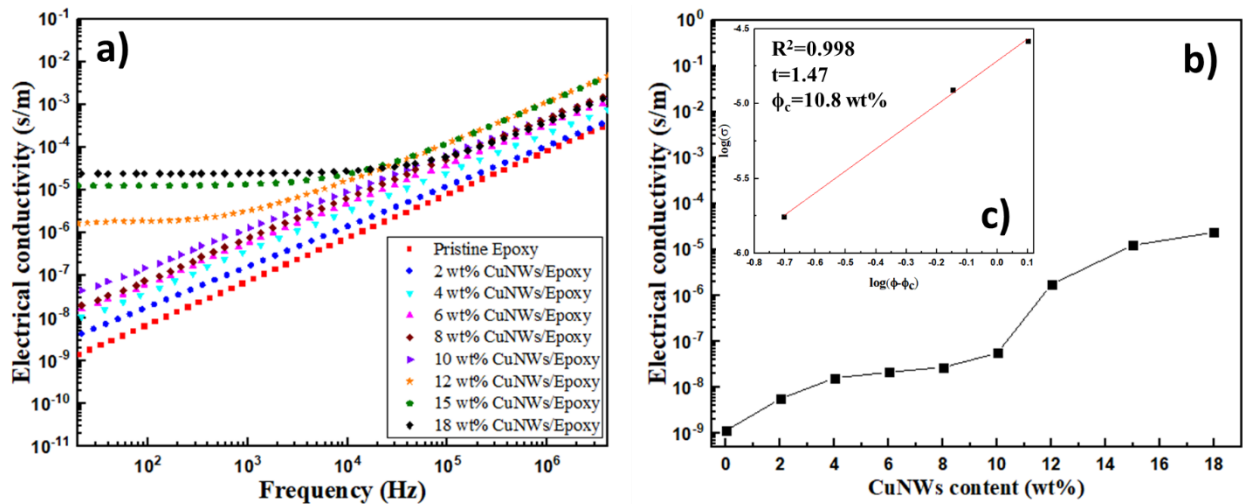
Fig.3. 5. (a) the plot of electrical conductivity of CuNW-epoxy composites as a function of frequency (b) electrical conductivity values at 25 Hz of composites as a function of CuNW filler loading(s) (c) Percolation power-law fitting of electrical conductivity data.

3.3.4 EMI Shielding Effectiveness of CuNW-Epoxy Nanocomposites

The EMI shielding effectiveness was measured for neat epoxy and CuNW-epoxy nanocomposites of 1 mm thickness in the X-band frequency range of 8–12.4 GHz. The SE_T values of CuNW-epoxy nanocomposites and neat epoxy over the X-band frequency range are shown in Fig.3.6 (a). The neat epoxy exhibited a SE_T value of 1 dB, which indicates the transparent nature of the epoxy matrix to the EM waves over the X-band. Similar results were obtained for the epoxy matrix in earlier studies.[242] However, the composites containing CuNW exhibited SE_T values that were dependent on the filler loading and increased with increasing the CuNW content. The composite containing 12 wt% CuNW exhibited the highest total shielding effectiveness value of 6.5 dB over the X-band frequency range. This increase in SE_T with increased CuNW content can be attributed to multiple interfacial polarization losses arising due to the presence of multiple dielectric-to-conductor interfaces.[3,111,243–245]

The EMI shielding effectiveness values of CuNW epoxy composites were comparatively lower than reported values in the literature for other composite systems.[92,93,240] This may be attributed to more oxidation of CuNW's in the presence of epoxy polymer, which degrades the electrical conductivity of the CuNW, thereby reducing the interfacial losses. It is reported that prepared CuNW containing epoxy exhibits inferior electrical conductivity as compared to those containing surface pacified CuNW. [241] Nevertheless, it should be noted here that only 1 mm thick epoxy composite with 12 wt.% CuNW demonstrated a capability to attenuate 77.1% of incident wave power in the X-band. This further suggests that CuNW has the potential to enhance the SE_T of a widely useful engineering thermoset, i.e., epoxy.

To further understand the shielding mechanism, the SE_R and SE_A values of the composites and neat epoxy were determined, and the results are shown in Fig.3.6 (b) and 3.6(c), respectively. It

can be seen from the results that both SE_R and SE_A values increase with increasing the CuNW content in the epoxy. The increase in SE_R with increasing the CuNW content may be attributed to an increase in the composite conductivity. With an increase in composite conductivity, the impedance mismatch at the epoxy-air interface increases, thereby increasing the reflective power. Similar observations were made for other conductive polymer composites as well [3,96,246]. Furthermore, the SE_A may be attributed to increasing interfacial area with increasing CuNW loading, thereby increasing the interfacial polarization losses. It should be noted here that absorption losses were more when compared to reflection losses for all concentrations of CuNW-containing epoxy composite, which suggests an absorption-dominated shielding mechanism in these materials. Similar observations were made for other conductive filler systems [130,247–249].
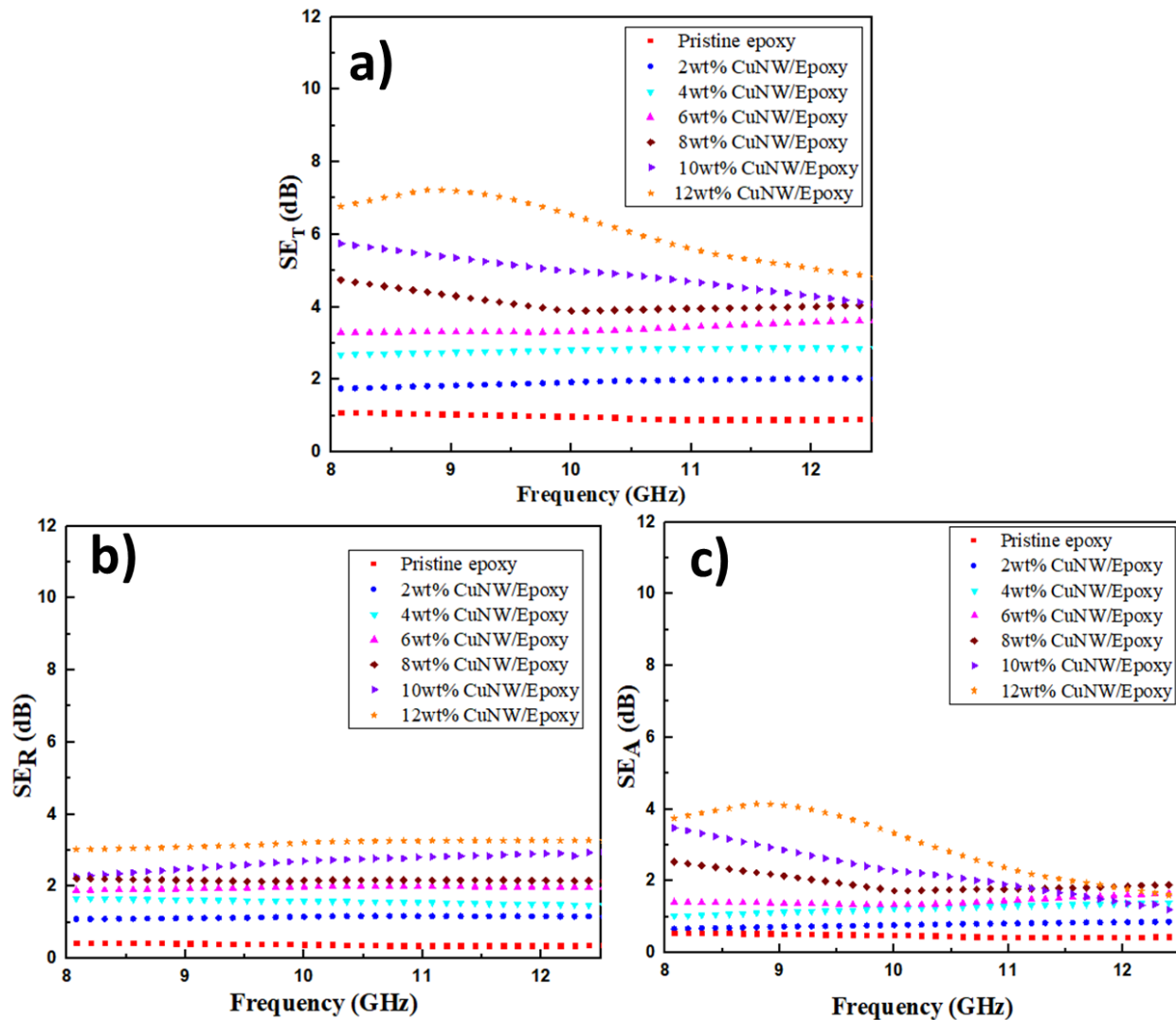
Fig.3.6. (a) SE_T (b) SE_R (c) SE_A of CuNW epoxy nanocomposites with a variation of CuNW filler loading content(s)

3.4 Conclusion

Copper nanowires (CuNW) are an important class of materials with excellent electrical and thermal conductivities. Owing to their cost advantage over other conductive fillers, their use as a filler for enhancing the properties of polymers is aptly justifiable. In this work, the performance of epoxy nanocomposites containing CuNW as an EMI shielding material is presented. The CuNW were produced using a facile one-pot hydrothermal synthesis method, and the EMI shielding effectiveness of the composites in the X-band frequency range (i.e., 8-12.4 GHz) is investigated.

The presence of CuNW in the synthesized product was confirmed by XRD and SEM, respectively. The presence of copper was confirmed by the XRD studies, and the SEM revealed an average diameter of 24.3 nm and a length of 44.9 μm of the CuNW. The CuNW-epoxy nanocomposites were fabricated via an industrially relevant solvent-free melt blending process. A series of CuNW-epoxy nanocomposites containing various filler contents were fabricated and compared for their electrical conductivity and EMI shielding effectiveness. The SEM performed on the freeze-fractured cross-section of the composite reveals uniform dispersion of CuNW in the epoxy matrix. The electrical conductivity of epoxy composites was measured, and the composites containing 12 wt% CuNW demonstrated percolated behavior and exhibited a frequency-independent conductivity value of 1.76×10^{-6} S/m in 25-200 Hz range. The 12 wt% CuNW sample demonstrated an EMI shielding effectiveness value of 6.5 dB, which corresponds to 77.1 % attenuation of incident EM wave.

Chapter-4

4 Influence of the addition of Fe₃O₄ particles on the EMI shielding properties of CuNW-filled epoxy composite

4.1 Introduction

Electromagnetic (EM) waves have been widely used in many applications, such as personal digital assistants, local area networks, wireless communication tools, etc.,[21]. Furthermore, concepts such as smart villages and the IoT are now quickly gathering momentum, which will further expand device footprint and wireless networking [3]. Nevertheless, this rapid development in modern electronics has brought about a new undesired effect known as electromagnetic interference (EMI). The EMI has arisen as an exceedingly severe problem that affects the proper functioning of electronic devices, and some studies also report its adverse effects on human health [250]. Therefore, EMI prevention is necessary to protect electronic systems such as control systems, power systems, communication systems, aerospace, aircraft, automobiles, flexible electronics, and wearable devices [251–253]. However, the current situation needs an effective EMI shielding material that can aid this by attenuating microwaves, thus reducing signal interference problems. Owing to such implications, continued efforts have been made to find an absorption-dominated EMI shielding material that can attenuate microwaves over broadband.

There are two major mechanisms by which EMI shielding materials attenuate the impinging of EM waves, i.e., reflection and absorption, as seen in Fig.4.1. The absorption-driven shielding properties in a material are a consequence of either magnetic or dielectric losses inside the material, whereas the reflection losses arise primarily due to impedance mismatch [12]. Additionally, a good EMI shielding material must have several desirable characteristics for practical applications, like small size, lightweight, flexibility, cost-effectivity, and easy processability [18]. As a result, continued efforts have been made over the past two decades to reduce EMI by using several

strategies and a variety of materials that include metals, carbon-based materials, dielectric/magnetic materials, and conducting polymers [3,8,49]. Metals are excellent conductors of electricity and can be used to shield from electromagnetic waves [12]. Owing to this, metals have been widely employed for EMI shielding applications. However, the shielding mechanism in metals is dominated by the reflection of the incident electromagnetic wave, which is not always a desirable option. In addition to this, a relatively large density and high cost of fabrication limit its widespread use in EMI shielding applications [210,211].

Polymer composites represent a special class of materials with tailorable properties that could be tuned by the addition of suitable filler particles. By incorporating suitable filler(s), the electrical, magnetic, and dielectric properties of polymeric materials could be significantly enhanced, which makes them a good alternative to metals for EMI shielding applications [64,212,213,216]. Moreover, by employing nanosized fillers, the low-density advantage of polymeric materials could further be retained as relatively low loadings of nanosized fillers are required to realize significant property enhancement.

Electrically conductive polymer composites (CPC), often containing carbon-based nanoparticles, are used as EMI shielding materials. The major mechanisms of microwave absorption in CPC are the dielectric and conduction losses. In addition to these losses, the conductive composites also generate eddy current losses in the presence of the magnetic field [52]. Even though CPC offers wide bandwidth microwave absorption, relatively high filler loadings are usually required to achieve reasonable absorption. Such high conductive filler content in these composites increases the impedance mismatch, thereby increasing the undesirable reflection of microwaves [3,72,312]. Moreover, high filler loadings in CPC may further induce mechanical properties deterioration, cost enhancement, and processing difficulties [313]. Thus, it is of practical interest to develop efficient

CPC-based EMI shielding materials that offer large bandwidth absorption with the minimum reflection of microwaves [49,64,254,255].

Magnetic materials such as ferrites and their composites are suitable materials for EMI shielding materials because of their good magnetic and dielectric properties. Consequently, spinel and hexaferrite have been widely used for microwave absorption applications [35], [256,257]. In ferrites-polymer composites, the primary mechanism responsible for the absorption of EM waves is the magnetic loss which comprises natural resonance, domain wall resonance, and/or hysteresis loss. However, low absorption bandwidth, large density, and difficult processing limit their widespread utilization as EMI shielding material of choice [257]. The incorporation of magnetic particles in conductive polymer composite (CPC) further enhances their microwave absorption due to the addition of magnetic loss capability in these hybrid composites, along with dielectric and conduction losses. For example, adding conductive fillers such as graphene, graphene oxide, and nickel, along with magnetic fillers (i.e., Fe_3O_4) in the polymer matrix, has been shown to increase the microwave absorption in the composites [80,85,128–132,86,121–127]. The properties of Fe_3O_4 particles make it as a potential candidate over other magnetic materials, such as chemical stability, inexpensiveness, ease of processing, large magnetic anisotropy, magnetic susceptibility, magnetic permeability, and saturation magnetization [90]. Furthermore, the addition of Fe_3O_4 particles in the polymer composites facilitates the attenuation of microwaves through hysteresis losses, eddy current, and natural resonance [258].

Furthermore, the hexaferrites are classified into different types based on the complexity of the hexaferrite's unit cell, such as M, Y, W, Z, X, and U types [259]. Among these, M-type barium hexaferrite nanoparticles (BaM) have gathered significant interest for a variety of applications due to their exceptional properties such as wideband magnetic resonance frequency, large coercivity,

high electric resistivity, high Curie temperature, excellent chemical stability, strong saturation magnetization, uniaxial anisotropy, and magneto-crystalline anisotropy [35,260,261]. Owing to such desirable properties, the use of BaM for high-frequency EMI shielding applications is of great significance [262].

Accordingly, M-type barium hexaferrite has been used in the design of EMI shielding materials, but their widespread applicability is limited by their high density and lower dielectric losses [263]. To overcome these limitations, conductive fillers such as graphene, carbon nanotubes, flexible graphite, expanded graphite, GO, RGO, and GNP are added [3,125,267,285–292]. It is postulated that the addition of a conductive filler to a polymer matrix increases the dielectric losses above the percolation threshold owing to the generation of leakage currents in the composite [121–124]. Furthermore, The increased dielectric losses in percolated polymer composites are also attributed to interfacial polarization effects (at high frequencies) and direct current conductance losses (at low frequencies) [125]. Hence, the addition of conductive fillers along with hexaferrite could further increase the dielectric losses and can enhance the EMI shielding properties of composites containing these nanoparticles.

Despite such potential, very few studies have been reported on the EM wave absorption properties of hexaferrite with divalent and trivalent ion substitution [262,273]. Furthermore, the EMI shielding performance of polymer composites containing barium ferrite and electrically conductive nanoparticles is also not explored at large [274–276]. It would be worth mentioning here that there has been no published study where the EMI shielding performance of a nanocomposite containing GNP and BaM nanoparticles over the X-band frequency range is reported, which drives the motivation for current work. Graphene is one of the most promising two-dimensional materials with unique electrical properties that have been widely used as an EMI

shielding material. In addition, graphenes and their derivatives, such as GO and RGO, are widely explored for EMI shielding applications alone or in combination with certain other conductive and magnetic materials [21,64,129,277]. Despite such merits, the lack of production-friendly strategies for developing high-quality single-layer graphene limits its utilization. Furthermore, exfoliated graphene layers of GO contain defects that reduce their electrical conductivity [278]. On the other hand, GNP, which can be considered an intermediate between graphene and graphite, is a commercially viable product that can be manufactured on a large scale. As a result, the use of GNP as a conductive filler in EMI shielding polymer composites is of commercial significance.

In an epoxy composite containing GNP and BaM nanoparticles, the polymer matrix will act as a low-loss electrical barrier. Due to the presence of conductive GNP, space charges build up at the interfaces in nanocomposites which leads to interfacial polarization losses. Thus, nanocomposites combining the magnetic characteristics of BaM along with the dielectric properties of GNP in an epoxy matrix may yield a high overall loss (i.e., dielectric and magnetic losses) in the epoxy matrix, making them ideal for realistic EMI applications. Driven by the above motivation, we report the EMI shielding performance of epoxy nanocomposites containing GNP and BaM nanoparticles. Firstly, a facile method for the synthesis of barium hexaferrite is reported.

However, the direct addition of conductive and magnetic particles in the polymer matrix can lead to phase separation, which can deteriorate the microwave absorption performance of EMI shielding materials [100]. One strategy to overcome the phase separation in hybrid polymer nanocomposites is to employ a hybrid nanostructure comprising magnetic and/or dielectric nanoparticles anchored to an electrically conductive nanoparticle. Accordingly, many studies have been reported where the use of hybrid nanostructures such as magnetic@conductive and dielectric@conductive has resulted in an enhancement of the microwave absorption capability of

polymer composites [3,101–113]. The increase in microwave absorption in hybrid composites may be ascribed to the multiple interfacial polarization along with the conduction, magnetic, and dielectric losses [3],[136].
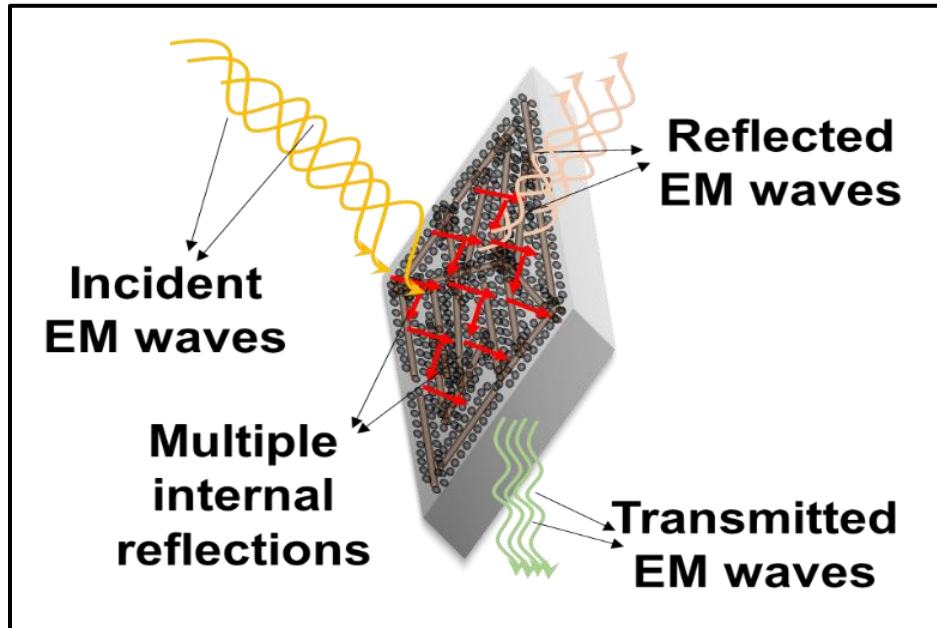
Fig.4. 1. Schematic representation of microwave attenuation in the epoxy composite

Copper nanowires (CuNW) are fascinating nanomaterials owing to their good electrical and thermal conductivities, high aspect ratio, and relatively lower cost compared to carbon-based nanomaterials. The electrical conductivity of CuNW is comparable to that of silver and thus is of interest to be used as a conductive filler in polymers to produce EMI shielding materials [26]. In spite of such merit, very few attempts have been made where CuNW-filled polymer composites were analyzed for their microwave absorption characteristics in the X-band [92,93,232,279]. This may be due to the inferior performance of CuNW-filled polymer composites compared to nano-carbon-filled composites. For example, a 12 wt% CuNW-filled epoxy exhibited an attenuation of 77.1 % incidence microwave power which is significantly lower than the values achievable with other carbon-based nanofillers [280]. Thus, there is a need to improve the microwave absorbing

power of CuNW-based CPC to ensure their widespread utilization, which drives the motivation for the current study.

For the first time, this study reports on the microwave-absorbing properties of CuNW-based hybrid epoxy nanocomposites over the X-band. A simple water-based synthesis protocol was employed for producing CuNW, Fe_3O_4, and Fe_3O_4@CuNW hybrid nanoparticles used in this work. Next, a facile method for the synthesis of barium hexagonal ferrites is reported. The microstructural properties and crystallographic phases of nanoparticles were analyzed using scanning electron microscopy (SEM) and X-ray diffraction (XRD), respectively. A series of hybrid composites containing different ratios of GNP and BaM nanoparticles and CuNW and/or Fe_3O_4 nanoparticles, and Fe_3O_4@CuNW hybrids were prepared and characterized for their microstructure and electrical conductivity. The microwave absorption capability of the composites was determined over the X-band frequency range of 8-12.4 GHz. Furthermore, the magnetic permeability and dielectric permittivity of the composites as a function of filler loadings over the X-band were also included.

4.2 Influence of the addition of Fe_3O_4 particles on the EMI shielding properties of CuNW/epoxy nanocomposite

4.2.1 Materials and methods

4.2.1.1 Materials

Ammonia Solution extra pure (AR), ferric chloride anhydrous pure (AR), and ferrous chloride tetrahydrate extra pure (AR) were procured from Sisco research laboratories (Mumbai, Maharashtra). Liquid Epoxy Resin Araldite® CY230 and hardener Aradur® HY-951 were purchased from Huntsman (Mumbai, Maharashtra).

4.2.1.2 Synthesis of Fe_3O_4 @CuNW hybrid, Fe_3O_4 nanoparticles and CuNW

First, the Fe_3O_4 nanoparticles were prepared through the facile coprecipitation method. An aqueous iron salt solution was prepared by mixing $FeCl_3$ and $FeCl_2.4H_2O$ at the stoichiometric ratio in the round bottom flask. The molar ratio of $Fe^{2+}:Fe^{3+}$ of 1:1.5 was maintained as per the literature [281,282]. The solution was stirred for 15 minutes to obtain a homogeneous mixture of iron salts. Subsequently, the solution was stirred for 45 minutes with a magnetic stirrer at room temperature. Afterward, the ammonia solution (30 wt.%) was added to the solution at a 1 mL/min rate. Next, the final solution was stirred for 30 minutes to complete the precipitation process at room temperature. The solution was centrifuged at 10000 rpm then the precipitate was separated from the solution. The residue was washed and dried at 60 ℃. The obtained Fe_3O_4 nanoparticles were used for the preparation of nanocomposites.

4.2.1.3 Preparation of Fe_3O_4 nanoparticles and CuNW epoxy nanocomposites

A previously published study reports a detailed description of the composite preparation through the resin blending process [9]. The CuNW-epoxy composites containing Fe_3O_4 were made by adding the required quantity of Fe_3O_4 and CuNW hybrid content(s) in the epoxy resin using ARE-250 Thinky Mixer (Thinky, USA) for 12 minutes. Afterward, the resin mixture was treated in an

ultrasonic liquid processor (Sonics & Materials, USA) operated at 20 kHz and 500 W for 8 minutes to facilitate good dispersion of the hybrid(s) in the epoxy matrix. Subsequently, the required quantity of hardener was added, and the mixture was further mixed in ARE-250 Thinky Mixer for 4 minutes to enable good mixing of the hardener. The resin mixture was then degassed using the degassing chamber, cast in a glass mold, and cured at room temperature for 24 hours. The thickness of the composites was measured to be 1 mm and was controlled by the mold dimensions. Similarly, the CuNW and/or Fe_3O_4 composites were prepared by a similar procedure. Table 4.1. shows the composition of the composites used in this study.

Table 4.1. The composition of the composites used in this study.

Filler	Sample Code	CuNW (wt%)	Fe_3O_4(wt%)
Pristine epoxy	NE	0	0
Fe_3O_4	F8	0	8
CuNW	Cu12	12	0
Fe_3O_4-CuNW (**Non-hybrid**)	Cu12F2D	12	2
	Cu12F4D	12	4
	C12F8D	12	8

4.2.2 Results and Discussion

4.2.2.1 XRD characterization of Fe_3O_4 particles and CuNW

To identify the crystallographic phases, X-ray powder diffraction (XRD) was performed on CuNW, and Fe_3O_4 particles, as shown in Fig.4.2. It can be observed that the XRD patterns of the Fe_3O_4 particles were well-matched with the standard peaks of JCPDS #75−0033. It confirms the presence of Fe_3O_4 particles in the synthesized powder sample. Furthermore, the XRD patterns were relatively broad, which indicates the formation of fine nanoparticles. Similar results were

also reported in the literature [281–284]. In the XRD patterns of CuNW, the prominent peak corresponding to 2θ value of 43.3 °, matched with standard peaks of copper as per JCPDS #03–1018. It was in good agreement with previously reported literature for CuNW [234,235,280,285,286].
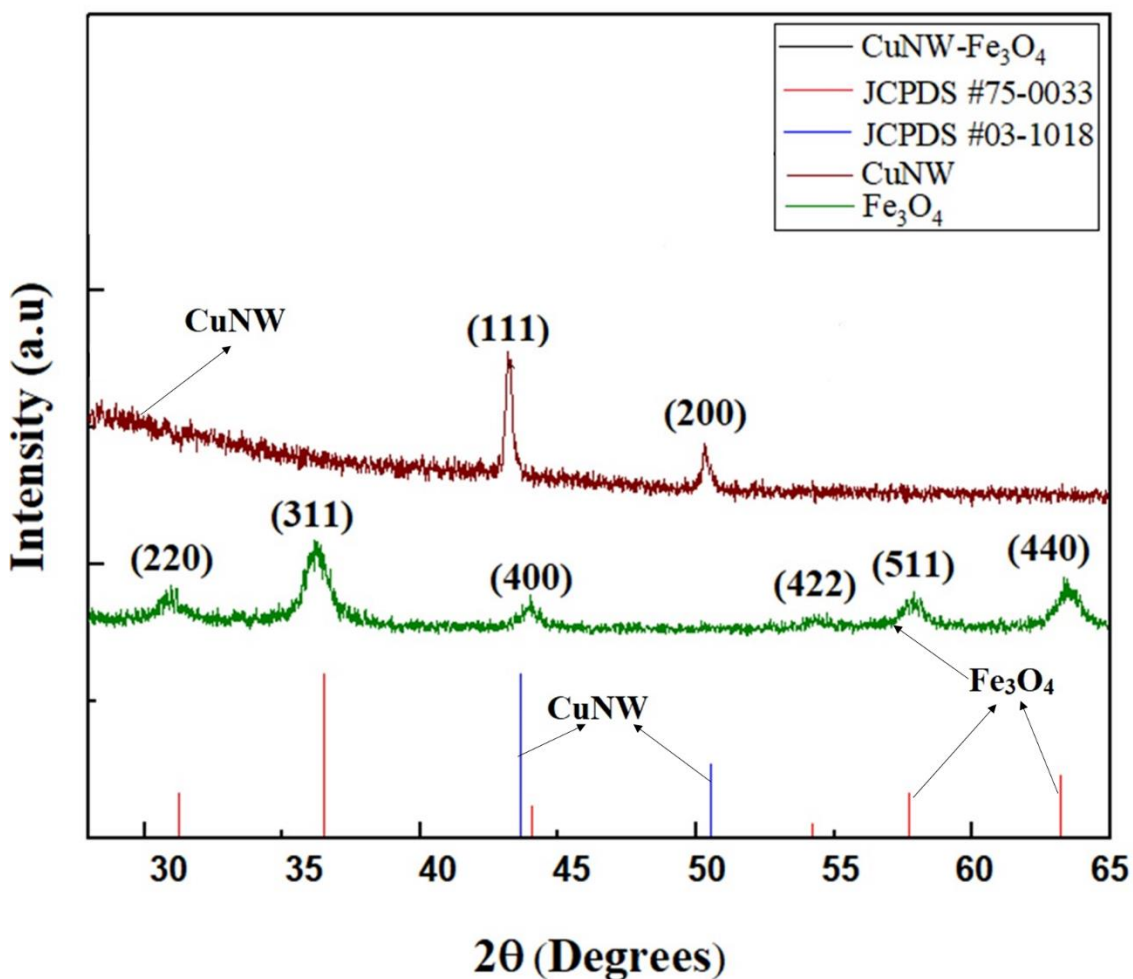
Fig.4.2. XRD spectra of (a) Fe_3O_4 (b)CuNW along with corresponding JCPDS of CuNW and Fe_3O_4.

4.2.2.2 SEM characterization of CuNW and Fe_3O_4 particles

To investigate the microstructure of particles, SEM was performed on the Fe_3O_4 particles, and images are shown in Fig.4.3. It can be observed from Fig.4.3(a) that the synthesized Fe_3O_4 particles formed spherical-shaped particles with an average particle diameter of 28 nm. Similar results were

also reported in the literature [39],[40]. Furthermore, EDX analysis of Fe_3O_4 particles confirmed the presence of Fe and O elements in the powder, as shown in Fig.4.3(b). The microstructure of CuNW was clearly described in Chapter-3. It can be recalled here that CuNW exhibited smooth surfaces with wire-like morphology [280], and the EDX analysis of CuNW confirms the presence of the copper element. Furthermore, the SEM was performed on the freeze-fractured CuNW-epoxy composite containing Fe_3O_4 particles (non-hybrid) and was shown in Fig.4.3(d). It can be observed that both CuNW and Fe_3O_4 particles were distributed in the epoxy composite. The EDX analysis on the same composite as shown in Fig 4.3(c), confirms the presence of Cu, Fe, and O elements in non-hybrid.
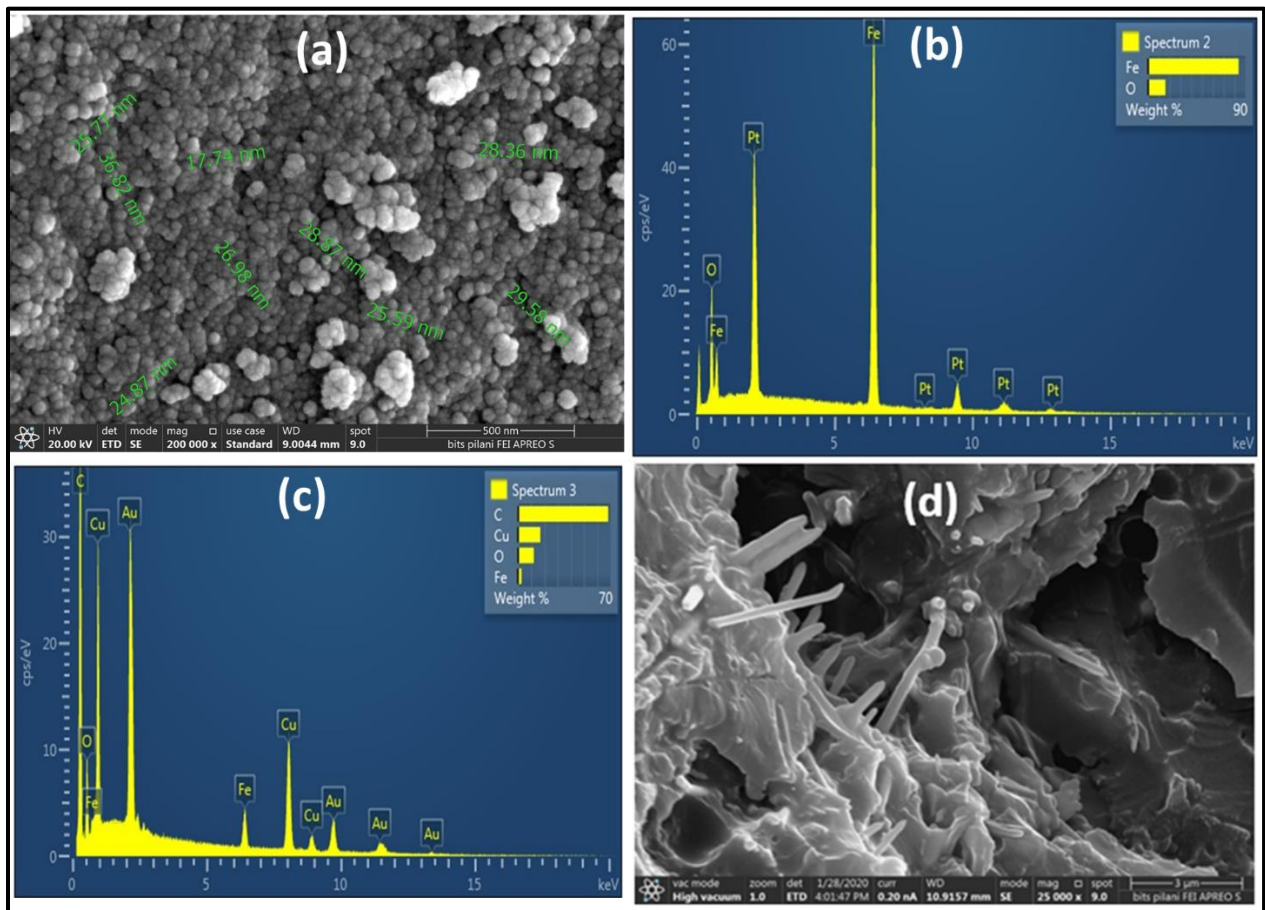
Fig.4.3. SEM images of (a) Fe_3O_4 nanoparticles (b) EDX of Fe_3O_4 (c) EDX of freeze fractured cross-section of Cu12F8D sample (d) freeze fractured cross-section of Cu12F8D sample.

4.2.2.3 XPS characterization of CuNW-epoxy composites containing Fe_3O_4 particles

The wide scan XPS spectrum of hybrid and non-hybrid composites is shown in Fig. 4.4. The XPS data of composites confirms the presence of C1s, Cu2P, Fe2P, and O1s bands in the composites, as shown in Fig 4.4 (a). It can be observed from Fig. 4.4 (e) that O1s peak was observed at 531.5 eV in Fig. 4.4 (e), which was attributed to oxygen anion (O^{-2}) in Fe_3O_4. Similar observations were reported for the O1s band [287]. The C1s spectrum of composites has shown in Fig. 4.4 (b). The composites exhibited a C1s peak at 284.4 eV. Similar results were reported in the literature [288]. The deconvolution peaks of C1s were observed at 284.4 eV, 286.4 eV, and 287.8 eV containing main components of the epoxy matrix, corresponding to aromatic rings (C=C/C–C), epoxy and alkoxy (C–O), and C=O groups. Similar observations were reported [289]. The Cu2P spectrum of composites is shown in Fig. 4.4 (c). The non-hybrid composites exhibited the Cu2p peaks at 932.5 and 952.5 eV, corresponding to Cu $2p_{3/2}$ and Cu $2p_{1/2}$, respectively. Similar observations were reported for Cu2p bands [290]. In contrast, in Fig. 4.4 (d), the Fe2p peaks in non-hybrid composites located at 714.8 eV and 723.8 eV correspond to Fe $2p_{3/2}$ and Fe $2p_{1/2}$, respectively. There are no extra satellites observed in both Fe2p band, which confirms that the composite contains only Fe_3O_4 nanoparticles [289].
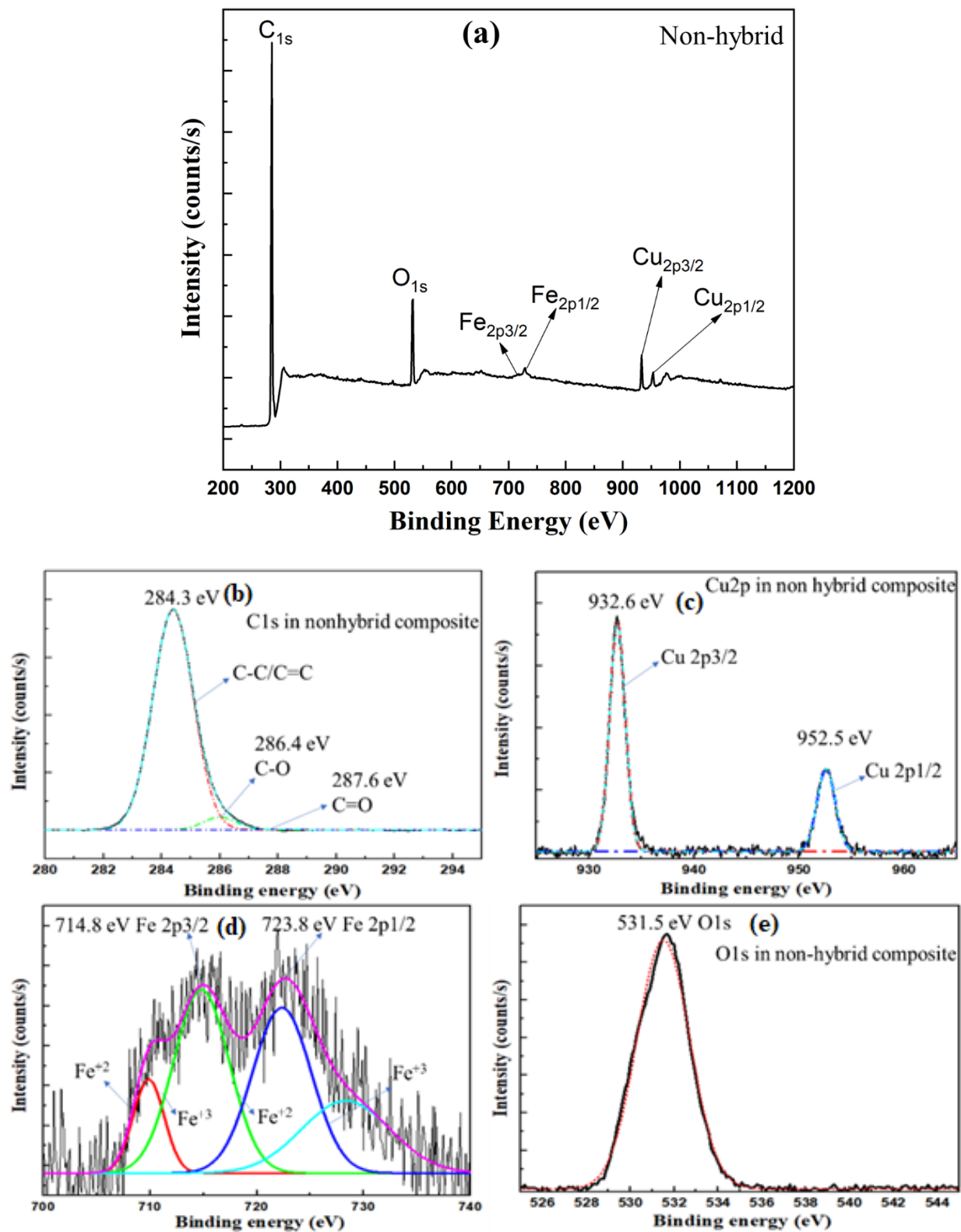
Fig.4. 4. The XPS spectra of (a) non-hybrid composites (b) C1s (c) Cu2P (d) Fe2P (e) O1s of non-hybrid composites

4.2.2.4   Electrical conductivity of epoxy composites

In an effort to study the influence of the adding CuNW and /or Fe_3O_4 nanoparticles on the electrical conductivity of the epoxy nanocomposites, the measurements were carried out on samples in the frequency range of 20 Hz to 25 MHz, as shown in Fig.4.5. The Cu12 nanocomposites demonstrated frequency independent electrical conductivity curves. This suggests that the nanocomposite formed a percolated network at 12 wt% loading of CuNW and significantly increased electrical conductivity. The Cu12 sample exhibited electrical conductivity values of 5.3×10^{-7} S/m at 25 Hz. The electrical conductivity of the nanocomposites at a frequency of 100 Hz was used in the analysis. It can be observed from Fig.4.5(b) that the electrical conductivity was increased with the addition of Fe_3O_4 filler loadings in the composite. It can be observed that composites containing non-hybrid structures (i.e., Fe_3O_4 and CuNW) demonstrated a percolated behavior. This can be attributed to the presence of Fe_3O_4 nanoparticles in epoxy composites containing CuNW was enhanced its conductivity. This is suggested that the presence of Fe_3O_4 improves the formation of the percolated network structure of CuNW in the composite [40]. Similar observations were reported in the literature [128], [291].
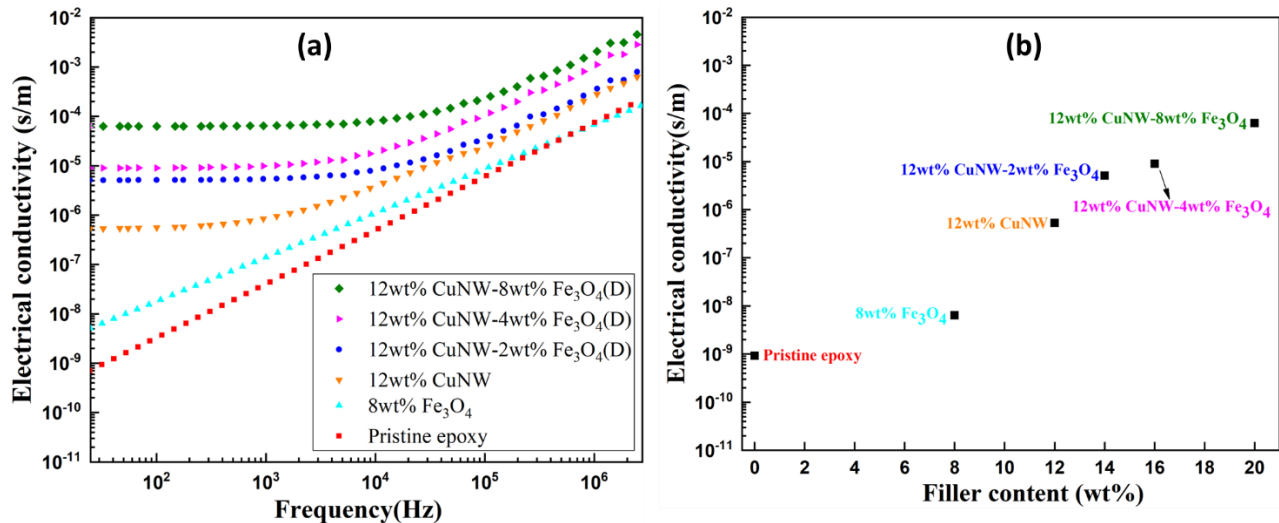
Fig.4. 5 (a) electrical conductivity of CuNW- Fe_3O_4- epoxy composites as a function of frequency (b) electrical conductivity at 100 Hz of CuNW- Fe_3O_4- epoxy composites as a function filler loading

4.2.2.5   EMI shielding effectiveness of epoxy composites.

The EMI shielding effectiveness of the epoxy composites containing CuNW and/or Fe_3O_4 over the X-band in the frequency range of 8-12.4 GHz was determined, and the results are shown in Fig. 4.6. It can be observed from Fig. 4.6(a) that the pristine epoxy sample was exhibited a very low total shielding effectiveness (SE_T) value of 1.7 dB. This is attributed to the epoxy matrix's electrically insulating and non-magnetic nature, which renders it transparent to microwaves [3]. The addition of 8 wt% of Fe_3O_4 nanoparticles to epoxy marginally increased its SE_T value to 2.5 dB in the X-band frequency range. In contrast, the addition of 12 wt% CuNW to the epoxy matrix increases the SE_T value 3 times more than a pristine epoxy sample. These results suggest that CuNW is more effective in improving the EMI shielding performance as compared to Fe_3O_4. The composites Cu12F2D and Cu12F4D exhibited a SE_T value of 11.8 dB and 13.2 dB, respectively, which is higher than that of a Cu12 sample. This further suggests that the direct addition of Fe_3O_4 nanoparticles in the presence of CuNW in epoxy composites enhances the EMI shielding performance of the composites. It can also be seen from Fig. 4.6(a) that the epoxy composites containing both the particles, i.e., CuNW and $Fe_3O_4,$ exhibited higher EMI shielding effectiveness values when compared to the sum of SE_T values of composites containing equivalent filler loadings of only CuNW or Fe_3O_4. This suggested that the increase SE_T value of the non-hybrid sample is due to the synergistic effect between the particles.

The increased EMI shielding in composites containing hybrid nanoparticles can be attributed to the coexistence of magnetic and dielectric loss, and the interfacial polarization loss makes the better attenuation of microwaves. In the Fe_3O_4 nanoparticles are added along with the CuNW, which enhances the dielectric losses due to interfacial polarization effects between the Fe_3O_4 and

CuNW. In addition, the CuNW acts as a center for a dielectric polarization, thereby improving dielectric loss and a good impedance match. Similarly, the Fe_3O_4 serves as a center for magnetic dipole, resulting in increasing the magnetic loss. This further suggests that Fe_3O_4 content in the hybrid influences its EMI shielding capability in the composites. In contrast, the non-hybrid samples have exhibited marginally higher SE_R values than epoxy composites containing 12 wt% CuNW. Furthermore, the composites were demonstrated higher SE_A values than those SE_R values. The non-hybrid samples demonstrated higher SE_A values compared to epoxy composites containing 12 wt% CuNW. This suggested that a significant increase in absorption capability was observed over a physically mixed composite containing Fe_3O_4 and CuNW. Similar observations were reported in the literature [292]. The results suggested that the composites exhibited an absorption-dominant shielding mechanism.
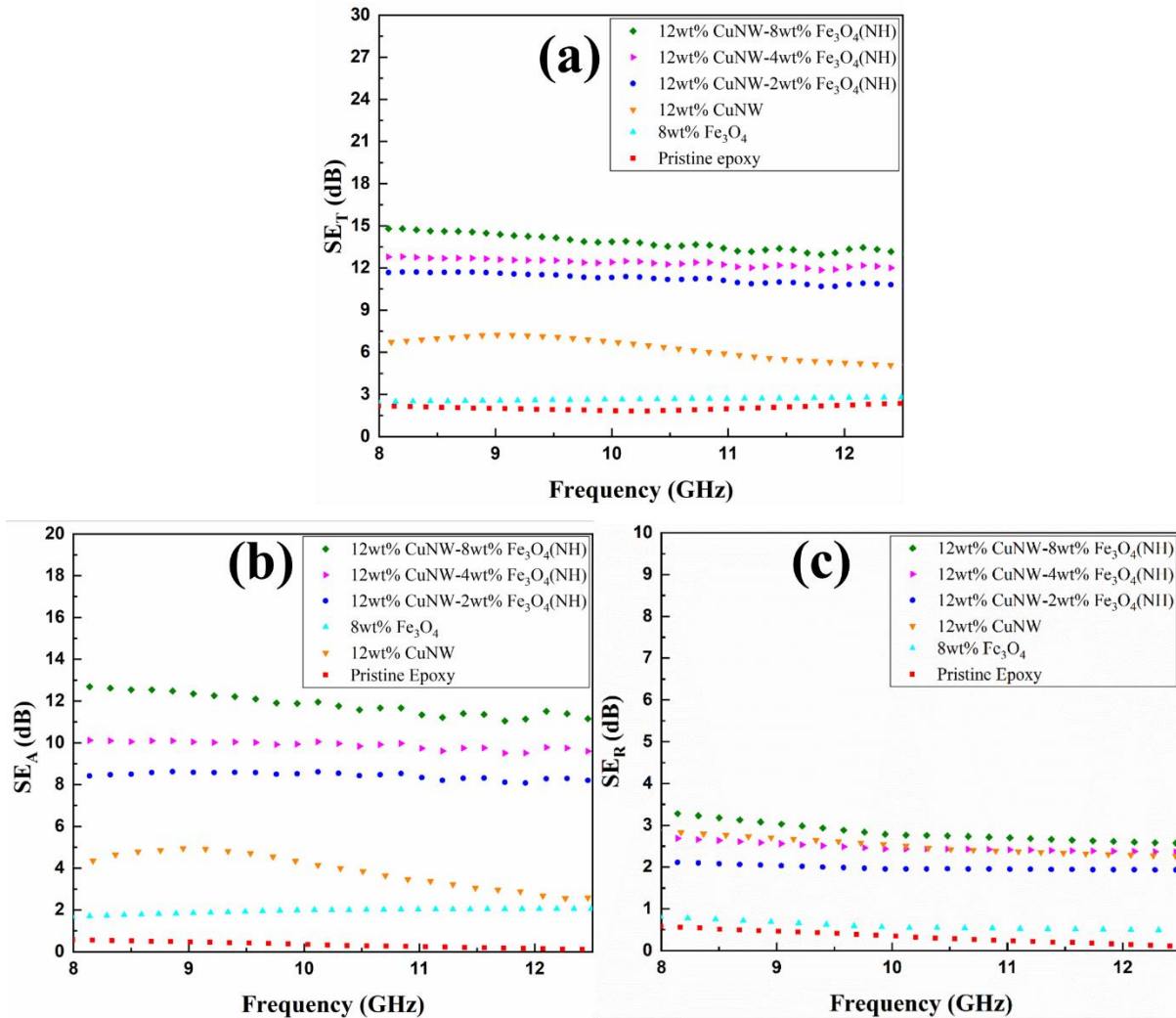
Fig.4.6.(a) (a) SE_T (b) SE_A, (c) SE_R values of CuNW-epoxy composites containing Fe_3O_4 particles as a function of frequency.

4.2.2.6 Complex permeability and permittivity of epoxy composites

To further investigate the dielectric and magnetic losses of epoxy composites, complex permittivity, and permeability were calculated using the NRW method in the X-band frequency range of 8-12.4 GHz. The complex permittivity values (i.e., ε' and ε'') of non-hybrid composites were shown in Fig.4.7. It can be observed from Fig. 4.7(a) that ε' values of the composites were increased with the addition of the Fe_3O_4 filler loadings. It can be observed that non-hybrid samples demonstrated a higher ε' value than epoxy composite containing 12 wt% of CuNW. The pristine

epoxy composite has demonstrated the ε' value of 3.5. This is attributed to the insulative nature of the epoxy matrix. The C12F8D non-hybrid sample has demonstrated 52% higher than the epoxy composite. In addition, ε'' values of the composites were increased with the addition of the Fe_3O_4 filler loadings and demonstrated a similar trend with the frequency. The ε'' value of the pristine epoxy has demonstrated the lowest value of 0.1. The non-hybrid composites exhibited higher ε'' values as compared to an epoxy composite containing 12wt% CuNW. These ε'' values of the composites are attributed to the formation of interface polarization among CuNW and Fe_3O_4, and epoxy, thereby increasing the dielectric losses of the composite. Thus, strong attenuation of the EM wave in the composite can be achievable.
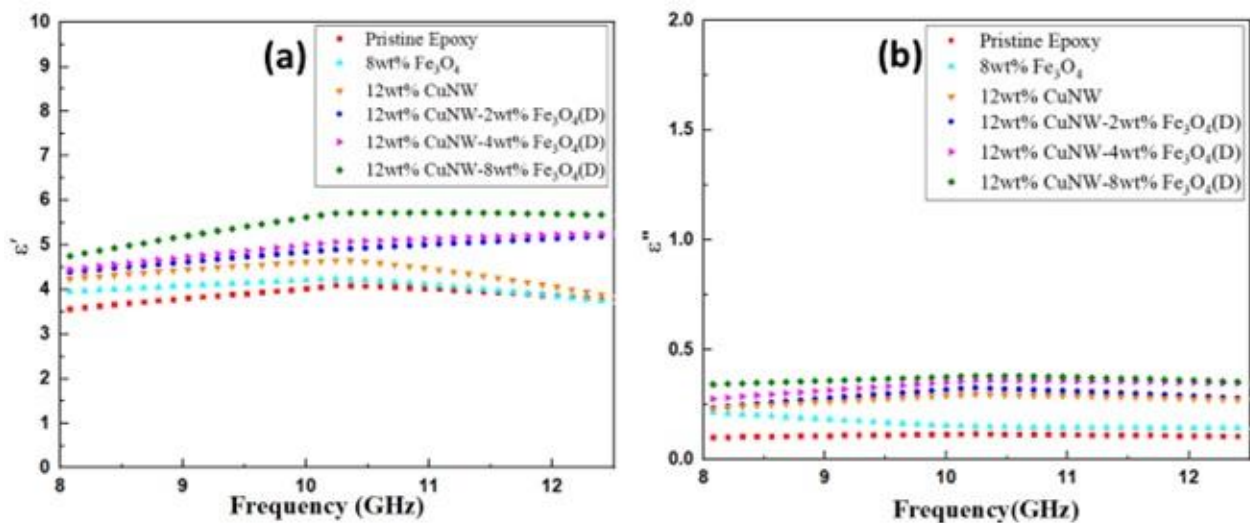
Fig.4.7. The plot of (a) ε' and (b) ε'' of CuNW- Fe_3O_4- epoxy composites as a function of frequency

Furthermore, the permeability (i.e., μ' and μ'') of epoxy composites in the X-band frequency range of 8-12.4 GHz, as shown in Fig.4.8. It can be observed that the μ' values of the epoxy composites were increased with the addition of the Fe_3O_4 filler loadings and demonstrated a similar trend with the frequency. The μ' and μ'' values of the pristine epoxy sample exhibited are 0.52 and 0.5, respectively, which are the lowest values compared to all other composites. This suggested that

the epoxy exhibited low magnetic loss to the incident EM wave. It can be observed from Fig.4.8 that for the composites containing Fe_3O_4, the μ' value of 1 and the μ'' value of 0.6, which indicates that Fe_3O_4 has a reasonable magnetic loss. Furthermore, the non-hybrid composites demonstrated better values of μ' as compared to an epoxy composite containing only Fe_3O_4 or CuNW. The results suggested that the addition of Fe_3O_4 to CuNW-epoxy composites helped in the enhancement of μ' values for the composites. The Cu12F8D sample exhibited higher μ' values compared to all other epoxy composites. Furthermore, μ'' values of the non-hybrid samples exhibited higher than epoxy composites containing 8wt% of Fe_3O_4. This suggested that non-hybrid composites formed a higher magnetic loss than epoxy composites containing 8wt% of Fe_3O_4. It can imply that the addition of Fe_3O_4 particles enhances magnetic loss, which plays an essential role in absorbing EM waves. It can be observed from the results that the dielectric loss values of the nanocomposites are more than their magnetic loss values. Therefore, the main contributor to the shielding performance of the composites is a dielectric loss rather than a magnetic loss.
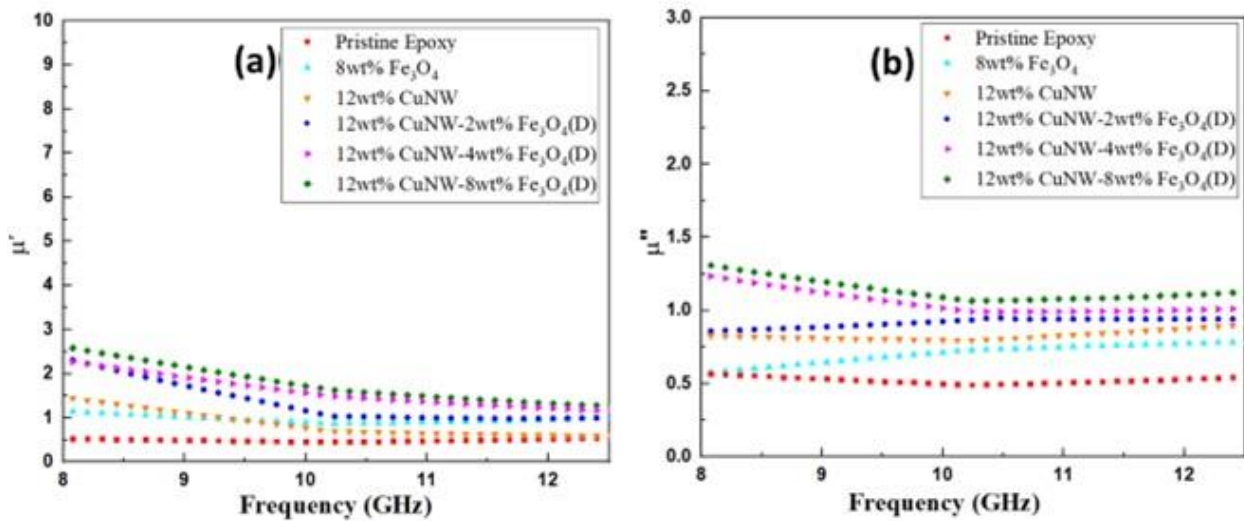
Fig.4.8. The plot of (a) ε' and (b) ε'' of CuNW- Fe_3O_4- epoxy composites as a function of frequency

4.3 Influence of Barium Hexaferrite nanoparticles for enhancing the EMI shielding performance of GNP/epoxy nanocomposites

4.3.1 Materials and methods

4.3.1.1 Materials

Graphene nanoplatelets (GNP) were purchased from Sigma Aldrich (Bengaluru, Karnataka). Barium nitrate (purity of 98%) and Iron (III) nitrate nonahydrate (98%) were purchased from Molychem (Mumbai, Maharashtra). Sodium hydroxide was procured from Glaxo Laboratories (Mumbai, Maharashtra). Liquid epoxy resin Araldite® CY230 and hardener Aradur® HY-951 were procured from Huntsman (Mumbai, Maharashtra).

4.3.1.2 Synthesis of Barium hexaferrite nanoparticles

The procedure for the synthesis of barium ferrite nanoparticles (BaM) is shown in Fig.4.9. BaM ($BaFe_{12}O_{19}$) nanoparticles were prepared by the co-precipitation method. Firstly, the salt solution was prepared by dissolving stoichiometric amounts of Iron(III) nitrate nonahydrate, and barium nitrate in millipore water and stored in a conical flask. The solution was kept under continuous mixing using a magnetic stirrer for 3 hours at 80 °C. The stoichiometric ratio of Ba^{2+}:Fe^{3+} in the solution was maintained as 1:12 based on the reported literature [293]. The sodium hydroxide solution was added to the reaction mixture drop-wise at a specific flow rate of 0.5 mL/ min under vigorous stirring for 1 hour at 80 °C to form a viscous solution. Subsequently, a highly viscous product was obtained, and the suspended BaM particles in the solution were separated using a CPR 24 centrifuge (REMI Compufuge, India) operated at 10000 RPM for 10 minutes. The sediment was washed several times with millipore water and dried at 60 °C for 1 hour. Then, the sediment was calcined in a muffle furnace for 3 h at 900 °C to obtain the final product of BaM particles. The calcined BaM particles were stored in air-tight containers before using them for composite preparation.

4.3.1.3 Preparation of Epoxy Nanocomposite

The nanocomposites were prepared by incorporating the necessary quantity of GNP and/or BaM fillers in the epoxy using an ARE-250 planetary resin mixer (Thinky Corporation, Japan) for 12 minutes. Then, the epoxy mixture was sonicated in an ultrasonic liquid processor (Johnson Plastosonic, Pune) operated for 10 minutes at 20 kHz and 250 W to enable good dispersion of the GNP and/or BaM fillers in the epoxy matrix [280]. Afterward, the necessary quantity of hardener was added, and the resin mixture was well mixed in an ARE-250 planetary resin mixer (Thinky Corporation, Japan)) for 8 minutes to facilitate well mixing of the hardener and then degassed in a vacuum degassing chamber. After degassing, the mixture was cast in a glass mold and cured at room temperature for 12 hours. The nanocomposite's thickness of 1 mm was measured and controlled by the dimensions of the mold. The composition of the composites utilized in this work is listed in Table 4.2.

Table 4.2. The composition of composites used in this study

Sample code	GNP (wt%)	BaM (wt%)	Epoxy (wt%)
Pristine epoxy	0	0	100
G4B8	4	8	88
G6B8	6	8	86
G8B8	8	8	84
G10B8	10	8	82
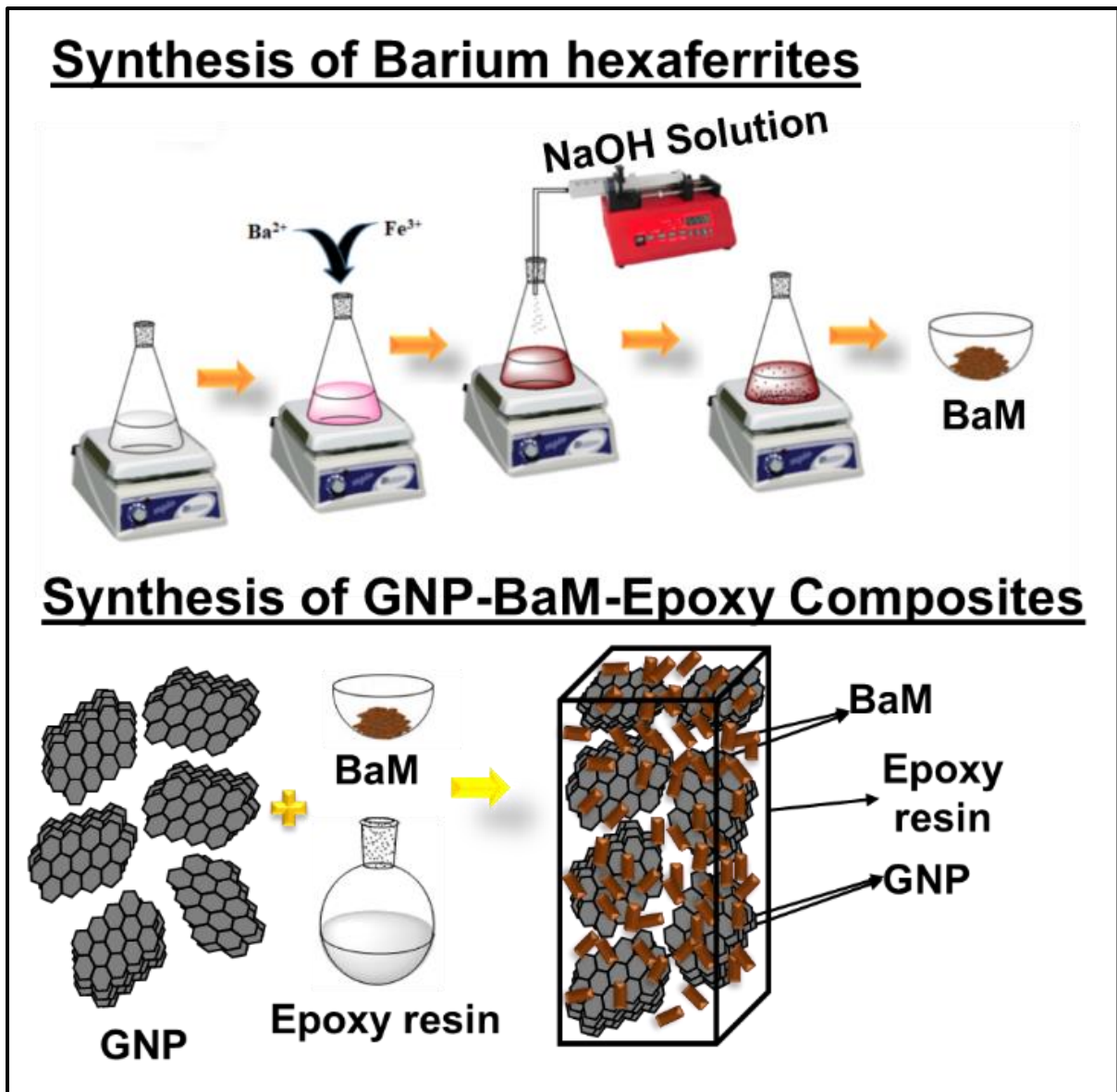
Fig.4.9. Schematic diagram of the synthesis of barium hexaferrites and preparation of epoxy composites containing GNP and BaM.

4.3.2 Results and discussion

4.3.2.1 XRD characterization of BaM and GNP

To investigate the crystallographic phases, present in the synthesized barium hexaferrite nanoparticles, X-ray powder diffraction was performed, and the results are shown in Fig.4.10. It can be observed from Fig.4.10 that all XRD peaks obtained from the nanoparticle powder matched well with the standard peaks of BaM as per JCPDS #84–0757, which confirms the successful

formation of BaM nanoparticles. The prominent peaks were observed at 2θ values of 32.32° and 34.17°, which corresponds to (107) and (114) planes suggesting that BaM particles were oriented towards the c-axis [267]. It can also be seen that all the prominent peaks in Fig.4.10 are broad. The average crystallite size of 37.2 nm was calculated using the Scherrer equation employing the peak corresponding to the (114) plane, which suggests that synthesized BaM particles have a nanocrystalline microstructure. Furthermore, no additional peaks were recorded in the XRD patterns, which suggested that the synthesized product contains pure BaM without any impurities. Moreover, in the XRD spectra of GNP, the peak corresponding to the 2θ value of 26.52° matched the characteristic peak of graphene as per JCPDS #75–1621. Additionally, the average crystallite size of GNP was calculated using Scherrer's equation by taking the value of K as 0.89 [267]. The peak corresponding to the (002) plane was chosen for the analysis, and the crystallite size was calculated as 29.5 nm [267]. These results suggest that the BaM and GNP particles exhibit a nanocrystalline microstructure.
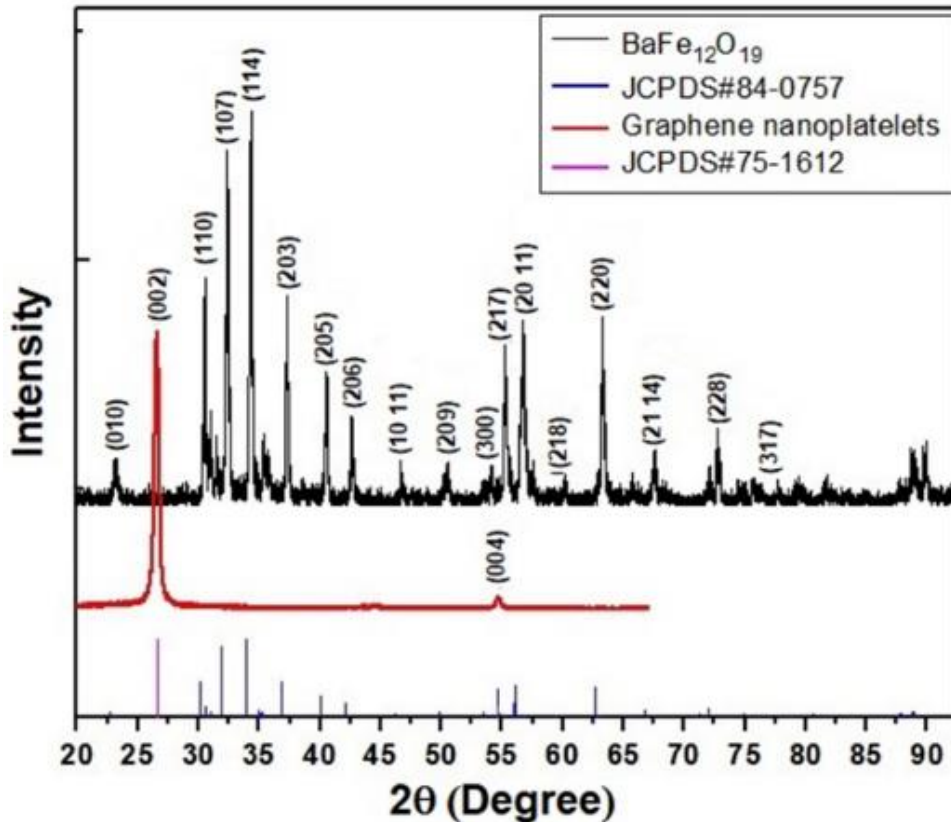
Fig.4.10 XRD patterns of (a) Barium hexaferrite (b) JCPDS of barium hexaferrite. (c) graphene

nanoplatelets (d) JCPDS of graphene nanoplatelets

4.3.2.2 SEM-EDS characterization of BaM and GNP

To further investigate the microstructure of the synthesized BaM nanoparticles and the GNP, SEM

was performed, and the results are shown in Fig.4.11. It can be seen from Fig.4.11(a) that the

synthesized BaM particles had a platelet-like morphology, and the particle size varies between

50.9–72.40 nm (Thickness), 112.3-153.3 nm (Width), 224-254 nm (Length). The plate-like

morphology observed in SEM images for BaM nanoparticles suggests that preferential growth

occurred in 2-directions, while minimal growth was observed in the perpendicular direction.

Similar results were obtained for BaM nanoparticles, where it was demonstrated that the growth

preferably occurs along with the a and b planes with minimum growth along the c-

axis.[267,270] To confirm the chemical composition of the BaM particles, EDS was performed,

and the results are shown in Fig.4.11(b). The observed Fe, Ba, and O peaks in the EDS spectra confirm the presence of these elements in the BaM nanoparticles. This further suggests that the synthesized nanoparticles do not contain any other impurities. Furthermore, the SEM micrograph of GNP nanoparticles is shown in Fig.4.11(c). It can be observed that GNP nanoparticles exhibit platelet-like morphology with smooth surfaces. To investigate the nanoparticle microstructure in the composites, SEM was performed on the freeze fractured cross-section of an epoxy composite containing BaM and GNP nanoparticles, and the result is shown in Fig.4.11(d). It can be observed that both GNP and BaM particles are well mixed and uniformly distributed in the composite, which suggests that good dispersion of the filler particles was achieved.
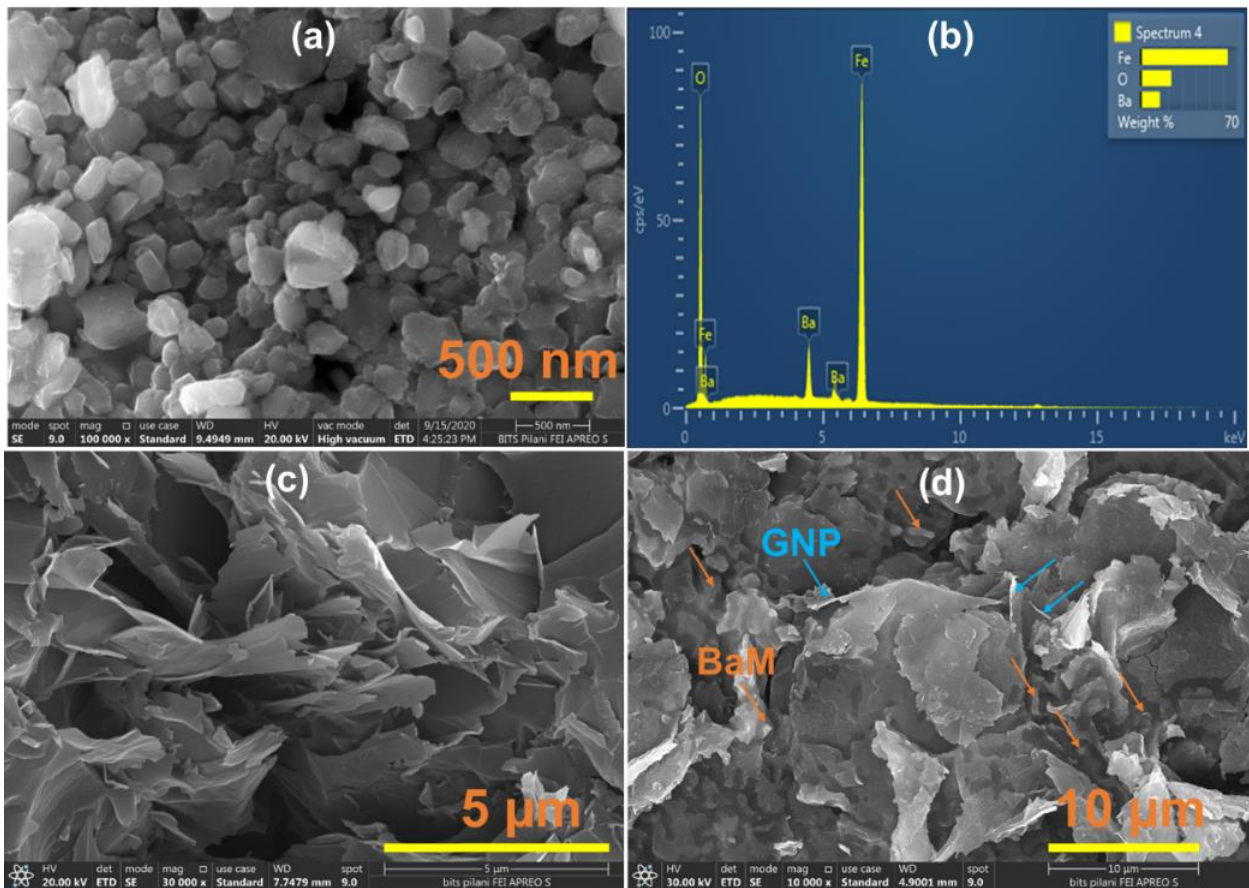
Fig.4.11. SEM micrographs of (a)Barium hexaferrite at a magnification of 100000 (b) EDS spectra of barium hexaferrite (c) Graphene nanoplatelets at a magnification of 30000 (d) epoxy composite containing BaM and GNP at a magnification of 10000

4.3.2.3   Electrical conductivity of epoxy composites

A good EMI shield should possess moderate electrical conductivity to allow good wave interaction. To probe the electrical properties of the nanocomposites, electrical conductivity measurements were carried out on samples in the frequency range of 20 Hz to 25 MHz, and the results are shown in Fig.4.12. It can be observed from Fig.4.12(a) that the pristine epoxy, B8, and G4B8 composites demonstrated a frequency-dependent electrical conductivity in the entire frequency range investigated, suggesting the dielectric nature of these materials [3,239]. However, the composites containing 10 wt% GNP alone or 8 wt% BaM along with GNP content greater than 4 wt% demonstrated frequency-independent electrical conductivity values in the low-frequency range. Such frequency-independent behavior in the low-frequency region is attributed to the formation of 3-D percolated networks in the composites [3,239]. Based on this reasoning, it is apt to deduce that percolated network of GNP was formed in these composites. It can be observed from Fig.4.12(b) that the electrical conductivity values of the composites at a frequency of 100 Hz were increased with the addition of GNP. The G10B8 composite demonstrated the highest conductivity of 5.13×10^{-4} S/m at 100 Hz among all the samples measured. Furthermore, the conductivity of the G10 composite at 100 Hz frequency was measured to be 2.42×10^{-6} S/m, which is two orders in magnitude less than that of the G10B8 sample. It should be noted here that both G10 and G10B8 samples contain equal loading of conductive fillers, i.e., GNP. The increase in the electrical conductivity with BaM addition could be attributed to synergistic effects due to which

efficient network formation of GNP occurs in the composite. Similar synergistic effects were exhibited in epoxy composites containing conductive and dielectric filler particles [271].

The percolation threshold (ϕ_c) for GNP epoxy composites was calculated using the classical percolation power law shown in Eq. (18) below.

$$\sigma = \sigma_o \, (\phi - \phi_c)^t \quad\text{..} (4.6)$$

Where σ refers to conductivity, ϕ refers to filler loading in volume percent, and t refers to the conductivity exponent [3,239]. The conductivity of the composites at a frequency of 100 Hz was used in the analysis. The value of the conductivity exponent t was determined to be 0.872 and was obtained by linear fitting of log-log plots of σ vs. ($\phi - \phi_c$), as shown in Fig.4.12(c). The percolation threshold for the epoxy composite containing 8 wt% BaM was found to be 4.21 wt% of GNP, which is significantly lower than that of epoxy composites containing only GNP (~8 wt%) [3,239]. Such lowering of the percolation threshold is attributed to better network formation in GNP in the presence of BaM.
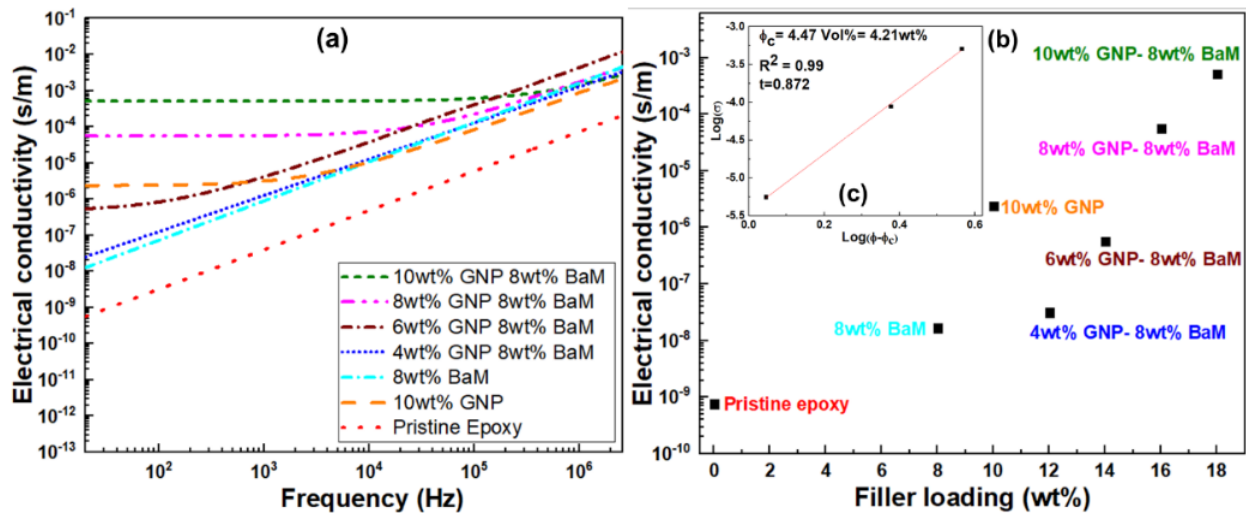
Fig.4.12 (a) The plot of electrical conductivity of epoxy composites containing GNP and BaM as a function of frequency (b) electrical conductivity values at 100 Hz of epoxy composites

containing GNP and BaM as a function filler loading(s) (c) Percolation power-law fitting of

electrical conductivity data.

4.3.2.4   EMI shielding effectiveness of epoxy composites

The EMI shielding effectiveness of the composites in the frequency range of 8-12.4 GHz was measured, and the results are shown in Fig.4.13. It can be seen that the pristine epoxy sample is transparent to EM waves and exhibits a very low SE_T value of 2 dB, which is attributed to the epoxy's electrically insulating and non-magnetic nature [3],[8]. Furthermore, the addition of 8 wt% of BaM nanoparticles to epoxy only marginally increases the SE_T to 2.6 dB. However, with the addition of 10 wt% of GNP in epoxy, a significant enhancement in shielding effectiveness is observed, and the composite exhibits a SE_T value of 7.5 dB, which corresponds to 87.2 % attenuation of incident power. The addition of GNP increases the electrical conductivity of the epoxy, which increases the SE_T values. It is known that composites should possess desirable electrical conductivity to demonstrate good EMI shielding effectiveness. These results also suggest that GNP are more effective in increasing the total EMI shielding performance as compared to BaM nanoparticles in the X-Band frequency range. It can also be seen from Fig.4.13(a) that composites containing both the particles (i.e., GNP and BaM) demonstrated higher EMI shielding effectiveness compared to the composites containing only GNP or BaM nanoparticles. This suggests that the addition of BaM nanoparticles enhances the EMI shielding effectiveness of GNP-epoxy composites. Furthermore, the EMI shielding effectiveness of composite having 10 wt% GNP was found to be 7.5 dB, and 8wt% BaM was found to be 2.6 dB. It is only reasonable to deduce from the rules of mixtures that a composite containing 10 wt% GNP and 8 wt% BaM should exhibit a shielding effectiveness value of 10.1 dB (i.e., 7.5 dB due to GNP and 2.6 dB due to BaM). However, the G10B8 composite sample, which contains a mixture of 10 wt% and 8 wt%

of GNP and BaM, respectively, exhibited an EMI shielding effectiveness value of 17.2 dB in the X-band, which is significantly greater than the anticipated value. The enhancement of EMI shielding in the composites containing both GNP and BaM may be attributed to a synergy between the GNP and BaM nanoparticles that facilitates better dispersion and efficient network formation of GNPs in the epoxy matrix. It is anticipated that better dispersion of GNP in the presence of the BaM would significantly enhance the GNP-epoxy interfacial area, thereby increasing the interfacial polarization losses. Additionally, the presence of BaM nanoparticles might enhance the magnetic losses in the composites, which further increases the total EMI shielding in the composites [3,262,276,294].

To further understand the EMI shielding mechanism, the shielding effectiveness by reflection (SE_R) and absorption (SE_A) of the composites were calculated, and the results are depicted in Fig. 4.13 (b and c). It can be observed that for all the composites, SE_A values are found to be higher compared to the SE_R values, which suggests that the shielding mechanism in the composites is absorption-dominated. Similar observations were made for epoxy composites containing other fillers [3,8,49],[277]. Furthermore, it can be seen from Fig.4.13(d) that SE_R and SE_A values in composites that contain both BaM and GNP nanoparticles depend on GNP content and increase with increasing the GNP content. For example, the composite G4B8 samples exhibited 2.5 dB and 5 dB of SE_R and SE_A values, respectively. Upon increasing the GNP content to 8 wt%, i.e., the G8B8 sample, the SE_R and SE_A values increased to 4.8 dB and 9.7 dB, respectively. However, with a further increase in the GNP content, i.e., in the G10B8 sample, the only marginal increase in the SE_R but a significant increase in the SE_A was observed. It can also be seen from Fig.4.13(d) that compared the SE_R, and SE_A appears to be more sensitive to the GNP content in the composites as the latter exhibits a greater change in its value with the addition of GNP. These results further

suggest that increasing the GNP content in BaM epoxy composites increase the absorption-dominated shielding mechanism in these materials.
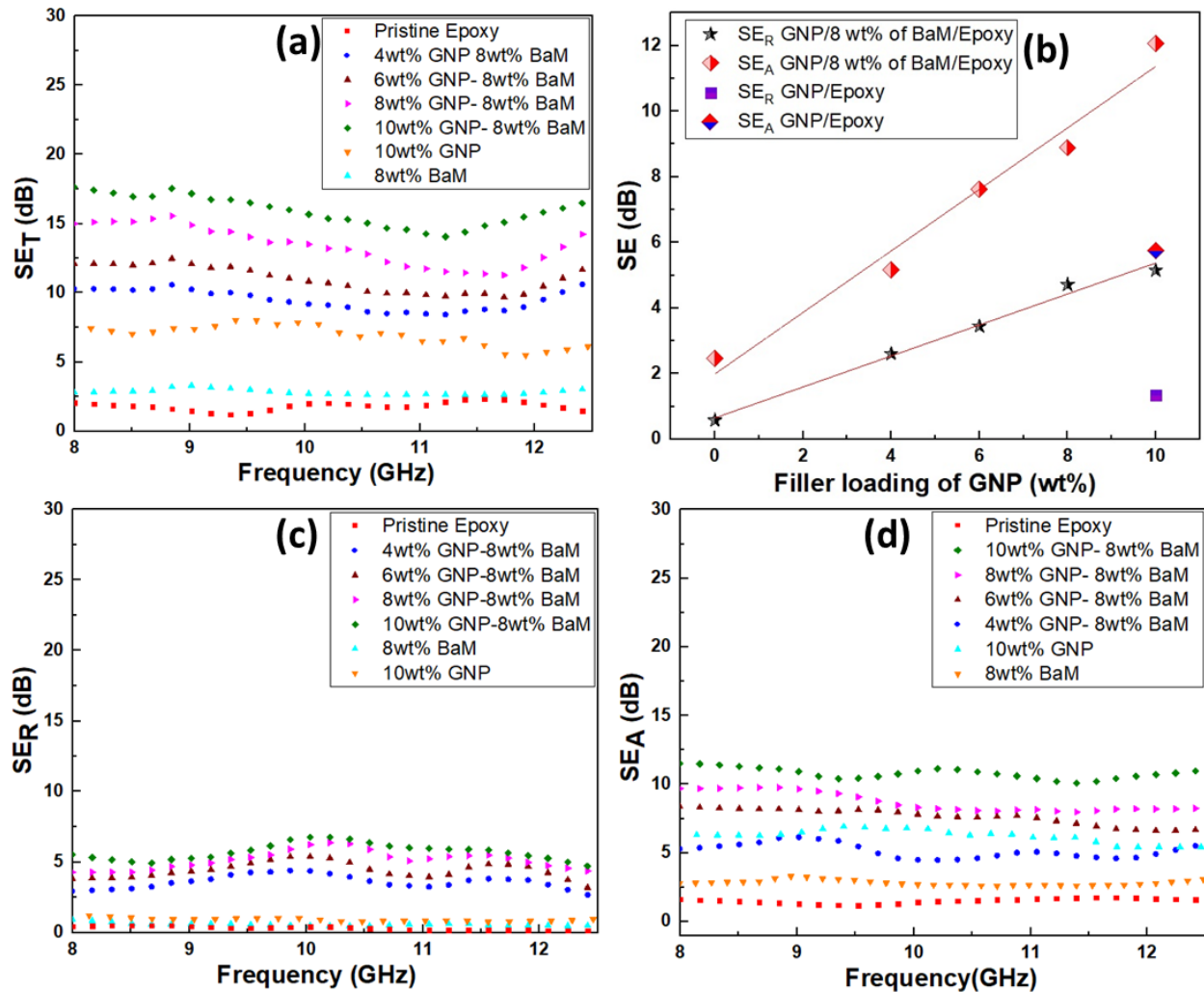
Fig.4.13 Plots of (a) SE_T, (b) average values of SE_R and SE_A, (c) SE_R, and (d) SE_A as a function of frequency for epoxy composites containing GNP and BaM.

4.3.2.5 The permittivity and permeability of epoxy composites

To investigate the magnetic and dielectric properties of the composites, the complex permeability (i.e., $\mu = \mu' - j\mu''$) and complex permittivity (i.e., $\varepsilon = \varepsilon' - j\varepsilon''$) using the NRW method in the X-band frequency range was calculated, and the results are shown in Fig.4.14. It can be seen from Fig.4.14 (a and b) that the pristine epoxy demonstrated an ε' and ε'' values of 3.6 and 0.5, respectively. The

B8 composite exhibited a marginally higher ε' and ε" values of 3.72 and 0.52, respectively. The G10 composite exhibited a significantly higher ε' (i.e., 4.3) and ε"(i.e., 0.7) compared to the pristine epoxy and B8 composite, suggesting its larger polarizability to the incident EM wave. Furthermore, it can also be observed that in composites containing both GNP and BaM, ε' and ε" values increased with increasing GNP content. These composites demonstrated lower ε" values as compared to the G10 composite. The results suggest that the addition of BaM to the epoxy composite containing GNP can reduce the interfacial area between GNP and epoxy, thereby marginally reducing the dielectric loss. However, the same composite demonstrated higher ε' values as compared to the G10 composite suggesting an increased energy storage capacity in the epoxy composites containing both GNP and BaM.

The μ' and μ" values of epoxy composites containing GNP and/or BaM over the 8–12 GHz frequency range are shown in Fig.4.14(c and d). It can be seen that the pristine epoxy sample exhibited a μ' and μ" value of 0.5 and 0.33, respectively, which is the lowest value compared to all other composites. Furthermore, the G10 composite also exhibited μ' and μ" values of only 0.7 and 0.34, respectively, which suggests that the pristine epoxy and G10 composites have low magnetic loss capability. However, the B8 composite exhibited μ' and μ" values of 1.1 and 0.51, respectively. Furthermore, it can be observed that both the μ' and μ" values in the BaM/epoxy composites increased with the addition of GNP. For example, the G10B8 epoxy composite yielded the highest μ' value of 2.5 and μ" value of 0.7 compared to all other composites. These results suggest that the addition of BaM to epoxy composites containing GNP increases its magnetic loss capability. Based on the permittivity and permeability results, it would be reasonable to deduce that the enhanced EMI shielding effectiveness observed in composites containing GNP and BaM is a consequence of good dielectric and magnetic losses in these materials. It is known that a good

EMI shielding material should have good complex permeability or permittivity, but these results indicated that an optimum combination of these properties could also be of significant interest.
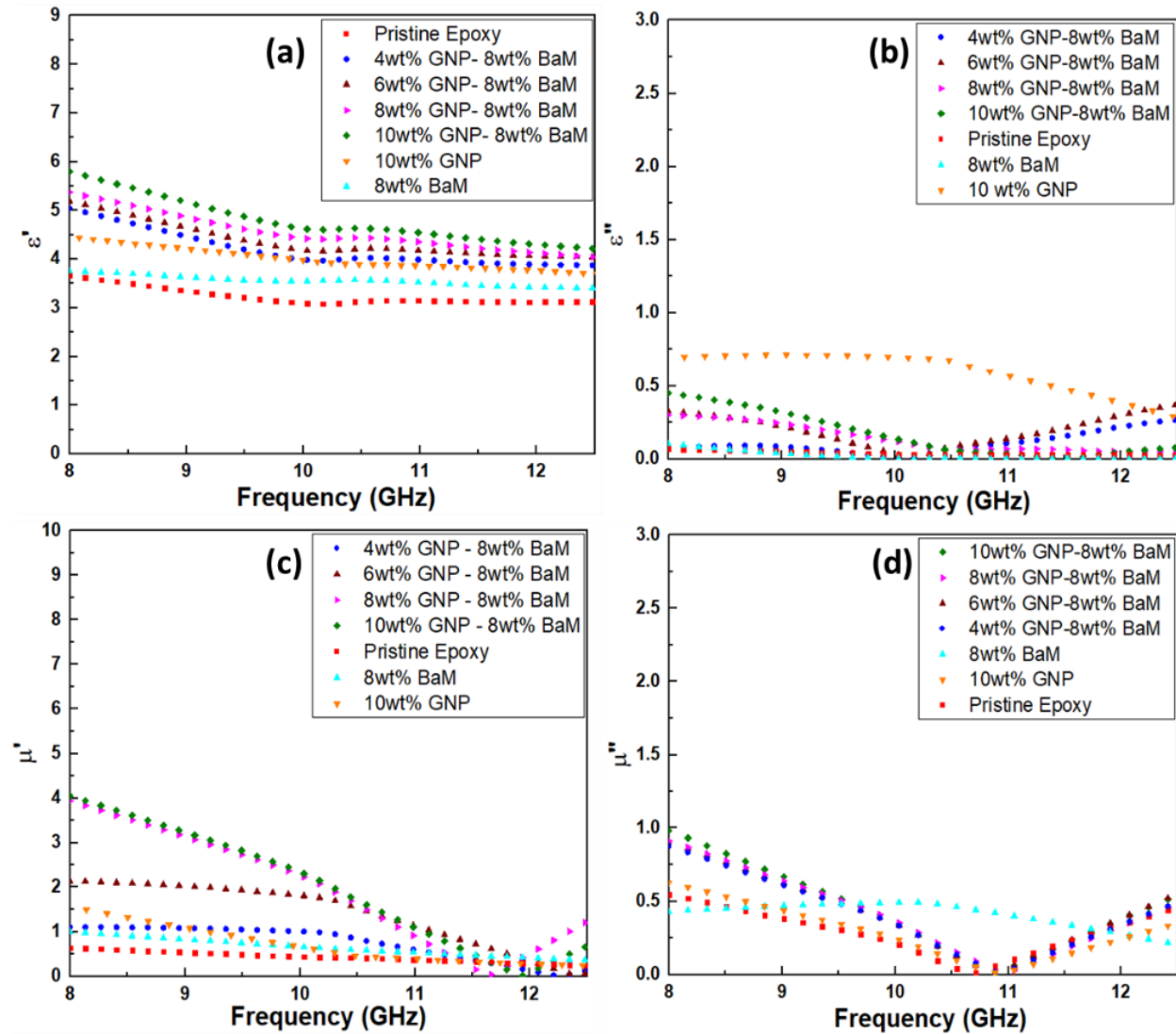
Fig.4.14 Plots of (a) ε′ (b) ε″ (c) μ′ (d) μ″ as a function of frequency for epoxy composites containing GNP and BaM.

Table 4.3. The following table contains the EMI shielding performance of various polymeric systems containing barium hexaferrite and different conductive fillers.

S.No	Polymer used	Filler used		Frequency range (GHz)	SE$_T$ value (dB)	Thick ness (mm)	Ref
		Conductive	Magnetic				
1	Wax	42wt% of polyaniline	8w% of barium hexaferrite	8-18	28.6	5	[295]
2	No polymer	10 parts of reduced graphene oxide	1 part of barium hexaferrite	12-18	15.5	1	[275]
3	Poly(ure thane)	2 wt% of thermally reduced graphene oxide	20 wt% of barium hexaferrite	0.1-20	40	4	[274]
4	Wax	42% of polyaniline	8wt% of barium hexaferrite	8-18	15-17.5	4	[296]
5	Poly(vin ylchlorid e)	7.5wt% of polypyrrole	10wt% of barium hexaferrite	0.1-20	88.5	0.5	[297]
6	Poly(thi ophene)		50wt% of barium hexaferrite	8-13	43.27	1	[298]

7	Poly(vinyl alcohol)	25wt% of carbon black	35wt% of barium hexaferrite	8-18	16.6-23.6	2	[299]
8	Natural rubber	20wt% of carbon black	20wt% of barium hexaferrite	0.1-12	43-70	1	[300]
9	Epoxy	10 wt% GNP	8 wt% barium hexaferrite	8-12.4	17.2	1	Present study

4.4 Influence of Fe_3O_4@Cunw Hybrid Nanoparticles on EMI Shielding Properties Of Epoxy Nanocomposites

4.4.1 Materials and methods

4.4.1.1 Materials

Liquid araldite® CY230 epoxy resin and aradur® HY-951 hardener were purchased from Huntsman Corporation (Mumbai, India). Cupric chloride dihydrate extra pure (ACS), ferrous chloride tetrahydrate (AR), ammonia solution extra pure (AR), dextrose extra pure (ACS), oleic acid extra pure (AR), ferric chloride anhydrous pure (AR), and oleyl amine pure (AR) were procured from Sisco research laboratories (Mumbai, India).

4.4.1.2 Synthesis of Fe_3O_4 @CuNW hybrid, Fe_3O_4 nanoparticles and CuNW

The Fe_3O_4@CuNW hybrid nanoparticles synthesis procedure is depicted in Fig.4.15. The hybrid particles were prepared through a facile water-based co-precipitation method. Firstly, an aqueous solution of iron salts was prepared by blending $FeCl_3$ and $FeCl_2.4H_2O$ at the stoichiometric ratio in the round bottom flask. The molar ratio of $Fe^{2+}:Fe^{3+}$ of 1:1.5 was maintained as per the literature [281,282]. The solution was stirred for 15 minutes to obtain a homogeneous mixture of iron salts. Afterward, a measured quantity of CuNW was mixed with the salt solution. A previous study reports a detailed description of the CuNW synthesis process [280]. Subsequently, the solution was stirred for 45 minutes with a magnetic stirrer at room temperature (RT). Afterward, ammonia solution (30 wt.%) was added at a 1 mL/min rate to the salt solution. The final solution was agitated for 30 minutes to complete the precipitation process. The final solution was centrifuged at 10000 rpm then the precipitate was separated. The residue was washed with ethanol and water. The obtained Fe_3O_4@CuNW hybrid was used for the preparation of nanocomposites.
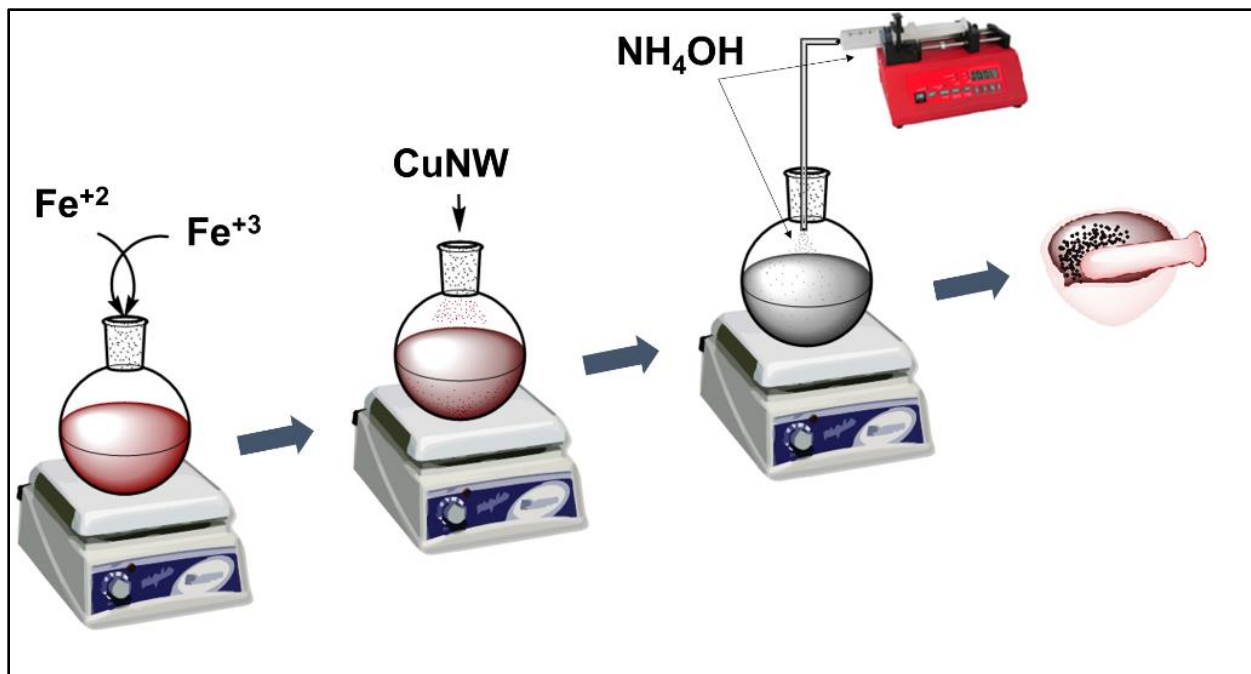
Fig.4.15. Schematic of preparation of Fe_3O_4@CuNW hybrid particles

4.4.1.3 Preparation of epoxy nanocomposites

The epoxy composite were prepared through the resin blending process [3,133,280]. The epoxy composites containing Fe_3O_4@CuNW hybrid structures were prepared by adding the necessary quantity of Fe_3O_4@CuNW hybrid content(s) in an epoxy resin using Thinky Mixer ARE-250 (Thinky, USA) for 14 minutes. Following that, the epoxy mixture was treated for 8 minutes in an ultrasonic liquid processor (Sonics & Materials, USA) set to 500 W and 20 kHz to ensure good distribution of the hybrid(s) in an epoxy. Afterward, the appropriate amount of hardener was mixed into the resin mixture and properly blended in Thinky Mixer for 4 minutes to ensure proper hardener mixing. The epoxy mixture was degassed in the degassing chamber, cast in a mould, and then cured at RT for a day. The composite's thickness was found to be one millimeter and regulated by the mould's dimensions. The epoxy composites used in this study are listed in Table 4.4.

Table 4. 4. The composition of the composites used in this study.

Filler	Composite Code	CuNW (wt%)	Fe_3O_4(wt%)
Pristine epoxy	PE	0	0
Fe_3O_4	F8	0	8
CuNW	Cu12	12	0
Fe_3O_4@CuNW hybrid	Cu12F2H	12	2
	Cu12F4H	12	4
	C12F8H	12	8

4.4.2 Results and Discussion

4.4.2.1   XRD characterization of Fe_3O_4 @CuNW hybrid, CuNW, and Fe_3O_4 particles

To identify crystallographic phases present in particles, X-ray diffraction (XRD) was performed on Fe_3O_4 @CuNW hybrid, CuNW, and Fe_3O_4 particles and patterns depicted in Fig.4.16. The Fe_3O_4 particles' XRD patterns were well matched with the standard peaks of Fe_3O_4 as per JCPDS #75-0033, confirming the Fe_3O_4 particles present in the synthesized powder sample. Furthermore, XRD patterns were relatively broad, which indicates the formation of fine nanoparticles. Similar results were also reported in the literature [281–284]. In the CuNW XRD patterns, a prominent peak at 2θ value of 43.3 º, is well-matched with standard peaks of copper according to JCPDS #03–1018. It is in good agreement with previously reported literature for CuNW [234,235,280,285,286]. Furthermore, the peaks corresponding to 2θ values of 43.3 ° and 50.5 ° in the XRD patterns of hybrid structures correspond with the standard peaks of copper, and the remaining peaks are well-matched with the standard peaks of Fe_3O_4 particles. The results suggested that both CuNW and Fe_3O_4 were present in hybrid structures. In addition, the average crystallite size of Fe_3O_4 nanoparticles present in the Fe_3O_4@CuNW hybrid structures

corresponding to the 2θ value of 36.56 ° was determined as 8.876 nm [301]. This indicates that Fe_3O_4 particles present in hybrid structures have a nanocrystalline microstructure.
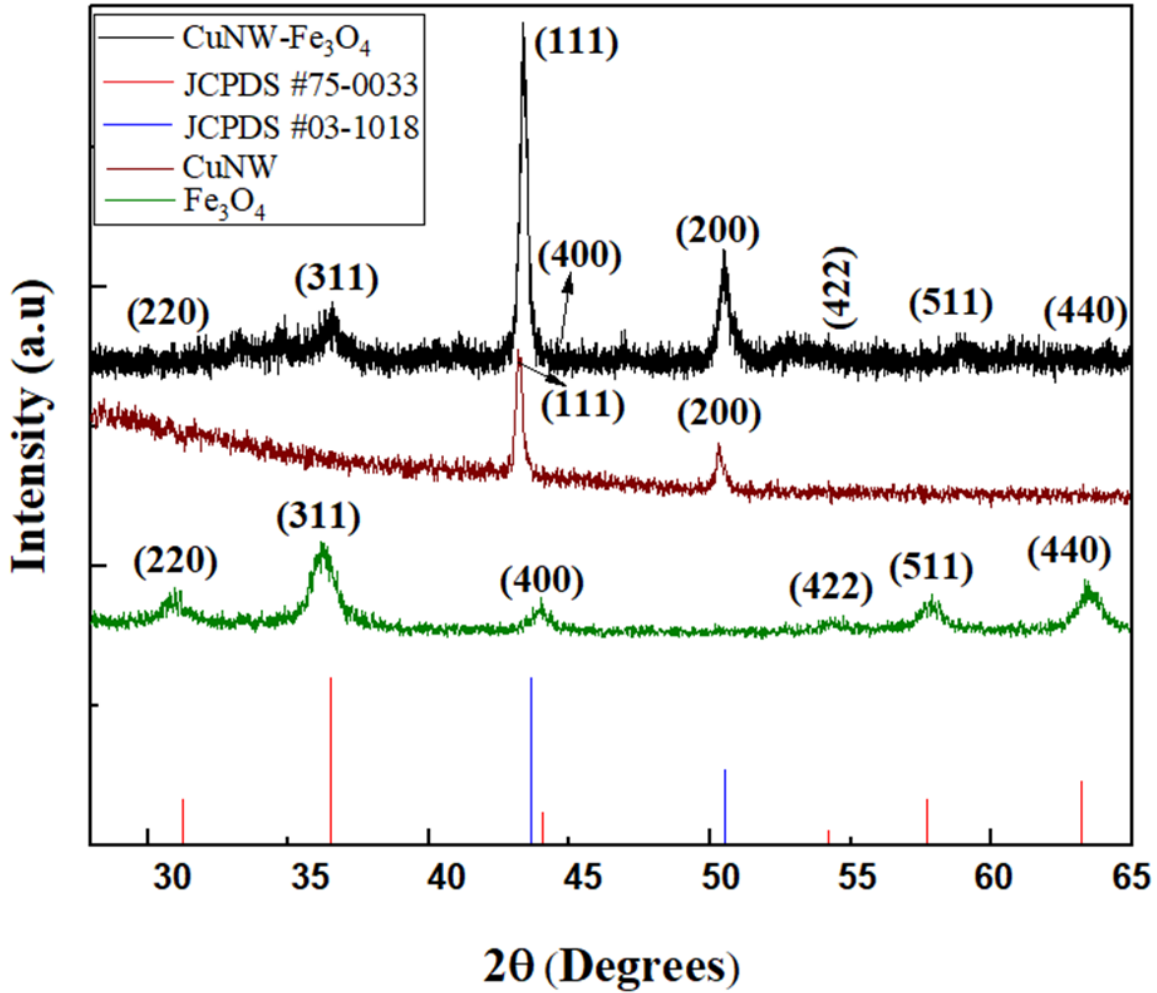
Fig.4.16. XRD spectra of (a) CuNW@Fe₃O₄ nanoparticles (b) Fe₃O₄ (c)CuNWalong with corresponding JCPDS of CuNW and Fe₃O₄.

4.4.2.2   SEM characterization of Fe₃O₄ @CuNW hybrid, CuNW, and Fe₃O₄ particles

To study the microstructure of synthesized particles, SEM analysis was performed on Fe_3O_4@CuNW hybrid, CuNW, and Fe_3O_4, as shown in Fig.4.17. The synthesized Fe_3O_4 particles have a spherical shape with an average diameter of 23 nm, as shown in Fig.4.17(a), which agrees well with the literature [3,284]. The CuNW exhibited smooth surfaces with wire-like morphology,

as depicted in Fig.4.17(b). However, as shown in Fig. 4.17(c), the surface of CuNW appears to contain many particles firmly anchored on its surface. It can be observed from Fig.4.17(d) that the EDS spectra obtained on the hybrid particles confirm the Fe and O elements present in the anchored particles. Based on the above observations, it is apt to deduce the Fe_3O_4 particles have been anchored at the CuNW surface in Fe_3O_4@CuNW hybrid nanoparticles. The cross-section SEM images of freeze fractured composite to investigate further the hybrid microstructure stability in the epoxy composite, as shown in Fig.4.17(e). It was clear from Fig.4.17(e) that the microstructure of hybrids was retained in the composites in spite of all the processing steps. This further suggests that the Fe_3O_4 nanoparticles are firmly deposited on the CuNW surfaces.
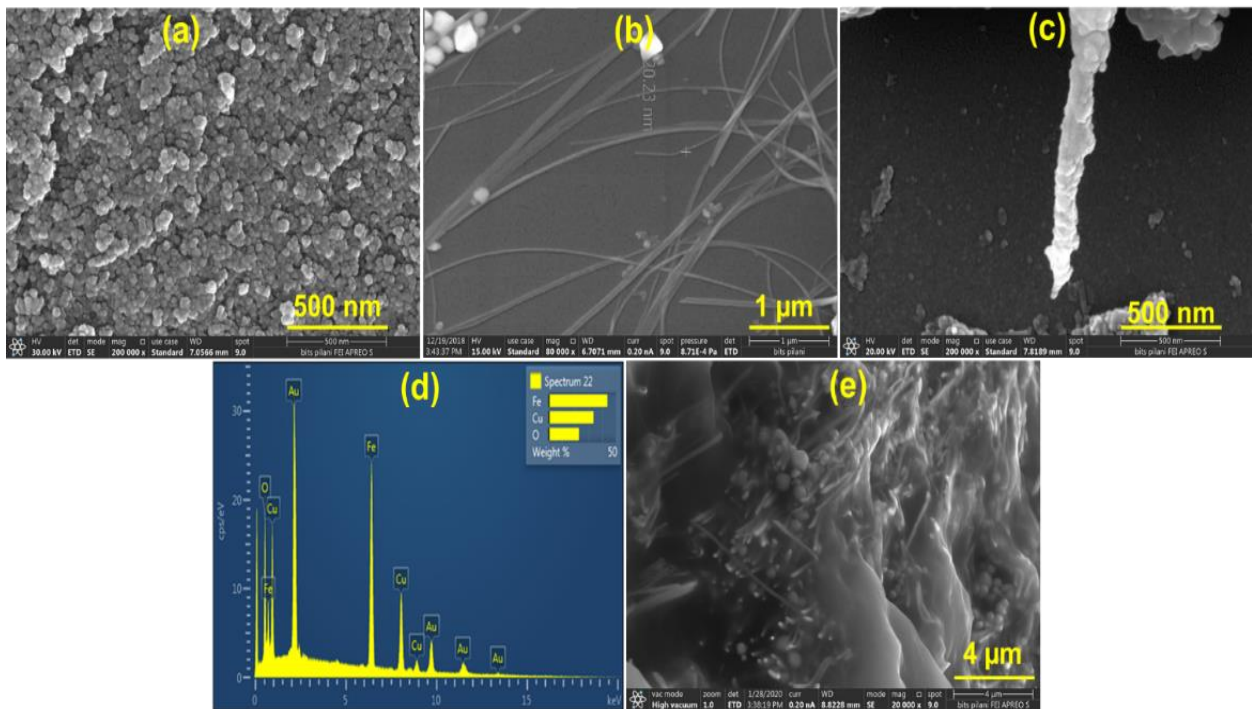
Fig.4.17. SEM images of (a) Fe_3O_4 nanoparticles (b) CuNW (c) Fe_3O_4@CuNW hybrid (d) EDS of Fe_3O_4@CuNW hybrid (e) SEM image of freeze fractured cross-section of Cu12F8H sample.

4.4.2.3 XPS characterization of epoxy composites

The wide scan XPS spectrum of hybrid and non-hybrid composites is shown in Fig. 4.18. The XPS data of composites confirms the presence of C1s, Cu2P, Fe2P, and O1s bands in the composites. It can be observed from Fig. 4.18 (e) and 4.4 (e) that O1s peak observed at 531.3 and 531.5 eV in Fig. 4.18 (e) and 4.4 (e), respectively, which were attributed to oxygen anion (O^{-2}) in Fe_3O_4. Similar observations were reported for the O1s band [287]. The C1s spectrum of composites has shown in Fig. 4.18 (b) and 4.4 (b). Both C1s bands are almost similar in the composites. The composites exhibited a C1s peak at 284.4 eV. Similar results were reported in the literature [288]. The deconvolution peaks of C1s were observed at 284.4 eV, 286.4 eV, and 287.8 eV containing main components of the epoxy matrix, corresponding to aromatic rings (C=C/C–C), epoxy and alkoxy (C–O), and C=O groups. Similar observations were reported [289]. The Cu2P spectrum of composites is shown in Fig. 4.18 (c) and 4.4(c). In hybrid composite, the peaks are observed at 933.6 and 953.5 eV, corresponding to Cu $2p_{3/2}$ and Cu $2p_{1/2}$, respectively. The non-hybrid composites exhibited the Cu2p peaks at 932.5 and 952.5 eV, corresponding to Cu $2p_{3/2}$ and Cu $2p_{1/2}$, respectively. Similar observations were reported for Cu2p bands [290]. Similarly, the Fe2p bands in hybrid composites are located at 709.8 eV and 722.5 eV corresponding to Fe $2p_{3/2}$ and Fe $2p_{1/2}$, respectively, in Fig. 4.18 (d). Similar results were reported for Fe_3O_4 hybrid structures [287]. In contrast, in Fig. 4.4 (d), the Fe2p peaks in non-hybrid composites located at 714.8 eV and 723.8 eV correspond to Fe $2p_{3/2}$ and Fe $2p_{1/2}$, respectively. There are no extra satellites observed in both Fe2p band, which confirms that the composite contains only Fe_3O_4 nanoparticles. There is a slight shift in the binding energy in both composites due to the formation of hybrid structures of CuNW and Fe_3O_4 particles. Similar studies reported the peak shift of bands in the literature due to the formation of hybrid structures [289].
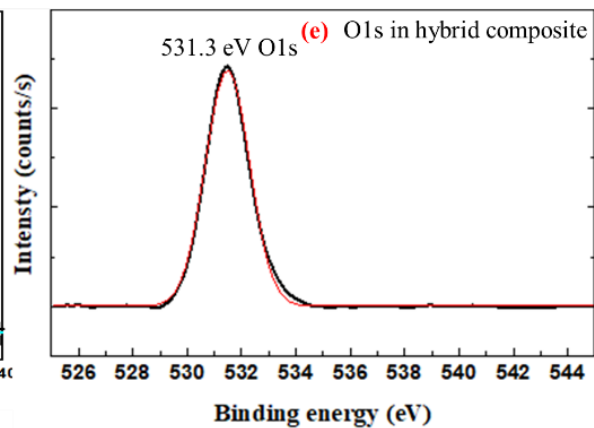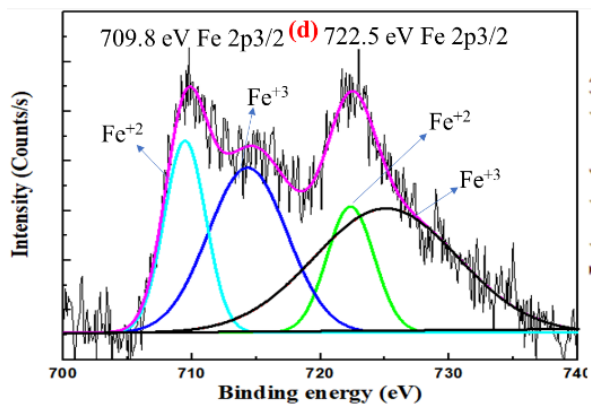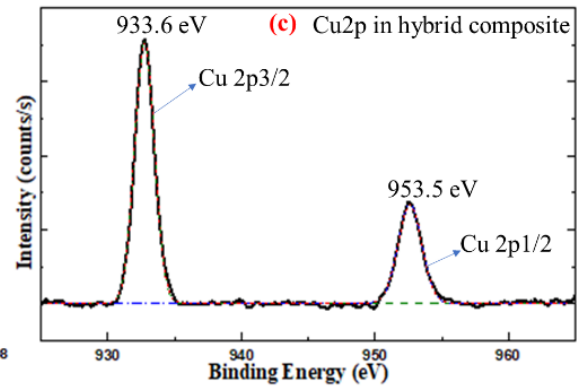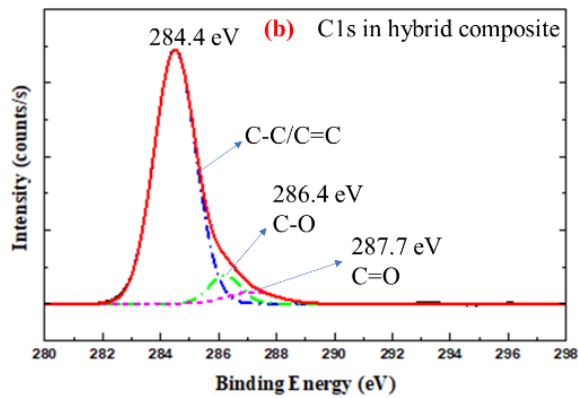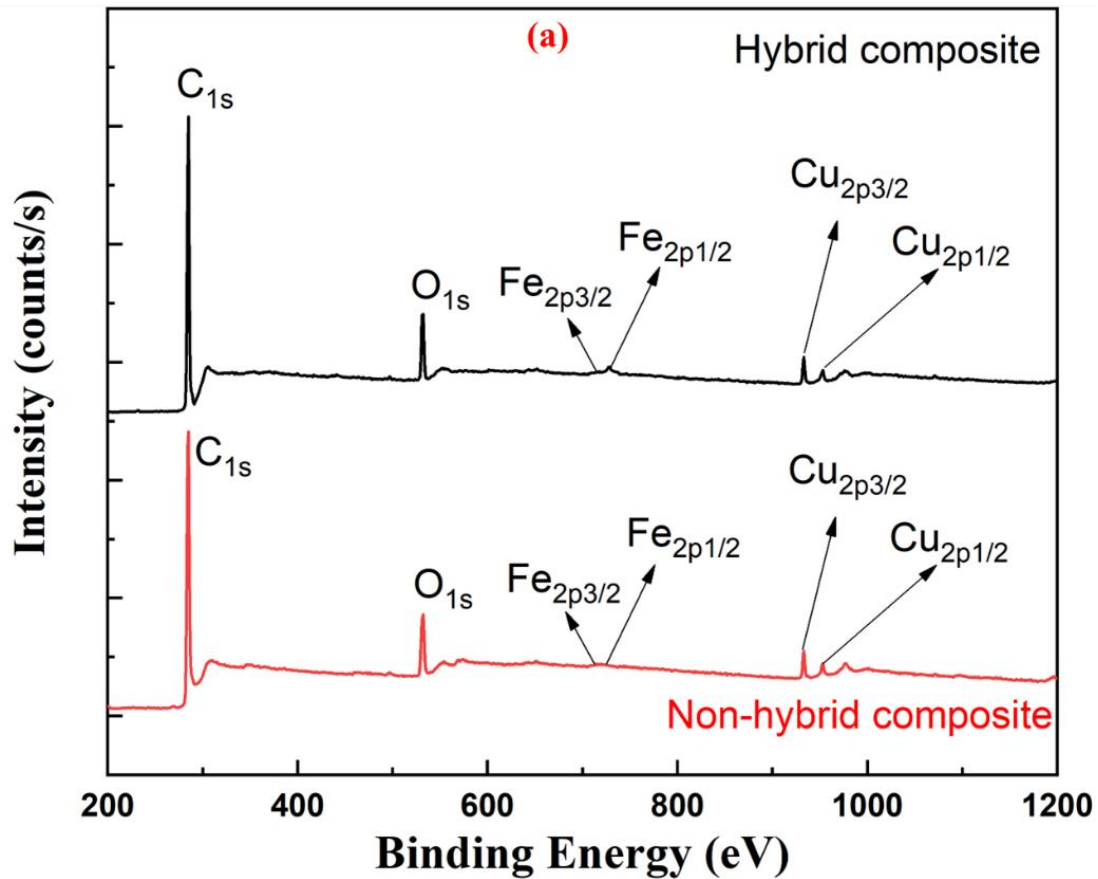
Fig.4.18. The XPS spectra of (a) hybrid and non-hybrid composites (b) C1s (c) Cu2P (d)Fe2P (e) O1s of hybrid composites

4.4.2.4   Electrical conductivity of epoxy composites

To further characterize the electrical characteristics of the epoxy composites, the AC electrical conductivity measurements over the 25 Hz to 25 MHz frequency range were performed on epoxy composites, as shown in Fig.4.19. Among all the composites, only samples Cu12 and Cu12F8NH demonstrated frequency-independent electrical conductivity in the 25 Hz – 1 kHz frequency range suggesting the formation of a percolated network of CuNW in these composites [3,133,239,280]. These samples contain a loading of 12 wt% of conductive filler (i.e., CuNW), which is above the percolation threshold limit reported for CuNW-polymer composites [280]. However, in stark contrast, the composites containing hybrid filler (i.e., Fe_3O_4@CuNW) across the frequency range exhibited a frequency-dependent conductivity, suggesting a non-percolated microstructure in these composites. This can be ascribed to the existence of Fe_3O_4 nanoparticles on the CuNW surface in the hybrid structures that degrade the electrical networking between the nanowires and hinders electron transport [128]. Similar observations were also reported in the literature for other particulate systems [302]. Based on the above observation, it is only reasonable to deduce that the hybrid microstructure of Fe_3O_4@CuNW nanoparticles is largely preserved in the epoxy composites. It can also be observed that the sample Cu12F8NH exhibited a significantly higher electrical conductivity value than Cu12 nanocomposite, although both samples contained 12 wt% CuNW content. This suggests that the presence of Fe_3O_4 nanoparticles in Cu12F8NH enables the formation of efficient CuNW networks in these composites. Similar observations were made where

the presence of dielectric particles significantly enhanced the electrical conductivity of CPC [3,133,302].
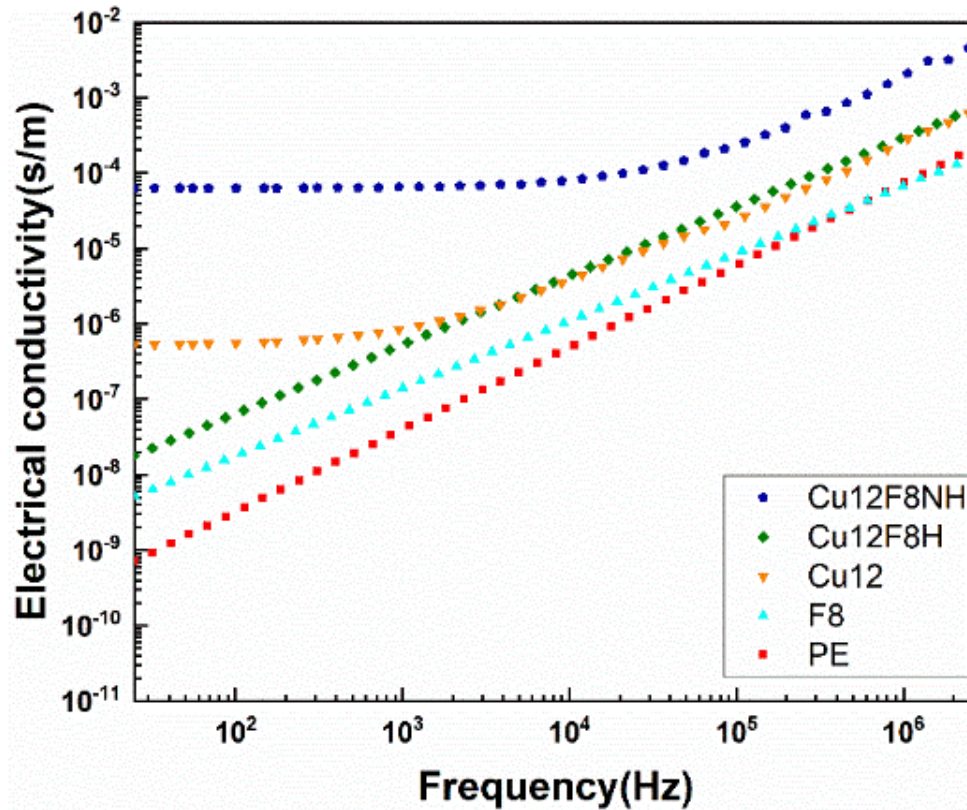
Fig.4.19. Electrical conductivity values of epoxy composites containing CuNW and/or Fe_3O_4 as a function of frequency.

4.4.2.5   EMI shielding effectiveness of epoxy composites.

The EMI shielding effectiveness of the epoxy composites containing CuNW and/or Fe_3O_4 and Fe_3O_4@CuNW hybrid structures over the X-band in the frequency range of 8-12.4 GHz was determined, and the results are shown in Fig. 4.20. It can be observed from Fig. 4.20(a) that the pristine epoxy sample exhibited a very low shielding effectiveness value of 1.7 dB. This is attributed to the electrically insulating and non-magnetic nature of the epoxy matrix, which renders it transparent to EM waves [3]. The addition of 8 wt% of Fe_3O_4 nanoparticles to epoxy marginally increased its total EMI shielding effectiveness (SE_T) to 2.5 dB in the X-band frequency range. In

contrast, the addition of 12 wt% CuNW to the epoxy matrix increases the total shielding effectiveness 3 times more than neat epoxy. These results suggest that CuNW is more effective in improving the EMI shielding performance as compared to Fe_3O_4.

In contrast, composites containing Fe_3O_4@CuNW hybrid nanoparticles exhibit Fe_3O_4 filler content-dependent EMI shielding effectiveness. In particular, the sample Cu12F8H, which contained a hybrid nanoparticle having Fe_3O_4: CuNW in the weight ratio of 8:12, exhibited the highest SE_T value of 19.1 dB in the X band frequency range. It should be noted here that the total filler loading in the hybrid composite sample Cu12F8H was 20 wt%, which is equivalent to having 12 wt% Cu and 8 wt% of Fe_3O_4 in the composite. However, it should be recalled here that the EMI shielding effectiveness of Cu12F8D composite was found to be 14.6 dB in the X-band frequency range, which is lower than the hybrid sample. This suggests that the hybrid nanoparticles containing equivalent loading of fillers were better than the direct mixing of fillers for enhancing EMI shielding effectiveness in composites.

The increased EMI shielding in composites containing hybrid nanoparticles can be attributed to the combined effects of multiple interfacial polarization coupled with the magnetic losses arising due to the presence of Fe_3O_4 nanoparticles. It can be observed that Fe_3O_4 nanoparticles are firmly anchored to the CuNW surfaces. This anchoring of Fe_3O_4 on the CuNW surface enhances the dielectric losses due to interfacial polarization effects between the Fe_3O_4 and CuNW. It should be noted here that the hybrid samples Cu12F2H and Cu12F4H exhibited lower SE_T values as compared to Cu12F8H. This further suggests that Fe_3O_4 content in the hybrid influences its EMI shielding capability in the composites. This may be attributed to reduced interfacial polarization losses in Cu12F2H samples due to the low Fe_3O_4 content in the hybrids as compared to Cu12F8H. However, with the higher loadings of Fe_3O_4 contents in the hybrids, there may be an agglomeration

of nanoparticles, impacting proper filler dispersion and shielding performance. This further suggests an optimum loading of Fe_3O_4 on the CuNW, which is beneficial for increasing the EMI shielding performance. Furthermore, it can be observed from Fig.4.20 that the hybrid composites have exhibited lower SE_R values than epoxy composites containing 12 wt% CuNW.
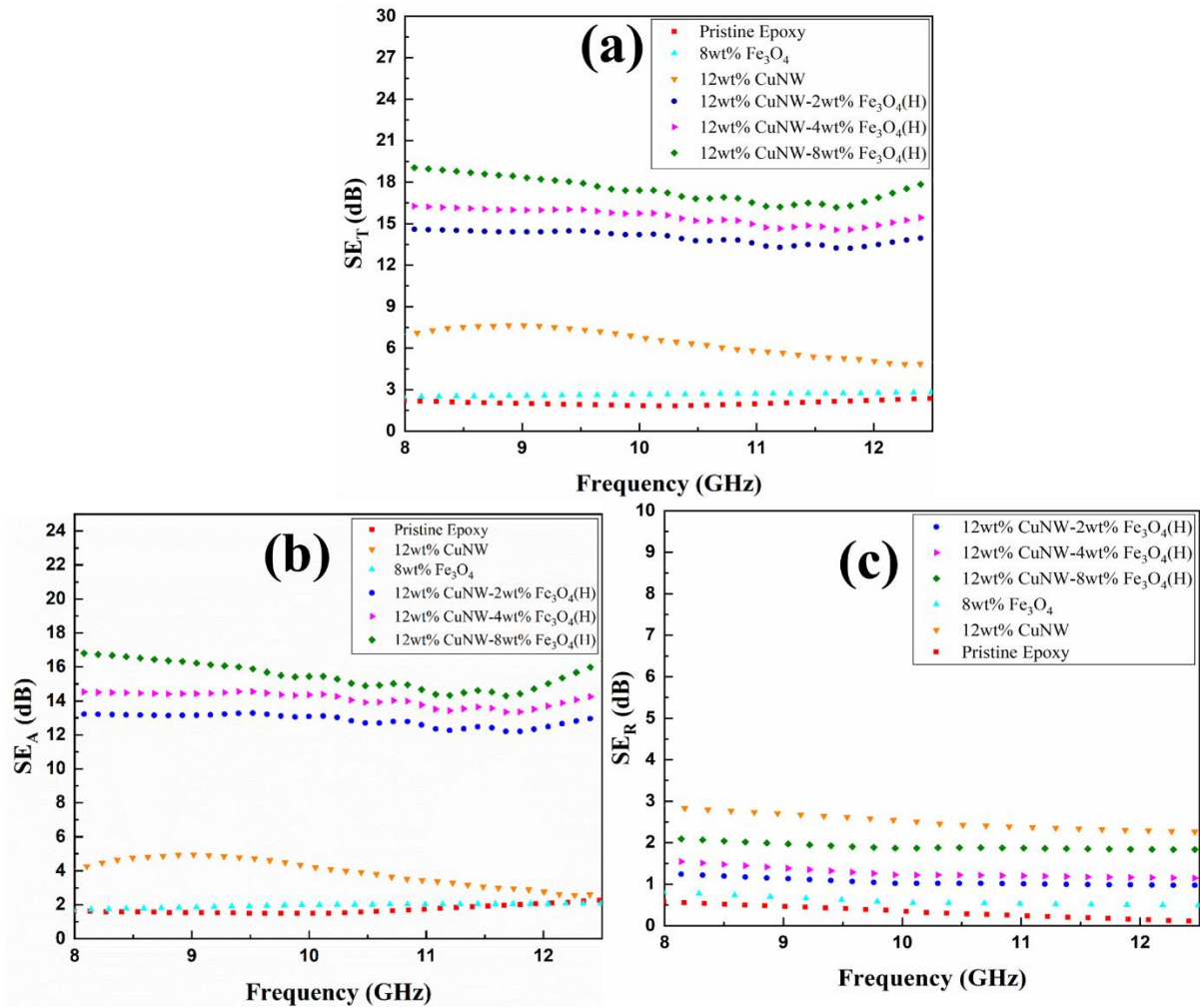
Fig.4. 20. (a) SE_T (b) SE_A, (c) SE_R values of Fe_3O_4@CuNW hybrid epoxy composites as a function of frequency

It can be recalled from chapter 4.1 that the non-hybrid samples have exhibited marginally higher SE_R values than epoxy composites containing 12 wt% CuNW. This further suggests the composites containing hybrid nanoparticle(s) demonstrated lower reflection loss than non-hybrid

samples. In contrast, the composites were demonstrated higher SE_A values than those SE_R values. The non-hybrid samples demonstrated higher SE_A values compared to epoxy composites containing 12 wt% CuNW. This suggested that a significant increase in absorption capability was observed over a physically mixed composite containing Fe_3O_4 and CuNW. Similar observations were reported in the literature [292]. Furthermore, the hybrid samples demonstrated higher SE_A values than those of non-hybrid samples. This may be attributed to increasing EM wave absorption due to the unique hybrid structure. The results suggested that the composites exhibited an absorption-dominant shielding mechanism.

4.4.2.6 Complex permeability and permittivity of epoxy composites

To further study the magnetic and dielectric properties of epoxy composites, complex permeability and permittivity were determined using the NRW method in the X-band. The complex permittivity values (i.e., ε' and ε'') of hybrid and non-hybrid composites are depicted in Fig.4.21. It can be observed that the ε' values of the epoxy depend on the filler incorporated and increased with the addition of the filler content, as shown in Fig. 4.21 (a). The pristine epoxy composite demonstrated an ε' value of 3.5, which suggests an insulative nature of an epoxy matrix. The presence of 8 wt% Fe_3O_4 nanoparticles in epoxy marginally increased the ε' values in the frequency range of 8-10 GHz. However, the addition of 12 wt% CuNW (i.e., the Cu12 composite) significantly enhances the ε' values of the epoxy over the entire X-band frequency range suggesting strong interfacial polarization effects in the composite. It can also be observed that both the hybrid and non-hybrid composites demonstrated a higher ε' value compared to the Cu12 composite. Furthermore, the ε' values for the hybrid composites were found to be marginally higher than the non-hybrid composites suggesting greater polarizability of the former in the X-band.

The ε'' values, also shown in Fig.4.21(a), followed a similar trend with the frequency as observed for the ε' values of the epoxy composites. The pristine epoxy demonstrated the lowest value of 0.1 for ε'', and the hybrid composite Cu12F8H exhibited the highest ε'' values among all the composites investigated in this study. The interfacial polarization between nanofiller-epoxy interfaces contributes to the dielectric losses in the composite, which results in increased ε'' values. Based on the above, it can be deduced that the Fe_3O_4@CuNW filled composites offer higher interfacial polarization capability compared to non-hybrid composites containing equivalent loading of both these nanofillers.

The complex permeability (i.e., μ' and μ'') of epoxy composites in the X-band is shown in Fig.4.21(b). The μ' and μ'' values of the pristine epoxy sample were found to be 0.52 and 0.5, respectively, and are the lowest values as compared to other composites. The addition of Fe_3O_4 increases the epoxy composites' μ' and μ'' values. For example, the composites containing 8wt% Fe_3O_4 (i.e., F8 sample) demonstrated an μ'' and μ' values of 0.6 and 1, respectively, which are more than that observed for pristine epoxy. Furthermore, both the non-hybrid and hybrid composites exhibited larger values of μ' compared to pristine epoxy or its composite containing 8 wt% of Fe_3O_4. This suggests that the magnetic permeability of composites is enhanced, in the 8-10 GHz range, when both CuNW and Fe_3O_4 are present in the composite. This may be ascribed to the good distribution of Fe_3O_4 in the presence of CuNW, which can reduce the domain wall resistance [100,303–305]. The small increase in μ'' values observed for hybrid and non-hybrid composites over the F8 composite may be attributed to strong interactions between the CuNW and Fe_3O_4, which may hinder the domain alignment with the changing electromagnetic fields.
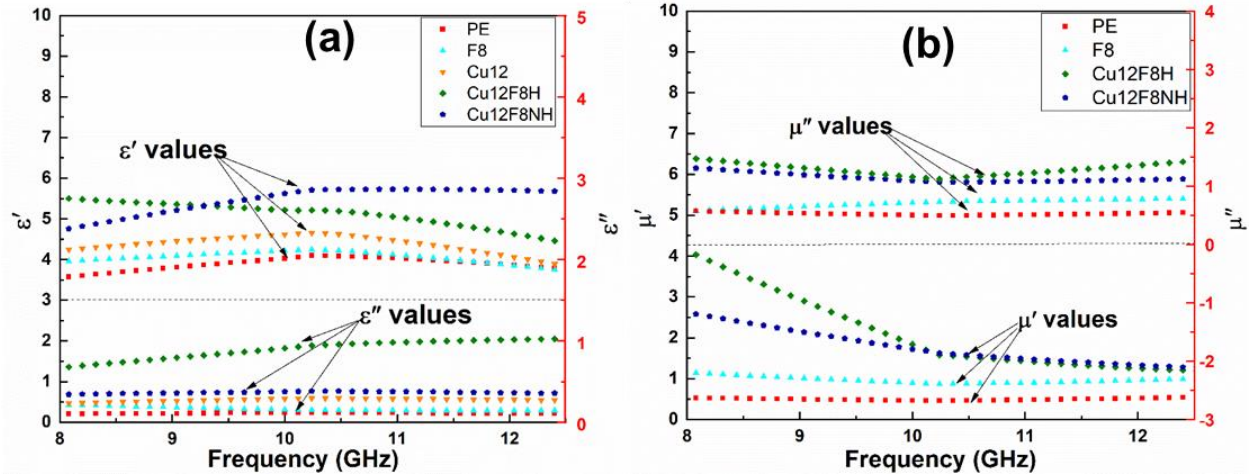
Fig.4.21. Plot of (a) ε′ and ε″ (b) μ' and μ″ of CuNW- Fe_3O_4- epoxy composites as a function of frequency

4.4.2.7 Reflection and Absorption losses of epoxy composites

The reflection and absorption of microwaves are mainly responsible for their attenuation while passing through a medium [28,92,306]. In an effort to characterize the microwave interaction behavior of the epoxy composites, the absorption, transmission, and reflection power ratios of the epoxy composites were calculated and shown in Fig.4.22. The contributions arising from the multiple internal reflections were excluded in this analysis since they cannot be measured independently. The pristine epoxy samples reflected 2% and absorbed 18% of the incident microwave power across the X-band, as depicted in Fig.4.22. Incorporation of 12wt% CuNW (i.e., Cu12 sample) to epoxy increased both the reflected and absorbed power to 41% and 37%, respectively. The rise in the reflected power can be ascribed to an increased conductivity in the sample, while the increase in absorbed power may be a result of the interfacial polarization effects [116]. However, only 8 wt.% of Fe_3O_4 addition to epoxy did not significantly alter the microwave absorption or reflection behavior, which suggests a low magnetic loss in the composite. It can also be noted that the addition of Fe_3O_4 nanoparticles to an epoxy-containing 12wt% CuNW (i.e., the

non-hybrid composites) affects the reflection and absorption power. For example, the addition of 4wt% and 8wt% of Fe_3O_4 along with 12 wt% CuNW in epoxy increased the reflection power by 22% and 32%, respectively, when compared to the composite containing equivalent loading of CuNW alone. The increase in reflected power with the addition of Fe_3O_4 particles to epoxy containing 12wt% CuNW can be ascribed to a rise in the conductivity of these composites, as evidenced by the electrical conductivity measurements [271,280]. These results suggest that in the presence of Fe_3O_4, efficient CuNW networks are formed, which leads to increase electrical conduction pathways that ultimately enhance the electrical conductivity in the composites. Similar results were observed for other filler systems where the presence of electrically inert particles augmented the electrical conductivity of the conductive polymer composites [271].

However, no significant change was observed in the microwave absorption characteristics of these samples when compared to a composite containing only CuNW. This further suggests only a weak contribution from Fe_3O_4 nanoparticles for enhancing the microwave absorption in composites in the X-band. It is worth mentioning here that reduced transmission, as shown in Fig 4.22(c), from the non-hybrid composites compared to 12wt% CuNW composite is a consequence of increased reflection from these composites rather than absorption of microwave power. In sharp contrast to non-hybrid composites, the composites containing Fe_3O_4@CuNW hybrid fillers exhibited significantly lower reflected power, significantly higher absorbed power, and lower transmitted power in the X-band. For example, the hybrid composite Cu12F8H, which contained the same amount of Fe_3O_4 and CuNW nanoparticles as the non-hybrid composite Cu12F8NH, demonstrated 60.8 % higher absorption and approximately 68% lower microwave power transmittance. These results indicate that hybrid nanostructures offer an advantage to physically mixed filler systems for enhancing the absorption of microwaves in the X-band region. However, there is currently no

evidence to demonstrate the effect of the Cu–O–Fe bond on microwave absorption characteristics. However, the addition of Fe_3O_4 nanoparticles considerably improved the microwave absorption capability of the epoxy composites. According to electromagnetic theory, the dielectric loss of the Fe_3O_4@CuNW composites can be attributed to electron polarization relaxation, dipolar relaxation, natural resonance, unique hybrid structures, etc. Firstly, the presence of Fe_3O_4 nanoparticles on CuNW can serve as polarized centers that promote the absorption of microwave energy [289]. Secondly, the wide aspect ratio, wire-like structure, and high conductivity of CuNW are further reasons why these composites have superior microwave absorption characteristics. Thirdly, Fe_3O_4 has dipoles, particularly when their dimensions are nanoscale. As the size decreases, the number of surface atoms with unsaturated bonds automatically increases, resulting in an increase in dipoles. Consequently, dipole polarizations can contribute to dielectric loss. If we just directly mix CuNW and Fe_3O_4 in the epoxy composite, then Fe_3O_4 nanoparticles will conglomerate, then the dipole polarization will be decreased. Moreover, the interfaces between the CuNW and Fe_3O_4 nanoparticles enhance the interfacial polarization and the accompanying relaxation, which contribute to the dielectric loss. This is another reason why Fe_3O_4@CuNW composites absorb microwaves more efficiently than Fe_3O_4 nanoparticles. Fourth, multiple reflections across the interfaces can significantly increase the microwave travel path in the composite, making them more susceptible to reabsorption by the Fe_3O_4@CuNW particles via magnetic and dielectric loss mechanisms [307]. Based on the above observations, it is reasonable to deduce that the enhanced microwave absorption in the hybrid composites may be a result of increased interfacial polarization effects coupled with the existence of multiple reflections and magnetic loss within the composite material [307].
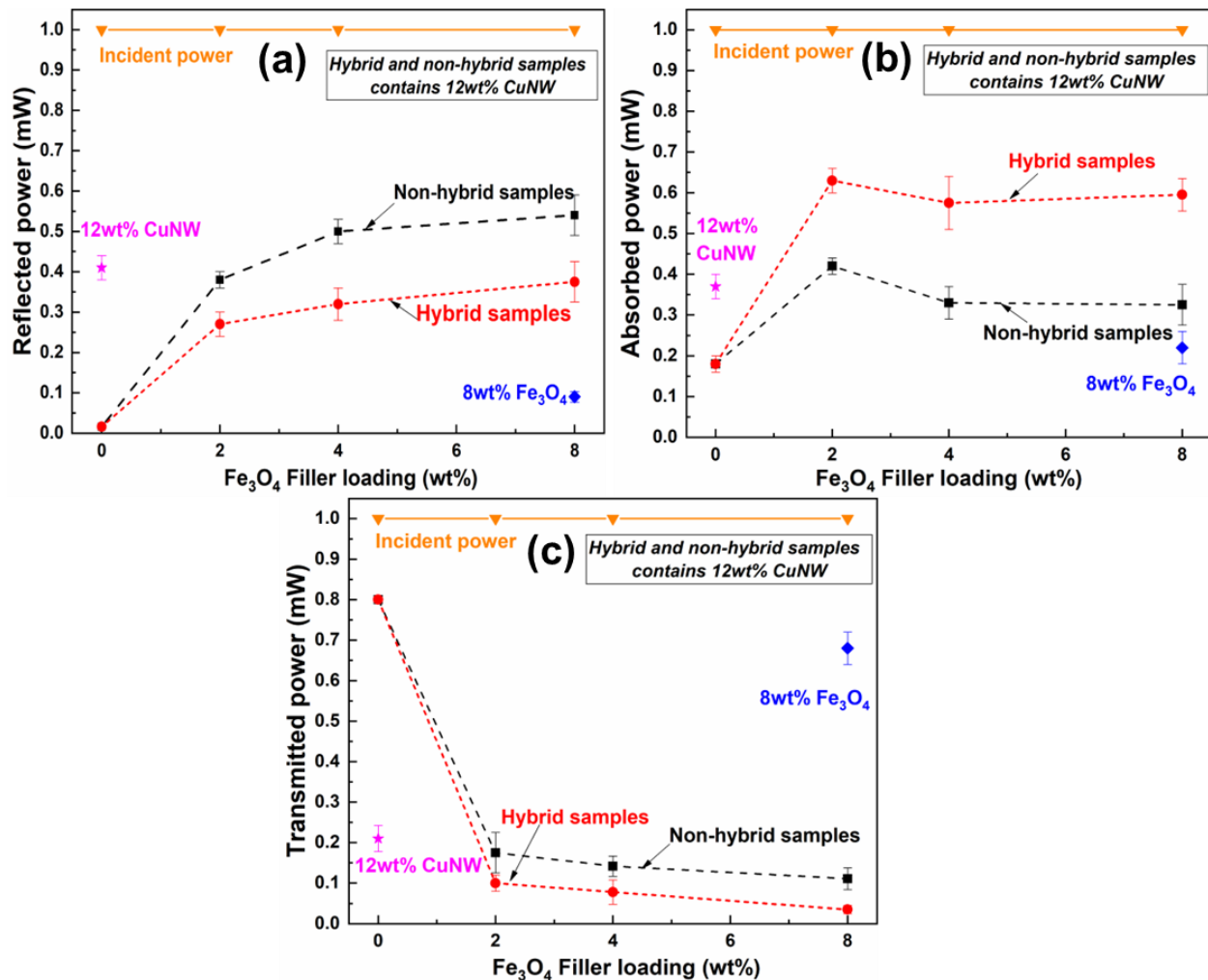
Fig.4.22. (a) Reflected (b) Absorbed and (c) Transmitted power of CuNW- Fe_3O_4- epoxy composites as a function of frequency

4.5 Conclusion

An epoxy-based microwave absorbing material comprising Fe_3O_4@CuNW hybrid nanoparticles is successfully developed through the resin blending process, which offers large bandwidth absorption with minimal microwave reflection in the X-band frequency range. Firstly, the synthesis of Fe_3O_4@CuNW hybrid nanoparticles through a simple water-based co-precipitation technique was clearly explained. The presence of CuNW and Fe_3O_4 particles in the hybrid powder sample was confirmed using the XRD analysis. Furthermore, the morphology of hybrid

nanostructures obtained using SEM analysis demonstrated the deposition of Fe_3O_4 nanoparticles on the surface of CuNW. Based on the XRD, XPS, and SEM results, it was deduced that Fe_3O_4 nanoparticles are anchored to the CuNW in the hybrid nanostructure. A series of epoxy nanocomposites with different amounts of Fe_3O_4@CuNW, CuNW, and/or Fe_3O_4 nanoparticles were prepared and characterized for morphological, electrical, and EMI shielding properties. The freeze-fractured cross-section SEM images of hybrid composites revealed that hybrid particles were uniformly distributed and retained their morphology despite the processing conditions used in composite preparation. In addition, the electrical conductivity data confirms that non-hybrid composites and 12wt% CuNW demonstrated a percolated behavior, whereas hybrid composites did not exhibit a percolated behavior. The Cu12F8NH sample exhibited the highest electrical conductivity value of 9.8×10^{-5} s/m compared to all other composites analyzed. The ε' and ε'' values for the hybrid composites were higher than the nonhybrid composites with equivalent loading of both these nanofillers. This is attributed to more interfacial polarization in hybrid composites owing to a better distribution of Fe_3O_4 nanoparticles. Furthermore, the complex magnetic permeability (i.e., μ' and μ'') values were found to be larger for Fe_3O_4@CuNW composites than the epoxy composite containing only Fe_3O_4 further suggesting a good linkage between Fe_3O_4 and CuNW. The hybrid composites containing 12 wt % CuNW and 8 wt % Fe_3O_4 exhibited the highest dielectric loss of 0.9 and magnetic loss of 1.4 as compared to other composites. The absorption and reflection power of the composite revealed that Fe_3O_4@CuNW filled hybrid composites demonstrated substantially lower reflected power and higher absorbed power, and very low transmitted power in comparison to non-hybrid composites in the X-band. The hybrid composites containing 12 wt% CuNW and 2 wt% Fe_3O_4 exhibited the lowest reflection power of 26% and the highest absorption power of 64% of the incident microwave as compared to all other composites.

A one-millimeter thick 12:8 (wt%/wt%) CuNW: Fe_3O_4 hybrid epoxy composite attenuated 98% of the microwave power with 60% absorption in the X-band frequency range of 8–12.4 GHz.

In order to understand the universal improvement of EMI shielding and microwave absorption performance of the addition of magnetic particles along with conductive particles, epoxy nanocomposites were fabricated using the solvent-free resin blending technique utilizing GNP and BaM nanoparticles. A one-millimeter-thick composite sample containing 10 wt% GNP and 8 wt% BaM exhibited an EMI shielding effectiveness value of 17.2 dB over the entire X-band frequency, which equates to 98.17 % attenuation of the incident wave power. The results obtained in this study suggest that the addition of magnetic particles along with conductive particles exhibited a synergetic effect in epoxy that contributes to a better EMI shielding performance in the composites containing a combination of these particles. Furthermore, an absorption-dominated shielding mechanism was found responsible for the observed enhancement in the EMI shielding effectiveness values in these composites.

5 Influence of BST particles on EMI shielding properties of the CuNW/epoxy Nanocomposite

5.1 Introduction

The rapid development of electronic technology has resulted in a greater reliance on electronic devices. These products made our day-to-day life very convenient, but this development in consumer electronics caused EMI problems [308]. This signal interference not only impacts the regular performance of electronic gadgets but also has an adverse impact on human life [309]. Hence, shielding materials with good EMI shielding performances are necessary to ensure the reliability and stability of electronic devices. Over the decade, conventional metals and metallic alloys have been generally utilized for EMI shielding applications [3,8,133,280]. However, these materials have specific limitations such as large density, heavyweight, high cost, low flexibility, corrosion, etc. [133]. The quest continues for an effective material for the absorption of EM waves that have lightweight, flexible, cost-effective, and corrosion inhibition. As a result, designing and producing polymer composites with excellent EMI shielding properties has become a research hotspot. Therefore, our main goal is to design a high-performance EMI shielding material in an X-band frequency range of 8-12.4 GHz.

Conductive polymer composites (CPC) containing carbon-based or metal-based fillers (i.e., copper nanowires (CuNW)) are often used as EMI shielding materials. The metal-filled composites may have inferior performance over the nano carbon-filled composites. Moreover, CuNW is appealing because of its unique structure, cost-effectiveness, high aspect ratio, outstanding thermal conductivity, and electrical conductivity equivalent to silver [141]. Thus, CuNW-filled composites have been addressed as a potential routine for producing EMI shielding materials. In spite of this potential, very few studies have been conducted to study the EMI shielding characteristics of polymers containing CuNW in the X-band. This might be related to the lower performance of

composites containing CuNW when compared to composites containing nano carbons [49,141]. Thus, there is a need to increase the EMI shielding performance of CuNW-filled composites to enable their broad use, which motivates the current work.

However, the direct incorporation of dielectric and conductive particulates in the epoxy matrix might cause phase separation [100], which means the presence of individual particles at certain locations can generate interfacial polarization between CuNW and epoxy or BST to epoxy. This suggested there is a decrease in the interfacial polarization in the epoxy composite, thereby reducing EMI shielding performance of the composite. One approach for resolving phase separation in polymer composites is to use a hybrid nanostructure composed of dielectric nanoparticles tethered to conductive nanoparticles. Accordingly, a few studies have been reported on the utilization of hybrid nanostructures, such as dielectric@conductive and magnetic@dielectric@conductive, which have improved the microwave absorption performance of polymer composites [3,101,102]. In spite of immense potential, very few studies reported on dielectric-based hybrid nanostructures in microwave absorption and EMI shielding applications. This has piqued the interest of researchers in conducting research on hybrid structures applied in these applications. Driven by this motivation, the hybrid nanostructures were prepared, the first one with conductive particles (i.e., CuNW) and dielectric particles (i.e., BST) employed in the microwave absorption and EMI shielding application. The hybrid structure of BST@CuNW and the unique characteristics of these materials have drawn the attention of both industrial and scientific institutions.

 In BST@CuNW hybrid structures, BST has a high dielectric constant; therefore, BST particles on CuNW act as tiny dipoles that get polarized in the presence of an electromagnetic field, which enhances the microwave absorption in the hybrid structures [310]. The unique BST@CuNW

hybrid structures enhance the multiple scattering, multiple internal reflections, and absorption of microwaves. In particular, the existence of imperfections at the interfaces of hybrid structures may be readily excited by an electromagnetic field, and these imperfections can operate as polarized centers that enhance the space charge polarizations by trapping space charges, hence enhancing microwave absorption capability. Furthermore, the hybrid structures allow the dielectric constant to be altered, which is advantageous for impedance matching and hence favorable to the attenuation of microwaves [10]. In the hybrid epoxy composites, the existence of combining interfaces between BST−CuNW, epoxy−BST particles, and CuNW−epoxy are responsible for combining interfacial polarization, which further can contribute to higher dielectric losses. It should be noted here that interfacial polarization develops because of the formation of large diploes, and an accumulation of charges develops at the interfaces of hybrid composites. Thus, it drives the motivation for the development of nanocomposites with BST@CuNW for microwave absorption and EMI shielding applications. This improvement in microwave absorption in composites comprising hybrid nanostructures may be attributed to the combined effects of dielectric, multiple interfacial polarization, and conduction losses [3,133,136].

This work reported a facile synthesis of BST@CuNW hybrid particles through the co-precipitation method. The morphological properties of the CuNW, BST, and hybrid nanoparticles were obtained using scanning electron microscopy. XRD analysis revealed the crystallographic phases present in the synthesized BST@CuNW hybrid particles. A set of epoxy composites containing different ratios of BST@CuNW hybrids, CuNW, BST, and Fe_3O_4 nanoparticles were prepared, and their electrical conductivity and microstructure were discussed. The dielectric, magnetic, microwave absorption and EMI shielding characteristics of the nanocomposites are also reported over the X-band frequency range of 8–12.4 GHz.

5.1.1 Materials and methods

5.1.1.1 Materials

Tetraisopropyl orthotitanate (AR) was purchased from Sigma Aldrich (Karnataka, India). Copper chloride dihydrate (AR), strontium nitrate (AR), dextrose extra pure (AR), oleic acid (AR), barium nitrate (AR), and oleyl amine (AR) were purchased from Merck (Maharashtra, India). Ammonia solution (AR) was procured from Glaxo Laboratories (Mumbai, Maharashtra). Liquid Epoxy Resin Araldite® CY230 and hardener Aradur® HY-951 were purchased from Huntsman (Maharashtra, India).

5.1.1.2 Synthesis of BST @CuNW hybrid, CuNW, and BST nanoparticles

The synthesis of BST particles followed a similar protocol to those previously reported in the literature [311]. Firstly, the BST @CuNW hybrid nanostructure particles were synthesized through the co-precipitation process. An appropriate stoichiometric ratio of copper salt, i.e., $CuCl_2$ $2H_2O$, was added to double distilled water to prepare the copper salt solution and stored in a conical flask. The oleyl amine, oleic acid, and ethanol are mixed thoroughly using a magnetic stirrer in the ratio of 10:0.1:17.5 for 15 minutes to obtain a homogenous mixture and added to the copper salt solution. Next, the measured quantity of BST nanoparticles was added to the copper salt solution. After that, the copper salt solution was stirred for 45 minutes at room temperature. Afterward, a reducing agent, i.e., dextrose solution, was prepared and added dropwise to copper- BST solution at a specific flow rate of 1mL/ min under vigorous stirring for 2 hours to form a homogenous viscous solution. Then the copper- BST solution was diluted by adding double distilled water and thoroughly stirred for 8 hours at a temperature of 50 °C. Subsequently, the solution's color changed from blue to caesious at this stage. Additionally, the solution was processed at 130 °C for 8 hours in an autoclave, then the solution's color turned reddish-brown, suggesting the formation of BST

@CuNW hybrid nanostructure particles. Subsequently, the final product was separated using a centrifuge (CPR 24, REMI Compufuge, India) operated at 10000 RPM for 10 minutes to obtain the sediment. Then the residue was washed several times with hexane and stored under the hexane prior to using it for composite preparation. The synthesis of CuNW followed a similar protocol, with the exception that BST was not applied to the solution. Recently published research provided a thorough overview of the synthesis process of CuNW.

5.1.1.3 Preparation of epoxy nanocomposites

The nanocomposites were produced by mixing the required quantity of fillers, comprising BST @CuNW hybrid nanostructure particle, CuNW and/or BST particles, in the epoxy resin for 12 minutes with an ARE-250 Mixer (Thinky, USA). Subsequently, the epoxy mixture was processed in an ultrasonic processor (Sonics, USA) operated at 500 W for 5 minutes in order to facilitate uniform dispersion of the fillers in the epoxy matrix [133,141]. Afterward, the requisite quantity of curing agent was added, and the epoxy mixture was even further mixed in the ARE-250 Mixer for 3 minutes to ensure proper mixing of the curing agent. The epoxy mixture was then degassed in the degassing chamber before being cast in a glass mold and cured at room temperature for 12 hours. The thickness of the nanocomposite was measured to be 1 mm and was also set by the mold's dimensions. Table 5.1 illustrates the composition of the composites utilized in this study.

Table.5. 1. The composition of the composites used in this study.

Filler	Sample Code	CuNW (wt%)	BST (wt%)
Pristine epoxy	PE	0	0
BST particles	BST15	0	15
CuNW	Cu10	10	0
BST@CuNW hybrid	Cu10BST5H	10	5

	Cu10BST10H	10	10
	Cu10BST15H	10	15
BST-CuNW (Non-hybrid)	Cu10BST5NH	10	5
	Cu10BST10NH	10	10
	Cu10BST15NH	10	15

5.1.1.4 Characterization

The XRD diffractograms of BST @CuNW hybrid nanostructures, CuNW, and BST particles were collected using a Miniflex X-ray diffractometer (Rigaku, USA). The diffractograms were recorded at a scan rate of 2 °/min over a 2θ range of 20 ° to 80 °, using the Cu- Kα radiation source of wavelength (λ) = 1.54 Å. The microstructure of BST @CuNW hybrid nanostructures, CuNW, and BST particles was observed using an FEI-APREO scanning electron microscope (Thermo Fisher, USA). The XPS data were recorded by K-Alpha X-ray photoelectron spectrometer system (Thermo Fisher Scientific, India) using Al Kα (hν = 1486.3 eV) X-ray source with a step size of 0.05 eV at an average of ten scans. It was observed that the analyzer chamber had a residual pressure of 1.3 x 10 -8 Pa. A nonlinear curve-fitting method was used so that the core level changes and relative intensities of these components could be determined. The electrical conductivity was measured using an E4990A impedance analyzer (Keysight Technologies, India) in a frequency range of 25 Hz to 25 MHz. The composite samples used for measurement were in the size of 10 mm× 10 mm× 1 mm. The electrical conductivity was calculated from the electrical resistivity of the composite. The EMI shielding effectiveness of the composites was measured using a 2-port N5230C PNA-L vector network analyzer (Keysight Technologies, India). A detailed description of the setup and measurement method is reported in the research methodology. A full 2-port calibration was performed before each measurement, and the scattering parameters (S_{11} or S_{22} and

S_{21} or S_{12}) were measured over the X-band frequency range of 8 –12.4 GHz. The power coefficients, absorption coefficient (A), reflection coefficient (R), and transmission coefficient (T) were calculated by the equations of A=1-R-T where $R=|S_{11}|^2$ and $T=|S_{21}|^2$, respectively. The real and imaginary part of the complex permittivity ($\varepsilon^* = \varepsilon' - i\varepsilon''$) was determined from the obtained S-parameters by using the standard Nicholson–Ross–Weir (NRW) method.

5.1.2 Results and Discussion

5.1.2.1   XRD characterization of BST@CuNW hybrid, CuNW, and BST particles

To identify the crystallographic phases existing in the BST@CuNW hybrid nanostructure, CuNW, and BST particles, X-ray powder diffraction (XRD) was performed, and data were shown in Fig.5.1. The XRD data of the BST sample are well-matched with standard peaks of BST as per JCPDS #34-0411 [312]. It indicates that BST particles are present in the powder sample. Furthermore, in the XRD data of BST particles, the most prominent peak observed at 2θ of the value of 32.17 ° corresponds projected phase of (101), indicating that BST has a simple cubic structure [311]. Importantly, no additional peaks are observed in the XRD data, indicating the absence of any impurities and the formation of pure BST. It was similar to previously published literature on BST [311–313]. In addition, the prominent peak corresponding to the 2θ value of 43.59 ° observed in the XRD data of CuNW made a good agreement with conventional peaks of copper as per JCPDS #03–1018. Additionally, no additional peaks are seen, confirming that the powder sample contains pure and single-phase CuNW free from impurities. Furthermore, the XRD peaks of CuNW were very broad, as demonstrated in Fig.5.1, which implies the formation of nanoparticles. It was in good agreement with previous studies on the CuNW.

Nonetheless, the XRD data obtained for BST@CuNW hybrid particles demonstrates that the most prominent peak of hybrid particles corresponding to the 2θ value of 43.59 ° was well-matched with

the conventional peak of CuNW as per JCPDS #03–1018. It can be observed that the other peaks

of XRD data were well matched with the conventional peaks of BST particles as per JCPDS #34–

0411 and CuNW as per JCPDS #03–1018. These results indicated that the hybrid powder sample

contained both CuNW and BST particles. Furthermore, the average crystallite size of BST particles

present in the hybrid particles was calculated using Scherrer's formula by considering the K value

as 0.89. In the results, the peak corresponding to the 2θ value of 32.17 ° from the XRD data of the

hybrid sample was chosen for the analysis, and the crystallite size of BST particles was calculated

as 18.10 nm. This suggests that the BST particles present in the hybrid particles have a

nanocrystalline morphology.
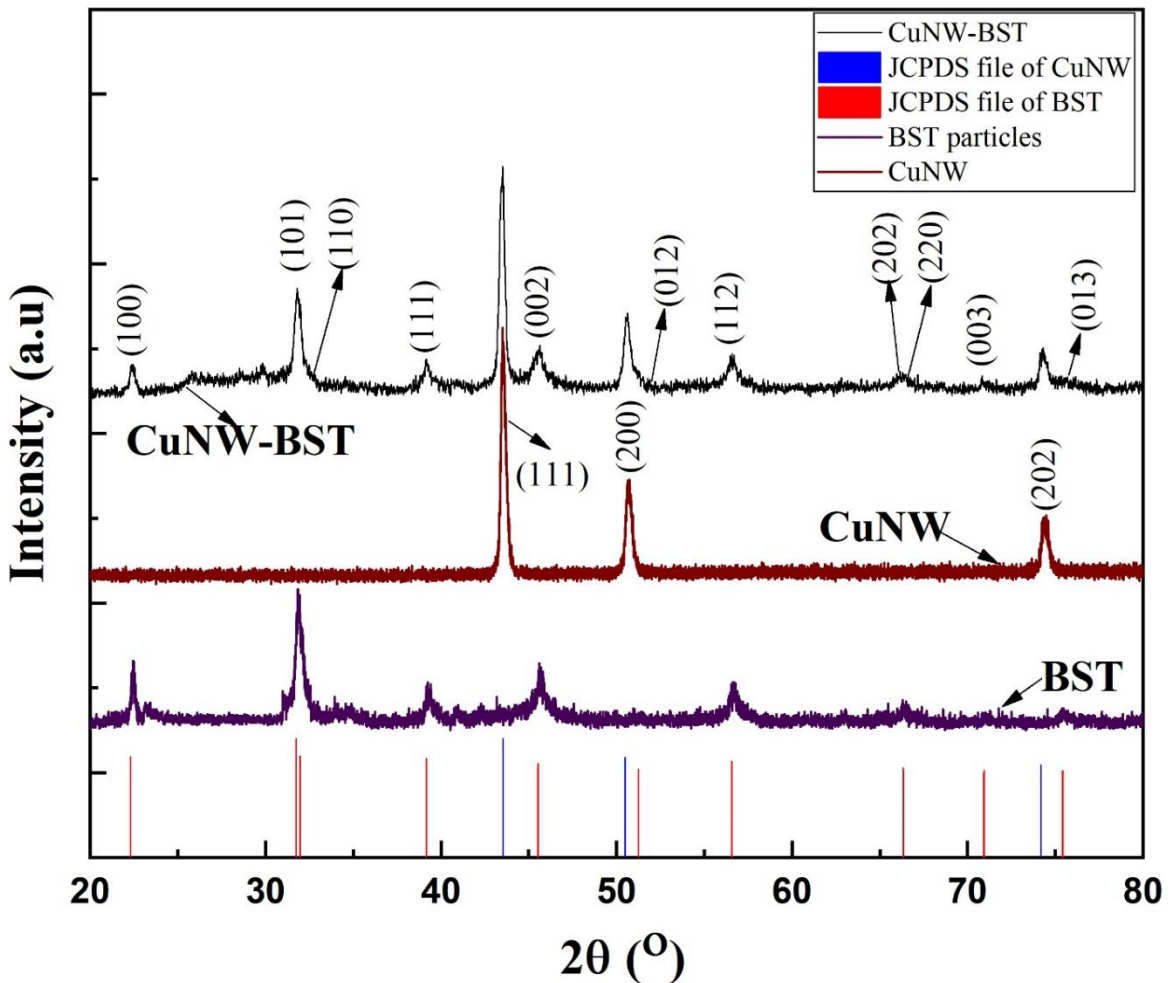
Fig.5. 1. XRD spectra of (a) BST@CuNW hybrid nanoparticles (b)BST particles (c) CuNW
along with corresponding JCPDS of CuNW and BST particles.

5.1.2.2 SEM characterization of BST@CuNW hybrid, CuNW, and BST particles

To further investigate the morphology of the synthesized particles, SEM analysis was performed on BST@CuNW hybrids, BST particles, and CuNW and the results are shown in Fig.5.2. It can be observed from Fig.5.2(e) that the CuNW has extended its structure in 1D and formed wire-like morphology. Also, the CuNW possesses a uniform diameter and length. It was in good agreement with previous studies on the CuNW [280]. Furthermore, Fig.5.2(d) depicts the microstructure of the BST nanoparticles. It can be noticed that the synthesized BST particles formed sphere-like morphology with a rough surface. It can be observed that each BST particle is a conglomeration of several grains. The unique shape of BST is generated during the calcining process. The average particle size of BST particles was calculated, and the average particle diameter of 68.63 nm. The results suggest that the BST particles synthesized by the present method are believed to have good sintering activity owing to their sub-micron particle size and nano-powder surface area. Similar results were also reported in the literature [311]. Moreover, Fig. 5.2 (a and b) exhibit the microstructure of BST@CuNW hybrid nanoparticles. It can be observed from Fig.5.2 (a) that CuNW exhibited smooth surfaces with wire-like morphology [311]. In contrast, the hybrids exhibited that the surface of copper nanowires was covered with BST nanoparticles. In addition, the presence of Cu, Ba, Sr, Ti, and O elements in BST@CuNW hybrids was confirmed with the energy dispersion spectroscopy analysis, as shown in Fig. 5.2 (c). It is also suggested that the BST nanoparticles were anchored onto the surface of CuNW in the hybrid sample, as shown in Fig. 5.2 (b).
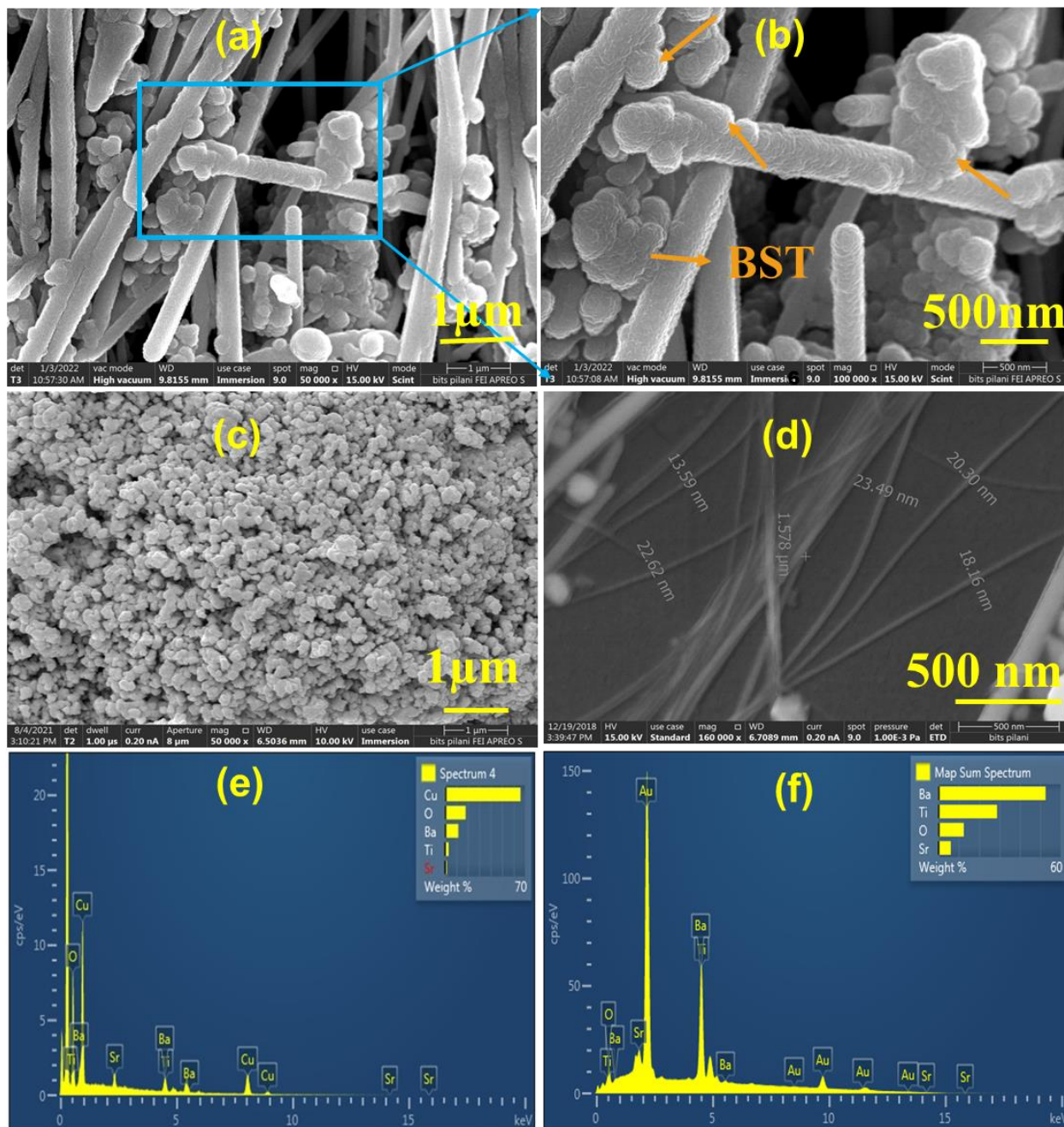
Fig.5. 2. The SEM images of (a& b) BST@CuNW hybrids, (c) BST particles, (d) CuNW, (e) EDS of BST@CuNW hybrids, (f) EDS of BST

5.1.2.3 XPS characterization of CuNW-epoxy composites containing BST particles

The wide scan XPS spectrum of the hybrid epoxy composite was shown in Fig. 5.3 . It can be observed from the XPS spectrum that the presence of barium (Ba), copper (Cu), carbon (C), strontium (Sr), titanium (Ti) and oxygen (O) with chemical states of Ba 3d, C1s, Cu 2p, Sr 3d, Ti

2p and O 1s. Peak deconvolution can be accomplished after fitting the curves using the Gauss-Lorentz function. The carbon (C) chemical state C 1s spectrum of composites was shown in Fig. 5.3(c). The epoxy composite exhibited a prominent C 1s peak at a binding energy of 284.6 eV. Similar results were reported in the literature [288]. The C 1s spectrum's deconvoluted peaks were observed at a binding energy of 284.4 eV and 286.4 eV corresponding to aromatic rings (C=C/C–C), epoxy, and alkoxy (C–O) groups, which contain main components of the epoxy matrix. Similar observations were reported [289]. The copper (Cu) chemical state Cu 2P spectrum of composites was shown in Fig. 5.3 (b). Furthermore, in the Cu 2P spectrum in epoxy composite, the Cu 2p3/2 peak was observed at a binding energy of 932.5, and Cu 2p1/2 peak was observed at a binding energy of 952.5 eV. Similar observations were reported for Cu 2p peaks [290]. The oxygen (O) chemical state O1s spectrum and curve fitting were shown in Fig. 5.3 (e). It can be noticed that O1s deconvoluted peaks were observed at a binding energy of 529.3 eV and 531.7 eV. Similar observations were reported for the O1s band [287]. The peak at 529.3 eV attributed to the oxygen ions are coordinated in TiO_6 octahedra, and the peak at 531.7 eV attributed to the presence of oxygen vacancies on the surface of the ceramic.

It can be observed from Fig. 5.3 (d) that Ba 3d peaks consisted of a Ba 3d$_{3/2}$ peak with a binding energy of 795.1 eV and a Ba 3d$_{5/2}$ peak with a binding energy of 779.6 eV. These peaks confirm the presence of barium in the BST. The peak at a binding energy of 779.6 eV corresponds to the barium oxide (O−Ba−O) in the lattice. An actual spin-orbit distance of about 15.28 eV (793.34 eV–778.06 eV) exists between the two peaks. Similar results were published for Ba 3d [314,315]. Fig. 5.3 (g) illustrated that the strontium chemical state Sr 3d is composed of deconvoluted peaks of Sr 3d$_{3/2}$ and Sr 3d$_{5/2}$ at a binding energy of 134.8 eV and 133.4 eV, respectively. These results suggest the presence of an O−Sr−O bonding structure of strontium and oxygen ligands in the

perovskite lattice. Similar observations were reported for sr 3d [315,316]. Both profiles Ti 2p, i.e., Ti $2p_{3/2}$ and Ti $2p_{1/2}$ demonstrated the binding energy of 457.94 eV and 463.74 eV, as shown in Fig. 5.3 (f). The gap in binding energy between Ti $2p_{3/2}$ and Ti $2p_{1/2}$, which was determined to be -5.8 eV, may be attributed to the Ti^{4+}-O bonding. Similar results were reported for Ti 2P [317,318]. The broadening of the Ti $2p_{3/2}$ peak indicates the presence of Ti^{3+} ions because of the presence of two or more chemical states. Hence, it follows that very little or no Ti^{3+} is formed on the particle's surface. These results confirmed that the BST has formed a perovskite structure [315,319].
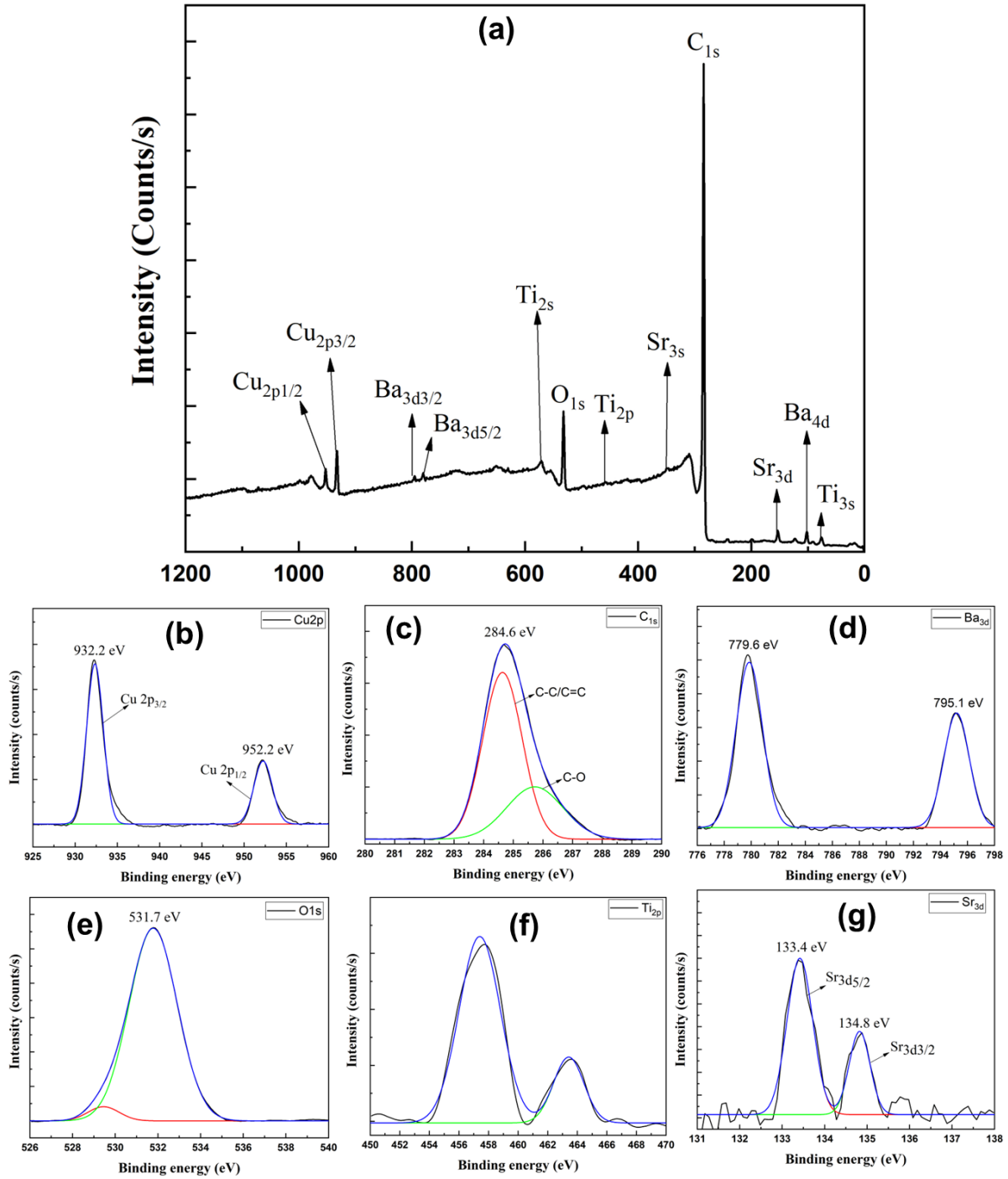
Fig.5. 3. The XPS spectra of (a) hybrid composites (b) Cu2P (c) C1s (d) Ba 3d (e) O1s (f) Ti 2p (g) Sr 3d

5.1.2.4 Electrical conductivity of epoxy composites

In an effort to study the influence of CuNW, and/or BST particles, and BST@CuNW hybrid structures addition on the electrical conductivities of the composites in the frequency range of 20 Hz to 25 MHz, as shown the Fig.5.4. The 10 wt% of CuNW-filled epoxy (i.e., Cu10) composite has demonstrated frequency-dependent electrical conductivity across the frequency range of 20Hz to 25MHz. This Cu10 composite has exhibited an electrical conductivity value of 9.7×10^{-8} S/m at a frequency of 100 Hz. Similar results were reported in the literature [141]. In contrast, the non-hybrid samples demonstrated frequency-independent electrical conductivity values in the frequency range of 25- 900 Hz, as seen in Fig.5.4(a). Furthermore, the Cu10BST15 sample exhibited the highest electrical conductivity value of 2.32×10^{-5} S/m at a frequency of 100 Hz as compared to all other composites. These suggested that adding 15wt% of BST particles to the epoxy composite containing 10wt% CuNW has increased their electrical conductivity values by 3 orders of magnitude.

The Cu10BST10 and Cu10BST5 samples demonstrated electrical conductivity values of 3.52×10^{-6} S/m and 6.48×10^{-7} S/m at a frequency of 100 Hz, respectively. These results suggested that the addition of BST particles in the presence of CuNW has increased the electrical conductivity of the epoxy composite, as shown in Fig.5.4 (c). Similar observations were reported in the literature for other particulate systems [3,133,302]. However, it was observed from Fig. 5.4 (d) that the Cu10BST5 sample exhibited higher electrical conductivity than the Cu10 sample and an electrical conductivity value of 1.4×10^{-7} S/m. The remaining composites containing hybrid particles (i.e., BST@CuNW) exhibited frequency-dependent electrical conductivity values, as seen in Fig.5.4(b). These results suggested that the composites demonstrated non-percolated behavior. This can attribute to the presence of BST decorations on CuNW in the hybrids reducing the interactions

between CuNW, which breaks the percolated network of CuNW in the composite. The results can also further suggest that the hybrid microstructure of BST@CuNW nanoparticles is preserved in the epoxy composites.
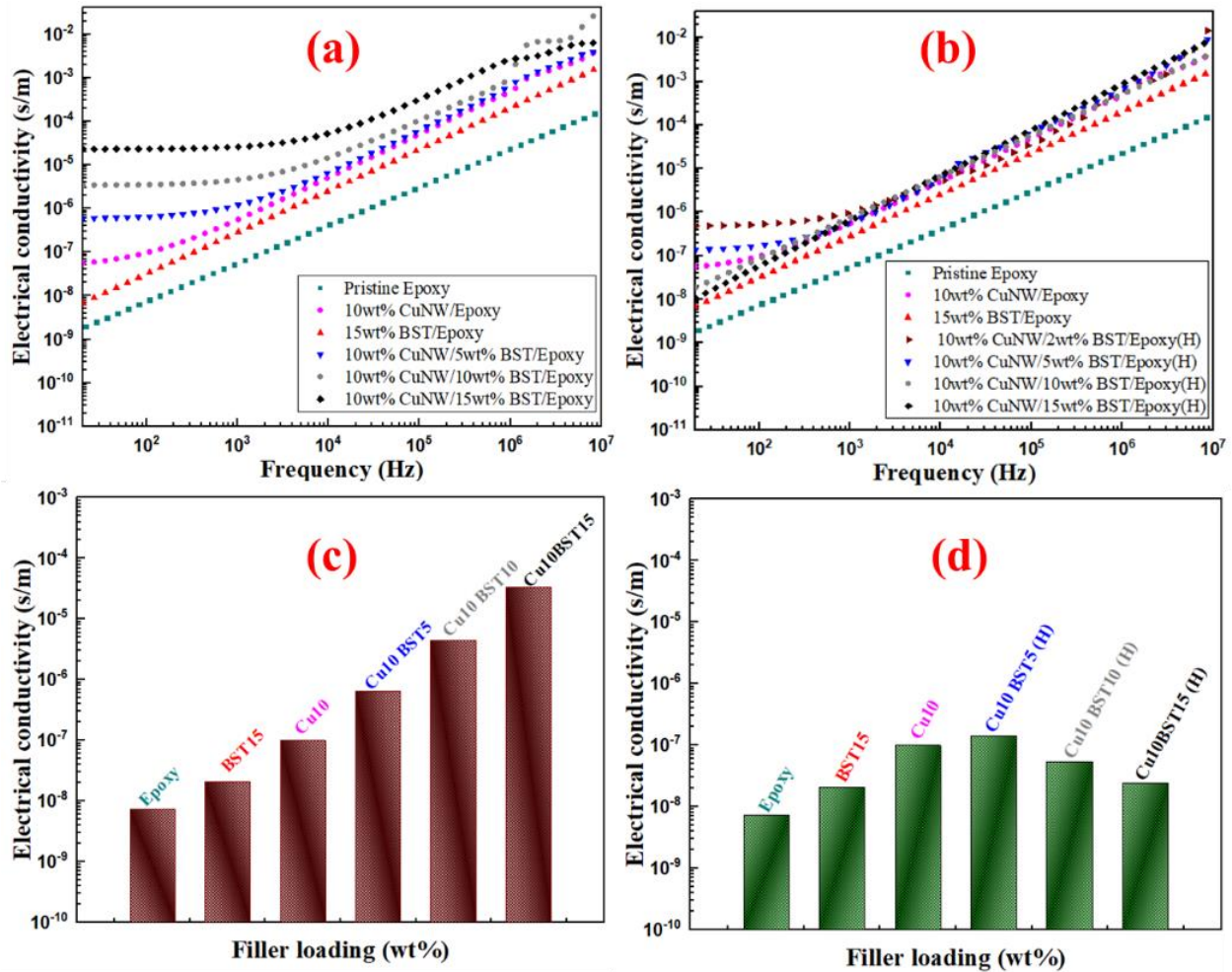
Fig.5. 4. The electrical conductivity values of (a) CuNW-BST-epoxy non-hybrid composite, (b) BST@CuNW hybrid composites as a function of frequency, and (c) CuNW-BST-epoxy non-hybrid composite, (d) BST@CuNW hybrid composites as a function of filler loading

5.1.2.5 EMI shielding effectiveness of epoxy composites.

To further investigate the EMI shielding effectiveness of the epoxy composites containing CuNW and/or BST particles and BST@CuNW hybrid structures in the X-band frequency range of 8-12.4 GHz was determined, and the results are shown in Fig.5.5. The epoxy matrix's electrical insulating and nonmagnetic properties make it transparent to EM waves, resulting in the pristine epoxy

sample demonstrating a very low SE_T value of 1.5 dB. On the other hand, the Cu10 sample containing only 10wt% CuNW increases the SE_T value 5 times compared to pristine epoxy. In contrast, the BST15 sample, which contains only 15wt% of BST particles, exhibits an albeit increase in SE_T value to 2 dB.

It can be observed from the results that the addition of CuNW is more effective in increasing the shielding performance as compared to BST nanoparticles. The composites containing both these particles, i.e., CuNW and BST, higher SE_T values as compared to composites containing only CuNW or BST, were observed. Specifically, the Cu10BST4 and Cu10BST8 samples exhibited SE_T values of 10.1 dB and 12.3 dB, respectively, which is higher than the SE_T value of the Cu10 sample containing only 10 wt% CuNW in the X-band frequency range. This further suggests that the direct addition of BST nanoparticles in the presence of CuNW in epoxy composites enhances the EMI shielding performance of the composites. However, it should be recalled here that SE_T value of Cu10BST15NH mixed directly was found to be 16.9 dB which is higher than the sum of SE_T values of Cu10 and BST 15 samples in the X band frequency range.

On the other hand, composites containing BST@CuNW hybrid nanoparticles, the sample Cu10BST15H, which contained a hybrid nanoparticle BST: CuNW having the weight ratio of 3:2, exhibited the highest SE_T values, with a maximum of 21.2 dB in the X band frequency range. However, it should be recalled here that the EMI shielding effectiveness of composite having 10 wt% CuNW and 15wt% BST mixed directly was found to be 16.9 dB in the X-band frequency range, which is lower than the hybrid sample. This suggests that the hybrid nanoparticles containing equivalent loading of fillers are better than the direct mixing of fillers for enhancing EMI shielding effectiveness in composites. The increased EMI shielding in composites containing hybrid nanoparticles can be attributed to the combined effects of multiple interfacial polarization

coupled with the conduction losses arising due to the presence of BST nanoparticles. It can be seen from Fig. 5.5 (c),(d) that BST nanoparticles are strongly anchored to the CuNW surfaces. This anchoring of BST on the CuNW surface enhances the dielectric losses due to interfacial polarization effects between the BST nanoparticles and CuNW.

It could be observed that the Cu10BST5H and Cu10BST10H hybrid samples exhibited lower SE_T values as compared to Cu10BST15H. These results further suggest that the BST filler content influences its EMI shielding capability in the hybrid composites. This can be attributed to lower interfacial polarization losses in Cu10BST2H and Cu10BST5H samples due to the less BST filler content in the hybrid sample as compared to Cu10BST15H. However, with the higher BST filler contents in the hybrid sample, there may be an agglomeration of nanoparticles which could impact proper filler dispersion and shielding performance. This further suggests that there is an optimum loading of BST nanoparticles on the CuNW, which is beneficial for increasing the EMI shielding performance. Similar observations were made for other hybrid systems [90,96,320,321].
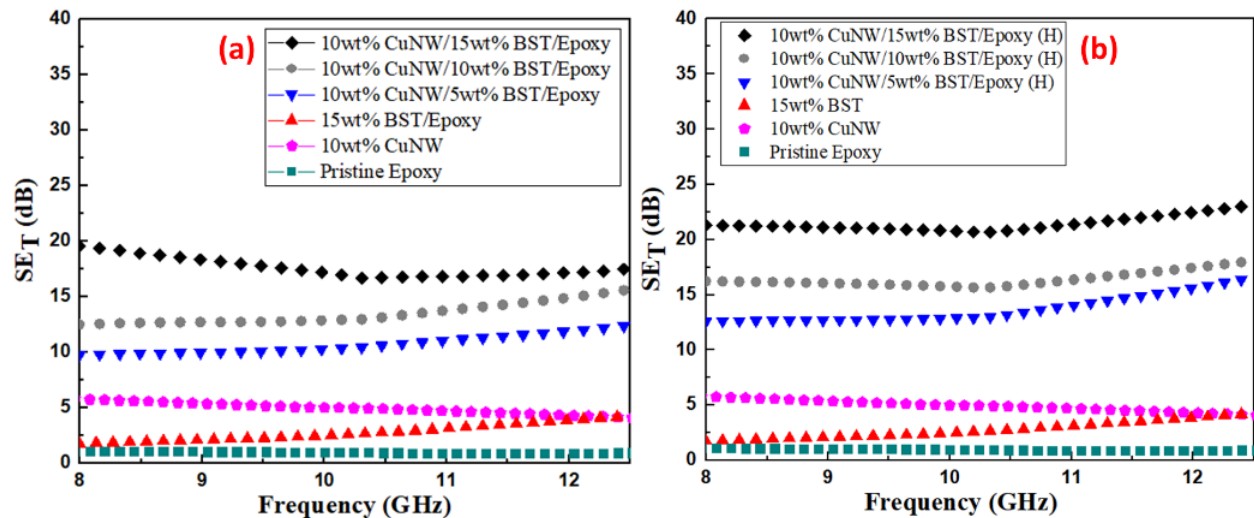
Fig.5. 5. SE_T values of (a) CuNW-BSTnon-hybrid epoxy composite and (b) BST@CuNW hybrid epoxy composites as a function of frequency

5.1.2.6 Complex permeability and permittivity of epoxy composites

To investigate the energy storage capability and loss ability of the EMI shielding materials, the complex permittivity (i.e., $\varepsilon = \varepsilon' - j\varepsilon''$) was calculated using the NRW method from scattering parameters (S_{11} and S_{21}) recorded from VNA. The variation of complex permittivity (ε' and ε'') with a frequency range over 8–12.4 GHz frequency range is depicted in Fig. 5.6. The ε' value of the pristine epoxy sample exhibited is 3.2, which is the lowest value compared to all other composites. This suggested that the epoxy exhibited a small dipole and low polarizability to the incident EM wave. The Cu10 and BST15 samples demonstrated a value of 4.1 and 8, respectively. This suggested that the BST exhibits dielectric loss, mainly depending on interfacial polarization to absorb the EM waves. Furthermore, it can observe that the ε' values were increased with the addition of BST fillers to the epoxy composite containing CuNW. The Cu10BST15 composite demonstrated the highest ε' value of 15.5 compared to all other composites. It can be seen that the ε' values for the Cu10BST15 composite are larger than other samples. It can be suggested that the composites exhibited a remarkable interface polarization. The difference in complex permittivity between BST, CuNW, and Epoxy could generate interface scattering, leading to increased shielding effectiveness of nanocomposites. Furthermore, The BST can form a dielectric network for dispersing charges and can improve the dielectric loss. The CuNW with a large high aspect ratio can form a complete conductive network for dispersing charges, improving the conduction loss. Furthermore, the existence of multiple reflections can enhance the microwave absorption ability of the composites. The addition of BST to epoxy composites containing CuNW could also be used as multiple polarization centers that enhance the electronic polarization of the nanocomposites. Thus, strong attenuation of the EM wave in the composite can be achievable. The 10 wt% of CuNW in composites was enough to blend with BST, which suggests that more CuNW

in nanocomposites could result in an agglomeration of CuNW, which impacts the proper dispersion of filler content and shielding performance of nanocomposite. Similar behavior was observed for ε'' values over the X- band frequency range of 8-12.4 GHz. A good EMI shielding material should have a dielectric loss and should be as high as possible. It can imply that the addition of BST combined with CuNW enhances the dielectric loss, which plays an essential role in the absorption of EM waves. The effective complementarities between these two losses, i.e., conduction loss and dielectric loss, would encourage the incoming of incident EM waves into the shielding materials. The results further suggested that the synergetic effect between CuNW and BST could also enhance EM waves' attenuation. The synergetic effect between CuNW and BST could govern the complex permittivity, which is beneficial for the impedance match. This suggested that epoxy nanocomposite containing CuNW, and BST formed an electric dipole, which enhanced the dielectric polarization of the composite. It can benefit to enhance the absorption loss in composites, thus promoting the EMI shielding materials' performance. Furthermore, the polarization and their related relaxation processes at the heterogeneous junctions of BST and CuNW and epoxy matrix can enhance the EMI shielding material's performance. The causes for dielectric loss are mainly due to interfacial polarization occurring between BST and CuNW in the epoxy matrix. In addition, the presence of CuNW in the epoxy matrix can create an electric dipole, which further enhances the dielectric loss. This further suggests an optimum loading of BST on the CuNW sheets, which is beneficial for increasing the EMI shielding performance. This further suggests the relatively enhanced absorptive nature of the composite containing BST and CuNW. This may be attributed to increasing wave absorption due to the synergetic behavior between BST and CuNW nanoparticles. Similar observations were made for composites containing BST, where

a remarkable increase in attenuating capability was observed over a physically mixed composite containing these particles.
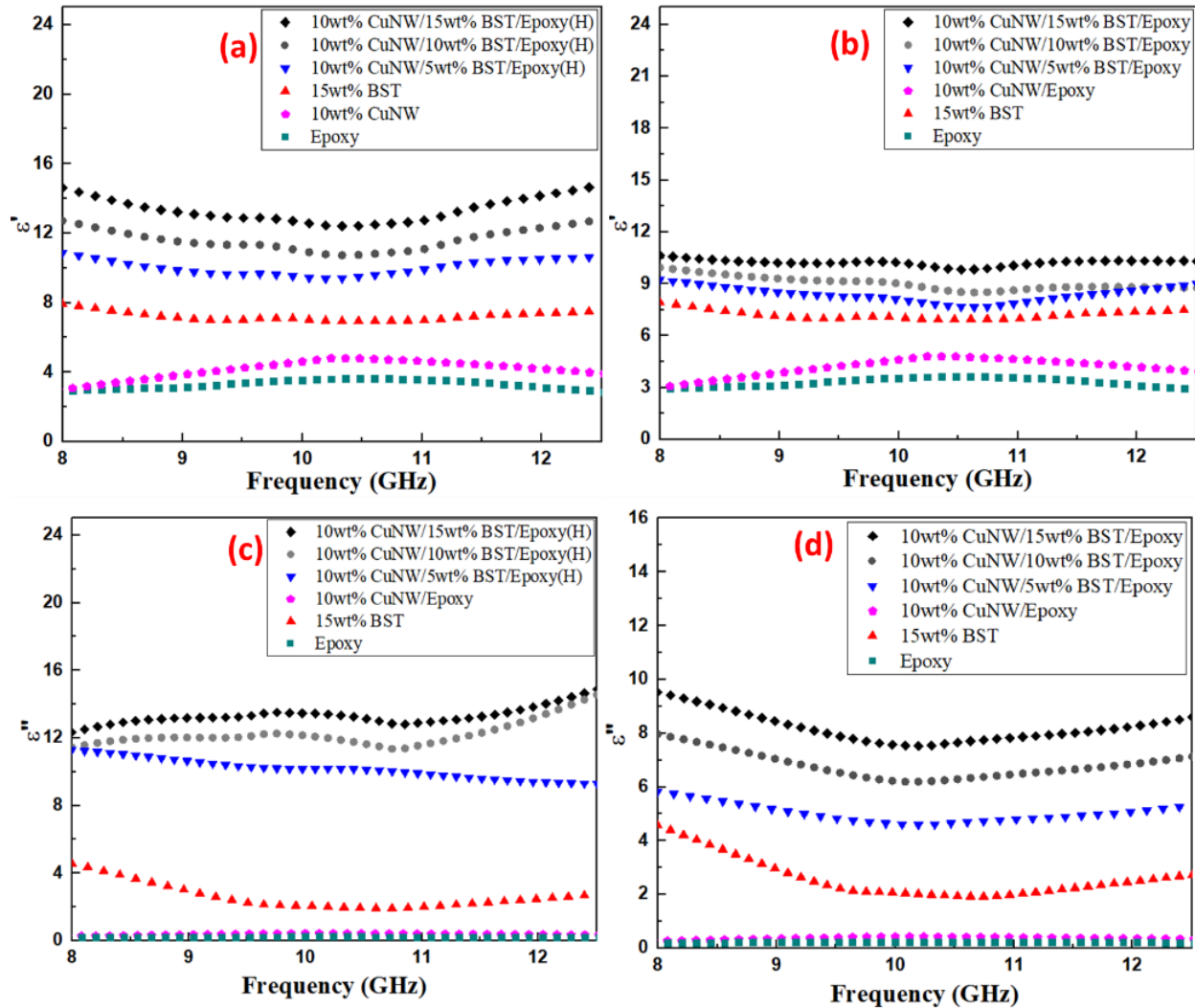
Fig.5.6. The plot of (a) ε' and (b) ε'' values of hybrid composites (c) ε' and (d) ε'' values of non-hybrid composites as a function of frequency

5.1.2.7 Reflection and Absorption losses of epoxy composites

The absorption, transmission, and reflection power ratios of the epoxy composites were determined in order to characterize the microwave interaction behavior of the epoxy composites, as shown in Fig.5.7. The contributions resulting from several internal reflections were eliminated from this study since they cannot be quantified separately. Firstly, the epoxy (PE) sample absorbed

4% and reflected 6% of the microwave power across the X-band, as shown in Fig.5.7. The Cu10 sample has demonstrated 7.6 times rise in absorbed power and 6 times rise in reflected power with the addition of 10wt% CuNW to epoxy sample. The improvement in reflected power may be attributed to a rise in the sample's electrical conductivity, while the increase in absorbed power can be attributed to interfacial polarisation effects. In contrast, adding merely 15% BST to epoxy had increased absorption power by 5.3 and reflected power by 1.5 times as compared to an epoxy sample. This result indicated that the composite had a minimal dielectric loss and had no significant influence on microwave absorption or reflection. Furthermore, the incorporation of BST to Cu10 (i.e., non-hybrid composites) alters both the reflected and absorbed power of the composites. The reflected power of the Cu10BST5NH and Cu10BST10NH samples was reduced with the addition of 5wt% and 10wt% BST together with 10 wt% CuNW in an epoxy, decreasing the reflection power by 11% and 7%, respectively, as compared to the composite having similar loading of CuNW alone. In contrast, the reflected and absorbed power of the Cu10BST15NH composite has increased by 3% and 52% greater than the Cu10 sample. However, non-hybrid composites demonstrated 53% rise in the microwave absorption characteristics of these samples when compared to a composite containing only CuNW. This also implies that BST particles can help improve microwave absorption in composites in the X-band. It is worth noting that the lower transmission from non-hybrid composites compared to the Cu10 sample is due to enhanced reflection rather than absorption of microwave power, as seen in Fig 5.7 (c). It is also worth noting that the reflection power of non-hybrid composites is greater than that of hybrid composites. The improvement in reflected power in the non-hybrid can be attributed to an increase in the composite electrical conductivity of the non-hybrid composites. These findings imply that in the presence of BST, efficient CuNW networks develop, resulting in increased electrical conduction networks and,

ultimately, increased electrical conductivity in the composites. Similar results were obtained for additional filler systems in which the incorporation of electrically inert particles increased the electrical conductivity of the conductive polymer composites. In comparison to non-hybrid composites, composites containing BST@CuNW hybrid fillers had considerably reduced reflected power, significantly greater absorbed power, and substantially lower transmitted power in the X-band. The hybrid composite Cu10BST15H, which comprised the same quantity of BST and CuNW nanoparticles as the non-hybrid composite Cu10BST15NH, displayed 33% greater absorption and 35% and 62.5% reduced microwave power reflection and transmittance, respectively. These findings suggest that hybrid structures provide benefits over physically mixed filler systems in terms of microwave absorption in the X-band. The enhanced microwave absorption in hybrid composites might be attributed to greater interfacial polarization effects and the existence of numerous reflections and dielectric loss inside the composite material. Furthermore, Multiple reflections across boundaries can greatly increase the microwave travel path in the composite, increasing its propensity to re-absorption by the BST@CuNW particles via conduction and dielectric loss mechanisms.
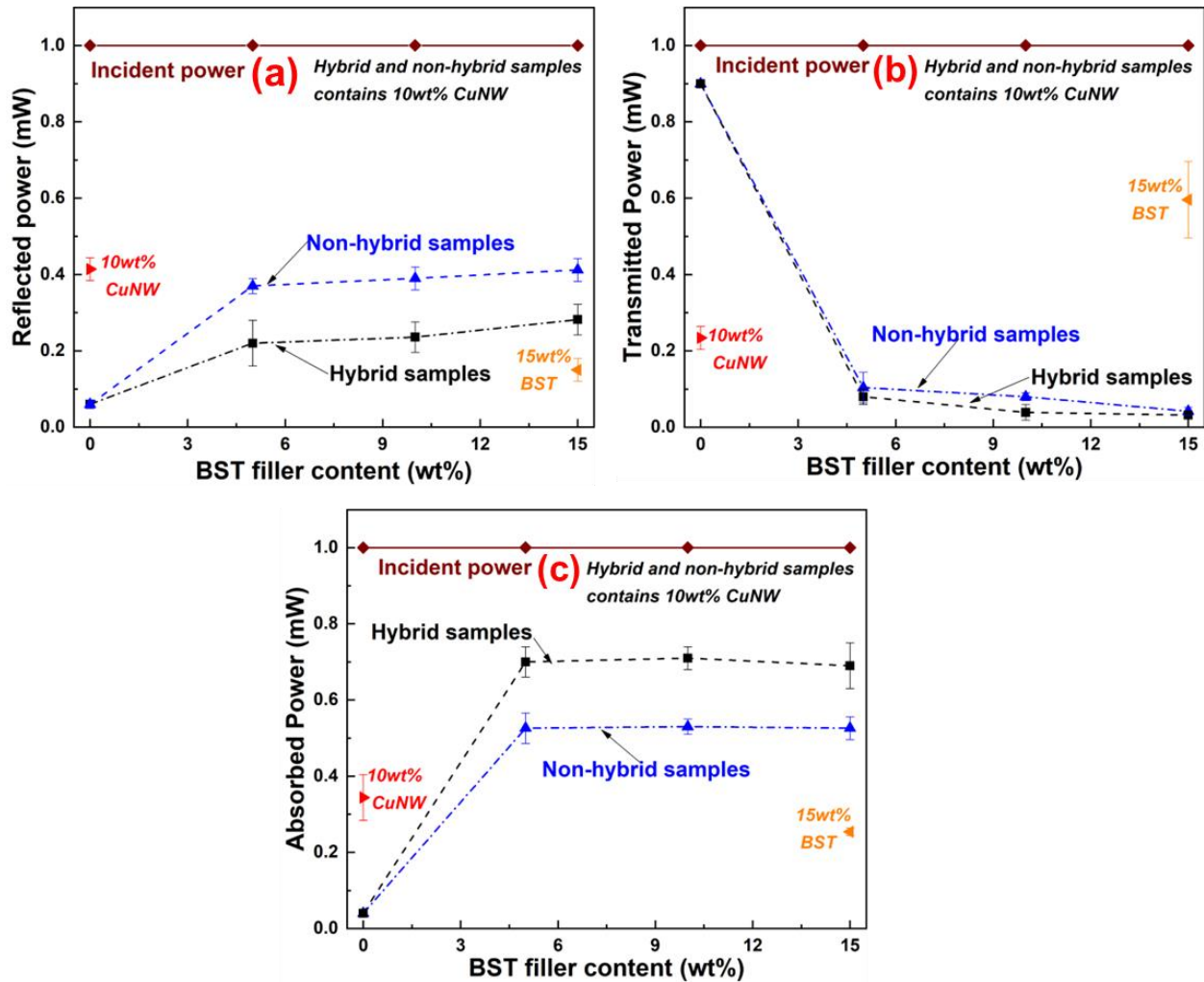
Fig.5.7. The plots of (a) reflected, (b) transmitted, and (c) absorbed power of epoxy composites containing CuNW and BST particles

5.1.3 Conclusion

Copper nanowires (CuNW) are a prominent class of materials with unique properties, such as one-dimensional structure with a high aspect ratio and electrical and thermal conductivity with a cost advantage over other conductive fillers, making them attractive choices as fillers for a wider range of applications. In this work, the microwave absorption characteristics of epoxy composites containing CuNW and/or BST (non-hybrids) and BST@CuNW hybrid structures have been reported. This work clearly explains the advantage of hybrid structure composites containing a

unique combination of conductive filler along with dielectric filler over direct mix composites. Thus, the performance of epoxy composites containing CuNW and/or BST (non-hybrids) and BST@CuNW hybrid structures has been reported. Firstly, the hybrid nanoparticles were synthesized using a facile co-precipitation technique. The XRD data confirms the presence of BST and CuNW particles in the sample. The SEM data collected on the hybrid particles demonstrate good dispersion of BST particles on the CuNW. Based on the XRD, XPS, and SEM results, it was deduced that BST particles are anchored on the surface of CuNW. A series of epoxy composites containing CuNW and/or BST were prepared and characterized for electrical, EMI shielding, and microwave absorption properties. The non-hybrid composites demonstrated frequency-independent electrical conductivity, which confirms the formation of percolated network structure in the composite. However, the hybrid nanoparticles filled epoxy composites did not exhibit a percolated electrical network even though the CuNW content in them was 10 wt% which was much higher than the percolation threshold for the CuNW-epoxy system. The hybrid composites exhibited superior absorption and lower transmission and reflection power of microwaves when compared to non-hybrid composites. The addition of BST to epoxy composites containing CuNW has improved the dielectric loss of the composites. The hybrid composites demonstrated higher dielectric loss as compared to non-hybrid composites. Overall, the nanocomposites containing BST@CuNW hybrids exhibited enhanced EMI shielding performance when compared to samples containing equivalent loading of only CuNW and/or BST. The 1 mm thick composite sample containing 10:15 (wt/wt) CuNW: BST hybrid attenuated 99.2 % of incident wave power and exhibited an EMI shielding effectiveness value of 21.2 dB in the X-band. Thus, these composites with high absorption properties will be promising materials for futuristic microwave shielding material.

6 Influence of Fe$_3$O$_4$@BST@Cunw Hybrid Nanoparticles on EMI Shielding Properties Of Epoxy Nanocomposites

6.1 Introduction

Electromagnetic interference (EMI) among business electronics and telecommunication devices is generated when the device is under signal interference from unwanted sources when these devices operate at higher frequency ranges which is a significant side-effect developed due to the rapid development in electronics and communication sectors [141]. EMI shielding at higher frequencies remains a critical concern to maintain the uninterrupted performance of electronic devices and avoid any negative impacts on human health [3,309]. To address this issue, lightweight EMI shielding materials are required to protect electronic devices from EM waves [7,322].

The primary mechanisms observed in the EMI shielding materials are reflection and absorption [12]. The reflection mechanism is predominant in metal-based EMI shielding materials, while the absorption is dominated in polymer-based EMI shielding materials [3,8,114,133,141,190,216, 285,340–345]. These polymer composites can absorb or convert the energy of EM waves into heat or other types of energy, limiting the reflection and transmission of EM waves. Polymer composites with absorption-dominated shielding mechanisms have an advantage over metal-based EMI shielding materials. Furthermore, Polymer composites are a type of material that may have their properties tailored by incorporating nanoparticles. In addition, polymer composites provide desirable properties, such as light-weight, ease of processing, and low manufacturing cost, which are mainly required in the application of EMI shielding materials [16,321,329,330]. Due to these advantages, polymer composites have been employed in the use of EMI shielding materials.

The ferrites-filled composites utilize for EMI shielding applications, but low absorption bandwidth, high density, and processing difficulty limit their usage as EMI shielding material [256,257]. Furthermore, conductive polymer composites (CPC), which are generally filled with

carbon nanoparticles, offer wide bandwidth absorption and are an excellent replacement for ferrite-filled systems as EMI shielding materials. However, while polymer composites offer benefits, they also have certain challenges, such as low dielectric permittivity or magnetic permeability at gigahertz frequencies, manufacturing difficulties, heavy-weight, and narrow-band absorption [34,131,271,331–337]. In addition, these materials primarily suffer from difficulties such as inferior electromechanical properties and irreproducibility due to agglomeration, phase separation, and poor dispersion effects associated with these fillers, which results in the deterioration of the shielding efficiency [257].

In order to overcome these challenges, hybrid nanostructures have been developed with a combination of dielectrics and magnetic and/or conductive nanomaterials. Furthermore, hybrids are a unique class of nano-structural systems that exhibit superior electric as well as magnetic characteristics (i.e., dielectric and magnetic losses), which play an important role in increasing the absorption capacity of EMI shielding materials [131,136,338–340]. This is primarily attributed to their unique synthetic nanostructures, which allow them to accomplish significant absorption of EM waves that can surpass the same synthetic nanomaterials [10]. The dielectric and magnetic losses in the EMI shielding materials can be controlled by creating a united array of hybrid structures. Furthermore, dielectric, magnetic, and conductive losses in the EMI shielding materials can be generated in the polymer matrix by adding suitable particles with a high dielectric permittivity such as $BaTiO_3$, ZnO, SiO_2, MnO_2, and TiO_2, magnetic permeability such as ferrites and hexaferrite and/or electrical conductivity such as carbon-based materials or metal-based fillers and/or conductive polymers [88,99,295,341–345,105–107,112,171,260,264,274]. Furthermore, the addition of particles in the form of nanostructures, either combined or alone, exhibits the dielectric loss, magnetic loss, and/or conductive loss-dominated shielding mechanism,

respectively [40,79,99,216,325,338,346]. Furthermore, hybrid nanostructures can limit the reflection of incident EM waves by reducing the impedance mismatch, hence enhancing shielding performance [10]. In spite of immense potential, very few studies reported on hybrid nanostructures in EMI shielding applications. This has piqued the interest of researchers in conducting research on hybrid structures applied in EMI shielding applications. Driven by this motivation, the hybrid nanostructure was prepared with conductive particles (i.e., CuNW), magnetic particles (i.e., Fe_3O_4), and dielectric particles (i.e., BST) and employed in the EMI shielding application. Moreover, CuNW is appealing because of its unique structure, cost-effectiveness, high aspect ratio, outstanding thermal conductivity, and electrical conductivity equivalent to silver [141]. Thus, CuNW-filled composites have been addressed as a potential routine for producing EMI shielding materials. In spite of this potential, very few studies have been conducted to study the EMI shielding characteristics of polymers containing CuNW in the X-band. This might be related to the lower performance of composites containing CuNW when compared to composites containing nano carbons [49,141]. Thus, there is a need to increase the EMI shielding performance of CuNW-filled composites to enable their broad use, which motivates the current work.

Driven by this motivation, the CuNW-based hybrid nanostructure was developed along with magnetic and dielectric fillers such as Fe_3O_4 and BST to generate the magnetic losses and dielectric losses, respectively, in the epoxy matrix. The hybrid structure of Fe_3O_4@BST@CuNW unique characteristics of these materials have drawn the attention of both industrial and scientific institutions. It should be noted here that a good EMI shielding material should possess reasonable electrical conductivity, magnetic loss, and dielectric loss to mitigate the EM wave propagation through the material. Thus, the development of nanocomposites with Fe_3O_4@BST@CuNW has

been proposed as a promising approach to making EMI shielding materials. Firstly, this work reported a facile synthesis of $Fe_3O_4@BST@CuNW$ hybrid particles through the coprecipitation method. The morphological properties of the CuNW, Fe_3O_4, and hybrid nanoparticles were obtained using scanning electron microscopy. X-ray diffraction analysis revealed the crystallographic phases present in the synthesized $Fe_3O_4@BST@CuNW$ hybrid particles. A set of epoxy composites containing different ratios of $Fe_3O_4@BST@CuNW$ hybrids, CuNW, BST, and Fe_3O_4 nanoparticles were prepared, and their electrical conductivity and microstructure were discussed. The EMI shielding effectiveness of the nanocomposites is also compared over the X-band frequency range of 8–12.4 GHz.

6.2 Materials and methods

6.2.1 Materials

Tetraisopropyl orthotitanate (AR) was purchased from Sigma Aldrich (Karnataka, India). Copper chloride dihydrate (AR), strontium nitrate (AR), dextrose extra pure (AR), oleic acid (AR), barium nitrate (AR), and oleyl amine (AR) were purchased from Merck (Maharashtra, India). Ammonia solution (AR) was procured from Glaxo Laboratories (Mumbai, Maharashtra). Liquid Epoxy Resin Araldite® CY230 and hardener Aradur® HY-951 were purchased from Huntsman (Maharashtra, India).

6.2.2 Synthesis of Fe_3O_4 @BST @CuNW hybrid, CuNW, and BST nanoparticles

Firstly, the last study reports a detailed description of the preparation of the BST@CuNW hybrid nanostructure particles through the facile coprecipitation process. An aqueous iron salt solution was prepared by mixing $FeCl_3$ and $FeCl_2.4H_2O$ in the stoichiometric ratio. The molar ratio of $Fe^{2+}:Fe^{3+}$ of 1:1.5 was maintained as per the literature [281,282]. The solution was stirred for 15 minutes to obtain a homogeneous mixture of iron salts. After that measured quantity of BST@CuNW was added to the salt solution. The preparation of BST@CuNW followed a similar

protocol described in the previous chapter. Subsequently, the solution was stirred for 45 minutes with a magnetic stirrer at room temperature. Afterward, the ammonia solution (30 wt.%) was added at a 1 mL/min rate to the solution. Subsequently, the final solution was stirred for 30 minutes to complete the precipitation process at room temperature. The solution was centrifuged at 10000 rpm then the precipitate was separated from the solution. The residue was washed several times with water and dried. The obtained Fe_3O_4@BST@CuNW hybrid was used for the preparation of nanocomposites. Subsequently, the final product was separated using a centrifuge (CPR 24, REMI Compufuge, India) operated at 10000 RPM for 10 minutes to obtain the sediment. Then the residue was washed several times with hexane and stored under the hexane prior to using it for composite preparation.

6.2.3 Preparation of epoxy nanocomposites

The nanocomposites were produced by mixing the required quantity of fillers, comprising Fe_3O_4@BST @CuNW hybrid nanostructure particle, CuNW and/or BST particles, in the epoxy resin for 12 minutes with an ARE-250 Mixer (Thinky, USA) [133,141]. Subsequently, the epoxy mixture was processed in an ultrasonic processor (Sonics, USA) operated at 500 W for 5 minutes in order to facilitate uniform dispersion of the fillers in the epoxy matrix. Afterward, the requisite quantity of curing agent was added, and the epoxy mixture was even further mixed in the ARE-250 Mixer for 3 minutes to ensure proper mixing of the curing agent. The epoxy mixture was then degassed in the degassing chamber before being cast in a glass mold and cured at room temperature for 12 hours. The thickness of the nanocomposite was measured to be 1 mm and was also set by the mold's dimensions. Table 6.1 illustrates the composition of the composites utilized in this study.

Table 6. 1. The composition of the composites used in this study.

Filler	Sample Code	CuNW (wt%)	Fe_3O_4 (wt%)	BST (wt%)
Pristine epoxy	PE	0	0	0
BST particles	BST8	0	0	8
CuNW	Cu10	10	0	0
Fe_3O_4@BST@CuNW hybrid	Cu10F4BST2H	10	4	2
	Cu10 F4BST4H	10	4	4
	Cu10 F4BST8H	10	4	8
	Cu10 BST2H	10	0	2

6.2.4 Characterization

The XRD patterns of Fe_3O_4@BST@CuNW hybrid nanostructure particles were collected using an X-ray diffractometer (Rigaku Miniflex, USA). The diffractograms were recorded using the Cu-Kα radiation source of wavelength (λ) = 1.54 Å at a scan rate of 2 °/min over a 2θ angle range of 20° to 80°. The microstructure of Fe_3O_4@BST@CuNW hybrid nanostructure particle and cross-section images of freeze fractured composite were observed using a scanning electron microscope FEI-APREO (Thermo Fisher, USA). The electrical resistivity was measured using a Keysight E4990A impedance analyzer in a frequency range of 25 Hz to 25 MHz. The test specimens used for resistivity measurements were of the size of 10 mm× 10 mm× 1 mm. The electrical conductivity was calculated from the resistivity value of the composite. The EMI shielding effectiveness of the nanocomposite was measured using a 2-port vector network analyzer N5230C PNA-L (Keysight Technologies, India). The vector network analyzer setup contains a coaxial to-waveguide adapter coupled to an X-band waveguide (i.e., WR-90), and a full 2-port calibration was performed before each measurement. The composite's dimension of 22.86 mm×10.16 mm was used to fit into the cavity of the sample holder, and 5 samples were measured for each composite. Then sample holder

was placed in between the two waveguides, and the scattering parameters (S_{11} or S_{22} and S_{21} or S_{12}) were measured at various frequencies over the X-band frequency range of 8 –12.4 GHz. The power coefficients, absorption coefficient (A), reflection coefficient (R), and transmission coefficient (T) were calculated by the equations of A=1-R-T where R=$|S_{11}|^2$ and T=$|S_{21}|^2$, respectively. The real and imaginary part of the complex permittivity ($\varepsilon^* = \varepsilon' - i\varepsilon''$) was determined from the obtained S-parameters by using the Nicholson–Ross–Weir (NRW) method [70,347–349]

6.3 Results and discussion

6.3.1.1 XRD characterization of Fe₃O₄@BST@CuNW hybrid, CuNW, BST, and Fe₃O₄ particles

To identify the crystallographic phases present in the Fe_3O_4@BST@CuNW hybrid, X-ray powder diffraction (XRD) was performed on particles, and data were shown in Fig.6.1. It can be observed that the XRD diffractograms were indexing different phases of Fe_3O_4, BST, and CuNW powder with respect to 2θ angles. It can be observed from Fig.6.1 that the XRD patterns of the powder sample are well-matched with standard peaks of Fe_3O_4, BST, and CuNW as per JCPDS #75−0033, JCPDS #34-0411, and JCPDS #03–1018, respectively. Furthermore, the peaks corresponding to the 2θ value of 43.3 ° and 50.5 ° in the XRD patterns of hybrid structures were well matched with the standard peaks of CuNW, and the other peak corresponding to 2θ of the value of 32.17° matched with the standard peaks of BST and remaining peaks were matched with the standard peaks of Fe_3O_4 particles. The results suggested the presence of Fe_3O_4, BST, and CuNW particles in the synthesized powder sample [312]. Importantly, no additional peaks are observed in the XRD data, indicating the absence of any impurities and the formation of pure Fe_3O_4@BST@CuNW. Moreover, it can be observed that the XRD data of the powder sample were quite broad, which suggests the formation of fine particles. It was similar to previously published literature [234,235,280–286]. Additionally, the average crystallite size of Fe_3O_4 nanoparticles present in the

Fe$_3$O$_4$@BST@CuNW hybrid structures corresponding to the 2θ value of 36.56 ° was calculated as 8.876 nm [301]. This indicates that the Fe$_3$O$_4$ particles present in hybrid structures have a nanocrystalline microstructure.
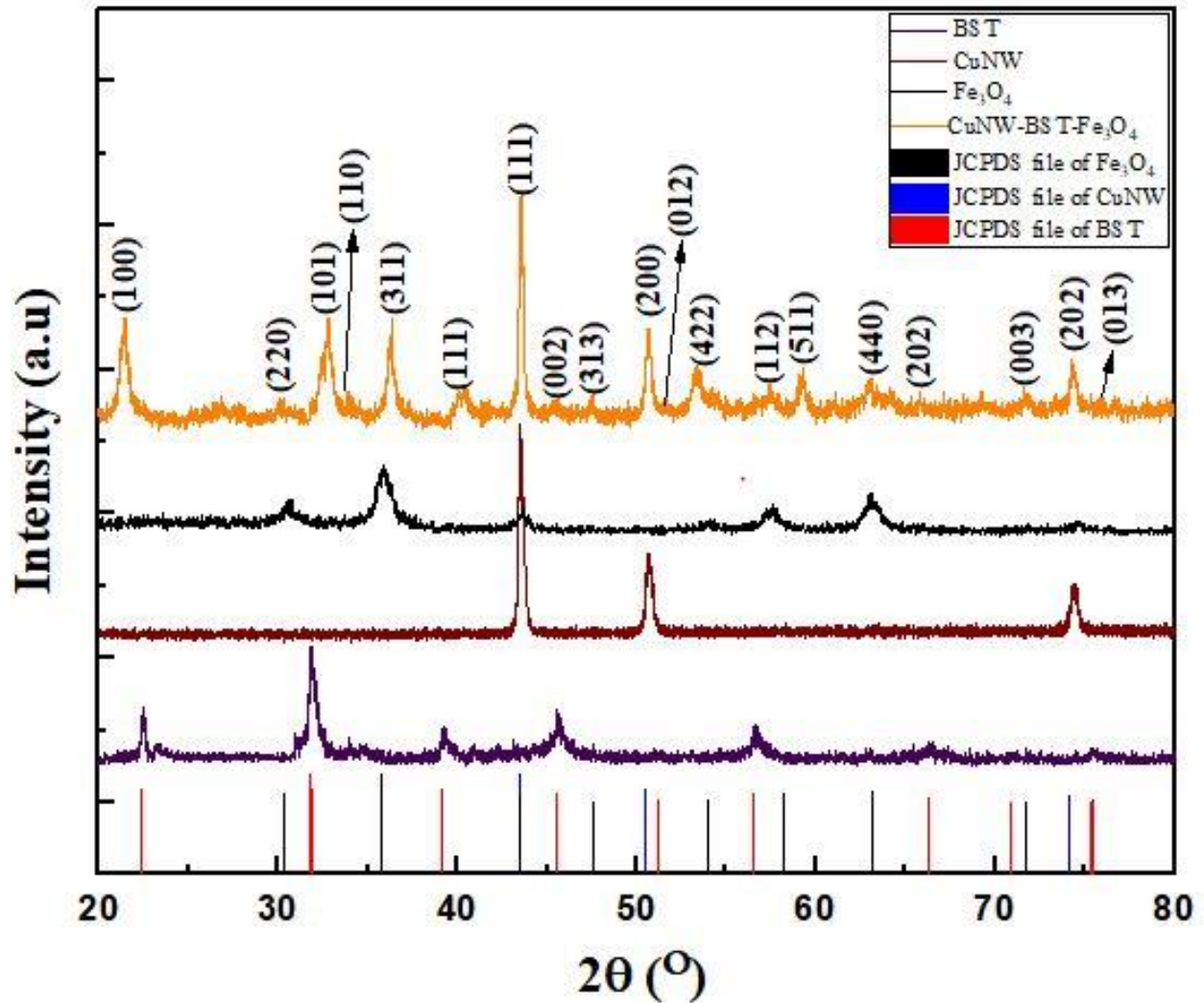
Fig.6. 1. XRD diffractograms of Fe$_3$O$_4$@BST@CuNW, CuNW, Fe$_3$O$_4$, and BST with their respective JCPDS curves

6.3.1.2 SEM characterization of Fe$_3$O$_4$@BST@CuNW hybrid, CuNW, BST, and Fe$_3$O$_4$ particles

To investigate the microstructure of Fe$_3$O$_4$@BST@CuNW hybrid structures, BST and Fe$_3$O$_4$ particles scanning electron microscopy (SEM) was performed, and the results are shown in Fig.6.2.

Furthermore, Fig.6.2 depicts the microstructure of the BST nanoparticles. It can be noticed that the synthesized BST nanoparticles formed sphere-like morphology with a rough surface. The average particle size of BST particles was calculated, and the average particle diameter of 68.63 nm. The unique shape of BST is generated during the calcining process. The results suggest that the BST particles synthesized by the present method are believed to have good sintering activity owing to their sub-micron particle size and nano-powder surface area. Similar results were also reported in the literature [312,313]. It can be observed from Fig.6.2(a) that the synthesized Fe_3O_4 particles formed spherical-shaped particles with an average particle diameter of 23 nm. Similar results were also reported in the literature [39],[40]. A previously published study reports a detailed description of the morphological properties of CuNW [280]. It can be observed that CuNW exhibited smooth surfaces with wire-like morphology [280].

Furthermore, Fig.6.2 depicts the microstructure of the Fe_3O_4@BST@CuNW hybrid structures. In contrast to smooth surface CuNW, the hybrids demonstrated that the surface of copper nanowires was covered with BST and Fe_3O_4 nanoparticles, and the results are shown in Fig.6.2(b). In addition, the presence of Cu, Fe, and O elements in Fe_3O_4@CuNW hybrid structures was confirmed with the energy dispersive X-ray analysis (EDX), as shown in Fig.6.2(d). It is also suggested that the BST and Fe_3O_4 nanoparticles were anchored onto the surface of CuNW in the hybrid sample, as shown in Fig.6.2(b). SEM was performed on the cross-section of freeze-fractured composite to investigate further the stability of the hybrid microstructure in the composites, and the result was shown in Fig.6.2(d). It was evident from Fig.6.2(d) that the hybrid structure was retained even after processing in the composites. This is attributed to the BST and Fe_3O_4 nanoparticles being firmly anchored to CuNW surfaces.
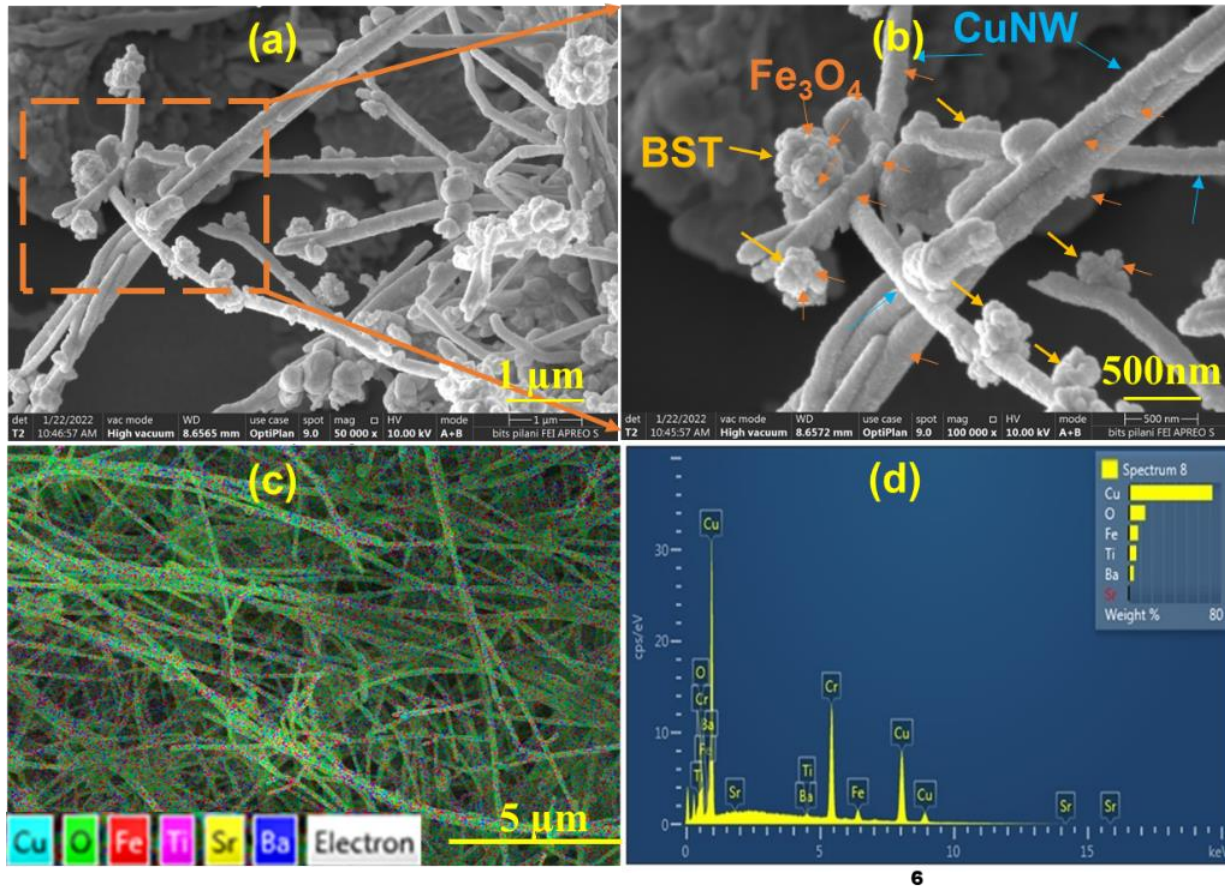
Fig.6. 2. The SEM images of Fe$_3$O$_4$@BST@CuNW hybrid nanostructures at a magnification of (a)50000 and (b) 100000, (c) element mapping of Fe$_3$O$_4$@BST@CuNW hybrid nanostructures, and (d) EDX image of Fe$_3$O$_4$@BST@CuNW hybrid nanostructures

6.3.1.3 Electrical conductivity of epoxy composites

In an effort to study the influence of the addition of CuNW, Fe$_3$O$_4$ nanoparticles, BST particles, and Fe$_3$O$_4$@BST@CuNW hybrid structures on the electrical conductivity of the nanocomposites, the electrical conductivity measurements were carried out on samples in the frequency range of 20 Hz to 25 MHz as shown in Fig.6.3(a). The Cu10BST2 composite demonstrated the highest electrical conductivity values of 4.9×10^{-7} S/m at 25 Hz. The Cu10 composite demonstrated an electrical conductivity value of 5.9×10^{-8} S/m at 25 Hz. This suggests that the nanocomposite formed a percolated network at 10 wt% loadings and demonstrated frequency-independent electrical conductivity values from 25 Hz to 100Hz. Furthermore, it was observed that no

composites containing hybrid filler (i.e., $Fe_3O_4@BST@CuNW$) exhibited percolated behavior. This can be attributed to the presence of BST and Fe_3O_4 particle decoration in the hybrid structures, reducing the interactions between CuNW, which breaks the formation of a percolated network of CuNW in the composite [128]. It can also be further suggested from the results that the hybrid microstructure of $Fe_3O_4@BST@CuNW$ nanoparticles is preserved in the epoxy composites. Similar observations were reported in the literature [3,8,133,141]. The electrical conductivity of the nanocomposites at a frequency of 25 Hz was used in the analysis. It can be observed from Fig.6.3(b) that the electrical conductivity of hybrid particles was decreased with the addition of BST filler loadings in the composite. This can be attributed to the decoration of $Fe_3O_4@BST$ nanoparticles on CuNW, reducing its electrical conductivity.
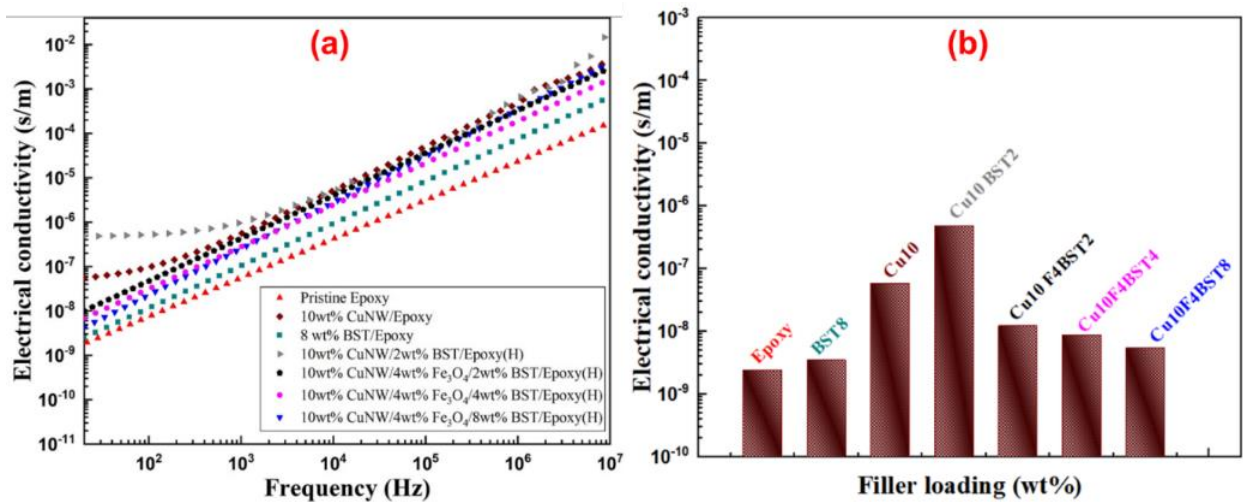
Fig.6. 3. The electrical conductivity values (a) as a function of frequency and (b) as a function of filler loading

6.3.1.4 EMI shielding effectiveness of epoxy composites.

The EMI shielding effectiveness of the epoxy composites containing CuNW, BST, Fe_3O_4, and $Fe_3O_4@BST@CuNW$ hybrid structures over the X-band in the frequency range of 8-12.4 GHz was determined, and the results are shown in Fig.6.4. It can be observed from Fig.6.4(a) that the pristine epoxy sample was exhibited a very low total shielding effectiveness value (SE_T) of 1.7

dB. This is attributed to the electrically insulating and non-magnetic nature of the epoxy matrix, which renders it transparent to EM waves [3]. The addition of 4 wt% of Fe_3O_4 nanoparticles to epoxy marginally increased its SE_T value to 2.2 dB in the X-band frequency range. The addition of 8 wt% of BST to epoxy increased its SE_T value to 2 dB. In contrast, the addition of 10 wt% CuNW to the epoxy matrix increases the SE_T value 5 times more than pristine epoxy. These results suggest that CuNW is more effective in improving the EMI shielding performance as compared to BST and Fe_3O_4 nanoparticles. It can also be seen from Fig.6.4(a) that the epoxy composites containing these particles, i.e., CuNW and BST, and Fe_3O_4, exhibited higher EMI shielding effectiveness values when compared to composites containing only CuNW or BST, or Fe_3O_4. In this work, we reported that the direct addition of BST particles and Fe_3O_4 nanoparticles in the presence of CuNW in epoxy composites enhance the EMI shielding performance of the composites.

In contrast, composites containing Fe_3O_4@BST@CuNW hybrid nanoparticles exhibit BST filler content-dependent EMI shielding effectiveness. In particular, the sample Cu10F4BST8H, which contained a hybrid nanoparticle having BST: Fe_3O_4: CuNW in the weight ratio of 8:4:10, exhibited the highest SE_T value of 36.5 dB in the X band frequency range. It should be noted here that the total filler loading in the hybrid composite sample Cu10F4BST8H was 22 wt%, which is equivalent to having 10 wt% CuNW and 4 wt% of Fe_3O_4 and 8wt% of BST in the composite. This suggests that the hybrid nanoparticles containing equivalent loading of fillers were better than when compared to composites containing only CuNW, BST, or Fe_3O_4 for enhancing EMI shielding effectiveness in composites.

The increased EMI shielding in composites containing hybrid nanoparticles can be attributed to the combined effects of multiple interfacial polarization coupled with the magnetic losses arising

from the presence of BST particles and Fe_3O_4 nanoparticles [90,99,306,350–352]. It can be observed from SEM images that BST particles are firmly decorated on the CuNW surfaces, which enhances the dielectric losses due to interfacial polarization effects between the BST and CuNW. It can also be observed that Fe_3O_4 nanoparticles are firmly anchored to the BST@CuNW surfaces. This anchoring of Fe_3O_4 on the BST@CuNW surface enhances the magnetic losses due to the presence of Fe_3O_4 on BST@CuNW. It should be noted here that the hybrid samples Cu10F4BST2H and Cu10F4BST4H exhibited lower SE_T values as compared to Cu10F4BST8H. This further suggests that BST content in the hybrid influences its EMI shielding capability in the composites. This may be attributed to reduced interfacial polarization losses in Cu10F4BST2H samples due to the low BST content in the hybrids as compared to Cu10F4BST8H. However, with the higher loadings of BST contents in the hybrids, there may be an agglomeration of nanoparticles, impacting proper filler dispersion and shielding performance. This further suggests an optimum loading of BST on the CuNW, which is beneficial for increasing the EMI shielding performance. Furthermore, it can be observed from Fig.6.4(b) that the hybrid composites have exhibited lower SE_R values than epoxy composites containing 10 wt% CuNW. This further suggests the composites containing hybrid nanoparticle(s) demonstrated lower reflection loss than epoxy composites containing 10 wt% CuNW. In contrast, the composites demonstrated higher SE_A values than those SE_R values. Furthermore, the hybrid samples demonstrated higher SE_A values than those 10 wt% CuNW. This may be attributed to increasing EM wave absorption due to the unique hybrid structure. The results suggested that the composites exhibited an absorption-dominant shielding mechanism.
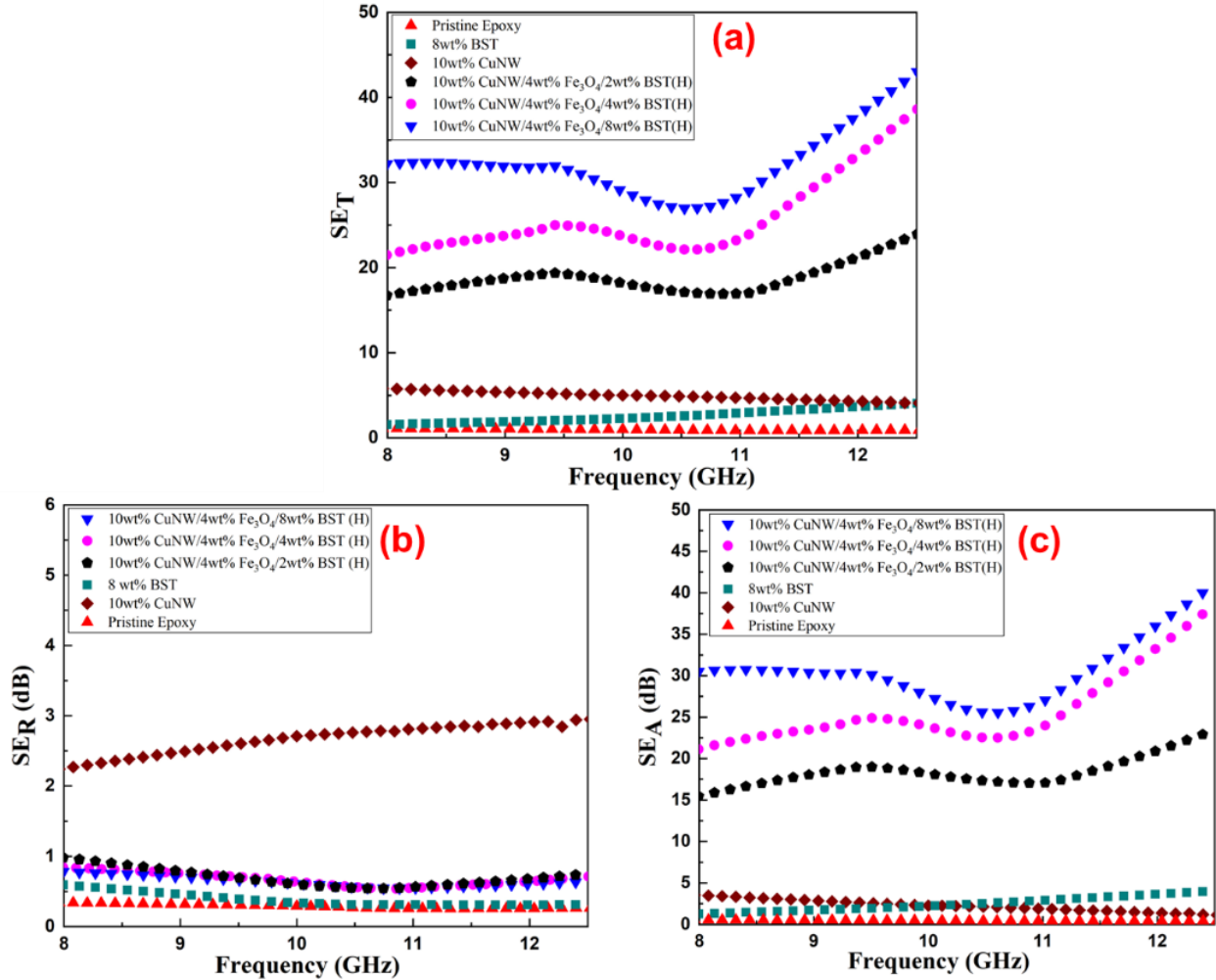
Fig.6. 4. Plots of (a) SE_T, (b) SE_R, and (c) SE_A of epoxy composites as a function of frequency

6.3.1.5 Complex permeability and permittivity of epoxy composites

To further investigate the dielectric and magnetic losses of epoxy composites, complex permittivity, and permeability were calculated using the NRW method in the X-band frequency range of 8-12.4 GHz. The complex permittivity values (i.e., ε' and ε'') of hybrid composites were shown in Fig.6.5. It can be observed from Fig.6.5 (a and b) that ε' values of the composites were increased with the addition of the BST filler loadings. It can be observed that the hybrid samples demonstrated a higher ε' value than the epoxy composite containing 10 wt% of CuNW. Similar behavior was reported in the literature [3]. The pristine epoxy composite has demonstrated the ε' value of 3.5. This is attributed to the insulative nature of the epoxy matrix. The Cu10F4BST8H

hybrid sample has demonstrated 5 times higher than the epoxy composite. In addition, ε'' values of the composites were increased with the addition of the BST filler loadings and demonstrated a similar trend with the frequency.

The ε'' value of the pristine epoxy has demonstrated the lowest value of 0.1. The hybrid composites exhibited higher ε'' values as compared to the Cu10 sample. These ε'' values of the composites are attributed to the formation of interface polarization among CuNW, BST, Fe_3O_4, and epoxy, thereby increasing the dielectric losses of the composite. The results suggested that the hybrid composites exhibited higher dielectric losses as compared to the Cu10 sample. The hybrid structure in the composite could also help to improve the multiple polarizations at the interface of hybrid structures that enhance the dielectric loss of the hybrid composites. Thus, strong attenuation of the EM wave in the composite can be achievable
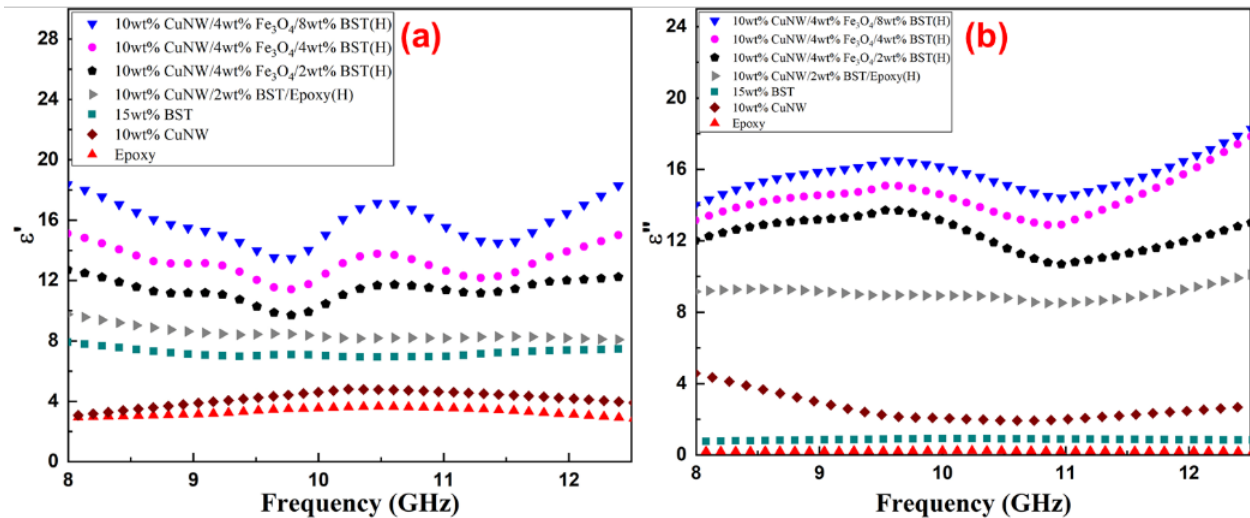
Fig.6. 5. The (a) ε' values and (b) ε'' values of the epoxy composites as a function of frequency

Furthermore, the permeability (i.e., μ' and μ'') of epoxy composites in the X-band frequency range of 8-12.4 GHz, as shown in Fig.6.6. It can be observed that the μ' values of the epoxy composites were increased with the addition of filler loadings and demonstrated a similar trend with the frequency. Similar behavior was reported in the literature [3,133]. The μ' and μ'' values of the

pristine epoxy sample exhibited are 0.52 and 0.5, respectively, which are the lowest values compared to all other composites. This suggested that the epoxy exhibited low magnetic loss to the incident EM wave. It was reported that the composites containing Fe_3O_4, the μ' value of 1 and the μ'' value of 0.6, which indicates that Fe_3O_4 has a reasonable magnetic loss. Furthermore, the hybrid and hybrid composites demonstrated better values of μ' as compared to an epoxy composite containing only Fe_3O_4 or CuNW. The results suggested that the hybrid structures helped in the enhancement of μ' values for the composites. The Cu10F4BST8H sample exhibited higher μ' values compared to all other epoxy composites. Furthermore, μ'' values of the hybrid samples exhibited higher than epoxy composites containing 10wt% of CuNW. This suggested that hybrid composites formed a higher magnetic loss than 10wt% of CuNW composites. The Cu10F4BST8H sample exhibited higher μ'' values compared to all other epoxy composites. The hybrid composites exhibited more magnetic loss than 10wt% of CuNW composites in the X-band frequency range. It can imply that the formation of hybrid structures enhances magnetic loss, which plays an essential role in the absorption of EM waves. It can be observed from the results that the dielectric loss values of the nanocomposites are more than their magnetic loss values. Therefore, the main contributor to the shielding performance of the composites is a dielectric loss rather than a magnetic loss.
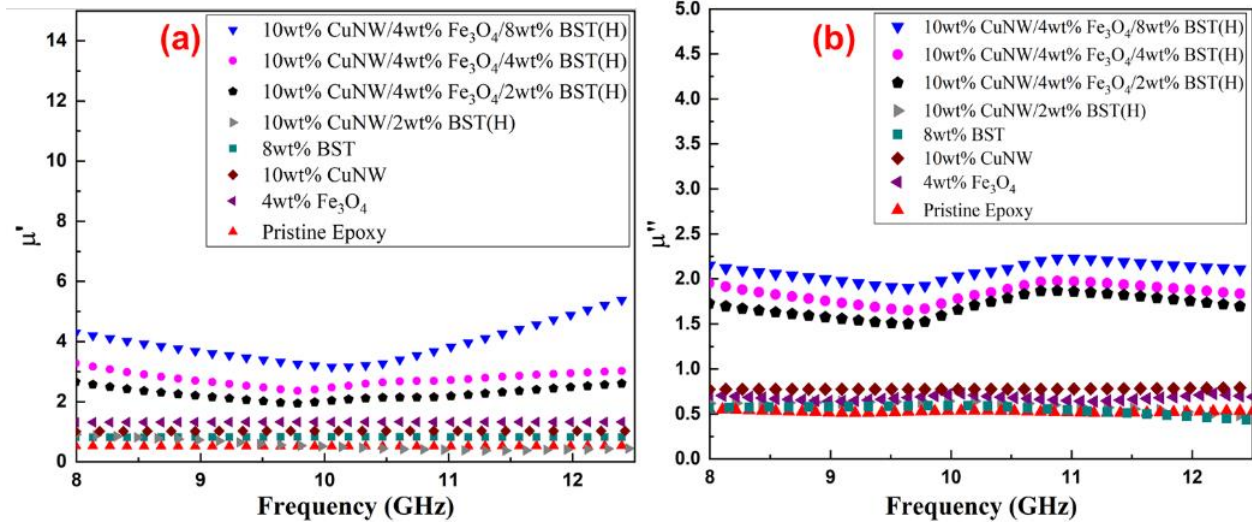
Fig.6. 6. The (a) μ' values and (b) μ'' values of the epoxy composites as a function of frequency

6.3.1.6 Reflection and Absorption losses of epoxy composites

To evaluate the electromagnetic interaction behavior of the hybrid composites, the absorption, reflection, and transmission power ratios of the Fe_3O_4@BST@CuNW hybrid composites were calculated and shown in Fig.6.7. The contributions arising from multiple internal reflections were excluded from this study since they could not be measured independently. It can be observed from Fig.6.7 that the pristine epoxy (PE) reflected 6% and absorbed 4% of the incident EM power in the X-band. Furthermore, the addition of 10wt% CuNW (i.e., Cu10) has increased reflected power by 7 times and absorbed power by 8.5 times when compared to the PE sample. The results suggested that the boost in absorbed power may be ascribed to interfacial polarisation effects, while the gain in reflected power can be ascribed to an improvement in the electrical conductivity of the composite. On the other hand, incorporating 8wt% of BST (i.e., BST8) into an epoxy boosted reflected power by 1.84 times and absorbed power by 3.2 times more than the PE sample. It indicates that the BST8 composite exhibited a low dielectric loss and no noticeable impact on the reflection or absorption of microwaves. In similar, the addition of 4wt% Fe_3O_4 (i.e., F4) to the

epoxy has increased the reflected power by 1.5 times and absorbed power by 3 times more than the PE sample.

The reflection and absorbed power of hybrid epoxy composites were calculated and shown in Fig.6.7. The results suggested that the addition of BST to the epoxy composite containing 10wt% CuNW and 4wt% Fe_3O_4 modifies both the absorption and reflection of incident microwave power of the composites. In comparison to Cu10 composite, hybrid composites exhibited significantly greater absorbed power, noticeably lower reflected power, and transmitted power in the X-band. The hybrid composite Cu104FBST2H, which contains the same quantity of CuNW, displayed 2.31 times greater absorption and 2.74 times and 5.08 times lower reflected and transmitted EM power, respectively. These results suggest that the addition of BST and Fe_3O_4 along with CuNW provides benefits over only the addition of CuNW in terms of absorption of EM power in the X-band. Similarly, the Cu10F4BST4H and Cu10F4BST8H composites demonstrated higher absorption and lower reflection and transmitted power as compared to the Cu10F4BST2H composite. This suggested that the addition of BST, along with 4wt% Fe_3O_4 and 10wt% CuNW, has improved the absorption, thereby reducing the reflected and transmitted power. The Cu10F4BST8H composite demonstrated higher absorption power of 82.6% and lower transmittance and reflected power of 3.2% and 13.7%, respectively. The improved microwave absorbance in hybrid composites might be due to higher interfacial polarisation effects, as well as the presence of multiple reflections and dielectric loss within the composite. Moreover, multiple internal reflections across interfaces can significantly lengthen the microwave travel route in the composite, increasing its susceptibility to re-absorption by the Fe_3O_4@BST@CuNW hybrid particles through both conduction and dielectric loss mechanisms.
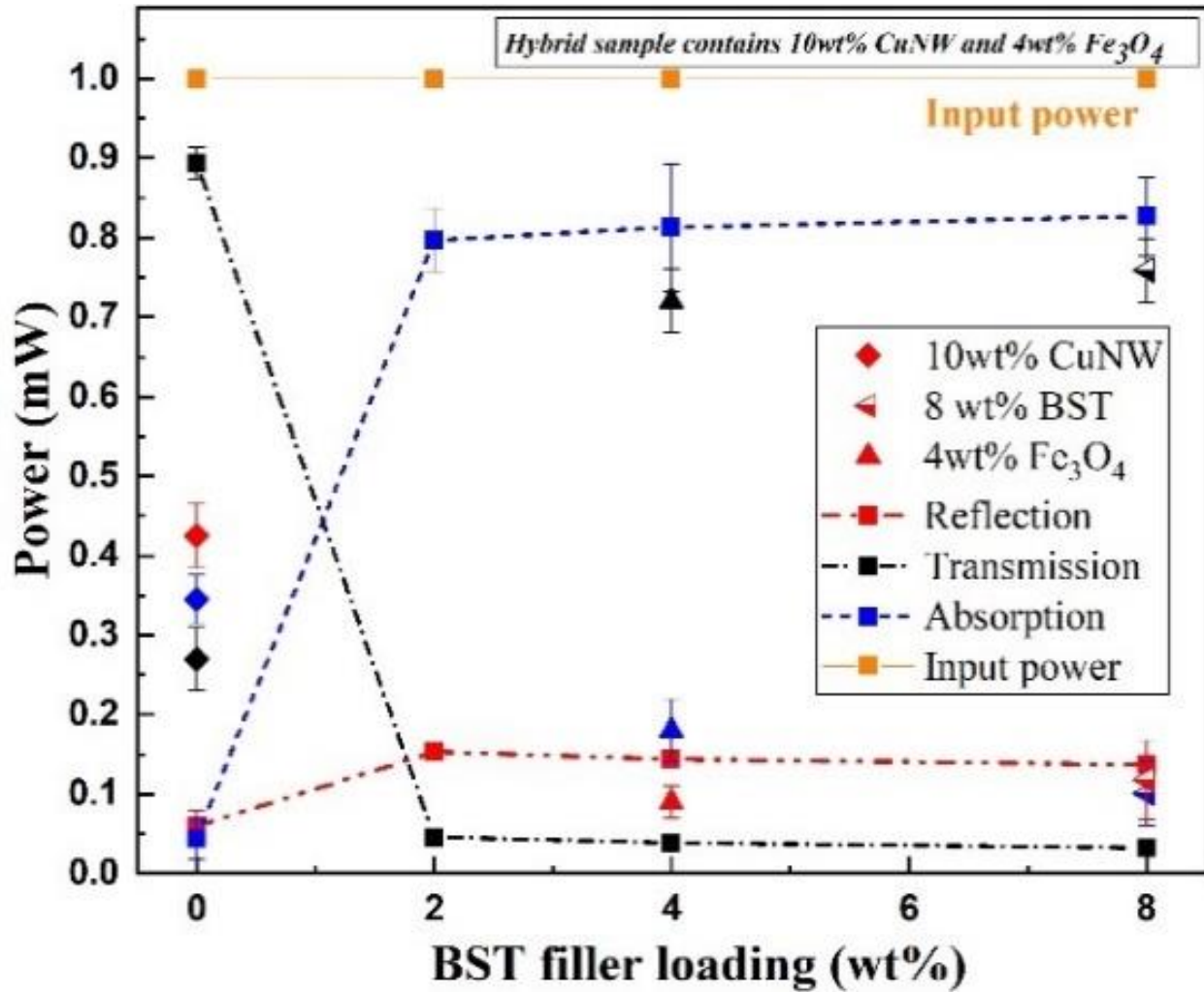
Fig.6. 7. The absorbed, reflected, and transmitted power of epoxy composites as a function of BST filler loading

6.4 Conclusion

The hybrid composites containing Fe₃O₄@BST@CuNW were prepared through a resin blending process which is a fast, highly reproducible, and production-friendly approach to preparing an epoxy composite. First of all, the facile synthesis process of hybrid nanostructures formed with conductive, dielectric, and magnetic filler (i.e., Fe₃O₄@BST@CuNW) through coprecipitation was clearly explained. The XRD patterns of Fe₃O₄@BST@CuNW particles confirm the presence of CuNW, BST, and Fe₃O₄ nanoparticles synthesized powder. SEM images obtained on the hybrid nanostructures demonstrate the anchoring of BST and Fe₃O₄ nanoparticles on the surface of

CuNW. A series of epoxy nanocomposites with different amounts of Fe_3O_4@BST@CuNW, CuNW, BST, or Fe_3O_4 nanoparticles were prepared and characterized for electrical conductivity, magnetic, dielectric, microwave absorption, and EMI shielding properties. The electrical conductivity data collected on the epoxy composites reveals that the epoxy composites containing hybrid structures did not exhibit a percolated behavior. The Cu10BST2D sample exhibited a higher electrical conductivity value of 6.8×10^{-7} s/m compared to all other epoxy composites. The hybrid epoxy samples have demonstrated higher dielectric loss when compared to the Cu10 sample having the same amount of CuNW filler loading. Similarly, the hybrid composites have exhibited higher magnetic loss as compared to the F4 sample having the same filler loading of Fe_3O_4. The epoxy composite containing Fe_3O_4@BST@CuNW hybrids exhibited greater SE_T values. The hybrid composites demonstrated higher EMI shielding performance when compared to samples containing equivalent loading of only CuNW, BST, or Fe_3O_4. Furthermore, the epoxy composites containing CuNW and Fe_3O_4 exhibited an absorption-dominated mechanism which was found responsible for the improvement in the EMI shielding effectiveness in these composites. The hybrid composites demonstrated superior absorption power and lower reflected and transmitted power. The 1-mm thick composite sample containing 4:8:10 (wt/wt) Fe_3O_4:BST: CuNW hybrid attenuated 99.92 % in that majority portion 80.6% of the incident microwave power was absorbed in the X-band.

7 Conclusions and Future work

7.1 Conclusions

The main goal of good EMI shield is to keep sensitive electronics from being affected by electromagnetic interference (EMI) or radio frequency interference (RFI). The choice of an EMI shielding material depends on several factors, including the frequency of the electromagnetic radiation, the size and shape of the electronic device, and the required level of shielding effectiveness. Traditionally, metals were used for EMI shielding but they are prone to corrosion, are bulky, and can only reflect the electromagnetic energy, which at best only partially mitigates the EMI issue. Polymer composites offers an attractive alternative to metals for use as EMI shielding owing to their lightweight and tailorable properties. In this work, the EMI shielding and microwave absorption performance of CuNWs based epoxy nanocomposites in the X-band frequency range, i.e., 8-12.4 GHz, was investigated. The addition of Fe_3O_4 or BST nanoparticles to CuNW-epoxy composites resulted in enhanced of the EMI shielding effectiveness. Furthermore, CuNW based hybrid nanoparticles were found to significantly enhance the shielding performance in the epoxy composites when compared to those containing equivalent loading non-hybrid nanoparticles. The outcomes from the research work presented in this thesis can be summarized as the following:

- CuNWs were prepared through a facile one pot hydrothermal method and XRD and SEM characterizations were performed to confirm their synthesis.

- A series of CuNW-filled epoxy composites containing different loadings of CuNWs were prepared and were characterized for their microstructure, electrical conductivity and EMI shielding effectivenss.

- The percolation threshold in these composites was determined to be 10.8 wt% CuNW through the electrical conductivity measurements and fitting the data to the power law model.

- The 12 wt% CuNW containing epoxy composites demonstrated the highest EMI shielding effectiveness (i.e., SE_T) of 6.5dB which translated to 77.1% attenuation of the incident EM wave power. The loss due to absorption mechanism was determined to be 37% of the incident wave power in the composite.

- The addition of magnetic (i.e., Fe_3O_4) or dielectric (i.e., $BaSrTiO_3$) materials added along with CuNW successfully increased the microwave absorption and EMI shielding performance of hybrid epoxy composites.

- A series of composites containing 12 wt% CuNW and varying weight percentages of Fe_3O_4 were prepared and tested. The composite sample containing 12 wt% CuNW and 8 wt% Fe_3O_4 demonstrated the highest SE_T value of 14.6 dB in the X-band frequency range among all the composites tested.

- The SE_T value for a composite containing both particles was found to be significantly more than the composites containing equivalent loading of only either of these particles, which suggested a synergistic effect between these particles that enhances the EMI shielding performance in the composites.

- To explore further on the observed synergy between conductive and magnetic nanoparticles, an epoxy composite containing an altogether different filler system, i.e., graphene nanoplatelets (GNP) and Barium hexaferrite (BaM), was prepared and characterized.

- A set of epoxy composites were made using varying weight ratios of GNP:BaM and when tested for their EMI shielding performance revealed similar synergistic enhancement in SE_T as observed for the CuNW/Fe_3O_4 epoxy composites.

- An one-millimeter-thick composite sample containing 8 wt% BaM and 10 wt% GNP exhibited a SE_T value of 17.2 dB in the X-band frequency range, which equates to attenuation of 98.17% of incident wave power.

- The hybrid particles (i.e., Fe_3O_4@CuNW) containing varying weight ratio of Fe_3O_4:CuNW were hydrothermally synthesized and characterized using XRD, SEM, and XPS.

- The epoxy composites containing Fe_3O_4@CuNW were made and tested for their EMI shielding performance..

- An one-millimeter thick 12:8 (wt%:wt%) CuNW: Fe_3O_4 hybrid containing epoxy composite exhibited a SE_T value of 19.3 dB in the X-band, which translates to attenuation of 98.8% of the microwave power. When compared to the non-hybrid composite containing equivalent loadings of Fe_3O_4 and CuNW nanoparticles, these composites exhibited 60.8% higher absorption and approximately 68% lower microwave power transmittance.

- To understand the influence of dielectric filler on the SE_T values, epoxy composite filled with CuNW and/or $BaSrTiO_3$(BST) and their hybrid, i.e., BST@CuNW, were prepared and tested.

- The BST@CuNW hybrid composite exhibited superior EMI shielding performance when compared to samples containing equivalent loading of only CuNW and/or BST.

- An one millimeter thick 10:15 (wt%:wt%) CuNW:BST hybrid containing composite sample attenuated 99.2 % of incident wave power and exhibited a SE_T value of 21.2 dB in the X-band. The composite demonstrated 40 % higher absorption and approximately 80% lower microwave power reflection as compared to the non-hybrid composite, which contained the same amount of BST and CuNW nanoparticles.

- To study the simultaeneous addition of both BST and Fe_3O_4 in CuNW/epoxy composites, Fe_3O_4@BST@CuNW hybrid particles were synthesized by a facile co-precipitation method and characterized with XRD and SEM

- The SE_T values obtained on epoxy composites containing Fe_3O_4@BST@CuNW hybrid were significantly more than those containing equivalent loading of CuNW, BST, or Fe_3O_4.

- An one-millimeter thick composite containing 4:8:10 (wt%:wt%:wt%) Fe_3O_4: BST: CuNW hybrid filler attenuated 99.91 % of incident wave power with absorption power of 80.2% in the X-band.

- Based on the results obtained in this research, it is demonstrated that EMI shielding of CuNW-epoxy composites can be significantly improved with the addition of CuNW-based hybrid nanostructures and an absorption-dominated attenuation mechanism exists in these composites.

7.2 Future work

The present studies were focussed on epoxy composites containing CuNWs and their hybrids to determine their EMI shielding and microwave absorption capabilities in the X-band frequency range. It is evident from the research results obtained in this study that conductive particles modified with magnetic or dielectric particles could significantly enhance the EMI shielding properties of polymer composites containing such particles. Moreover, an absorption dominant shielding mechanism is observed in these composites. However, only a limited number of polymer-filler systems could be analysed in this study and there exists a definite scope for further research to better understand the influence of dielectric and/or magnetic nanoparticles on EMI shielding capabilities of polymer composites. The following summarizes a few pointers for further research in this direction:

- Various types of potential conductive particles, such as nickel, silver, and MXenes, have significant potential to be employed as conductive fillers in alternative to CuNW for the EMI shielding applications.

- There is a wide range of scope available when it comes to the preparation of hybrid materials. Even yet, there is a majority of work that may be accomplished in this field.

- The hybrid structures can be developed with various combinations of magnetic materials such as ferrites, AFe_2O_4 where (A = divalent metal ions like Cu, Co, Mn, Ni, Zn) and hexaferrite, $X_2Y_2Fe_{12}O_{22}$ (where X=Ba, Sr, Mg, Pb, and Y= Cu, Co, Zn) and dielectric materials such as MoO_3, $BaTiO_3$, TiO_2, $SrTiO_3$, ZnO, ZnS, SnO_2.

- The combination of these materials has the potential to develop novel hybrid materials, which have the capability of being used in the production of materials that can absorb microwaves.

- For example, the EMI shielding performance and microwave absorbing properties of epoxy composites containing BST/ GNP and Fe_3O_4 /BST/GNP particles and their hybrids will be investigated.

- Yet another, the development of foaming structures and multilayer structures, is considered one of the important aspects in the preparation of EMI shielding materials. These aspects can effectively block EM waves.

- It is hypothesized that these structures improve the multiple internal reflections inside the material, which boosts shielding effectiveness. Therefore, applying these aspects in the preparation of EMI shielding materials will establish a new pathway for the development of effective shielding materials.

- Throughout the course of our research study, our studies majorly focused on X-band frequency. However, the S-band frequency range is used by many electronic devices that we use in our day-to-day lives, such as mobile phones, Wi-Fi routers, and other devices.

- In addition, Ku-band is being utilized by satellites as well as other military applications. As a result, it is essential to design shielding materials that can limit the amount of signal interference in the S-band and Ku-band frequency ranges.

- It is worth mentioning that the majority of EMI shielding materials are limited to the laboratory level. It is important to commercialize these products for real-time applications.

References

[1]   K. Nasouri, A.M. Shoushtari, M.R.M. Mojtahedi, Theoretical and experimental studies on EMI shielding mechanisms of multi-walled carbon nanotubes reinforced high performance composite nanofibers, J. Polym. Res. 23 (2016) 3–10. https://doi.org/10.1007/s10965-016-0943-3.

[2]   L. Huang, J. Li, Y. Li, X. He, Y. Yuan, Lightweight and flexible hybrid film based on delicate design of electrospun nanofibers for high-performance electromagnetic interference shielding, Nanoscale. 11 (2019) 8616–8625. https://doi.org/10.1039/c9nr02102g.

[3]   K. Bhaskaran, R.K. Bheema, K.C. Etika, The influence of Fe3O4@GNP hybrids on enhancing the EMI shielding effectiveness of epoxy composites in the X-band, Synth. Met. 265 (2020). https://doi.org/10.1016/j.synthmet.2020.116374.

[4]   D. Jiang, V. Murugadoss, Y. Wang, J. Lin, T. Ding, Z. Wang, Q. Shao, C. Wang, H. Liu, N. Lu, R. Wei, A. Subramania, Z. Guo, Electromagnetic Interference Shielding Polymers and Nanocomposites - A Review, Polym. Rev. 59 (2019) 280–337. https://doi.org/10.1080/15583724.2018.1546737.

[5]   J. Kruželák, A. Kvasničáková, K. Hloževeková, I. Hudec, Progress in polymers and polymer composites used as efficient materials for EMI shielding, Nanoscale Adv. 3 (2021) 123–172. https://doi.org/10.1039/d0na00760a.

[6]   S. Geetha, K. K. Satheesh Kumar, Chepuri R. K. Rao, M. Vijayan, D. C. Trivedi, EMI Shielding: Methods and Materials—A Review S., J. Appl. Polym. Sci. 116 (2010) 2658–2667. https://doi.org/10.1002/app.

[7]   S. Verma, M. Dhangar, S. Paul, K. Chaturvedi, M.A. Khan, A.K. Srivastava, Recent Advances for Fabricating Smart Electromagnetic Interference Shielding Textile: A Comprehensive Review, Electron. Mater. Lett. 18 (2022) 331–344. https://doi.org/10.1007/s13391-022-00344-w.

[8]   V. Uma Varun, B. Rajesh Kumar, K.C. Etika, Hybrid polymer nanocomposites as EMI shielding materials in the X-band, Mater. Today Proc. (2020) 10–12. https://doi.org/10.1016/j.matpr.2019.12.300.

[9]   Y. Yao, S. Jin, H. Zou, L. Li, X. Ma, G. Lv, F. Gao, X. Lv, Q. Shu, Polymer-based lightweight materials for electromagnetic interference shielding: a review, J. Mater. Sci. 56 (2021) 6549–6580. https://doi.org/10.1007/s10853-020-05635-x.

[10]   H. Pang, Y. Duan, L. Huang, L. Song, J. Liu, T. Zhang, X. Yang, J. Liu, X. Ma, J. Di, X. Liu, Research advances in composition, structure and mechanisms of microwave absorbing materials, Compos. Part B Eng. 224 (2021) 109173. https://doi.org/10.1016/j.compositesb.2021.109173.

[11]   P. Saini, M. Arora, G. Gupta, B.K. Gupta, V.N. Singh, V. Choudhary, High permittivity polyaniline-barium titanate nanocomposites with excellent electromagnetic interference shielding response, Nanoscale. 5 (2013) 4330–4336. https://doi.org/10.1039/c3nr00634d.

[12]   X.C. Tong, Advanced materials and design for electromagnetic interference shielding text book,2009, (n.d.).

[13]   G.G. Bush, Measurement techniques for permeability, permittivity and EMI shielding: A review, IEEE Int. Symp. Electromagn. Compat. (1994) 333–339. https://doi.org/10.1109/isemc.1994.385635.

[14]   V. Choudary, S.K. Dhawan, P. Saini, Polymer based nanocomposites for electromagnetic

interference (EMI) shielding, 2012.

[15] D.D.L. Chung, Materials for electromagnetic interference shielding, Mater. Chem. Phys. 255 (2020) 123587. https://doi.org/10.1016/j.matchemphys.2020.123587.

[16] H. Abbasi, M. Antunes, J.I. Velasco, Recent advances in carbon-based polymer nanocomposites for electromagnetic interference shielding, Prog. Mater. Sci. 103 (2019) 319–373. https://doi.org/10.1016/j.pmatsci.2019.02.003.

[17] S. Thomas, Advanced Materials for Electromagnetic Shielding, 2018. https://doi.org/10.1002/9781119128625.

[18] G. Sun, B. Dong, M. Cao, B. Wei, C. Hu, Hierarchical dendrite-like magnetic materials of Fe3O 4, γ-Fe2O3, and Fe with high performance of microwave absorption, Chem. Mater. 23 (2011) 1587–1593. https://doi.org/10.1021/cm103441u.

[19] M. Shahbaz, I. Sadiq, M.M.H. Butt, A. Basit Javaid, M. Idrees, S. Hussain, F. Sadiq, S. Riaz, S. Naseem, H.M. Khan, Peculiar magnetic behavior and structural, electrical, dielectric properties of substituted R-type hexagonal ferrites, J. Magn. Magn. Mater. 499 (2020) 166309. https://doi.org/10.1016/j.jmmm.2019.166309.

[20] S. Qu, G. Wu, J. Fang, D. Zang, H. Xing, L. Wang, H. Wu, Dielectric and Magnetic Loss Behavior of Nanooxides, Spectrosc. Methods Nanomater. Charact. 2 (2017) 301–319. https://doi.org/10.1016/B978-0-323-46140-5.00011-X.

[21] X. Sun, J. He, G. Li, J. Tang, T. Wang, Y. Guo, H. Xue, Laminated magnetic graphene with enhanced electromagnetic wave absorption properties, J. Mater. Chem. C. 1 (2013) 765–777. https://doi.org/10.1039/c2tc00159d.

[22] W.C. Yu, T. Wang, Y.H. Liu, Z.G. Wang, L. Xu, J.H. Tang, K. Dai, H.J. Duan, J.Z. Xu, Z.M. Li, Superior and highly absorbed electromagnetic interference shielding performance achieved by designing the reflection-absorption-integrated shielding compartment with conductive wall and lossy core, Chem. Eng. J. 393 (2020) 124644. https://doi.org/10.1016/j.cej.2020.124644.

[23] S.M. Abbas, A.K. Dixit, R. Chatterjee, T.C. Goel, Complex permittivity, complex permeability and microwave absorption properties of ferrite-polymer composites, J. Magn. Magn. Mater. 309 (2007) 20–24. https://doi.org/10.1016/j.jmmm.2006.06.006.

[24] A. Raveendran, M.T. Sebastian, S. Raman, Applications of Microwave Materials: A Review, J. Electron. Mater. 48 (2019). https://doi.org/10.1007/s11664-019-07049-1.

[25] B.S. Kwak, W.H. Choi, Y.H. Noh, G.W. Jeong, J.G. Yook, J.H. Kweon, Y.W. Nam, Nickel-coated glass/epoxy honeycomb sandwich composite for broadband RCS reduction, Compos. Part B Eng. 191 (2020) 107952. https://doi.org/10.1016/j.compositesb.2020.107952.

[26] Y. Jiang, Y. Chen, Y.J. Liu, G.X. Sui, Lightweight spongy bone-like graphene@SiC aerogel composites for high-performance microwave absorption, Chem. Eng. J. 337 (2018) 522–531. https://doi.org/10.1016/j.cej.2017.12.131.

[27] H. Wang, F. Meng, F. Huang, C. Jing, Y. Li, W. Wei, Z. Zhou, Interface Modulating CNTs@PANi Hybrids by Controlled Unzipping of the Walls of CNTs to Achieve Tunable High-Performance Microwave Absorption, ACS Appl. Mater. Interfaces. 11 (2019) 12142–12153. https://doi.org/10.1021/acsami.9b01122.

[28] A. Wigfield, J. Eccles, D. Rodriguez, Introduction to Electromagnetic compatability, (2013) 404.

[29] M. Green, X. Chen, Recent progress of nanomaterials for microwave absorption, J. Mater. 5 (2019) 503–541. https://doi.org/10.1016/j.jmat.2019.07.003.

[30] P. Saini, V. Choudhary, Enhanced electromagnetic interference shielding effectiveness of polyaniline functionalized carbon nanotubes filled polystyrene composites, J. Nanoparticle Res. 15 (2013). https://doi.org/10.1007/s11051-012-1415-2.

[31] F. Meng, H. Wang, F. Huang, Y. Guo, Z. Wang, D. Hui, Z. Zhou, Graphene-based microwave absorbing composites: A review and prospective, Compos. Part B Eng. 137 (2018) 260–277. https://doi.org/10.1016/j.compositesb.2017.11.023.

[32] J. Liu, W.Q. Cao, H.B. Jin, J. Yuan, D.Q. Zhang, M.S. Cao, Enhanced permittivity and multi-region microwave absorption of nanoneedle-like ZnO in the X-band at elevated temperature, J. Mater. Chem. C. 3 (2015) 4670–4677. https://doi.org/10.1039/c5tc00426h.

[33] A. Elahi, M. Ahmad, I. Ali, M.U. Rana, Preparation and properties of sol-gel synthesized Mg-substituted Ni 2Y hexagonal ferrites, Ceram. Int. 39 (2013) 983–990. https://doi.org/10.1016/j.ceramint.2012.07.016.

[34] S.K. Singh, M.J. Akhtar, K.K. Kar, Hierarchical Carbon Nanotube-Coated Carbon Fiber: Ultra Lightweight, Thin, and Highly Efficient Microwave Absorber, ACS Appl. Mater. Interfaces. 10 (2018) 24816–24828. https://doi.org/10.1021/acsami.8b06673.

[35] M. Verma, A.P. Singh, P. Sambyal, B.P. Singh, S.K. Dhawan, V. Choudhary, Barium ferrite decorated reduced graphene oxide nanocomposite for effective electromagnetic interference shielding, Phys. Chem. Chem. Phys. 17 (2015) 1610–1618. https://doi.org/10.1039/c4cp04284k.

[36] N. Yousefi, X. Sun, X. Lin, X. Shen, J. Jia, B. Zhang, B. Tang, M. Chan, J.K. Kim, Highly aligned graphene/polymer nanocomposites with excellent dielectric properties for high-performance electromagnetic interference shielding, Adv. Mater. 26 (2014) 5480–5487. https://doi.org/10.1002/adma.201305293.

[37] B. Cherqaoui, J. Guillet, G. Seytre, Etude des propriétés diélectriques du polyfluorure de vinylidène chargé de titanate de baryum, Die Makromol. Chemie, Rapid Commun. 6 (1985) 133–136. https://doi.org/10.1002/marc.1985.030060303.

[38] N. Mansouri, N. Benbrahim-Cherief, E. Chainet, F. Charlot, T. Encinas, S. Boudinar, B. Benfedda, L. Hamadou, A. Kadri, Electrodeposition of equiatomic FeNi and FeCo nanowires: Structural and magnetic properties, J. Magn. Magn. Mater. 493 (2020) 165746. https://doi.org/10.1016/j.jmmm.2019.165746.

[39] J. Guo, M. Lan, S. Wang, Y. He, S. Zhang, G. Xiang, F.S. Boi, Enhanced saturation magnetization in buckypaper-films of thin walled carbon nanostructures filled with Fe3C, FeCo, FeNi, CoNi, Co and Ni crystals: the key role of Cl, Phys. Chem. Chem. Phys. 17 (2015) 18159–18166. https://doi.org/10.1039/c5cp02425k.

[40] V. Shukla, Review of electromagnetic interference shielding materials fabricated by iron ingredients, Nanoscale Adv. 1 (2019) 1640–1671. https://doi.org/10.1039/c9na00108e.

[41] S. Ye, A. Sridhar, L. Del Carro, P. McCloskey, A. Masood, T. Brunschwiler, Anisotropic composite core material for inductor-based fully integrated voltage regulator, 2019 22nd Eur. Microelectron. Packag. Conf. Exhib. EMPC 2019. (2019). https://doi.org/10.23919/EMPC44848.2019.8951870.

[42] R. Rohini, S. Bose, Electrodeposited carbon fiber and epoxy based sandwich architectures suppress electromagnetic radiation by absorption, Compos. Part B Eng. 161 (2019) 578–585. https://doi.org/10.1016/j.compositesb.2018.12.123.

[43] L. Schrempp-Koops, Size effects on the efficiency of neutron shielding in nanocomposites-A full-range analysis, Int. J. Nanosci. 12 (2013) 1–8. https://doi.org/10.1142/S0219581X13500154.

[44] Z. Chen, C. Xu, C. Ma, W. Ren, H.M. Cheng, Lightweight and flexible graphene foam composites for high-performance electromagnetic interference shielding, Adv. Mater. 25 (2013) 1296–1300. https://doi.org/10.1002/adma.201204196.

[45] D. Feng, D. Xu, Q. Wang, P. Liu, Highly stretchable electromagnetic interference (EMI) shielding segregated polyurethane/carbon nanotube composites fabricated by microwave selective sintering, J. Mater. Chem. C. 7 (2019) 7938–7946. https://doi.org/10.1039/c9tc02311a.

[46] S. Pande, B.P. Singh, R.B. Mathur, T.L. Dhami, P. Saini, S.K. Dhawan, Improved electromagnetic interference shielding properties of MWCNT-PMMA composites using layered structures, Nanoscale Res. Lett. 4 (2009) 327–334. https://doi.org/10.1007/s11671-008-9246-x.

[47] Z. Osawa, S. Kuwabara, of composites to electromagnetic interference . Effects of matrix polymers and surface, 35 (1992).

[48] C.-Y. Huang, J.-F. Pai, Studies on processing parameters and thermal stability of ENCF/ABS composites for EMI shielding, J. Appl. Polym. Sci. 63 (2004) 115–123. https://doi.org/10.1002/(sici)1097-4628(19970103)63:1<115::aid-app12>3.0.co;2-4.

[49] R. Kumar, K. Kumar, N. Etakula, K.C. Etika, Enhanced thermo-mechanical , thermal and EMI shielding properties of MWNT / MAgPP / PP nanocomposites prepared by extrusion, Compos. Part C Open Access. 4 (2021) 100086. https://doi.org/10.1016/j.jcomc.2020.100086.

[50] S. Iqbal, G. Kotnala, J. Shah, S. Ahmad, Barium ferrite nanoparticles: A highly effective EMI shielding material, Mater. Res. Express. 6 (2019). https://doi.org/10.1088/2053-1591/ab02a4.

[51] J. Wu, D.D.L. Chung, Combined use of magnetic and electrically conductive fillers in a polymer matrix for electromagnetic interference shielding, J. Electron. Mater. 37 (2008) 1088–1094. https://doi.org/10.1007/s11664-008-0486-4.

[52] J. Sun, W. Wang, Q. Yue, Review on microwave-matter interaction fundamentals and efficient microwave-associated heating strategies, Materials (Basel). 9 (2016). https://doi.org/10.3390/ma9040231.

[53] J.D. Sudha, S. Sivakala, K. Patel, P. Radhakrishnan Nair, Development of electromagnetic shielding materials from the conductive blends of polystyrene polyaniline-clay nanocomposite, Compos. Part A Appl. Sci. Manuf. 41 (2010) 1647–1652. https://doi.org/10.1016/j.compositesa.2010.07.015.

[54] K. Chandra Babu Naidu, W. Madhuri, Microwave processed bulk and nano NiMg ferrites: A comparative study on X-band electromagnetic interference shielding properties, Mater. Chem. Phys. 187 (2017) 164–176. https://doi.org/10.1016/j.matchemphys.2016.11.062.

[55] D. Guo, W. Kong, J. Feng, X. Li, X. Fan, Synthesis, electromagnetic and microwave absorption properties of Ba3Co2Fe24O41 hexaferrites for GHz application, Mater. Sci. Eng. B Solid-State Mater. Adv. Technol. 228 (2018) 213–217. https://doi.org/10.1016/j.mseb.2017.12.008.

[56] G.R. Gordani, M. Mohseni, A. Ghasemi, S.R. Hosseini, Microstructure, magnetic and microwave absorptive behavior of doped W-type hexaferrite nanoparticles prepared by co-precipitation method, Mater. Res. Bull. 76 (2016) 187–194. https://doi.org/10.1016/j.materresbull.2015.12.021.

[57] Y. Chen, Y. Wang, H. Bin Zhang, X. Li, C.X. Gui, Z.Z. Yu, Enhanced electromagnetic interference shielding efficiency of polystyrene/graphene composites with magnetic

Fe3O4 nanoparticles, Carbon N. Y. 82 (2015) 67–76.
https://doi.org/10.1016/j.carbon.2014.10.031.

[58]   A.K. Singh, A. Shishkin, T. Koppel, N. Gupta, A review of porous lightweight composite materials for electromagnetic interference shielding, Compos. Part B Eng. 149 (2018) 188–197. https://doi.org/10.1016/j.compositesb.2018.05.027.

[59]   C. Liang, P. Song, H. Qiu, Y. Huangfu, Y. Lu, L. Wang, J. Kong, J. Gu, Superior electromagnetic interference shielding performances of epoxy composites by introducing highly aligned reduced graphene oxide films, Compos. Part A Appl. Sci. Manuf. 124 (2019) 105512. https://doi.org/10.1016/j.compositesa.2019.105512.

[60]   S. Gupta, S.K. Sharma, D. Pradhan, N.H. Tai, Ultra-light 3D reduced graphene oxide aerogels decorated with cobalt ferrite and zinc oxide perform excellent electromagnetic interference shielding effectiveness, Compos. Part A Appl. Sci. Manuf. 123 (2019) 232–241. https://doi.org/10.1016/j.compositesa.2019.05.025.

[61]   S.R. Ramasamy, A REVIEW OF EM1 SHIELDING AND SUPPRESSION MATERIALS, (n.d.).

[62]   D. Wanasinghe, F. Aslani, A review on recent advancement of electromagnetic interference shielding novel metallic materials and processes, Compos. Part B Eng. 176 (2019) 107207. https://doi.org/10.1016/j.compositesb.2019.107207.

[63]   R. Wilson, G. George, K. Joseph, An introduction to materials for potential EMI shielding applications: Status and future, Elsevier Inc., 2020. https://doi.org/10.1016/b978-0-12-817590-3.00001-4.

[64]   S. Sankaran, K. Deshmukh, M.B. Ahamed, S.K. Khadheer Pasha, Recent advances in electromagnetic interference shielding properties of metal and carbon filler reinforced flexible polymer composites: A review, Compos. Part A Appl. Sci. Manuf. 114 (2018) 49–71. https://doi.org/10.1016/j.compositesa.2018.08.006.

[65]   S.H. Kim, S.H. Jang, S.W. Byun, J.Y. Lee, J.S. Joo, S.H. Jeong, M.J. Park, Electrical properties and EMI shielding characteristics of polypyrrole-nylon 6 composite fabrics, J. Appl. Polym. Sci. 87 (2003) 1969–1974. https://doi.org/10.1002/app.11566.

[66]   M. Mishra, A.P. Singh, V. Gupta, A. Chandra, S.K. Dhawan, Tunable EMI shielding effectiveness using new exotic carbon: Polymer composites, J. Alloys Compd. 688 (2016) 399–403. https://doi.org/10.1016/j.jallcom.2016.07.190.

[67]   N. Li, Y. Huang, F. Du, X. He, X. Lin, H. Gao, Y. Ma, F. Li, Y. Chen, P.C. Eklund, Electromagnetic Interference (EMI) shielding of single-walled carbon nanotube epoxy composites, Nano Lett. 6 (2006) 1141–1145. https://doi.org/10.1021/nl0602589.

[68]   Y. Huang, N. Li, Y. Ma, F. Du, F. Li, X. He, X. Lin, H. Gao, Y. Chen, The influence of single-walled carbon nanotube structure on the electromagnetic interference shielding efficiency of its epoxy composites, Carbon N. Y. 45 (2007) 1614–1621. https://doi.org/10.1016/j.carbon.2007.04.016.

[69]   J. Liang, Y. Wang, Y. Huang, Y. Ma, Z. Liu, J. Cai, C. Zhang, H. Gao, Y. Chen, Electromagnetic interference shielding of graphene/epoxy composites, Carbon N. Y. 47 (2009) 922–925. https://doi.org/10.1016/j.carbon.2008.12.038.

[70]   M.H. Al-Saleh, W.H. Saadeh, U. Sundararaj, EMI shielding effectiveness of carbon based nanostructured polymeric materials: A comparative study, Carbon N. Y. 60 (2013) 146–156. https://doi.org/10.1016/j.carbon.2013.04.008.

[71]   A. Ameli, P.U. Jung, C.B. Park, Electrical properties and electromagnetic interference shielding effectiveness of polypropylene/carbon fiber composite foams, Carbon N. Y. 60

(2013) 379–391. https://doi.org/10.1016/j.carbon.2013.04.050.

[72] Z. Liu, G. Bai, Y. Huang, Y. Ma, F. Du, F. Li, T. Guo, Y. Chen, Reflection and absorption contributions to the electromagnetic interference shielding of single-walled carbon nanotube/polyurethane composites, Carbon N. Y. 45 (2007) 821–827. https://doi.org/10.1016/j.carbon.2006.11.020.

[73] P. Saini, V. Choudhary, N. Vijayan, R.K. Kotnala, Improved electromagnetic interference shielding response of poly(aniline)-coated fabrics containing dielectric and magnetic nanoparticles, J. Phys. Chem. C. 116 (2012) 13403–13412. https://doi.org/10.1021/jp302131w.

[74] R. Che, L.M. Peng, X. Duan, Q. Chen, X. Liang, Microwave Absorption Enhancement and Complex Permittivity and Permeability of Fe Encapsulated within Carbon Nanotubes, Adv. Mater. 16 (2004) 401–405. https://doi.org/10.1002/adma.200306460.

[75] S. Maensiri, U. Wongpratat, N. Chanlek, P. Tipsawat, S. Phumying, K. Chokprasombat, Magnetite (Fe3O4) nanoparticles: Synthesis, characterization and electrochemical properties, Appl. Surf. Sci. 446 (2017) 287–292. https://doi.org/10.1016/j.apsusc.2017.11.053.

[76] J. Wu, Z. Ye, H. Ge, J. Chen, W. Liu, Z. Liu, Modified carbon fiber/magnetic graphene/epoxy composites with synergistic effect for electromagnetic interference shielding over broad frequency band, J. Colloid Interface Sci. 506 (2017) 217–226. https://doi.org/10.1016/j.jcis.2017.07.020.

[77] J. Liu, H. Bin Zhang, Y. Liu, Q. Wang, Z. Liu, Y.W. Mai, Z.Z. Yu, Magnetic, electrically conductive and lightweight graphene/iron pentacarbonyl porous films enhanced with chitosan for highly efficient broadband electromagnetic interference shielding, Compos. Sci. Technol. 151 (2017) 71–78. https://doi.org/10.1016/j.compscitech.2017.08.005.

[78] M.K. Mohanapriya, K. Deshmukh, J. Kadlec, K.K. Sadasivuni, M. Faisal, N.A. Nambi Raj, S.K.K. Pasha, Dynamic mechanical analysis and broadband electromagnetic interference shielding characteristics of poly (vinyl alcohol)-poly (4-styrenesulfonic acid)-titanium dioxide nanoparticles based tertiary nanocomposites, Polym. Technol. Mater. 59 (2020) 847–863. https://doi.org/10.1080/25740881.2019.1695274.

[79] J. Abraham, M. Arif P, P. Xavier, S. Bose, S.C. George, N. Kalarikkal, S. Thomas, Investigation into dielectric behaviour and electromagnetic interference shielding effectiveness of conducting styrene butadiene rubber composites containing ionic liquid modified MWCNT, Polymer (Guildf). 112 (2017) 102–115. https://doi.org/10.1016/j.polymer.2017.01.078.

[80] L. yan Li, S. lin Li, Y. Shao, R. Dou, B. Yin, M. bo Yang, PVDF/PS/HDPE/MWCNTs/Fe3O4 nanocomposites: Effective and lightweight electromagnetic interference shielding material through the synergetic effect of MWCNTs and Fe3O4 nanoparticles, Curr. Appl. Phys. 18 (2018) 388–396. https://doi.org/10.1016/j.cap.2018.01.014.

[81] P. Lv, W. Xu, D. Li, Q. Feng, Y. Yao, Z. Pang, L.A. Lucia, Q. Wei, Metal-based bacterial cellulose of sandwich nanomaterials for anti-oxidation electromagnetic interference shielding, Mater. Des. 112 (2016) 374–382. https://doi.org/10.1016/j.matdes.2016.09.100.

[82] M.S. Cao, W.L. Song, Z.L. Hou, B. Wen, J. Yuan, The effects of temperature and frequency on the dielectric properties, electromagnetic interference shielding and microwave-absorption of short carbon fiber/silica composites, Carbon N. Y. 48 (2010) 788–796. https://doi.org/10.1016/j.carbon.2009.10.028.

[83]   X. Hao, X. Yin, L. Zhang, L. Cheng, Dielectric, Electromagnetic Interference Shielding
       and Absorption Properties of Si3N4-PyC Composite Ceramics, J. Mater. Sci. Technol. 29
       (2013) 249–254. https://doi.org/10.1016/j.jmst.2013.01.011.

[84]   Z. Jia, C. Wang, A. Feng, P. Shi, C. Zhang, X. Liu, K. Wang, G. Wu, A low-dielectric
       decoration strategy to achieve absorption dominated electromagnetic shielding material,
       Compos. Part B Eng. 183 (2020) 107690.
       https://doi.org/10.1016/j.compositesb.2019.107690.

[85]   M. Bayat, H. Yang, F.K. Ko, D. Michelson, A. Mei, Electromagnetic interference
       shielding effectiveness of hybrid multifunctional Fe3O4/carbon nanofiber composite,
       Polymer (Guildf). 55 (2014) 936–943. https://doi.org/10.1016/j.polymer.2013.12.042.

[86]   K. Yu, Y. Zeng, G. Wang, X. Luo, T. Li, J. Zhao, K. Qian, C.B. Park, RGO/Fe3O4 hybrid
       induced ultra-efficient EMI shielding performance of phenolic-based carbon foam, RSC
       Adv. 9 (2019) 20643–20651. https://doi.org/10.1039/c9ra04244j.

[87]   M.C. Bertolini, S.D.A.S. Ramoa, C. Merlini, G.M.O. Barra, B.G. Soares, A. Pegoretti,
       Hybrid Composites Based on Thermoplastic Polyurethane With a Mixture of Carbon
       Nanotubes and Carbon Black Modified With Polypyrrole for Electromagnetic Shielding,
       Front. Mater. 7 (2020) 1–9. https://doi.org/10.3389/fmats.2020.00174.

[88]   G. Sang, J. Dong, X. He, J. Jiang, J. Li, P. Xu, Y. Ding, Electromagnetic interference
       shielding performance of polyurethane composites: A comparative study of GNs-IL/Fe 3
       O 4 and MWCNTs-IL/Fe 3 O 4 hybrid fillers, Compos. Part B Eng. 164 (2019) 467–475.
       https://doi.org/10.1016/j.compositesb.2019.01.062.

[89]   Z. Guo, P. Ren, B. Fu, F. Ren, Y. Jin, Z. Sun, Multi-layered graphene-Fe3O4/poly
       (vinylidene fluoride) hybrid composite films for high-efficient electromagnetic shielding,
       Polym. Test. 89 (2020) 106652. https://doi.org/10.1016/j.polymertesting.2020.106652.

[90]   S. Chhetri, N.C. Adak, P. Samanta, N.C. Murmu, S.K. Srivastava, T. Kuila, Synergistic
       effect of Fe 3 O 4 anchored N-doped rGO hybrid on mechanical, thermal and
       electromagnetic shielding properties of epoxy composites, Compos. Part B Eng. 166
       (2019) 371–381. https://doi.org/10.1016/j.compositesb.2019.02.036.

[91]   F. Daneshvar, H. Chen, K. Noh, H.J. Sue, Critical challenges and advances in the carbon
       nanotube-metal interface for next-generation electronics, Nanoscale Adv. 3 (2021) 942–
       962. https://doi.org/10.1039/d0na00822b.

[92]   M.H. Al-Saleh, G.A. Gelves, U. Sundararaj, Copper nanowire/polystyrene
       nanocomposites: Lower percolation threshold and higher EMI shielding, Compos. Part A
       Appl. Sci. Manuf. 42 (2011) 92–97. https://doi.org/10.1016/j.compositesa.2010.10.003.

[93]   G.A. Gelves, M.H. Al-Saleh, U. Sundararaj, Highly electrically conductive and high
       performance EMI shielding nanowire/polymer nanocomposites by miscible mixing and
       precipitation, J. Mater. Chem. 21 (2011) 829–836. https://doi.org/10.1039/c0jm02546a.

[94]   R. Ravindren, S. Mondal, K. Nath, N.C. Das, Prediction of electrical conductivity, double
       percolation limit and electromagnetic interference shielding effectiveness of copper
       nanowire filled flexible polymer blend nanocomposites, Compos. Part B Eng. 164 (2019)
       559–569. https://doi.org/10.1016/j.compositesb.2019.01.066.

[95]   V.R. Sastri, Materials Used in Medical Devices, Plast. Med. Devices. (2022) 41–64.
       https://doi.org/10.1016/b978-0-323-85126-8.00015-1.

[96]   Y. Liu, D. Song, C. Wu, J. Leng, EMI shielding performance of nanocomposites with
       MWCNTs, nanosized Fe 3O4 and Fe, Compos. Part B Eng. 63 (2014) 34–40.
       https://doi.org/10.1016/j.compositesb.2014.03.014.

[97] B.M. Galeano-Villar, R.J. Caraballo-Vivas, E.C.S. Santos, R.C. Rabelo-Neto, S. Gemini-Piperni, P. V. Finotelli, N.R. Checca, C.S.B. Dias, F. Garcia, Core-shell Fe@FexOy nanoring system: A versatile platform for biomedical applications, Mater. Des. 213 (2022) 110303. https://doi.org/10.1016/j.matdes.2021.110303.

[98] P. Sambyal, A.P. Singh, M. Verma, M. Farukh, B.P. Singh, S.K. Dhawan, Tailored polyaniline/barium strontium titanate/expanded graphite multiphase composite for efficient radar absorption, RSC Adv. 4 (2014) 12614–12624. https://doi.org/10.1039/c3ra46479b.

[99] P. Sambyal, S.K. Dhawan, P. Gairola, S.S. Chauhan, S.P. Gairola, Synergistic effect of polypyrrole/BST/RGO/Fe3O4 composite for enhanced microwave absorption and EMI shielding in X-Band, Curr. Appl. Phys. 18 (2018) 611–618. https://doi.org/10.1016/j.cap.2018.03.001.

[100] S.P. Pawar, P. Rzeczkowski, P. Pötschke, B. Krause, S. Bose, Does the Processing Method Resulting in Different States of an Interconnected Network of Multiwalled Carbon Nanotubes in Polymeric Blend Nanocomposites Affect EMI Shielding Properties?, ACS Omega. 3 (2018) 5771–5782. https://doi.org/10.1021/acsomega.8b00575.

[101] R. Che, L.M. Peng, X. Duan, Q. Chen, X. Liang, Microwave Absorption Enhancement and Complex Permittivity and Permeability of Fe Encapsulated within Carbon Nanotubes, Adv. Mater. 16 (2004) 401–405. https://doi.org/10.1002/adma.200306460.

[102] H.L. Xu, H. Bi, R. Bin Yang, Enhanced microwave absorption property of bowl-like Fe 3O 4 hollow spheres/reduced graphene oxide composites, J. Appl. Phys. 111 (2012) 3–6. https://doi.org/10.1063/1.3691527.

[103] M. Gholampoor, F. Movassagh-Alanagh, H. Salimkhani, Fabrication of nano-Fe3O4 3D structure on carbon fibers as a microwave absorber and EMI shielding composite by modified EPD method, Solid State Sci. 64 (2017) 51–61. https://doi.org/10.1016/j.solidstatesciences.2016.12.005.

[104] S.Y. Hong, Y.C. Kim, M. Wang, J. Do Nam, J. Suhr, Anisotropic electromagnetic interference shielding properties of polymer-based composites with magnetically-responsive aligned Fe3O4 decorated reduced graphene oxide, Eur. Polym. J. 127 (2020) 109595. https://doi.org/10.1016/j.eurpolymj.2020.109595.

[105] J. Dalal, S. Malik, S. Dahiya, R. Punia, K. Singh, A.S. Maan, S.K. Dhawan, A. Ohlan, One pot synthesis and electromagnetic interference shielding behavior of reduced graphene oxide nanocomposites decorated with Ni0.5Co0.5Fe2O4 nanoparticles, J. Alloys Compd. 887 (2021) 161472. https://doi.org/10.1016/j.jallcom.2021.161472.

[106] M. Gurusiddesh, B.J. Madhu, G.J. Shankaramurthy, Structural, dielectric, magnetic and electromagnetic interference shielding investigations of polyaniline decorated Co0.5Ni0.5Fe2O4 nanoferrites, J. Mater. Sci. Mater. Electron. 29 (2018) 3502–3509. https://doi.org/10.1007/s10854-017-8285-4.

[107] S. Pradhan, D. Goswami, S.K. Ghorai, D. Ratna, S. Chattopadhyay, Excellent electromagnetic interference shielding and mechanical properties accomplished in a manganese dioxide decorated graphene/polymer composite, J. Appl. Polym. Sci. 138 (2021) 1–13. https://doi.org/10.1002/app.50785.

[108] M. Saini, R. Shukla, Silver nanoparticles-decorated NiFe2O4/polyaniline ternary nanocomposite for electromagnetic interference shielding, J. Mater. Sci. Mater. Electron. 31 (2020) 5152–5164. https://doi.org/10.1007/s10854-020-03075-6.

[109] S.P. Pawar, S. Stephen, S. Bose, V. Mittal, Tailored electrical conductivity, electromagnetic shielding and thermal transport in polymeric blends with graphene sheets decorated with nickel nanoparticles, Phys. Chem. Chem. Phys. 17 (2015) 14922–14930. https://doi.org/10.1039/c5cp00899a.

[110] R. Bera, A. Maitra, S. Paria, S.K. Karan, A.K. Das, A. Bera, S.K. Si, L. Halder, A. De, B.B. Khatua, An approach to widen the electromagnetic shielding efficiency in PDMS/ferrous ferric oxide decorated RGO–SWCNH composite through pressure induced tunability, Chem. Eng. J. 335 (2018) 501–509. https://doi.org/10.1016/j.cej.2017.10.178.

[111] T.K. Gupta, B.P. Singh, V.N. Singh, S. Teotia, A.P. Singh, I. Elizabeth, S.R. Dhakate, S.K. Dhawan, R.B. Mathur, MnO2 decorated graphene nanoribbons with superior permittivity and excellent microwave shielding properties, J. Mater. Chem. A. 2 (2014) 4256–4263. https://doi.org/10.1039/c3ta14854h.

[112] S. Pradhan, D. Goswami, D. Ganguly, S.K. Ghorai, D. Ratna, S. Chattopadhyay, Graphene and MnO2 decorated graphene filled composites for electromagnetic shielding applications having excellent dielectric properties, Polym. Test. 90 (2020) 106716. https://doi.org/10.1016/j.polymertesting.2020.106716.

[113] A. Sharma, R. Kumar, A. Gupta, P.R. Agrawal, N. Dwivedi, D.P. Mondal, A.K. Srivastava, S.R. Dhakate, Enhanced electromagnetic interference shielding properties of phenolic resin derived lightweight carbon foam decorated with electrospun zinc oxide nanofibers, Mater. Today Commun. 30 (2022) 103055. https://doi.org/10.1016/j.mtcomm.2021.103055.

[114] Y. Shi, H.J.H.L.H. Li, L.L. Chen, X. Huang, Fabrication and electromagnetic interference shielding effectiveness of carbon nanotube reinforced carbon fiber/pyrolytic carbon composites, Carbon N. Y. 41 (2014) 761–765. https://doi.org/10.1016/j.carbon.2013.11.027.

[115] X. Chen, L. Leng, H.H. Wang, H. Li, G. Zeng, Facile synthesis of polypyrrole decorated reduced graphene oxide–Fe3O4 magnetic composites and its application for the Cr(VI) removal, Nanotechnology. 27 (2019) 3505–3515. https://doi.org/10.1021/acs.chemmater.5b00944.

[116] K.S.A. Ali, M.M. Ravikumar, J. Mohammed, N. Farouk, V. Mohanavel, M. Ravichandran, Investigation of Ku band microwave absorption of three-layer BaFe12O19, carbon-fiber@Fe3O4, and graphene@BaFe12O19@Fe3O4 composite, J. Alloys Compd. 884 (2021) 161045. https://doi.org/10.1016/j.jallcom.2021.161045.

[117] J. Kittur, B. Desai, R. Chaudhari, P.K. Loharkar, A comparative study of EMI shielding effectiveness of metals, metal coatings and carbon-based materials, IOP Conf. Ser. Mater. Sci. Eng. 810 (2020). https://doi.org/10.1088/1757-899X/810/1/012019.

[118] L. Zhong, R. Yu, X. Hong, Review of carbon-based electromagnetic shielding materials: film, composite, foam, textile, Text. Res. J. 91 (2021) 1167–1183. https://doi.org/10.1177/0040517520968282.

[119] C. Liang, H. Qiu, Y. Han, H. Gu, P. Song, L. Wang, J. Kong, D. Cao, J. Gu, Superior electromagnetic interference shielding 3D graphene nanoplatelets/reduced graphene oxide foam/epoxy nanocomposites with high thermal conductivity, J. Mater. Chem. C. 7 (2019) 2725–2733. https://doi.org/10.1039/c8tc05955a.

[120] Q. Lu, F. Gao, D. Zhao, One-Step Synthesis and Assembly of Copper Sulfide Nanoparticles to Nanowires, Nanotubes, and Nanovesicles by a Simple Organic Amine-Assisted Hydrothermal Process, Nano Lett. 2 (2002) 725–728.

https://doi.org/10.1021/nl025551x.

[121] J. Ren, D. Yu, L. Feng, G. Wang, G. Lv, Nanocable-structured polymer/carbon nanotube composite with low dielectric loss and high impedance, Compos. Part A Appl. Sci. Manuf. 98 (2017) 66–75. https://doi.org/10.1016/j.compositesa.2017.03.014.

[122] C.L. Poh, M. Mariatti, A.F.M. Noor, O. Sidek, T.P. Chuah, S.C. Chow, Dielectric properties of surface treated multi-walled carbon nanotube/epoxy thin film composites, Compos. Part B Eng. 85 (2016) 50–58. https://doi.org/10.1016/j.compositesb.2015.09.024.

[123] Y. Abdullahi Hassan, H. Hu, Current status of polymer nanocomposite dielectrics for high-temperature applications, Compos. Part A Appl. Sci. Manuf. 138 (2020) 106064. https://doi.org/10.1016/j.compositesa.2020.106064.

[124] P. Barber, S. Balasubramanian, Y. Anguchamy, S. Gong, A. Wibowo, H. Gao, H.J. Ploehn, H.C. Zur Loye, Polymer composite and nanocomposite dielectric materials for pulse power energy storage, 2009. https://doi.org/10.3390/ma2041697.

[125] X. Zheng, Y. Huang, S. Zheng, Z. Liu, M. Yang, Improved dielectric properties of polymer-based composites with carboxylic functionalized multiwalled carbon nanotubes, J. Thermoplast. Compos. Mater. 32 (2019) 473–486. https://doi.org/10.1177/0892705718762614.

[126] H. Yuan, Y. Xu, H. Jia, S. Zhou, Superparamagnetic Fe3O4/MWCNTs heterostructures for high frequency microwave absorption, RSC Adv. 6 (2016) 67218–67225. https://doi.org/10.1039/c6ra11610h.

[127] J. Yang, X. Liao, J. Li, G. He, Y. Zhang, W. Tang, G. Wang, G. Li, Light-weight and flexible silicone rubber/MWCNTs/Fe3O4 nanocomposite foams for efficient electromagnetic interference shielding and microwave absorption, Compos. Sci. Technol. 181 (2019) 107670. https://doi.org/10.1016/j.compscitech.2019.05.027.

[128] J. Mathew, M. Sathishkumar, N.K. Kothurkar, R. Senthilkumar, B. Sabarish Narayanan, Polyaniline/Fe3O4-RGO Nanocomposites for Microwave Absorption, IOP Conf. Ser. Mater. Sci. Eng. 310 (2018). https://doi.org/10.1088/1757-899X/310/1/012138.

[129] X. Li, H. Yi, J. Zhang, J. Feng, F. Li, D. Xue, H. Zhang, Y. Peng, N.J. Mellors, Fe3O4-graphene hybrids: Nanoscale characterization and their enhanced electromagnetic wave absorption in gigahertz range, J. Nanoparticle Res. 15 (2013) 1–11. https://doi.org/10.1007/s11051-013-1472-1.

[130] S. Zhu, Q. Cheng, C. Yu, X. Pan, X. Zuo, J. Liu, M. Chen, W. Li, Q. Li, L. Liu, Flexible Fe3O4/graphene foam/poly dimethylsiloxane composite for high-performance electromagnetic interference shielding, Compos. Sci. Technol. 189 (2020). https://doi.org/10.1016/j.compscitech.2020.108012.

[131] H. Liu, C. Liang, J. Chen, Y. Huang, F. Cheng, F. Wen, B. Xu, B. Wang, Novel 3D network porous graphene nanoplatelets /Fe3O4/epoxy nanocomposites with enhanced electromagnetic interference shielding efficiency, Compos. Sci. Technol. 169 (2019) 103–109. https://doi.org/10.1016/j.compscitech.2018.11.005.

[132] H. Liu, C. Liang, J. Chen, Y. Huang, F. Cheng, F. Wen, B. Xu, B. Wang, Novel 3D network porous graphene nanoplatelets /Fe3O4/epoxy nanocomposites with enhanced electromagnetic interference shielding efficiency, Compos. Sci. Technol. 169 (2019) 103–109. https://doi.org/10.1016/j.compscitech.2018.11.005.

[133] R.K. Bheema, A.K. Ojha, A.V.P. Kumar, K.C. Etika, Synergistic influence of barium hexaferrite nanoparticles for enhancing the EMI shielding performance of GNP / epoxy

nanocomposites, J. Mater. Sci. (2022). https://doi.org/10.1007/s10853-022-07214-8.

[134] Z. Gholampour Shamami, M.S. Seyed Dorraji, S.F. Hosseini, M.H. Rasoulifard, I. Hajimiri, A. Amani-Ghadim, Targeted design of polyaniline-graphene oxide, barium-strontium titanate, hard-soft ferrite, and polyester multi-phase nanocomposite for highly efficient microwave absorption, Ceram. Int. (2021). https://doi.org/10.1016/j.ceramint.2021.04.141.

[135] A.J. Fairbanks, T.D. Crawford, J.A. Hernandez, J.D. Mateja, X. Zhu, T.N. Tallman, A.L. Garner, Electromagnetic measurements of composites containing barium strontium titanate or nickel zinc ferrite inclusions from 1 to 4 GHz, Compos. Sci. Technol. 210 (2021) 108798. https://doi.org/10.1016/j.compscitech.2021.108798.

[136] L. Wang, H. Qiu, C. Liang, P. Song, Y. Han, Y. Han, J. Gu, J. Kong, D. Pan, Z. Guo, Electromagnetic interference shielding MWCNT-Fe3O4@Ag/epoxy nanocomposites with satisfactory thermal conductivity and high thermal stability, Carbon N. Y. 141 (2019) 506–514. https://doi.org/10.1016/j.carbon.2018.10.003.

[137] Y. Zhan, J. Wang, K. Zhang, Y. Li, Y. Meng, N. Yan, W. Wei, F. Peng, H. Xia, Fabrication of a flexible electromagnetic interference shielding Fe3O4@reduced graphene oxide/natural rubber composite with segregated network, Chem. Eng. J. 344 (2018) 184–193. https://doi.org/10.1016/j.cej.2018.03.085.

[138] Y. Bhattacharjee, S. Bose, Core-Shell Nanomaterials for Microwave Absorption and Electromagnetic Interference Shielding: A Review, ACS Appl. Nano Mater. (2021). https://doi.org/10.1021/acsanm.1c00278.

[139] H. Jia, Q.Q. Kong, Z. Liu, X.X. Wei, X.M. Li, J.P. Chen, F. Li, X. Yang, G.H. Sun, C.M. Chen, 3D graphene/ carbon nanotubes/ polydimethylsiloxane composites as high-performance electromagnetic shielding material in X-band, Compos. Part A Appl. Sci. Manuf. 129 (2020) 105712. https://doi.org/10.1016/j.compositesa.2019.105712.

[140] N. Bagotia, V. Choudhary, D.K. Sharma, Synergistic effect of graphene/multiwalled carbon nanotube hybrid fillers on mechanical, electrical and EMI shielding properties of polycarbonate/ethylene methyl acrylate nanocomposites, Elsevier Ltd, 2019. https://doi.org/10.1016/j.compositesb.2018.10.009.

[141] B. Rajesh Kumar, K.C. Etika, Facile One-Pot Hydrothermal Synthesis of Copper Nanowires and Their Impact on the EMI Shielding Capability of Epoxy Composites, Chem. Eng. Technol. 45 (2022) 410–416. https://doi.org/10.1002/ceat.202100389.

[142] J. Chen, J. Wu, H. Ge, D. Zhao, C. Liu, X. Hong, Reduced graphene oxide deposited carbon fiber reinforced polymer composites for electromagnetic interference shielding, Compos. Part A Appl. Sci. Manuf. 82 (2016) 141–150. https://doi.org/10.1016/j.compositesa.2015.12.008.

[143] M. Verma, S.S. Chauhan, S.K. Dhawan, V. Choudhary, Graphene nanoplatelets/carbon nanotubes/polyurethane composites as efficient shield against electromagnetic polluting radiations, Compos. Part B Eng. 120 (2017) 118–127. https://doi.org/10.1016/j.compositesb.2017.03.068.

[144] C. Liu, X. Ye, X. Wang, X. Liao, X. Huang, B. Shi, Collagen Fiber Membrane as an Absorptive Substrate to Coat with Carbon Nanotubes-Encapsulated Metal Nanoparticles for Lightweight, Wearable, and Absorption-Dominated Shielding Membrane, Ind. Eng. Chem. Res. 56 (2017) 8553–8562. https://doi.org/10.1021/acs.iecr.7b01930.

[145] S. Shajari, M. Arjmand, S.P. Pawar, U. Sundararaj, L.J. Sudak, Synergistic effect of hybrid stainless steel fiber and carbon nanotube on mechanical properties and

electromagnetic interference shielding of polypropylene nanocomposites, Compos. Part B Eng. 165 (2019) 662–670. https://doi.org/10.1016/j.compositesb.2019.02.044.

[146] A.H.A. Hoseini, M. Arjmand, U. Sundararaj, M. Trifkovic, Significance of interfacial interaction and agglomerates on electrical properties of polymer-carbon nanotube nanocomposites, Mater. Des. 125 (2017) 126–134. https://doi.org/10.1016/j.matdes.2017.04.004.

[147] P. Saini, V. Choudhary, B.P. Singh, R.B. Mathur, S.K. Dhawan, Polyaniline-MWCNT nanocomposites for microwave absorption and EMI shielding, Mater. Chem. Phys. 113 (2009) 919–926. https://doi.org/10.1016/j.matchemphys.2008.08.065.

[148] J.M. Thomassin, C. Pagnoulle, L. Bednarz, I. Huynen, R. Jerome, C. Detrembleur, Foams of polycaprolactone/MWNT nanocomposites for efficient EMI reduction, J. Mater. Chem. 18 (2008) 792–796. https://doi.org/10.1039/b709864b.

[149] X. Yang, S. Fan, Y. Li, Y. Guo, Y. Li, K. Ruan, S. Zhang, J. Zhang, J. Kong, J. Gu, Synchronously improved electromagnetic interference shielding and thermal conductivity for epoxy nanocomposites by constructing 3D copper nanowires/thermally annealed graphene aerogel framework, Compos. Part A Appl. Sci. Manuf. 128 (2020) 105670. https://doi.org/10.1016/j.compositesa.2019.105670.

[150] X. Zhao, W. Xu, W. Yi, Y. Peng, A flexible and highly pressure-sensitive PDMS sponge based on silver nanoparticles decorated reduced graphene oxide composite, Sensors Actuators, A Phys. 291 (2019) 23–31. https://doi.org/10.1016/j.sna.2019.03.038.

[151] P. Xu, X. Han, J. Jiang, X. Wang, X. Li, A. Wen, Synthesis and characterization of novel coralloid polyaniline/BaFe 12O19 nanocomposites, J. Phys. Chem. C. 111 (2007) 12603–12608. https://doi.org/10.1021/jp073872x.

[152] W. Wang, S.P. Gumfekar, Q. Jiao, B. Zhao, Ferrite-grafted polyaniline nanofibers as electromagnetic shielding materials, J. Mater. Chem. C. 1 (2013) 2851–2859. https://doi.org/10.1039/c3tc00757j.

[153] S. Zhang, Y. Wang, Q. Ran, Q. Fu, Y. Gu, Electromagnetic interference shielding property of polybenzoxazine/graphene/nickel composites, React. Funct. Polym. 143 (2019). https://doi.org/10.1016/j.reactfunctpolym.2019.104324.

[154] S. Zeng, X. Li, M. Li, J. Zheng, S. E, W. Yang, B. Zhao, X. Guo, R. Zhang, Flexible PVDF/CNTs/Ni@CNTs composite films possessing excellent electromagnetic interference shielding and mechanical properties under heat treatment, Carbon N. Y. 155 (2019) 34–43. https://doi.org/10.1016/j.carbon.2019.08.024.

[155] I. Arief, S. Biswas, S. Bose, FeCo-Anchored Reduced Graphene Oxide Framework-Based Soft Composites Containing Carbon Nanotubes as Highly Efficient Microwave Absorbers with Excellent Heat Dissipation Ability, ACS Appl. Mater. Interfaces. 9 (2017) 19202–19214. https://doi.org/10.1021/acsami.7b04053.

[156] S. Gao, S.H. Yang, H.Y. Wang, G.S. Wang, P.G. Yin, Excellent electromagnetic wave absorbing properties of two-dimensional carbon-based nanocomposite supported by transition metal carbides Fe3C, Carbon N. Y. 162 (2020) 438–444. https://doi.org/10.1016/j.carbon.2020.02.031.

[157] A.A. Al-Ghamdi, O.A. Al-Hartomy, F.R. Al-Solamy, N. Dishovsky, P. Malinova, G. Atanasova, N. Atanasov, Conductive carbon black/magnetite hybrid fillers in microwave absorbing composites based on natural rubber, Compos. Part B Eng. 96 (2016) 231–241. https://doi.org/10.1016/j.compositesb.2016.04.039.

[158] S. Biswas, I. Arief, S.S. Panja, S. Bose, Electromagnetic screening in soft conducting

composite-containing ferrites: The key role of size and shape anisotropy, Mater. Chem. Front. 1 (2017) 2574–2589. https://doi.org/10.1039/c7qm00305f.

[159] S. Biswas, S.S. Panja, S. Bose, Physical Insight into the Mechanism of Electromagnetic Shielding in Polymer Nanocomposites Containing Multiwalled Carbon Nanotubes and Inverse-Spinel Ferrites, J. Phys. Chem. C. 122 (2018) 19425–19437. https://doi.org/10.1021/acs.jpcc.8b05867.

[160] H. Cheng, S. Wei, Y. Ji, J. Zhai, X. Zhang, J. Chen, C. Shen, Synergetic effect of Fe 3 O 4 nanoparticles and carbon on flexible poly (vinylidence fluoride) based films with higher heat dissipation to improve electromagnetic shielding, Compos. Part A Appl. Sci. Manuf. 121 (2019) 139–148. https://doi.org/10.1016/j.compositesa.2019.03.019.

[161] S.P. Pawar, M. Gandi, S. Bose, High performance electromagnetic wave absorbers derived from PC/SAN blends containing multiwall carbon nanotubes and Fe3O4 decorated onto graphene oxide sheets, RSC Adv. 6 (2016) 37633–37645. https://doi.org/10.1039/c5ra25435c.

[162] K. Sushmita, A. V. Menon, S. Sharma, A.C. Abhyankar, G. Madras, S. Bose, Mechanistic Insight into the Nature of Dopants in Graphene Derivatives Influencing Electromagnetic Interference Shielding Properties in Hybrid Polymer Nanocomposites, J. Phys. Chem. C. 123 (2019) 2579–2590. https://doi.org/10.1021/acs.jpcc.8b10999.

[163] R.S. Yadav, I. Kuřitka, J. Vilcakova, D. Skoda, P. Urbánek, M. Machovsky, M. Masař, L. Kalina, J. Havlica, Lightweight NiFe2O4-Reduced Graphene Oxide-Elastomer Nanocomposite flexible sheet for electromagnetic interference shielding application, Compos. Part B Eng. 166 (2019) 95–111. https://doi.org/10.1016/j.compositesb.2018.11.069.

[164] G. Datt, C. Kotabage, A.C. Abhyankar, Ferromagnetic resonance of NiCoFe2O4 nanoparticles and microwave absorption properties of flexible NiCoFe2O4-carbon black/poly(vinyl alcohol) composites, Phys. Chem. Chem. Phys. 19 (2017) 20699–20712. https://doi.org/10.1039/c7cp03953k.

[165] A. Kobyliukh, K. Olszowska, U. Szeluga, S. Pusz, Iron oxides/graphene hybrid structures – Preparation, modification, and application as fillers of polymer composites, Adv. Colloid Interface Sci. 285 (2020) 102285. https://doi.org/10.1016/j.cis.2020.102285.

[166] X. Li, Z. Sun, Y. Zhang, D. Huang, J. Hu, Effects of oxygen vacancies on dielectric properties and relaxor behavior of Ba(ZrxTi1-x)O3 ceramics, J. Phys. Conf. Ser. 2101 (2021). https://doi.org/10.1088/1742-6596/2101/1/012050.

[167] E. Cockayne, Influence of oxygen vacancies on the dielectric properties of hafnia: First-principles calculations, Phys. Rev. B - Condens. Matter Mater. Phys. 75 (2007) 1–8. https://doi.org/10.1103/PhysRevB.75.094103.

[168] B.K. Sahu, A. Das, Significance of in-plane oxygen vacancy rich non-stoichiometric layer towards unusual high dielectric constant in nano-structured SnO2, Phys. E Low-Dimensional Syst. Nanostructures. 103 (2018) 60–65. https://doi.org/10.1016/j.physe.2018.05.016.

[169] M.D. Li, X.G. Tang, S.M. Zeng, Y.P. Jiang, Q.X. Liu, T.F. Zhang, W.H. Li, Oxygen-vacancy-related dielectric relaxation behaviours and impedance spectroscopy of Bi(Mg1/2Ti1/2)O3 modified BaTiO3 ferroelectric ceramics, J. Mater. 4 (2018) 194–201. https://doi.org/10.1016/j.jmat.2018.03.001.

[170] S. Biswas, Y. Bhattacharjee, S.S. Panja, S. Bose, Graphene oxide co-doped with dielectric and magnetic phases as an electromagnetic wave suppressor, Mater. Chem. Front. 1

(2017) 1229–1244. https://doi.org/10.1039/c6qm00335d.

[171] L. Jin, X. Zhao, J. Xu, Y. Luo, D. Chen, G. Chen, The synergistic effect of a graphene nanoplate/Fe3O4@BaTiO3 hybrid and MWCNTs on enhancing broadband electromagnetic interference shielding performance, RSC Adv. 8 (2018) 2065–2071. https://doi.org/10.1039/c7ra12909b.

[172] S. Li, Y. Chen, L. Huang, D. Pan, Large-scale synthesis of well-dispersed copper nanowires in an electric pressure cooker and their application in transparent and conductive networks, Inorg. Chem. 53 (2014) 4440–4444. https://doi.org/10.1021/ic500094b.

[173] Y. Chang, M.L. Lye, H.C. Zeng, Large-scale synthesis of high-quality ultralong copper nanowires, Langmuir. 21 (2005) 3746–3748. https://doi.org/10.1021/la050220w.

[174] B.J. Wiley, A.R. Rathmell, Z.-Y. Li, S.M. Bergin, Y.-L. Hua, The Growth Mechanism of Copper Nanowires and Their Properties in Flexible, Transparent Conducting Films, Adv. Mater. 22 (2010) 3558–3563. https://doi.org/10.1002/adma.201000775.

[175] B. Zeng, Y. Wang, P. Liu, J. Yang, L. Liu, Facile Synthesis of Ultralong and Thin Copper Nanowires and Its Application to High-Performance Flexible Transparent Conductive Electrodes, Nanoscale Res. Lett. 13 (2018). https://doi.org/10.1186/s11671-018-2486-5.

[176] S. Ye, A.R. Rathmell, Y.C. Ha, A.R. Wilson, B.J. Wiley, The role of cuprous oxide seeds in the one-pot and seeded syntheses of copper nanowires, Small. 10 (2014) 1771–1778. https://doi.org/10.1002/smll.201303005.

[177] D. V. Ravi Kumar, K. Woo, J. Moon, Promising wet chemical strategies to synthesize Cu nanowires for emerging electronic applications, Nanoscale. 7 (2015) 17195–17210. https://doi.org/10.1039/c5nr05138j.

[178] Z. Liu, Y. Yang, J. Liang, Z. Hu, S. Li, S. Peng, Y. Qian, Synthesis of Copper Nanowires via a Complex-Surfactant-Assisted Hydrothermal Reduction Process, J. Phys. Chem. B. 107 (2003) 12658–12661. https://doi.org/10.1021/jp036023s.

[179] Y. Shi, H. Li, L. Chen, X. Huang, Obtaining ultra-long copper nanowires via a hydrothermal process, Sci. Technol. Adv. Mater. 6 (2005) 761–765. https://doi.org/10.1016/j.stam.2005.06.008.

[180] M. Mohl, P. Pusztai, A. Kukovecz, Z. Konya, J. Kukkola, K. Kordas, R. Vajtai, P.M. Ajayan, Low-temperature large-scale synthesis and electrical testing of ultralong copper nanowires, Langmuir. 26 (2010) 16496–16502. https://doi.org/10.1021/la101385e.

[181] D. V. Ravi Kumar, I. Kim, Z. Zhong, K. Kim, D. Lee, J. Moon, Cu(ii)-alkyl amine complex mediated hydrothermal synthesis of Cu nanowires: Exploring the dual role of alkyl amines, Phys. Chem. Chem. Phys. 16 (2014) 22107–22115. https://doi.org/10.1039/c4cp03880k.

[182] J.O. Park, K.Y. Rhee, S.J. Park, Silane treatment of Fe3O4 and its effect on the magnetic and wear properties of Fe3O4/epoxy nanocomposites, Appl. Surf. Sci. 256 (2010) 6945–6950. https://doi.org/10.1016/j.apsusc.2010.04.110.

[183] S. Sun, H. Zeng, Size-controlled synthesis of magnetite nanoparticles, J. Am. Chem. Soc. 124 (2002) 8204–8205. https://doi.org/10.1021/ja026501x.

[184] C. Shen, S. Sun, H. Gao, Z. Xu, Y. Hou, Oleylamine as Both Reducing Agent and Stabilizer in a Facile Synthesis of Magnetite Nanoparticles, Chem. Mater. 21 (2009) 1778–1780. https://doi.org/10.1021/cm802978z.

[185] S. Ge, X. Shi, K. Sun, C. Li, C. Uher, J.R. Baker, M.M. Banaszak Holl, B.G. Orr, Facile hydrothermal synthesis of iron oxide nanoparticles with tunable magnetic properties, J.

Phys. Chem. C. 113 (2009) 13593–13599. https://doi.org/10.1021/jp902953t.

[186] Y. Lu, Y. Yin, B.T. Mayers, Y. Xia, Modifying the Surface Properties of Superparamagnetic Iron Oxide Nanoparticles through a Sol-Gel Approach, Nano Lett. 2 (2002) 183–186. https://doi.org/10.1021/nl015681q.

[187] W. Chen, Z. Wang, C. Zhi, W. Zhang, High thermal conductivity and temperature probing of copper nanowire/upconversion nanoparticles/epoxy composite, Compos. Sci. Technol. 130 (2016) 63–69. https://doi.org/10.1016/j.compscitech.2016.05.004.

[188] M. Mahdavi, M. Bin Ahmad, M.J. Haron, F. Namvar, B. Nadi, M.Z. Ab Rahman, J. Amin, Synthesis, surface modification and characterisation of biocompatible magnetic iron oxide nanoparticles for biomedical applications, Molecules. 18 (2013) 7533–7548. https://doi.org/10.3390/molecules18077533.

[189] T.K. Jain, M.A. Morales, S.K. Sahoo, D.L. Leslie-Pelecky, V. Labhasetwar, Iron oxide nanoparticles for sustained delivery of anticancer agents, Mol. Pharm. 2 (2005) 194–205. https://doi.org/10.1021/mp0500014.

[190] Z. Zhou, X. Zhu, D. Wu, Q. Chen, D. Huang, C. Sun, J. Xin, K. Ni, J. Gao, Anisotropic shaped iron oxide nanostructures: Controlled synthesis and proton relaxation shortening effects, Chem. Mater. (2015). https://doi.org/10.1021/acs.chemmater.5b00944.

[191] Y. Chen, L. Huang, D. Pan, S.I. We, Tunable High Aspect Ratio Iron Oxide Nanorods for Enhanced Hyperthermia, Nanotechnology. 27 (2015) 4440–4444. https://doi.org/10.1021/acs.chemmater.5b00944.

[192] L. Shen, Y. Qiao, Y. Guo, S. Meng, G. Yang, M. Wu, J. Zhao, Facile co-precipitation synthesis of shape-controlled magnetite nanoparticles, Ceram. Int. (2013) 1–6. https://doi.org/10.1016/j.ceramint.2013.07.037.

[193] K. He, C.Y. Xu, L. Zhen, W.Z. Shao, Hydrothermal synthesis and characterization of single-crystalline Fe3O4 nanowires with high aspect ratio and uniformity, Mater. Lett. 61 (2007) 3159–3162. https://doi.org/10.1016/j.matlet.2006.11.023.

[194] H. Sun, B. Chen, X. Jiao, Z. Jiang, Z. Qin, D. Chen, Solvothermal synthesis of tunable electroactive magnetite nanorods by controlling the side reaction, J. Phys. Chem. C. 116 (2012) 5476–5481. https://doi.org/10.1021/jp211986a.

[195] P. Guégan, A.K. Khandpur, A. Nakayama, P. Marechal, T. Inoue, J. Polte, A.K. Singh, O.N. Srivastava, K. Singh, Towards cost-efficient EMI shielding materials using carbon nanostructure-based nanocomposites, Nanotechnology. 18 (2003) 4440–4444. https://doi.org/10.1088/0957-4484/18/34/345701.

[196] R. Pazik, D. Hreniak, W. Strek, Microwave driven hydrothermal synthesis of Ba1-xSrxTiO3 nanoparticles, Mater. Res. Bull. 42 (2007) 1188–1194. https://doi.org/10.1016/j.materresbull.2006.10.021.

[197] S. Fuentes, E. Chávez, L. Padilla-Campos, D.E. Diaz-Droguett, Influence of reactant type on the Sr incorporation grade and structural characteristics of Ba1-xSrxTiO3(x=0-1) grown by sol-gel-hydrothermal synthesis, Ceram. Int. 39 (2013) 8823–8831. https://doi.org/10.1016/j.ceramint.2013.04.070.

[198] S. Liu, S. Xiu, B. Shen, J. Zhai, L.B. Kong, Dielectric properties and energy storage densities of poly(vinylidenefluoride) nanocomposite with surface hydroxylated cube shaped Ba0.6Sr0.4TiO3 nanoparticles, Polymers (Basel). 8 (2016) 10–14. https://doi.org/10.3390/polym8020045.

[199] M.M. Shameem, S.M. Sasikanth, R. Annamalai, R.G. Raman, A brief review on polymer nanocomposites and its applications, Mater. Today Proc. 45 (2021) 2536–2539.

https://doi.org/10.1016/j.matpr.2020.11.254.

[200] S. Sinha Ray, M. Okamoto, Polymer/layered silicate nanocomposites: A review from preparation to processing, Prog. Polym. Sci. 28 (2003) 1539–1641. https://doi.org/10.1016/j.progpolymsci.2003.08.002.

[201] S. Pavlidou, C.D. Papaspyrides, A review on polymer-layered silicate nanocomposites, Prog. Polym. Sci. 33 (2008) 1119–1198. https://doi.org/10.1016/j.progpolymsci.2008.07.008.

[202] V. Mittal, Polymer layered silicate nanocomposites: A review, Materials (Basel). 2 (2009) 992–1057. https://doi.org/10.3390/ma2030992.

[203] S. Abedi, M. Abdouss, A review of clay-supported Ziegler-Natta catalysts for production of polyolefin/clay nanocomposites through in situ polymerization, Appl. Catal. A Gen. 475 (2014) 386–409. https://doi.org/10.1016/j.apcata.2014.01.028.

[204] Vikas Mittal, Optimization of Polymer Nanocomposite Properties, n.d.

[205] M. Alexandre, P. Dubois, Polymer-layered silicate nanocomposites: Preparation, properties and uses of a new class of materials, Mater. Sci. Eng. R Reports. 28 (2000) 1–63. https://doi.org/10.1016/S0927-796X(00)00012-7.

[206] S. Fu, Z. Sun, P. Huang, Y. Li, N. Hu, Some basic aspects of polymer nanocomposites: A critical review, Nano Mater. Sci. 1 (2019) 2–30. https://doi.org/10.1016/j.nanoms.2019.02.006.

[207] E.A. Zaragoza-Contreras, C.A. Hernández-Escobar, A. Navarrete-Fontes, S.G. Flores-Gallardo, Synthesis of carbon black/polystyrene conductive nanocomposite. Pickering emulsion effect characterized by TEM, Micron. 42 (2011) 263–270. https://doi.org/10.1016/j.micron.2010.10.005.

[208] H. Hu, X. Wang, J. Wang, L. Wan, F. Liu, H. Zheng, R. Chen, C. Xu, Preparation and properties of graphene nanosheets-polystyrene nanocomposites via in situ emulsion polymerization, Chem. Phys. Lett. 484 (2010) 247–253. https://doi.org/10.1016/j.cplett.2009.11.024.

[209] M. Hassan, K.R. Reddy, E. Haque, A.I. Minett, V.G. Gomes, High-yield aqueous phase exfoliation of graphene for facile nanocomposite synthesis via emulsion polymerization, J. Colloid Interface Sci. 410 (2013) 43–51. https://doi.org/10.1016/j.jcis.2013.08.006.

[210] J.M. Thomassin, C. Jérôme, T. Pardoen, C. Bailly, I. Huynen, C. Detrembleur, Polymer/carbon based composites as electromagnetic interference (EMI) shielding materials, Mater. Sci. Eng. R Reports. 74 (2013) 211–232. https://doi.org/10.1016/j.mser.2013.06.001.

[211] M.H. Al-Saleh, U. Sundararaj, Electromagnetic interference (EMI) shielding effectiveness of PP/PS polymer blends containing high structure carbon black, Macromol. Mater. Eng. 293 (2008) 621–630. https://doi.org/10.1002/mame.200800060.

[212] X. Xia, Y. Wang, Z. Zhong, G.J. Weng, A theory of electrical conductivity, dielectric constant, and electromagnetic interference shielding for lightweight graphene composite foams, J. Appl. Phys. 120 (2016). https://doi.org/10.1063/1.4961401.

[213] S.R. Dhakate, K.M. Subhedar, B.P. Singh, Polymer nanocomposite foam filled with carbon nanomaterials as an efficient electromagnetic interference shielding material, RSC Adv. 5 (2015) 43036–43057. https://doi.org/10.1039/c5ra03409d.

[214] Y. Wang, X. Jing, Intrinsically conducting polymers for electromagnetic interference shielding, Polym. Adv. Technol. 16 (2005) 344–351. https://doi.org/10.1002/pat.589.

[215] P. Balakrishnan, M.J. John, L. Pothen, M.S. Sreekala, S. Thomas, Natural fibre and

polymer matrix composites and their applications in aerospace engineering, Elsevier Ltd, 2016. https://doi.org/10.1016/b978-0-08-100037-3.00012-2.

[216] P. Kumar, U. Narayan Maiti, A. Sikdar, T. Kumar Das, A. Kumar, V. Sudarsan, Recent Advances in Polymer and Polymer Composites for Electromagnetic Interference Shielding: Review and Future Prospects, Polym. Rev. 59 (2019) 687–738. https://doi.org/10.1080/15583724.2019.1625058.

[217] S. Kumar, S.K. Samal, S. Mohanty, S.K. Nayak, Recent Development of Biobased Epoxy Resins: A Review, Polym. - Plast. Technol. Eng. 57 (2018) 133–155. https://doi.org/10.1080/03602559.2016.1253742.

[218] N.C. Das, T.K. Chaki, D. Khastgir, A. Chakraborty, Electromagnetic interference shielding effectiveness of conductive carbon black and carbon fiber-filled composites based on rubber and rubber blends, Adv. Polym. Technol. 20 (2001) 226–236. https://doi.org/10.1002/adv.1018.

[219] R. Manna, S.K. Srivastava, Reduced Graphene Oxide/Fe 3 O 4 /Polyaniline Ternary Composites as a Superior Microwave Absorber in the Shielding of Electromagnetic Pollution , ACS Omega. (2021). https://doi.org/10.1021/acsomega.1c00382.

[220] S. Khasim, Polyaniline-Graphene nanoplatelet composite films with improved conductivity for high performance X-band microwave shielding applications, Results Phys. 12 (2019) 1073–1081. https://doi.org/10.1016/j.rinp.2018.12.087.

[221] A.K. Singh, A. Shishkin, T. Koppel, N. Gupta, A review of porous lightweight composite materials for electromagnetic interference shielding, Compos. Part B Eng. 149 (2018) 188–197. https://doi.org/10.1016/j.compositesb.2018.05.027.

[222] F. Dalmas, R. Dendievel, L. Chazeau, J.Y. Cavaillé, C. Gauthier, Carbon nanotube-filled polymer composites. Numerical simulation of electrical conductivity in three-dimensional entangled fibrous networks, Acta Mater. 54 (2006) 2923–2931. https://doi.org/10.1016/j.actamat.2006.02.028.

[223] M. Foygel, R.D. Morris, D. Anez, S. French, V.L. Sobolev, Theoretical and computational studies of carbon nanotube composites and suspensions: Electrical and thermal conductivity, Phys. Rev. B - Condens. Matter Mater. Phys. 71 (2005) 1–8. https://doi.org/10.1103/PhysRevB.71.104201.

[224] A. Celzard, E. McRae, C. Deleuze, M. Dufort, Critical concentration in percolating systems containing a high-aspect-ratio filler, Phys. Rev. B - Condens. Matter Mater. Phys. 53 (1996) 6209–6214. https://doi.org/10.1103/PhysRevB.53.6209.

[225] S.H. Munson-Mcgee, Estimation of the critical concentration in an anisotropic percolation network, Phys. Rev. B. 43 (1991) 3331–3336. https://doi.org/10.1103/PhysRevB.43.3331.

[226] M.A. Osman, A. Atallah, High-density polyethylene micro- and nanocomposites: Effect of particle shape, size and surface treatment on polymer crystallinity and gas permeability, Macromol. Rapid Commun. 25 (2004) 1540–1544. https://doi.org/10.1002/marc.200400254.

[227] O. Microscope, F. Laser, O. Mdplan, D.M. Ctc-, M.C. Api, M.G. Hene, S. Electron, M. Imaging, J. Jsm-, perature during laser pruning has a lower bound of 1750 K, as suggested by the liquid-drop model for the size-dependent melting of nanoparticles. [11] The melting temperature of iron nanoparticles, T, 0044 (2003) 303–305.

[228] D. Mott, J. Galkowski, L. Wang, J. Luo, C.J. Zhong, Synthesis of size-controlled and shaped copper nanoparticles, Langmuir. 23 (2007) 5740–5745. https://doi.org/10.1021/la0635092.

[229] E. Ye, S.Y. Zhang, S. Liu, M.Y. Han, Disproportionation for growing copper nanowires and their controlled self-assembly facilitated by ligand exchange, Chem. - A Eur. J. 17 (2011) 3074–3077. https://doi.org/10.1002/chem.201002987.

[230] C. Yong, B.C. Zhang, C.S. Seet, A. See, L. Chan, J. Sudijono, S.L. Liew, C.H. Tung, H.C. Zeng, Cool copper template for the formation of oriented nanocrystalline α-tantalum, J. Phys. Chem. B. 106 (2002) 12366–12368. https://doi.org/10.1021/jp026668c.

[231] X. Li, Y. Wang, C. Yin, Z. Yin, Copper nanowires in recent electronic applications: Progress and perspectives, J. Mater. Chem. C. 8 (2020) 849–872. https://doi.org/10.1039/c9tc04744a.

[232] H.J. Yang, S.Y. He, H.Y. Tuan, Self-seeded growth of five-fold twinned copper nanowires: Mechanistic study, characterization, and SERS applications, Langmuir. 30 (2014) 602–610. https://doi.org/10.1021/la4036198.

[233] L. Lu, Y. Shen, X. Chen, L. Qian, K. Lu, Ultrahigh Strength and High Electrical Conductivity in Copper, Science (80-.). 304 (2004) 422–426. https://doi.org/10.1126/science.1092905.

[234] T. Gao, G. Meng, Y. Wang, S. Sun, L. Zhang, Electrochemical synthesis of copper nanowires, J. Phys. Condens. Matter. 14 (2002) 355–363. https://doi.org/10.1088/0953-8984/14/3/306.

[235] M. Tian, J. Wang, J. Kurtz, T.E. Mallouk, M.H.W. Chan, Electrochemical growth of single-crystal metal nanowires via a two-dimensional nucleation and growth mechanism, Nano Lett. 3 (2003) 919–923. https://doi.org/10.1021/nl034217d.

[236] C.N.R. Rao, F.L. Deepak, G. Gundiah, A. Govindaraj, Inorganic nanowires, Prog. Solid State Chem. 31 (2003) 5–147. https://doi.org/10.1016/j.progsolidstchem.2003.08.001.

[237] H. Yoon, D.S. Shin, B. Babu, T.G. Kim, K.M. Song, J. Park, Control of copper nanowire network properties and application to transparent conducting layer in LED, Mater. Des. 132 (2017) 66–71. https://doi.org/10.1016/j.matdes.2017.06.042.

[238] Z. Liu, Y. Yang, J. Liang, Z. Hu, S. Li, S. Peng, Y. Qian, Synthesis of Copper Nanowires via a Complex-Surfactant-Assisted Hydrothermal Reduction Process, J. Phys. Chem. B. 107 (2003) 12658–12661. https://doi.org/10.1021/jp036023s.

[239] T. Xia, D. Zeng, Z. Li, R.J. Young, C. Vallés, I.A. Kinloch, Electrically conductive GNP/epoxy composites for out-of-autoclave thermoset curing through Joule heating, Compos. Sci. Technol. 164 (2018) 304–312. https://doi.org/10.1016/j.compscitech.2018.05.053.

[240] R. Ravindren, S. Mondal, K. Nath, N.C. Das, Prediction of electrical conductivity, double percolation limit and electromagnetic interference shielding effectiveness of copper nanowire filled flexible polymer blend nanocomposites, Compos. Part B Eng. 164 (2019) 559–569. https://doi.org/10.1016/j.compositesb.2019.01.066.

[241] N. Zeng, J. Ma, Y. Zhang, G. Yang, S. Zhang, P. Zhang, Silver nanosheet-coated copper nanowire/epoxy resin nanocomposites with enhanced electrical conductivity and wear resistance, J. Nanoparticle Res. 19 (2017). https://doi.org/10.1007/s11051-017-3784-z.

[242] L. Wang, L. Chen, P. Song, C. Liang, Y. Lu, H. Qiu, Y. Zhang, J. Kong, J. Gu, Fabrication on the annealed Ti3C2Tx MXene/Epoxy nanocomposites for electromagnetic interference shielding application, Compos. Part B Eng. 171 (2019) 111–118. https://doi.org/10.1016/j.compositesb.2019.04.050.

[243] K. Zhang, J. Luo, N. Yu, M. Gu, X. Sun, Synthesis and excellent electromagnetic absorption properties of reduced graphene oxide/PANI/BaNd0.2Sm0.2Fe11.6O19

nanocomposites, J. Alloys Compd. 779 (2019) 270–279. https://doi.org/10.1016/j.jallcom.2018.11.284.

[244]   A. Kumar, P.S. Alegaonkar, Impressive Transmission Mode Electromagnetic Interference Shielding Parameters of Graphene-like Nanocarbon/Polyurethane Nanocomposites for Short Range Tracking Countermeasures, ACS Appl. Mater. Interfaces. 7 (2015) 14833–14842. https://doi.org/10.1021/acsami.5b03122.

[245]   H. Zhang, G. Zhang, Q. Gao, M. Tang, Z. Ma, J. Qin, M. Wang, J.K. Kim, Multifunctional microcellular PVDF/Ni-chains composite foams with enhanced electromagnetic interference shielding and superior thermal insulation performance, Chem. Eng. J. 379 (2020) 122304. https://doi.org/10.1016/j.cej.2019.122304.

[246]   H. Zhang, G. Zhang, Q. Gao, M. Zong, M. Wang, J. Qin, Electrically electromagnetic interference shielding microcellular composite foams with 3D hierarchical graphene-carbon nanotube hybrids, Compos. Part A Appl. Sci. Manuf. 130 (2020) 105773. https://doi.org/10.1016/j.compositesa.2020.105773.

[247]   S. Zhao, H. Bin Zhang, J.Q. Luo, Q.W. Wang, B. Xu, S. Hong, Z.Z. Yu, Highly Electrically Conductive Three-Dimensional Ti3C2Tx MXene/Reduced Graphene Oxide Hybrid Aerogels with Excellent Electromagnetic Interference Shielding Performances, ACS Nano. 12 (2018) 11193–11202. https://doi.org/10.1021/acsnano.8b05739.

[248]   H. Wang, K. Zheng, X. Zhang, T. Du, C. Xiao, X. Ding, C. Bao, L. Chen, X. Tian, Segregated poly(vinylidene fluoride)/MWCNTs composites for high-performance electromagnetic interference shielding, Compos. Part A Appl. Sci. Manuf. 90 (2016) 606–613. https://doi.org/10.1016/j.compositesa.2016.08.030.

[249]   L. Wang, Y. Wu, Y. Wang, H. Li, N. Jiang, K. Niu, Laterally compressed graphene foam/acrylonitrile butadiene styrene composites for electromagnetic interference shielding, Compos. Part A Appl. Sci. Manuf. 133 (2020). https://doi.org/10.1016/j.compositesa.2020.105887.

[250]   S. Iqbal, H. Khatoon, R.K. Kotnala, S. Ahmad, Bi-doped barium ferrite decorated polythiophene nanocomposite: influence of Bi-doping on structure, morphology, thermal and EMI shielding behavior for X-band, J. Mater. Sci. 55 (2020) 15894–15907. https://doi.org/10.1007/s10853-020-05134-z.

[251]   Y.Y. Wang, Z.H. Zhou, C.G. Zhou, W.J. Sun, J.F. Gao, K. Dai, D.X. Yan, Z.M. Li, Lightweight and Robust Carbon Nanotube/Polyimide Foam for Efficient and Heat-Resistant Electromagnetic Interference Shielding and Microwave Absorption, ACS Appl. Mater. Interfaces. 12 (2020) 8704–8712. https://doi.org/10.1021/acsami.9b21048.

[252]   Y. Yuan, W. Yin, M. Yang, F. Xu, X. Zhao, J. Li, Q. Peng, X. He, S. Du, Y. Li, Lightweight, flexible and strong core-shell non-woven fabrics covered by reduced graphene oxide for high-performance electromagnetic interference shielding, Carbon N. Y. 130 (2018) 59–68. https://doi.org/10.1016/j.carbon.2017.12.122.

[253]   J.H. Pu, X.J. Zha, L.S. Tang, L. Bai, R.Y. Bao, Z.Y. Liu, M.B. Yang, W. Yang, Human Skin-Inspired Electronic Sensor Skin with Electromagnetic Interference Shielding for the Sensation and Protection of Wearable Electronics, ACS Appl. Mater. Interfaces. 10 (2018) 40880–40889. https://doi.org/10.1021/acsami.8b15809.

[254]   J. Li, H. Liu, J. Guo, Z. Hu, Z. Wang, B. Wang, L. Liu, Y. Huang, Z. Guo, Flexible, conductive, porous, fibrillar polymer-gold nanocomposites with enhanced electromagnetic interference shielding and mechanical properties, J. Mater. Chem. C. 5 (2017) 1095–1105. https://doi.org/10.1039/c6tc04780g.

[255] X.M. Bian, L. Liu, H.B. Li, C.Y. Wang, Q. Xie, Q.L. Zhao, S. Bi, Z.L. Hou, Construction of three-dimensional graphene interfaces into carbon fiber textiles for increasing deposition of nickel nanoparticles: Flexible hierarchical magnetic textile composites for strong electromagnetic shielding, Nanotechnology. 28 (2017). https://doi.org/10.1088/1361-6528/28/4/045710.

[256] A. Houbi, Z.A. Aldashevich, Y. Atassi, Z. Bagasharova Telmanovna, M. Saule, K. Kubanych, Microwave absorbing properties of ferrites and their composites: A review, J. Magn. Magn. Mater. 529 (2021) 167839. https://doi.org/10.1016/j.jmmm.2021.167839.

[257] X.B. Xie, B. Wang, Y. Wang, C. Ni, X. Sun, W. Du, Spinel structured MFe2O4 (M = Fe, Co, Ni, Mn, Zn) and their composites for microwave absorption: A review, Chem. Eng. J. 428 (2022) 131160. https://doi.org/10.1016/j.cej.2021.131160.

[258] Y. Zhan, R. Zhao, Y. Lei, F. Meng, J. Zhong, X. Liu, Preparation, characterization and electromagnetic properties of carbon nanotubes/Fe 3 O 4 inorganic hybrid material, Appl. Surf. Sci. 257 (2011) 4524–4528. https://doi.org/10.1016/j.apsusc.2010.08.088.

[259] R.C. Pullar, Hexagonal ferrites: A review of the synthesis, properties and applications of hexaferrite ceramics, Prog. Mater. Sci. 57 (2012) 1191–1334. https://doi.org/10.1016/j.pmatsci.2012.04.001.

[260] M. Zahid, S. Siddique, R. Anum, M.F. Shakir, Y. Nawab, Z.A. Rehan, M-Type Barium Hexaferrite-Based Nanocomposites for EMI Shielding Application: a Review, J. Supercond. Nov. Magn. (2021). https://doi.org/10.1007/s10948-021-05859-1.

[261] T. Zhao, W. Jin, X. Ji, H. Yan, Y. Jiang, Y. Dong, Y. Yang, A. Dang, H. Li, T. Li, S. Shang, Z. Zhou, Synthesis of sandwich microstructured expanded graphite/barium ferrite connected with carbon nanotube composite and its electromagnetic wave absorbing properties, J. Alloys Compd. 712 (2017) 59–68. https://doi.org/10.1016/j.jallcom.2017.04.070.

[262] S.P. Gairola, V. Verma, A. Singh, L.P. Purohit, R.K. Kotnala, Modified composition of barium ferrite to act as a microwave absorber in X-band frequencies, Solid State Commun. 150 (2010) 147–151. https://doi.org/10.1016/j.ssc.2009.10.011.

[263] Y. Li, R. Yi, A. Yan, L. Deng, K. Zhou, X. Liu, Facile synthesis and properties of ZnFe2O4 and ZnFe2O4/polypyrrole core-shell nanoparticles, Solid State Sci. 11 (2009) 1319–1324. https://doi.org/10.1016/j.solidstatesciences.2009.04.014.

[264] S. Anand, S. Pauline, Electromagnetic Interference Shielding Properties of BaCo2Fe16O27 Nanoplatelets and RGO Reinforced PVDF Polymer Composite Flexible Films, Adv. Mater. Interfaces. 8 (2021) 1–18. https://doi.org/10.1002/admi.202001810.

[265] M. Trihotri, U.K. Dwivedi, M.M. Malik, F.H. Khan, M.S. Qureshi, Study of low weight percentage filler on dielectric properties of MWCNT-epoxy nanocomposites, J. Adv. Dielectr. 6 (2016) 1650024-1-1650024–9. https://doi.org/10.1142/S2010135X16500247.

[266] Y. Chen, B. Lin, X. Zhang, J. Wang, C. Lai, Y. Sun, Y. Liu, H. Yang, Enhanced dielectric properties of amino-modified-CNT/polyimide composite films with a sandwich structure, J. Mater. Chem. A. 2 (2014) 14118–14126. https://doi.org/10.1039/c4ta01818d.

[267] A.H. El-Sayed, O.M. Hemeda, A. Tawfik, M.A. Hamad, Remarkable magnetic enhancement of type-M hexaferrite of barium in polystyrene polymer, AIP Adv. 5 (2015). https://doi.org/10.1063/1.4934790.

[268] V. Uvarov, I. Popov, Metrological characterization of X-ray diffraction methods for determination of crystallite size in nano-scale materials, Mater. Charact. 58 (2007) 883–891. https://doi.org/10.1016/j.matchar.2006.09.002.

[269] N. Tahir, S.T. Hussain, M. Usman, S.K. Hasanain, A. Mumtaz, Effect of vanadium doping on structural, magnetic and optical properties of ZnO nanoparticles, Appl. Surf. Sci. 255 (2009) 8506–8510. https://doi.org/10.1016/j.apsusc.2009.06.003.

[270] M. Drofenik, I. Ban, D. Makovec, A. Žnidaršič, Z. Jagličić, D. Hanžel, D. Lisjak, The hydrothermal synthesis of super-paramagnetic barium hexaferrite particles, Mater. Chem. Phys. 127 (2011) 415–419. https://doi.org/10.1016/j.matchemphys.2011.02.037.

[271] K.C. Etika, L. Liu, L.A. Hess, J.C. Grunlan, The influence of synergistic stabilization of carbon black and clay on the electrical and mechanical properties of epoxy composites, Carbon N. Y. 47 (2009) 3128–3136. https://doi.org/10.1016/J.CARBON.2009.07.031.

[272] S. Zhang, B. Cheng, Z. Gao, D. Lan, Z. Zhao, F. Wei, Q. Zhu, X. Lu, G. Wu, Two-dimensional nanomaterials for high-efficiency electromagnetic wave absorption: An overview of recent advances and prospects, J. Alloys Compd. 893 (2022) 162343. https://doi.org/10.1016/j.jallcom.2021.162343.

[273] X. Chen, Y. Wang, H. Liu, S. Jin, G. Wu, Interconnected magnetic carbon@NixCo1-xFe2O4 nanospheres with core–shell structure: An efficient and thin electromagnetic wave absorber, J. Colloid Interface Sci. 606 (2022) 526–536. https://doi.org/10.1016/j.jcis.2021.07.094.

[274] K. Zubair, M.F. Shakir, A. Afzal, Z.A. Rehan, Y. Nawab, Effect of Barium Hexaferrites and Thermally Reduced Graphene Oxide on EMI Shielding Properties in Polymer Composites, J. Supercond. Nov. Magn. 34 (2021) 201–210. https://doi.org/10.1007/s10948-020-05669-x.

[275] M. Verma, A.P. Singh, P. Sambyal, B.P. Singh, S.K. Dhawan, V. Choudhary, Barium ferrite decorated reduced graphene oxide nanocomposite for effective electromagnetic interference shielding, Phys. Chem. Chem. Phys. 17 (2015) 1610–1618. https://doi.org/10.1039/c4cp04284k.

[276] S.D. Yoon, C. Vittoria, S.A. Oliver, Magnetic and microwave magnetic properties of barium hexaferrite permanent magnet films having the c-axis in the film plane, J. Appl. Phys. 93 (2003) 4023–4026. https://doi.org/10.1063/1.1544083.

[277] H. Guan, D.D.L. Chung, Absorption-dominant radio-wave attenuation loss of metals and graphite, J. Mater. Sci. 56 (2021) 8037–8047. https://doi.org/10.1007/s10853-021-05808-2.

[278] S. Pei, H.M. Cheng, The reduction of graphene oxide, Carbon N. Y. 50 (2012) 3210–3228. https://doi.org/10.1016/j.carbon.2011.11.010.

[279] M. Wang, X.H. Tang, J.H. Cai, H. Wu, J. Bin Shen, S.Y. Guo, Construction, mechanism and prospective of conductive polymer composites with multiple interfaces for electromagnetic interference shielding: A review, Carbon N. Y. 177 (2021) 377–402. https://doi.org/10.1016/j.carbon.2021.02.047.

[280] B. Rajesh Kumar, K.C. Etika, Facile one-pot hydrothermal synthesis of copper nanowires and its impact on the EMI shielding capability of epoxy composites in the X-band Experimental work Materials, (n.d.) 1–12. https://doi.org/10.1002/ceat.202100389.

[281] W. Jiang, K.L. Lai, H. Hu, X.B. Zeng, F. Lan, K.X. Liu, Y. Wu, Z.W. Gu, The effect of [Fe3+]/[Fe2+] molar ratio and iron salts concentration on the properties of superparamagnetic iron oxide nanoparticles in the water/ethanol/toluene system, J. Nanoparticle Res. 13 (2011) 5135–5145. https://doi.org/10.1007/s11051-011-0495-8.

[282] X. Wen, J. Yang, B. He, Z. Gu, Preparation of monodisperse magnetite nanoparticles under mild conditions, Curr. Appl. Phys. 8 (2008) 535–541.

https://doi.org/10.1016/j.cap.2007.09.003.

[283] S. Wu, A. Sun, F. Zhai, J. Wang, W. Xu, Q. Zhang, A.A. Volinsky, Fe 3 O 4 magnetic nanoparticles synthesis from tailings by ultrasonic chemical, Mater. Lett. 65 (2011) 1882–1884. https://doi.org/10.1016/j.matlet.2011.03.065.

[284] Y. Wei, B. Han, X. Hu, Y. Lin, X. Wang, X. Deng, Synthesis of Fe3O4 nanoparticles and their magnetic properties, Procedia Eng. 27 (2012) 632–637. https://doi.org/10.1016/j.proeng.2011.12.498.

[285] Y.Q. Liu, M. Zhang, F.X. Wang, G.B. Pan, Facile microwave-assisted synthesis of uniform single-crystal copper nanowires with excellent electrical conductivity, RSC Adv. 2 (2012) 11235–11237. https://doi.org/10.1039/c2ra21578k.

[286] M.E. Toimil Molares, V. Buschmann, D. Dobrev, R. Neumann, R. Scholz, I.U. Schuchert, J. Vetter, Single-Crystalline Copper Nanowires Produced by Electrochemical Deposition in Polymeric Ion Track Membranes, Adv. Mater. 13 (2001) 62–65. https://doi.org/10.1002/1521-4095(200101)13:1<62::aid-adma62>3.3.co;2-z.

[287] Q. Ai, Z. Yuan, R. Huang, C. Yang, G. Jiang, J. Xiong, Z. Huang, S. Yuan, One-pot co-precipitation synthesis of Fe3O4 nanoparticles embedded in 3D carbonaceous matrix as anode for lithium ion batteries, J. Mater. Sci. 54 (2019) 4212–4224. https://doi.org/10.1007/s10853-018-3141-3.

[288] F. Wang, Y. Li, Y. Wang, Z. Cao, Self-assembled monolayer of designed and synthesized triazinedithiolsilane molecule as interfacial adhesion enhancer for integrated circuit, Nanoscale Res. Lett. 6 (2011) 1–5. https://doi.org/10.1186/1556-276X-6-483.

[289] M. Zong, Y. Huang, Y. Zhao, X. Sun, C. Qu, D. Luo, J. Zheng, Facile preparation, high microwave absorption and microwave absorbing mechanism of RGO-Fe3O4 composites, RSC Adv. 3 (2013) 23638–23648. https://doi.org/10.1039/c3ra43359e.

[290] Z. Wang, M. Chen, J. Shu, Y. Li, One-step solvothermal synthesis of Fe3O4@Cu@Cu2O nanocomposite as magnetically recyclable mimetic peroxidase, J. Alloys Compd. 682 (2016) 432–440. https://doi.org/10.1016/j.jallcom.2016.04.269.

[291] T. Xia, D. Zeng, Z. Li, R.J. Young, C. Vallés, I.A. Kinloch, Electrically conductive GNP/epoxy composites for out-of-autoclave thermoset curing through Joule heating, Compos. Sci. Technol. 164 (2018) 304–312. https://doi.org/10.1016/j.compscitech.2018.05.053.

[292] S.P. Pawar, D.A. Marathe, K. Pattabhi, S. Bose, Electromagnetic interference shielding through MWNT grafted Fe3O4nanoparticles in PC/SAN blends, J. Mater. Chem. A. 3 (2015) 656–669. https://doi.org/10.1039/c4ta04559a.

[293] D.H. Chen, Y.Y. Chen, Synthesis of barium ferrite ultrafine particles by coprecipitation in the presence of polyacrylic acid, J. Colloid Interface Sci. 235 (2001) 9–14. https://doi.org/10.1006/jcis.2000.7340.

[294] J. Chen, P. Meng, M. Wang, G. Zhou, X. Wang, G. Xu, Electromagnetic and microwave absorption properties of BaMgxCo1-xTiFe10O19, J. Alloys Compd. 679 (2016) 335–340. https://doi.org/10.1016/j.jallcom.2016.04.001.

[295] H.K. Choudhary, S.P. Pawar, R. Kumar, A. V. Anupama, S. Bose, B. Sahoo, Mechanistic Insight into the Critical Concentration of Barium Hexaferrite and the Conductive Polymeric Phase with Respect to Synergistically Electromagnetic Interference (EMI) Shielding, ChemistrySelect. 2 (2017) 830–841. https://doi.org/10.1002/slct.201601895.

[296] H.K. Choudhary, R. Kumar, S.P. Pawar, S. Bose, B. Sahoo, Effect of Microstructure and Magnetic Properties of Ba-Pb-Hexaferrite Particles on EMI Shielding Behavior of Ba-Pb-

Hexaferrite-Polyaniline-Wax Nanocomposites, J. Electron. Mater. 49 (2020) 1618–1629. https://doi.org/10.1007/s11664-019-07478-y.

[297] S. Siddique, M. Zahid, R. Anum, H.F. Shakir, Z.A. Rehan, Fabrication and characterization of PVC based flexible nanocomposites for the shielding against EMI, NIR, and thermal imaging signals, Results Phys. 24 (2021) 104183. https://doi.org/10.1016/j.rinp.2021.104183.

[298] S. Iqbal, J. Shah, R.K. Kotnala, S. Ahmad, Highly efficient low cost EMI shielding by barium ferrite encapsulated polythiophene nanocomposite, J. Alloys Compd. 779 (2019) 487–496. https://doi.org/10.1016/j.jallcom.2018.11.307.

[299] S. Kumar, G. Datt, A. Santhosh Kumar, A.C. Abhyankar, Enhanced absorption of microwave radiations through flexible polyvinyl alcohol-carbon black/barium hexaferrite composite films, J. Appl. Phys. 120 (2016). https://doi.org/10.1063/1.4964873.

[300] F. Yakuphanoglu, A.A. Al-Ghamdi, F. El-Tantawy, Electromagnetic interference shielding properties of nanocomposites for commercial electronic devices, Microsyst. Technol. 21 (2015) 2397–2405. https://doi.org/10.1007/s00542-014-2394-2.

[301] H. Iida, K. Takayanagi, T. Nakanishi, T. Osaka, Synthesis of Fe 3 O 4 nanoparticles with various sizes and magnetic properties by controlled hydrolysis, 314 (2007) 274–280. https://doi.org/10.1016/j.jcis.2007.05.047.

[302] K.C. Etika, L. Liu, L.A. Hess, J.C. Grunlan, The influence of synergistic stabilization of carbon black and clay on the electrical and mechanical properties of epoxy composites, Carbon N. Y. 47 (2009) 3128–3136. https://doi.org/10.1016/j.carbon.2009.07.031.

[303] G. Rado, R. Wright, W. Emerson, Ferromagnetism at Very High Frequencies., Phys. Rev. Lett. 80 (1950) 273–281.

[304] S. Ni, S. Lin, Q. Pan, F. Yang, K. Huang, D. He, Hydrothermal synthesis and microwave absorption properties of Fe 3O4 nanocrystals, J. Phys. D. Appl. Phys. 42 (2009). https://doi.org/10.1088/0022-3727/42/5/055004.

[305] I. Maartense, C.W. Searle, Domain wall and magnetoelastic resonances in hematite, J. Appl. Phys. 42 (1971) 2349–2355. https://doi.org/10.1063/1.1660547.

[306] S.H. Ryu, Y.K. Han, S.J. Kwon, T. Kim, B.M. Jung, S.B. Lee, B. Park, Absorption-dominant, low reflection EMI shielding materials with integrated metal mesh/TPU/CIP composite, Chem. Eng. J. 428 (2022). https://doi.org/10.1016/j.cej.2021.131167.

[307] H. Duan, H. Zhu, J. Gao, D.X. Yan, K. Dai, Y. Yang, G. Zhao, Y. Liu, Z.M. Li, Asymmetric conductive polymer composite foam for absorption dominated ultra-efficient electromagnetic interference shielding with extremely low reflection characteristics, J. Mater. Chem. A. 8 (2020) 9146–9159. https://doi.org/10.1039/d0ta01393e.

[308] K. Li, S. Yang, M. Hu, J. Gao, R.K.-Y. Li, Y. Dong, G. Shan, Flexible Transparent PES/Silver Nanowires/PET Sandwich-Structured Film for High-Efficiency Electromagnetic Interference Shielding, Langmuir. 28 (2012) 7101–7106. https://doi.org/10.1021/la300720y.

[309] W.R. Hendee, J.C. Boteler, The question of health effects from exposure to electromagnetic fields, Health Phys. 66 (1994) 127–136. https://doi.org/10.1097/00004032-199402000-00001.

[310] P. Bhattacharya, C.K. Das, Investigation on microwave absorption capacity of nanocomposites based on metal oxides and graphene, J. Mater. Sci. Mater. Electron. 24 (2013) 1927–1936. https://doi.org/10.1007/s10854-012-1036-7.

[311] V. Somani, S.J. Kalita, Synthesis and characterization of nanocrystalline Barium

Strontium Titanate powder via sol-gel processing, J. Electroceramics. 18 (2007) 57–65. https://doi.org/10.1007/s10832-007-9008-7.

[312] C. Thongchanthep, S. Thountom, Effect of the fuel type on the synthesis of barium strontium titanate by sol-gel combustion method, Adv. Mater. Res. 802 (2013) 149–153. https://doi.org/10.4028/www.scientific.net/AMR.802.149.

[313] M.A. Ramirez, E. Longo, F. Moura, A.Z. Simões, J.A. Varela, T.B. Onofre, Microwave-hydrothermal synthesis of barium strontium titanate nanoparticles, J. Alloys Compd. 508 (2010) 620–624. https://doi.org/10.1016/j.jallcom.2010.08.143.

[314] S.A. Nasser, X-ray photoelectron spectroscopy study on the composition and structure of BaTiO3 thin films deposited on silicon, Appl. Surf. Sci. 157 (2000) 14–22. https://doi.org/10.1016/S0169-4332(99)00495-X.

[315] H. Farahani, R. Wagiran, G.A. Urban, Barium Strontium Titanate-Based Humidity Sensors: Microstructure, Surface Morphology, Dopant Influence, and Transduction Mechanism Investigations, ACS Appl. Electron. Mater. 3 (2021) 4919–4933. https://doi.org/10.1021/acsaelm.1c00744.

[316] J.D. Baniecki, M. Ishii, T. Shioga, K. Kurihara, S. Miyahara, Surface core-level shifts of strontium observed in photoemission of barium strontium titanate thin films, Appl. Phys. Lett. 89 (2006) 2004–2007. https://doi.org/10.1063/1.2357880.

[317] W. Xie, R. Li, Q. Xu, Enhanced photocatalytic activity of Se-doped TiO2 under visible light irradiation, Sci. Rep. 8 (2018) 1–10. https://doi.org/10.1038/s41598-018-27135-4.

[318] T. Singh, S. Öz, A. Sasinska, R. Frohnhoven, S. Mathur, T. Miyasaka, Sulfate-Assisted Interfacial Engineering for High Yield and Efficiency of Triple Cation Perovskite Solar Cells with Alkali-Doped TiO2 Electron-Transporting Layers, Adv. Funct. Mater. 28 (2018). https://doi.org/10.1002/adfm.201706287.

[319] K. Gebremedhn Kelele, H.C. Ananda Murthy, R. Balachandran, A. Tadesse, Y. Nikodimos, L. Teshome Tufa, J. Lee, The microstructural and morphological effects of doping barium strontium titanate nanocrystalline with selenium, Inorg. Chem. Commun. 145 (2022) 109954. https://doi.org/10.1016/j.inoche.2022.109954.

[320] A.A. Al-Ghamdi, F. El-Tantawy, New electromagnetic wave shielding effectiveness at microwave frequency of polyvinyl chloride reinforced graphite/copper nanoparticles, Compos. Part A Appl. Sci. Manuf. 41 (2010) 1693–1701. https://doi.org/10.1016/j.compositesa.2010.08.006.

[321] H. Duan, P. He, H. Zhu, Y. Yang, G. Zhao, Y. Liu, Constructing 3D carbon-metal hybrid conductive network in polymer for ultra-efficient electromagnetic interference shielding, Compos. Part B Eng. 212 (2021) 108690. https://doi.org/10.1016/j.compositesb.2021.108690.

[322] C. Wang, H. Gao, D. Liang, S. Liu, H. Zhang, H. Guan, Y. Wu, Y. Zhang, Effective fabrication of flexible nickel chains/acrylate composite pressure-sensitive adhesives with layered structure for tunable electromagnetic interference shielding, Adv. Compos. Hybrid Mater. (2022). https://doi.org/10.1007/s42114-022-00482-7.

[323] H. Guan, D.D.L. Chung, Absorption-dominant radio-wave attenuation loss of metals and graphite Electronic materials, J. Mater. Sci. 56 (n.d.). https://doi.org/10.1007/s10853-021-05808-2.

[324] V. Zaroushani, A. Khavanin, S.B. Mortazavi, A. Jonidi Jafari, Efficacy of Net Epoxy Resin for Electromagnetic Shielding in X-Band Frequency Range, Heal. Scope. 5 (2016). https://doi.org/10.17795/jhealthscope-30203.

[325] N. Maruthi, M. Faisal, N. Raghavendra, Conducting polymer based composites as efficient EMI shielding materials: A comprehensive review and future prospects, Synth. Met. 272 (2021) 116664. https://doi.org/10.1016/j.synthmet.2020.116664.

[326] A. Munir, Microwave Radar Absorbing Properties of Multiwalled Carbon Nanotubes Polymer Composites: A Review, Adv. Polym. Technol. 36 (2017) 362–370. https://doi.org/10.1002/adv.21617.

[327] C. Harnagea, R. Nechache, M.H. Phan, F. Rosei, H. Srikanth, Tunable High Aspect Ratio Iron Oxide Nanorods for Enhanced Hyperthermia, J. Phys. Chem. C. 27 (2015) 5476–5481. https://doi.org/10.1021/acs.chemmater.5b00944.

[328] S. Liu, S. Qin, Y. Jiang, P. Song, H. Wang, Lightweight high-performance carbon-polymer nanocomposites for electromagnetic interference shielding, Compos. Part A Appl. Sci. Manuf. 145 (2021) 106376. https://doi.org/10.1016/j.compositesa.2021.106376.

[329] S. Gupta, N.H. Tai, Carbon materials and their composites for electromagnetic interference shielding effectiveness in X-band, Carbon N. Y. 152 (2019) 159–187. https://doi.org/10.1016/j.carbon.2019.06.002.

[330] S. Das, S. Sharma, T. Yokozeki, S. Dhakate, Conductive layer-based multifunctional structural composites for electromagnetic interference shielding, Compos. Struct. 261 (2021) 113293. https://doi.org/10.1016/j.compstruct.2020.113293.

[331] P. Song, H. Qiu, L. Wang, X. Liu, Y. Zhang, J. Zhang, J. Kong, J. Gu, Honeycomb structural rGO-MXene/epoxy nanocomposites for superior electromagnetic interference shielding performance, Sustain. Mater. Technol. 24 (2020) e00153. https://doi.org/10.1016/j.susmat.2020.e00153.

[332] T. Omura, C.H. Chan, M. Wakisaka, H. Nishida, Organic Thin Paper of Cellulose Nanofiber/Polyaniline Doped with (±)-10-Camphorsulfonic Acid Nanohybrid and Its Application to Electromagnetic Shielding, ACS Omega. 4 (2019) 9446–9452. https://doi.org/10.1021/acsomega.9b00708.

[333] X. Yin, L. Kong, L. Zhang, L. Cheng, N. Travitzky, P. Greil, Electromagnetic properties of Si-C-N based ceramics and composites, Int. Mater. Rev. 59 (2014) 326–355. https://doi.org/10.1179/1743280414Y.0000000037.

[334] S. Bal, S. Saha, Scheming of microwave shielding effectiveness for X band considering functionalized MWNTs/epoxy composites, IOP Conf. Ser. Mater. Sci. Eng. 115 (2016). https://doi.org/10.1088/1757-899X/115/1/012027.

[335] Y. Xu, Y. Yang, D.X. Yan, H. Duan, G. Zhao, Y. Liu, Gradient Structure Design of Flexible Waterborne Polyurethane Conductive Films for Ultraefficient Electromagnetic Shielding with Low Reflection Characteristic, ACS Appl. Mater. Interfaces. 10 (2018) 19143–19152. https://doi.org/10.1021/acsami.8b05129.

[336] Z. Wang, X. Fu, Z. Zhang, Y. Jiang, M. Waqar, P. Xie, K. Bi, Y. Liu, X. Yin, R. Fan, Paper-based metasurface: Turning waste-paper into a solution for electromagnetic pollution, J. Clean. Prod. 234 (2019) 588–596. https://doi.org/10.1016/j.jclepro.2019.06.239.

[337] D. Tan, D. Hee, J.J. Yu, P. Eudeline, D. Baillargeat, B.K. Tay, Carbon nanotube cavity for compact Radar components, Proc. 2015 IEEE 5th Asia-Pacific Conf. Synth. Aperture Radar, APSAR 2015. (2015) 272–273. https://doi.org/10.1109/APSAR.2015.7306205.

[338] H. Zhang, G. Zhang, J. Li, X. Fan, Z. Jing, J. Li, X. Shi, Lightweight, multifunctional microcellular PMMA/Fe3O4@MWCNTs nanocomposite foams with efficient electromagnetic interference shielding, Compos. Part A Appl. Sci. Manuf. 100 (2017)

128–138. https://doi.org/10.1016/j.compositesa.2017.05.009.

[339] P. Bhattacharya, C.K. Das, In situ synthesis and characterization of CuFe10Al 2O19/MWCNT nanocomposites for supercapacitor and microwave-absorbing applications, Ind. Eng. Chem. Res. 52 (2013) 9594–9606. https://doi.org/10.1021/ie4005783.

[340] K. Manna, S.K. Srivastava, Fe3O4@Carbon@Polyaniline Trilaminar Core-Shell Composites as Superior Microwave Absorber in Shielding of Electromagnetic Pollution, ACS Sustain. Chem. Eng. 5 (2017) 10710–10721. https://doi.org/10.1021/acssuschemeng.7b02682.

[341] P. Sambyal, S.J. Noh, J.P. Hong, W.N. Kim, A. Iqbal, S.S. Hwang, S.M. Hong, C.M. Koo, FeSiAl/metal core shell hybrid composite with high-performance electromagnetic interference shielding, Compos. Sci. Technol. 172 (2019) 66–73. https://doi.org/10.1016/j.compscitech.2019.01.007.

[342] M. Gurusiddesh, B.J. Madhu, G.J. Shankaramurthy, B. Shruthi, Structural, dielectric and magnetic studies on polyaniline-decorated Ni0.5Cu0.5Fe2O4 nanoferrites for electromagnetic interference shielding applications, Appl. Phys. A Mater. Sci. Process. 126 (2020) 1–9. https://doi.org/10.1007/s00339-019-3268-3.

[343] A. V. Menon, B. Choudhury, G. Madras, S. Bose, 'Trigger-free' self-healable electromagnetic shielding material assisted by co-doped graphene nanostructures, Chem. Eng. J. 382 (2020) 122816. https://doi.org/10.1016/j.cej.2019.122816.

[344] H.K. Choudhary, R. Kumar, S.P. Pawar, U. Sundararaj, B. Sahoo, Enhancing absorption dominated microwave shielding in co@c-pvdf nanocomposites through improved magnetization and graphitization of the co@c-nanoparticles, Phys. Chem. Chem. Phys. 21 (2019) 15595–15608. https://doi.org/10.1039/c9cp03305j.

[345] S. Gupta, C. Chang, C.H. Lai, N.H. Tai, Hybrid composite mats composed of amorphous carbon, zinc oxide nanorods and nickel zinc ferrite for tunable electromagnetic interference shielding, Compos. Part B Eng. 164 (2019) 447–457. https://doi.org/10.1016/j.compositesb.2019.01.060.

[346] P. Bhattacharya, S. Dhibar, G. Hatui, A. Mandal, T. Das, C.K. Das, Graphene decorated with hexagonal shaped M-type ferrite and polyaniline wrapper: A potential candidate for electromagnetic wave absorbing and energy storage device applications, RSC Adv. 4 (2014) 17039–17053. https://doi.org/10.1039/c4ra00448e.

[347] A.N. Vicente, G.M.I. Dip, C. Junqueira, The step by step development of NRW method, SBMO/IEEE MTT-S Int. Microw. Optoelectron. Conf. Proc. (2011) 738–742. https://doi.org/10.1109/IMOC.2011.6169318.

[348] Y.L. Chan, F. Esa, K.Y. You, M.S. Sim, M.Z.H. Mayzan, M.A. Jusoh, Electromagnetic properties of magnetite/epoxy resin composites at x-band frequency, Prog. Electromagn. Res. Symp. 2017-Novem (2017) 3004–3010. https://doi.org/10.1109/PIERS-FALL.2017.8293649.

[349] Y. Yang, M.C. Gupta, K.L. Dudley, Towards cost-efficient EMI shielding materials using carbon nanostructure-based nanocomposites, Nanotechnology. 18 (2007). https://doi.org/10.1088/0957-4484/18/34/345701.

[350] V.D. Phadtare, V.G. Parale, K.Y. Lee, T. Kim, V.R. Puri, H.H. Park, Flexible and lightweight Fe3O4/polymer foam composites for microwave-absorption applications, J. Alloys Compd. 805 (2019) 120–129. https://doi.org/10.1016/j.jallcom.2019.07.048.

[351] B. Shen, W. Zhai, M. Tao, J. Ling, W. Zheng, Lightweight, multifunctional

polyetherimide/graphene@Fe3O 4 composite foams for shielding of electromagnetic pollution, ACS Appl. Mater. Interfaces. 5 (2013) 11383–11391. https://doi.org/10.1021/am4036527.

[352] Y. Wang, W. Zhang, C. Luo, X. Wu, G. Yan, W. Chen, Fabrication and high-performance microwave absorption of Ni@SnO2 @PPy Core-Shell composite, Synth. Met. 220 (2016) 347–355. https://doi.org/10.1016/j.synthmet.2016.07.005.

List of Publications

1. **R. K. Bheema**, A. V. Praveen Kumar, and K.C.Etika, "Broadband microwave absorption characteristics of BST@CuNW and Fe_3O_4@BST@CuNW hybrid epoxy composites in the X-band" (Communicated)

2. **R. K. Bheema**, Akshat Verma, and K.C.Etika, " A Review on recent progress in polymer composites for effective electromagnetic interference shielding properties- Structures, Process, Sustainability approaches" (To be communicated soon)

3. **R.K.Bheema**, Darmesh misra, et al., " An electrochemical sensor based on tetramethyl thiuram disulfide and multiwalled carbon nanotube electrode for sensitive detection of Lead" (To be communicated soon)

4. **R.K.Bheema**, K.C. Etika, Large microwave absorption By Fe_3O_4@CuNW hybrid nanoparticles filled epoxy nanocomposites in the X-Band, J. Alloys Compd. 938 (2023) 168405. https://doi.org/10.1016/j.jallcom.2022.168405.

5. **R.K.Bheema**, K.C. Etika, Materials Today : Proceedings The influence of hybrid decorated structures on the EMI shielding properties of epoxy composites over the X-Band, Mater. Today Proc. (2022) 2214-7853. https://doi.org/10.1016/j.matpr.2022.11.493.

6. I. Dogra, **R.K.Bheema**, K.C. Etika, M. Chavali, A.S. Khalifa, A.F. Gharib, Askary, Environmentally friendly low-cost graphene oxide-cellulose nanocomposite filter for dye removal from water, J. King Saud Univ. - Sci. 34 (2022) 102122. https://doi.org/10.1016/j.jksus.2022.102122.

7. **R.K.Bheema**, A.K. Ojha, A.V.P. Kumar, K.C. Etika, Synergistic influence of barium hexaferrite nanoparticles for enhancing the EMI shielding performance of GNP / epoxy nanocomposites, J. Mater. Sci. (2022) 8714–8726. https://doi.org/10.1007/s10853-022-07214-8.

8. **R.K.Bheema**, K.C. Etika, Facile One-Pot Hydrothermal Synthesis of Copper Nanowires and Their Impact on the EMI Shielding Capability of Epoxy Composites, Chem. Eng. Technol. 45 (2022) 410–416. https://doi.org/10.1002/ceat.202100389.

9. **R.K.Bheema**, K. Kumar, N. Etakula, K.C. Etika, Enhanced thermo-mechanical , thermal and EMI shielding properties of MWNT / MAgPP / PP nanocomposites prepared by extrusion, Compos. Part C Open Access. 4 (2021) 100086. https://doi.org/10.1016/j.jcomc.2020.100086.

10. K. Bhaskaran, **R.K. Bheema**, K.C. Etika, The influence of Fe3O4@GNP hybrids on enhancing the EMI shielding effectiveness of epoxy composites in the X-band, Synth. Met. 265 (2020). https://doi.org/10.1016/j.synthmet.2020.116374.

11. V. Uma Varun, **R.K.Bheema**, K.C. Etika, Hybrid polymer nanocomposites as EMI shielding materials in the X-band, Mater. Today Proc. (2020) 10–12. https://doi.org/10.1016/j.matpr.2019.12.300.

List of International Conferences

1. "Polymer composites for effective electromagnetic interference shielding properties-Structures, Process, Sustainability approaches" presented at International Conference on Nanotechnology for Sustainable Living & Environment-2022 (ICON-NSLE-2022), April 14-16, 2022, Organized by Chemical Engineering Department, BITS Pilani

2. "The influence of hybrid decorated structures on the EMI shielding properties of epoxy composites in the X-band" presented at International Conference on Nanotechnology for Sustainable Living & Environment-2022 (ICON-NSLE-2022), April 14-16, 2022, Organized by Chemical Engineering Department, BITS Pilani

3. "Biodegradable AESO-based nanocomposite for EMI Shielding applications" presented at International Conference on Nanotechnology for Sustainable Living & Environment-2022 (ICON-NSLE-2022), April 14-16, 2022, Organized by Chemical Engineering Department, BITS Pilani

4. "Synthesis and characterization of EMI shielding properties of copper nanowires epoxy nanocomposites" Presented at International Chemical Engineering Conferences-2021 (ICheEC-2021), September 17-19, 2021, Organized by Chemical Engineering Department, NIT Jalandhar

5. "Hybrid Polymer Nanocomposites as EMI. Shielding Materials in the X-Band" Presented at the 2nd International Conference on Recent Advances in Materials & Manufacturing Technologies (IMMT 2019), November 20-22, 2019, Organized by BITS Pilani Dubai Campus, UAE.

6. "Enhanced Thermal Stability And Mechanical Properties In Multi-Walled Carbon Nanotube Filled Polypropylene Nanocomposites Synthesized Using A Masterbatch," Presented at the 4th International Conference on Nanotechnology for Better Living: Theme: Technological Advancements of Polymer Composites, April 6-8, 2019, Organized by IIT Kanpur.

7. "Epoxy Nanocomposites For Electromagnetic Interference (EMI.) Shielding Applications," Presented at the 5th International Conference on Nanoscience and Nanotechnology (ICONN-2019), January 28–30, 2019, Organized by SRM Institute of Science and Technology, Chennai.

<u>Biographical sketch of supervisor (Dr. Krishna C.Etika)</u>

Dr. Krishna C.Etika graduated with a B.Tech degree in Chemical Engineering, securing University Rank 1 from Sri Venkateswara University in Tirupati, Andhra Pradesh. Further, he completed M.Tech degree in Materials Science and Engineering (Polymers) from IIT Kharagpur. After M.Tech he had a brief tenure at CEAT Ltd. in Bhandup, Mumbai prior to moving to the U.S.A for doctoral studies. He got enrolled at Cornell University for a Ph.D. program initially but later transferred to Texas A&M University in College Station, Texas from where he received his Ph.D. degree in Materials Science and Engineering. His Ph.D. research was primarily focused on controlling the dispersion state of nanoparticles using stimuli-responsive polymers. After his Ph.D, he worked for Intel Corporation in the U.S.A as a Technology Development Process Engineer for about three and half years and decided to relocate to India due to personal reasons. At Intel, his work spanned the areas of reactive ion etching and materials development for high-density interconnect applications. After moving back to India, he took up a temporary assignment with IIT Madras in terms of an Institute Post-Doctoral Fellowship and later joined as a faculty member (Associate Professor Grade) in the department of Chemical Engineering in the Vignan's University in Guntur, Andhra Pradesh. At Vignan, he served as both Head, Chemical Engineering and Dean, Academics during 2016-2018. Since March 2018, He is working as a faculty member in the department of Chemical Engineering at BITS Pilani, Pilani Campus. His research group at BITS Pilani is working on developing advanced materials and characterization methodology for tackling current engineering challenges. He is passionate about materials research, and He strongly believes that innovations at this end will make this world a great place to live.

Biographical sketch of a student (Bheema Rajesh Kumar)

Bheema Rajesh Kumar has been fascinated by the field of chemical engineering since his graduation, and he discovered an opportunity to implement it in a wide range of applications by integrating his fundamentals with current research findings. Hence, he applied and got admission into Anurag University, Hyderabad. He applied and got admission into Osmania University, Hyderabad, which is one of the top research institutes in India, by qualifying for the graduate aptitude test in engineering (GATE) with an all-India rank of 2744 and post-graduate engineering common entrance test (PGECET -2015) rank of 5. He successfully completed his M.Tech in Chemical Technology (Specialization: Material Science and Technology) tenure of 2015-2017 by submitting the dissertation under the supervision of E. Nagabhushana, Dean and HOD of College of Technology, Osmania University, Hyderabad. Further, he secured a Ph.D. position at the BITS, Pilani, to pursue his deep interest in Chemical Engineering.